BOSTON UNIVERSITY

SCHOOL OF MEDICINE

Dissertation

MECHANISM OF ELECTRON CAPTURE DISSOCIATION AND THE APPLICATION TO PROTEIN DEAMIDATION

by

XIAOJUAN LI

B.E., Jilin University, 2000

M.S., Jilin University, 2003

Submitted in partial fulfillment of the

requirements for the degree of

Doctor of Philosophy

2010

Approved by

First Reader _____

Peter B. O'Connor, Ph.D.

Associate Professor of Biochemistry

Second Reader _____

Cheng Lin, Ph.D.

Assistant Professor of Biochemistry

Acknowledgement

It is a great pleasure to thank all the people who supported and helped me during the whole period of my Ph.D. study at Boston University. I would like to express my deepest gratitude to my advisor, Prof. Peter B. O'Connor, for giving me the opportunity to join his lab and continuously supporting me to finish my work. He introduced me to the field of mass spectrometry and showed me the way to explore, so that I can enjoy the research in mass spectrometry and biochemistry. His guidance and encouragement are very important for my research. During every step of my study, from my first experiment design, to my first paper editing, and to my thesis writing, he is always ready to help me and give me valuable advices. I greatly appreciate his patience, kindness, and the time he spent helping me.

I would like to thank Prof. Cheng Lin, whom I always consult with about many things, from scientific research to daily life. I am really grateful to him for his constant and enthusiastic help in these five years. He also gave me extensive revision of my thesis. I would also like to thank Prof. Catherine E. Costello for her generous help and support. She kindly served on my committee and gave me many invaluable comments on our collaborated paper.

I am sincerely grateful to the members of my thesis advisory committee: Prof. Carmela Abraham, Prof. Richard A. Laursen, and Prof. Lawreen H. Connors, who spent their valuable time for serving on my committee and giving me constructive advices.

I would like to acknowledge all the past and present colleagues from Boston University. I thank Prof. Joseph Zaia, Prof. Mark McComb, Dr. Jason Cournoyer, Dr. Chunxiang Yao, Dr. Weidong Cui, Dr. Yiqun Huang, Dr. Cheng Zhao, Dr. Michael Bowman, Dr. Parminder Kaur, Dr. Vera Ivleva, Dr. Raman Mathur, Dr. Konstantine

Aizikov, Nadezda Sargaeva, Tzu-Yung (Terry) Lin, Xiang Yu, Yuhuan Ji, Dr. Nancy Leymarie, and Dr. Roger Theberge, for their scientific assistance and support. I thank Dr. Zhenning Hong, Dr. Hyejung Park, Dr. Yan Wang, Dr. Yan Jiang, Dr. Xiaofeng Shi, Ying Zhou, Yu Huang and Liang Han for their wonderful friendship. I also appreciate the administrative assistance from Denise Neves and Patricia Bullock.

Finally, I wish to thank my mother, my father, and my husband for their endless love and continuous support through all these years. My special gratitude goes to my parents-in-law for their support and taking care of our little baby, without their help I would not be able to focus on my study here. I also express my gratitude to all my other family members and friends in China.

MECHANISM OF ELECTRON CAPTURE DISSOCIATION AND THE APPLICATION TO PROTEIN DEAMIDATION

(Order No.)

XIAOJUAN LI

Boston University School of Medicine, 2010

Major Professor: Peter B. O'Connor, Ph.D., Professor of Biochemistry

ABSTRACT

Electron capture dissociation (ECD) is an important tandem mass spectrometry (MS) method, which features homolytic backbone fragmentation providing extensive sequence coverage and retention of post-translational modifications (PTMs). Two major applications of ECD in proteomics are protein sequencing and PTM characterizations using both top-down and bottom-up approaches. Among the several mechanisms proposed, the free-radical cascade (FRC) is the only one that adequately explains secondary fragmentations in ECD. To further test the FRC mechanism, ECD of fixed charge tag modified peptides was investigated. The data indicated that both the number and location of the fixed charge groups influenced the backbone and side-chain cleavages of these peptides in ECD. Secondary fragmentations of several synthetic peptides were also studied by both ECD and electron transfer dissociation (ETD). Charge remote fragmentations of z• ions were observed, which were more abundant in

ECD than in ETD, resulting in partial/entire side-chain losses and/or formation of internal fragments. ECD was performed on peptide b ions as well, which identified both linear and macro-cyclic structures. A sound understanding of b ion structure is important for spectra interpretation and peptide sequencing. ECD is a particularly useful method for studying deamidation. Deamidation is a spontaneous nonenzymatic PTM of proteins, which is involved in many diseases and postulated to function as a molecular clock in aging. Deamidation of asparagine/glutamine (Asn/Gln) introduces a negative charge to peptides/proteins and increases the molecular mass by +0.984 Da, which can be detected by many MS methods; however, diagnostic ions of isoaspartic and aspartic acid can only be generated by ECD. In order to differentiate the deamidation that occurred during sample preparation process from the pre-existing deamidation of biological interest, $H_2{}^{18}O$ labeling combined with ECD was used to monitor the artificial Asn deamidation of several peptides released from trypsin digestion. Due to the much slower deamidation rate of Gln than Asn, few Gln deamidation studies have been reported. The ECD method was further applied to investigate the isomeric Gln deamidation products in peptides. Diagnostic ions specific to γGlu were identified, indicating that ECD is also applicable to the study of Gln deamidation. Through this thesis, a better understanding of the ECD mechanism was gained, which helped protein characterization and study of deamidation.

Table of Contents

Title page……i

Reader's approval page……ii

Acknowledgement..…… iii

Abstract……v

Table of contents……..vii

List of figures……xii

List of abbreviations..……xvii

Chapter 1 Introduction 1

1.1 Introduction to protein deamidation study by mass spectrometry 1

1.2 Introduction to mass spectrometry and its applications in biology 2

1.2.1 Major ionization techniques..... 3

1.2.2 Mass analyzers 7

1.2.3 Tandem mass spectrometry methods 19

1.2.4 ESI qQq-FT ICR mass spectrometer 28

1.2.5 12 Tesla solariX FT ICR mass spectrometer 31

1.3 Introduction to protein deamidation and related diseases..... 33

1.3.1 Protein deamidation 33

1.3.2 Isomerization and racemization of asparatic acid 35

1.3.3 Protein L-isoaspartyl O-methyltransferase 36

1.3.4 Deamidation related diseases 38

1.4 Overview of this thesis 40

Chapter 2 The effect of fixed charge modifications on ECD 42

2.1 Introduction 42
2.1.1 ECD and primary mechanisms 42
2.1.2 ECD and secondary mechanism: free radical cascade (FRC) 44
2.2 Experimental section 46
2.2.1 Materials 46
2.2.2 Peptide derivatization 46
2.2.3 ECD experiments 47
2.3 Results and discussion 48
2.3.1 Backbone cleavages 49
2.3.2 Tag and alkyl group losses 58
2.3.3 Other small molecule and side-chain losses 62
2.3.4 Secondary and internal fragment ions 64
2.4 Conclusion 67

Chapter 3 Charge remote fragmentation in ECD and ETD 69
3.1 Introduction 69
3.1.1 Free radicals generated by various MS methods 69
3.1.2 Free radicals in ECD and ETD 70
3.2 Experimental section 72
3.2.1 Materials and ECD experiments 72
3.2.2 ETD experiments 73
3.3 Results and discussion 73
3.3.1 Entire side chain loss from z• Ions associated with γ-radical formation on the side chain 76

3.3.2 Partial side chain loss from z• ions associated with α-radical formation on the side chain 79
3.3.3 Internal fragments associated with β-radical formation on the side chain from z• ions 83
3.3.4 Side chain loss from z• ions and internal fragments studied in ETD 86
3.4 Conclusion 90

Chapter 4 Cyclic rotational heterogeneity of b ions 92
4.1 Introduction 92
4.1.1 MS^3 methods of CAD/CAD and CAD/ECD 92
4.1.2 The b ion structures 93
4.2 Experimental section 96
4.2.1 Materials 96
4.2.2 ECD experiments 97
4.2.3 Theoretical calculation 97
4.3 Results and discussion 98
4.3.1 ECD of b ions from neurokinin A and eledoisin 99
4.3.2 ECD of b ions from substance P 104
4.3.3 ECD of b ions from two variants of substance P 113
4.4 Conclusion 116

Chapter 5 Use of ^{18}O labels to monitor deamidation during protein trypsin digestion processes 118
5.1 Introduction 118
5.1.1 Deamidation and its mechanism 118

5.1.2 Asn deamidation detection methods 120
5.1.3 The $H_2{}^{18}O$ labeling method 122
5.2 Experimental section 123
5.2.1 Materials 123
5.2.2 Reduction and alkylation of ribonuclease A and lysozyme proteins 124
5.2.3 ^{18}O labeled time course digestion 124
5.2.4 ^{16}O labeled control experiments 124
5.2.5 Calmodulin ^{18}O labeled triplicate experiments 125
5.2.6 Mass spectrometry analysis 125
5.3 Results and discussion 126
5.3.1 Calmodulin tryptic peptide ESI FTMS spectra (^{16}O vs. ^{18}O) 126
5.3.2 RNase A and lysozyme tryptic peptides ESI FTMS spectra (^{16}O vs. ^{18}O) 129
5.3.3 Quantification of the extent of the ^{18}O incorporation and deamidation during the digestion time course 134
5.3.4 ECD of ^{18}O labeled calmodulin tryptic peptide at time points 2 hr and 24 hr 136
5.4 Conclusion 140

Chapter 6 Glutamine deamidation: differentiation of glutamic acid and γ-glutamic acid in peptides by ECD 141
6.1 Introduction 141
6.1.1 Asn deamidation and the fate of the deamidated proteins in cells 141
6.1.2 Gln deamidation 142
6.1.3 Gln deamidation detection methods 142
6.2 Experimental section 145
6.2.1 Materials 145

6.2.2 ECD experiments 146
6.3 Results and discussion 146
6.3.1 Identification of Gln deamidation site(s) 146
6.3.2 Characteristic ions for the differentiation of the α- and γ-Glu containing peptides 151
6.4 Conclusion 163

Chapter 7 Conclusion and future work 165
7.1 Conclusion 165
7.2 Future work 171

Bibliography..... 173
Curriculum vitae..... 213

List of Figures

Figure 1. 1 Theoretical stability diagram of three *m/z* values 10

Figure 1. 2 Scheme represents the cubic cell 15

Figure 1. 3 Scheme represents the cylindrical cell 16

Figure 1. 4 Nomenclature of peptide N- and C-terminal sequence ions used in mass spectrometry 20

Figure 1. 5 Scheme of ECD process. 23

Figure 1. 6 Scheme of 7 Tesla ESI qQq-FT ICR mass spectrometer. 29

Figure 1. 7 Pulse sequences used in a typical ECD experiment 31

Figure 1. 8 Schematic of 12 Tesla solariX FT mass spectrometer 33

Figure 1. 9 Asn and Gln deamidation process 34

Figure 1. 10 Scheme presents the relation among deamidation, isomerization, and the repairment by PIMT enzyme 37

Figure 2. 1 The ε-amino group of the lysine side-chain was selectively converted to a 2,4,6-trimethylpyridinium salt 49

Figure 2. 2 ECD spectra of the (a) unlabeled, (b) singly-labeled and (c) doubly-labeled Amyloid β peptide (20-29) 51

Figure 2. 3 ECD spectra of the (a) unlabeled, (b) singly-labeled and (c) doubly-labeled Amyloid β peptide (25-35) 52

Figure 2. 4 H loss from the TMP tag upon electron capture 53

Figure 2. 5 One possible mechanism for c/z ion formations in doubly tagged peptides.....55
Figure 2. 6 All observed ECD cleavages of the (a) unlabeled, (b) singly-labeled and (c) doubly-labeled Aβ peptide (20-29).....57
Figure 2. 7 All observed ECD cleavages of the (a) unlabeled, (b) singly-labeled and (c) doubly-labeled Aβ peptide (25-35).....58
Figure 2. 8 Tag loss after the electron capture.....59
Figure 2. 9 Methyl group loss from the tag loss product.....60
Figure 2. 10 Methyl loss from the valine (R = CH_3) and isoleucine (R = CH_2CH_3) side-chains.....62
Figure 2. 11 Methionine side-chain losses from z8 ion.....65

Figure 3. 1 ECD spectrum of αA crystallin peptide (1-11).....74
Figure 3. 2 ECD spectrum of amyloid β peptide (25-35).....75
Figure 3. 3 ECD spectrum of the deamidated form of βB2 crystallin peptide (4-14).....75
Figure 3. 4 Entire side chain loss from z• ions via gamma hydrogen abstraction...77
Figure 3. 5 Entire side chain loss from z• ions via gamma hydrogen abstraction involving aromatic amino acids.....77
Figure 3. 6 Partial side chain loss from z• ions via alpha hydrogen abstraction [through-bond, (a) and through-space, (b)].....80
Figure 3. 7 Postulated mechanisms for the formation of internal fragments.....85
Figure 3. 8 ETD spectra of the deamidated form of βB2 crystallin peptide (4-14)..87

Figure 3. 9 ETD spectrum of the doubly charged αA crystallin peptide (1-11).....88

Figure 3. 10 ETD spectrum of the doubly charged amyloid β peptide (25-35).....88

Figure 4. 1 The structures of b ions (a) acylium structure, (b) oxazolone structure, and (c) macro-cyclic structure 96

Figure 4. 2 ECD spectra of doubly charged b_9 (a), b_8 (b), and b_7 (c) ions from neurokinin A (HKTDSFVGLM-NH_2) 102

Figure 4. 3 Proposed ECD fragmentation pathway of neurokinin A b_9^{2+} ion..... 103

Figure 4. 4 ECD spectra of doubly charged b_{10} (a) and b_9 (b) ions from eledoisin ($_p$EPSKDAFIGLM-NH_2)..... 104

Figure 4. 5 ECD spectra of doubly charged b_{10} (a), b_9 (b), and b_8 (c) ions from substance P (RPKPQQFFGLM-NH_2)..... 107

Figure 4. 6 ECD spectra of doubly charged b_7 (a), b_6 (b), and b_5 (c) ions from substance P (RPKPQQFFGLM-NH_2)..... 108

Figure 4. 7 Proposed mechanism for the formation of c_m-Lys side chain ions in ECD of substance P b_{10}^{2+} ion..... 109

Figure 4. 8 Calculated lowest energy structures of substance P b_8^{2+} ion and their relative energetic stability obtained at B3LYP/6-31G(d)//HF/3-21G level of theory..... 111

Figure 4. 9 Calculated lowest energy structures of substance P b_6^{2+} ion and their relative energetic stability obtained at B3LYP/6-31G(d)//HF/3-21G level of theory..... 112

Figure 4. 10 ECD spectra of doubly charged b_{10} (a) and b_9 (b) ions from substance P variant peptide (RPKPEEFFGLM-OH) 114
Figure 4. 11 ECD spectra of doubly charged b_{10} (a) and b_9 (b) ions from substance P variant peptide (RPKPγEγEFFGLM-OH) 115

Figure 5. 1 Proposed mechanism for the formation of the $[(M+nH)^{(n-1)+\bullet}$ - 60] ions from Asp; and c• + 58 and z• – 57 ions from isoAsp in ECD 121
Figure 5. 2 Scheme of ^{18}O incorporation in asparagine deamidation 123
Figure 5. 3 Mass spectra of the triply charged calmodulin peptide (^{91}VFDKDGNGYISAAELR$_{106}$) extracted at different time from the tryptic digestion solution in $H_2{}^{16}O$ (left column) and in $H_2{}^{18}O$ (right column)..... 128
Figure 5. 4 Mass spectra of the doubly charged RNase A peptide (^{67}NGQTNCYQSYSTMSITDCR$_{85}$) extracted at different time from the tryptic digestion solution in $H_2{}^{16}O$ (left column) and in $H_2{}^{18}O$ (right column)..... 131
Figure 5. 5 Mass spectra of the doubly charged lysozyme peptide (^{46}NTDGSTDYGILQINSR$_{61}$) extracted at different time from the tryptic digestion solution in $H_2{}^{16}O$ (left column) and in $H_2{}^{18}O$ (right column)..... 132
Figure 5. 6 The percentage of each isotopic cluster at different digestion time as calculated using the least squares method 136
Figure 5. 7 ECD spectra of the triply charged calmodulin tryptic peptide (91-106) labeled in $H_2{}^{18}O$ at different time points 137

Figure 6. 1 ECD spectra of αA crystallin peptide (1-11) in its Gln (a), Glu (b), and γGlu (c) forms 147

Figure 6. 2 ECD spectra of βB2 crystallin peptide (4-14) in its Gln (a), Glu (b), and γGlu (c) forms 148

Figure 6. 3 ECD spectra of γS crystallin peptide (52-71) in its Gln (a), Glu (b), and γGlu (c) forms 150

Figure 6. 4 Comparison of several c ions from ECD of βB2 crystallin peptide (4-14) in its Gln and γGlu forms, upper and lower panel, respectively..... 151

Figure 6. 5 Mechanisms for the formation of z•-59 ions in ECD of the Glu containing αA crystallin peptide (1-11)..... 153

Figure 6. 6 Proposed mechanisms for the formation of z•-72 ions in the ECD of the γGlu containing peptide 154

Figure 6. 7 Proposed mechanisms for the formation of (a) c+59 and (b) c+72 ions in the γGlu containing peptide via proline ring opening process 158

Figure 6. 8 Proposed mechanisms for the loss of (a) -CH_2COOH and (b) -CH_2=CHCOOH molecules in the Glu containing peptide via proline ring opening process 158

Figure 6. 9 Proposed mechanisms for the formation of c+57 ions in the γGlu containing βB2 peptide 160

List of Abbreviations

Aβ	amyloid β
AdoMet	S-adenosylmethionine
AdoHcy	S-adeno-L-homocysteine
AI ECD	activated ion electron capture dissociation
APP	amyloid precursor protein
B3LYP	Lee-Yang-Parr's correlation functionals
CAD	collisionally activated dissociation
CDK	cyclin-dependent kinase
CHCA	α-cyano-4-hydroxycinnamic acid
CI	chemical ionization
CID	collision induced dissociation
CNF	cytotoxic necrotizing factors
C-I	carbon-iodine bond
CRFs	charge remote fragmentations
C-S	carbon-sulfur bond
DC	direct current
DE	delayed extraction
DFT	density functional theory
DHB	2,5-dihydroxybenzoic acid
DR-ECD	double resonance electron capture dissociation
ECD	electron capture dissociation
EDD	electron detachment dissociation
EED	electron excitation dissociation

EI	electron ionization
EI	electron impact
EID	electron-induced dissociation
EIEIO	electron-impact excitation of ion from organics
ESI	electrospray ionization
ETcaD	ETD with supplemental collisional activation
ETD	electron transfer dissociation
eV	electron volt
FAB	fast atom bombardment
FIL trap	filament trapping
FRC	free radical cascade
FT-ICR	Fourier transform ion cyclotron resonance
FWHM	full width at half maximum
HDACS	histone deacetylases
HECD	hot electron capture dissociation
HEX	hexapole
H/D	hydrogen/deuterium
HPLC	high performance liquid chromatography
IR	infrared
IRMPD	infrared multiphoton dissociation
IVR	intermolecular vibrational energy redistribution
KeV	kiloelectron volt
LC	liquid chromatography
LPC	lysine peroxycarbamates

MALDI	matrix assisted laser desorption/ionization
MD	molecular dynamics
MS	mass spectrometry
MS/MS	tandem mass spectrometry
m/z	mass-to-charge ratio
nanoES	nanoelectrospray
nETD	negative ETD
OR	orifice
PD	photodissociation
pE	pyroglutamic acid, Pyr
pI	isoelectric point
PIMT	protein L-isoaspartyl O-methyltransferase
ppm	part per million
PTM	post-translational modification
QLT	quadrupole linear ion trap
QqQ	triple quadrupole
RB	retinoblastoma protein
RF	radio frequency
RNG	ring electrode
SID	surface induced dissociation
SK	skimmer
S/N	signal-to-noise ratio
SORI	sustained off resonance irradiation
SPME	solid phase microextraction

ST	stubby quadrupole
TOF	time-of-flight
TLF	time-lag-focusing
TMP	2,4,6-trimethylpyridinium
TTR	transthyretin
UV	ultraviolet
VUV	vacuum ultraviolet

Chapter 1

Introduction

1.1 Introduction to protein deamidation study by mass spectrometry

Almost all life phenomena are carried out by proteins and the function of a protein depends on its structure, which is largely determined by its primary sequence. Therefore, the determination of the protein sequences is very important for the understanding of their functions in biological organisms. Many methods have been developed to facilitate the measurement of protein sequences. Among these, mass spectrometry (MS) is one of the most important analytical techniques, because of its sensitivity, accuracy, speed, and small sample amount requirement.

Initially, mass spectrometry was limited to the detection of small, volatile molecules. With the emergence of new ionization techniques and mass analyzers, the application of mass spectrometry has grown significantly in many research fields, especially in biochemistry and medicine. The development of tandem mass spectrometry (MS/MS) methods and the coupling of liquid chromatography (LC) to mass spectrometers further greatly improved its capabilities. Not only can MS detect the exact masses of many species, including large, nonvolatile biological molecules, it can also provide the detailed sequence information, and in many cases, the structure information as well. The contemporary tandem MS methods have the abilities to provide accurate sequence information for most proteins. Thus, the requirement for protein analysis by MS has moved to a higher level, which includes the post-translational modification (PTM) characterization, beyond the basic level of primary sequence measurement.

PTMs can regulate the activities and functions of many proteins, as well as a variety of signal transduction pathways, which are often associated with various diseases, such as tumorigenesis [1], Alzheimer's disease [2], etc. Phosphorylation/dephosphorylation is one of the most studied, which can function as a switch in many cell signaling pathways. In addition, there are many other kinds of PTMs that play important roles in cell machinery, including acetylation, methylation, glycosylation, deamidation, sulfation, ubiquitination, etc [3, 4]. One of most common and important PTMs is protein deamidation, which can significantly change the protein structure, affect its function and interactions with other proteins [4] and are involved in aging and many pathological processes.

This thesis focuses on the protein deamidation studies by using the electron capture dissociation (ECD) tandem MS method. This chapter includes two parts: the introduction to mass spectrometry (section 1.2) and the introduction to protein deamidation (section 1.3). In the first part, the components and techniques of mass spectrometry are discussed in detail. In the second part, basic principles of protein deamidation and its related diseases are described.

1.2 Introduction to mass spectrometry and its applications in biology

MS is a powerful technique in analytical chemistry which provides the molecular weight information and the structure details of biological molecules. For a protein, its molecular weight can be determined by MS, and its amino acid sequence can be determined by tandem MS methods. A mass spectrometer generally contains three major components: the ionization source, the mass analyzer, and the detector. Because mass spectrometers measure the mass-to-charge ratio (*m/z*), only charged particles can

be analyzed and detected in mass spectrometers. Thus, the first stage of MS is the ionization of analytes in the ionization sources.

1.2.1 Major ionization techniques

A variety of ionization techniques are available for the conversion of neutral molecules present in the gas or solution phase into charged particles. The classic ionization methods include electron ionization (EI) and chemical ionization (CI), etc. They are initiated by the gas-phase interactions of sample molecules with electrons and other chemical ions, which can eject an electron from or attach a proton to a neutral molecule, thus converting it into an ion. However, these methods usually require samples to be introduced into the gas phase and often break down the molecular ions due to the higher energy applied [5]. Recent development of soft ionization methods have enabled intact ions produced from large nonvolatile and fragile molecules [6]. Several major soft ionization methods discussed here are fast atom bombardment (FAB), matrix assisted laser desorption/ionization (MALDI), and electrospray ionization (ESI).

Electron ionization (EI)

The electron ionization, also known as the electron impact ionization, is usually used for the ionization of organic compounds. In EI, the sample molecules are first vaporized into the gas phase, where they collide with a beam of energetic electrons (~ 70 eV), which detach an electron from the analyte molecule to form a charged ion.

$$M + e^- \rightarrow M^{+\bullet} + 2e^- \qquad (1.1)$$

EI is limited to volatile samples and it also tends to fragment the molecular ions, because of the excess energy deposited during the EI process [7].

Chemical ionization (CI)

CI is an ionization process with less excess energy than the EI method. It involves multiple steps of ion-molecule interactions. The reagent gas molecules are first ionized by EI and further react with other neutral reagent gas molecules to produce reagent ions that can ionize analyte molecules [7, 8]. For example, if methane is used as a reagent gas, the analyte ions may be formed by the following process:

$$CH_4 + e^- \rightarrow CH_4^{\bullet +} + 2e^- \qquad (1.2)$$

$$CH_4^{\bullet +} + CH_4 \rightarrow CH_5^+ + CH_3^{\bullet} \qquad (1.3)$$

$$M + CH_5^+ \rightarrow CH_4 + MH^+ \qquad (1.4)$$

CI source usually generates simpler spectra than EI source, with less fragmentation of the molecular ions. It is particularly useful for providing the molecular weight information. However, CI also requires volatile and thermally stable samples.

Fast atom bombardment ionization (FAB)

The FAB ionization method was first devised in 1981 by Barber, et al. [9] In FAB, the impact of the high energy (kiloelectron volts) atom beam causes the analyte molecules to vaporize and ionize in a single step, before decomposition can occur [6]. The samples are usually dissolved in a drop of nonvolatile liquid matrix (glycerol, or thioglycerol, for example), which mediates the energy transfer to the analyte and reduces the amount of radiation damage to the analyte. Acids (e.g. trifluoroacetic acid, acetic acid, or HCl) can be added to the matrix to enhance the protonation efficiency. The fast neutral atoms employed include Ar and Xe. FAB is capable of producing intact ions from nonvolatile parent species, without the requirement of volatility, and minimizes

thermal decomposition during ionization [10]. The major drawback of FAB is the ion suppression effect, which may be influenced by the hydrophobicity of analytes and the contamination from the ionized matrix cluster. Although FAB is still used in the MS field, the more recently developed ESI and MALDI methods are far more superior and prevalently employed in modern mass spectrometry to explore sequence and structure information from biological and clinical samples.

Matrix assisted laser desorption/ionization (MALDI)

MALDI was first reported by Karas and Hillenkamp in 1987 [11]. MALDI is a pulsed ionization technique, which makes it particularly suitable for the time-of-flight mass analyzer [7]. In MALDI, analytes are first mixed with an excess of matrix molecules. The matrix has the abilities to isolate the analyte molecules; to absorb the laser energy via electronic [ultraviolet(UV)] or vibrational [infrared(IR)] excitation; and to vaporize the analytes into the gas phase and then ionize them [12, 13]. The matrix selection depends on both the type of the analyte and the laser wavelength used. The commonly used matrixes include 2,5-dihydroxybenzoic acid (DHB), α-cyano-4-hydroxycinnamic acid (CHCA), and sinapinic acid. The analyte/matrix mixture is allowed to dry on a steel target plate, which is then inserted into the vacuum of the mass spectrometer. Although the exact ionization mechanism of MALDI is still not well understood, it is proposed to be the result of following processes: the laser absorption and excitation of the matrix which facilitates the analyte vaporization to form a gaseous mixture of ionized matrix and neutral analyte followed by the ionization of neutral analytes via gas phase proton transfer.

MALDI generates singly charged molecular species, which simplifies the interpretation of the MALDI spectra. Other advantages of MALDI include easy sample preparation, good tolerance for salt adducts, and the increase of the mass range of proteins that can be measured. MALDI is widely used to measure synthetic polymers, as well as large, non-volatile biological compounds, such as proteins, oligonucleotides, and carbohydrates. Furthermore, MALDI is also well suited for imaging experiments.

Electrospray ionization (ESI)

ESI was first developed by John Fenn in 1989, whose contribution was recognized by the Nobel Prize in Chemistry in 2002 [5, 6, 14, 15]. In ESI, the samples are first dissolved in an easily evaporated solvent, such as a mixture of 50:50 methanol and water, with a small amount of acid (e.g. 1% formic acid) added to promote ionization. The solution then passes through a capillary tube, which is held at a high electrical potential (several kilovolts). The resulted strong electric field between the capillary and the counter electrode (e.g. orifice) induces the emerging surface of the analyte solution to form a Taylor cone and releases small droplets. As the evaporation of the solvent from the droplet is continuing, the radius of the droplet decreases and the charge density increases. When the radius of the droplet reaches the Rayleigh limit, the Coulombic repulsion exceeds the surface tension and leads to a “Coulombic explosion”, releasing smaller sized offspring ions. In addition, a countercurrent flow of dry curtain gas, normally nitrogen, or a heated capillary, can be applied to the interface to promote droplet evaporation, to sweep away the solvent molecules and other uncharged particles, and to ensure only ions can fly into the vacuum system [16]. A sheath gas is also used coaxially to reduce the radial dispersion of the spray [17]. The Coulombic fission keeps

on going, until finally, the unsolvated charged molecular ions are generated. In negative ESI, the polarities of the potentials applied in the positive mode are switched and a basic solvent is added instead to enhance the formation of negatively charged molecular ions.

Nanoelectropray ionization (nanoESI) was introduced by Wilm and Mann in 1994 [14, 18, 19]. In nanoESI, the glass capillary used typically has a very small tip with a diameter of 1-2 μm. Without the application of an external force, such as a solvent pump, the nanoESI has a very slow flow rate. Therefore, the sample consumption in nanoESI is much smaller than that in the conventional ESI source, which is especially useful for the analysis of biological samples often in limited amounts. Furthermore, the diameter of the droplets generated in nanoESI is less than 200 nm compared to the 1-2 μm diameter in conventional ESI, which greatly increases the desolvation and ionization efficiency.

Unlike MALDI, multiply charged molecular ions are commonly observed in ESI, which greatly extends the detection mass range of mass spectrometers. In ESI, the transition of the sample molecules to gas phase ions is not an energetic process, and the desolvation process effectively cools the ions [20, 21]. With the ability to ionize highly polar and involatile compounds, ESI has been widely used in many biological sample analyses, including peptides and proteins, carbohydrates, oligonucleotides, and other biomolecules. Finally, ESI is such a gentle ionization method that it can also be used to study noncovalent macromolecular complexes, such as protein interactions with cofactors, inhibitors, metal ions, or enzyme-substrate interaction [22].

1.2.2 Mass analyzers

After the analyte ions are generated in the ion source, they are directed into the mass analyzer region of the mass spectrometer usually by electric potentials. The mass analyzer is the most important part of the mass spectrometer which separates the analyte ions by their mass-to-charge ratios. There are many types of mass analyzers available, although each has its advantages and limitations. The operating principles of several commonly used mass spectrometers will be briefly discussed here.

The performance of a mass spectrometer can be described by a few important characteristic factors, including its mass accuracy, mass range, resolving power, and sensitivity. Mass accuracy is the accuracy of *m/z* value and is usually calculated by the difference between the experimental value and the theoretical value in part per million (ppm) units. Mass range is the range of *m/z* values which can be detected by the mass spectrometer.

Resolution or resolving power shows the ability of a mass spectrometer to distinguish two very close peaks in a mass spectrum. The resolving power (R) can be calculated as $R=m/\Delta m$, where m is the *m/z* value of the peak and Δm is its full width measured at half maximum (FWHM). Thus a higher resolution means a better ability to distinguish closely separated peaks.

The sensitivity of a mass spectrometer means the lowest amount of sample that can be analyzed, which is affected by transmission efficiency. Transmission efficiency measures the ratio of the actual number of ions reach the detector to the total number of ions generated in the ion source region.

Quadrupole mass analyzer

A quadrupole mass analyzer [7] contains four metal rods in parallel, with each opposing rod pair being electrically connected. A radio frequency (RF) voltage is applied between these two pairs of rods and a direct current (DC) voltage is also applied which superimposed on the RF voltage. This arrangement will generate an oscillating electric field within the four rods. The analyte ions are separated in the quadrupole mass analyzer based on their trajectory stabilities in this oscillating electric field. As the analyte ions fly along the z axis of the quadrupole, which is parallel to the quadrupole, the oscillating electric field will affect their stabilities on the x and y directions. The ion motion inside a quadrupole is governed by the Mathieu equations [7], and their trajectory stabilities are determined by the two characteristic values as described below:

$$a = \frac{8eU}{mr_0^2\omega^2} \qquad (1.5)$$

$$q = \frac{4eV}{mr_0^2\omega^2} \qquad (1.6)$$

where a and q are related to direct potential U and the magnitude of radio frequency V, respectively, ω is the angular frequency and r_0 is the half distance between the two opposing rods. For three different masses, the bounded solution to the Mathieu equations results in a stability diagram as shown in Figure 1.1 [7].

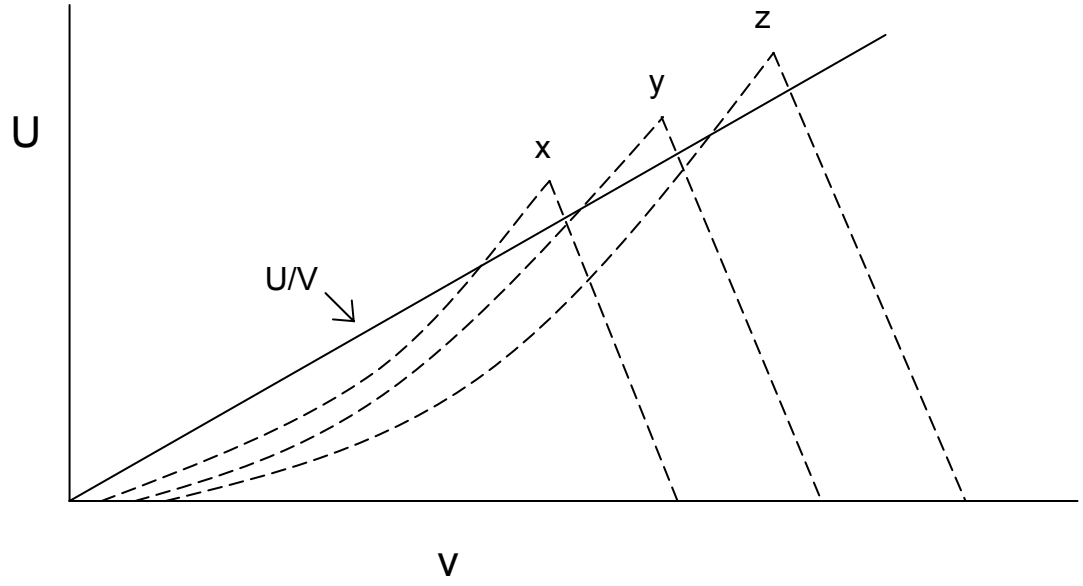

Figure 1. 1 Theoretical stability diagram of three *m/z* values.

Ions with different *m/z* values will have different stability areas. Specific U and V values will allow ions within a narrow *m/z* range to have stable trajectories and fly through the quadrupole to reach the detector; while ions with *m/z* values below or above this *m/z* range have unstable trajectories, and will strike the rods and become undetectable. This feature can be used in ion isolation.

When the U and V values are scanned along a constant U/V line, the quadrupole mass spectrometer detects the analyte ions successively. As shown in Figure 1.1, since the line only cross the vertices of the stable areas, only very small fraction of the analyte ions are actually detected in this process. By adjusting the U/V ratio, the resolution of the quadrupole can be varied.

When the DC potential U is turned off, the quadrupole becomes a RF only ion guide, which allows all the ions above a certain *m/z* value to pass through. The *m/z* cutoff depends on the amplitude and frequency of the RF applied.

Quadrupoles are easy to built, robust and of low cost, which makes them the most widely used mass analyzers. A quadrupole normally has an upper mass limit of *m/z* 4000, a mass resolution of 2000, with a typical mass accuracy about 100 ppm [7]. In addition to being used as stand-alone mass analyzers, quadrupoles are also used as ion guides, ion selectors, and ion storage devices in hybrid mass spectrometers.

Time-of-flight (TOF) mass analyzer

A time of flight mass analyzer [7, 23-26] separates the analyte ions by their flight time through a field free flight tube in vacuum between the ionization source and the mass detector. Ideally, all analyte ions should have the same initial kinetic energy (E) before entering the flight tube [26], which can be describe as:

$$E = \frac{1}{2}mv^2 = zeV \qquad (1.7)$$

where m and z are the mass and charge of the analyte ion, respectively. V is the accelerating potential and v is the velocity of the analyte ion as it exits the accelerating field. If the length of the flight tube is L, the flight time (t) of an ion can be calculated as:

$$t = L/V \qquad (1.8)$$

Combining equation 1.7 and equation 1.8, we have:

$$t^2 = \frac{m}{z}(L^2/2eV) \qquad (1.9)$$

It is clear from equation 1.9 that ions with different *m/z* values will take different times to reach the detector, thus they can be separated based on their *m/z* values.

In reality, analyte ions are not generated with the same initial velocity. The slight difference of the initial kinetic energy for the analyte ions with the same *m/z* will cause peak broadening and lower the mass resolution of the TOF mass analyzer. Several

methods have been developed to correct for the kinetic energy spread [7, 23, 26], including the time-lag-focusing (TLF) method, the retarding field, and the reflectron.

In TLF [26], also known as the delayed extraction (DE), the accelerating potential pulse is applied after a delay following the ion formation. This DE pulse compensates the slightly different kinetic energy of ions by accelerating the slower moving ions more, since they stay longer in the accelerating field, thus enabling them to catch up with the faster moving ions. For a given *m/z* value by carefully adjusting the delay and the accelerating potential, all ions can be focused at the detector at the same time.

The retarding field [23] is relatively easy to understand. In the retarding field, ions with higher initial kinetic energy travel through a larger radius and take more time to reach the detector than those with smaller kinetic energy. Eventually, ions with same *m/z* but different initial kinetic energy will strike the detector simultaneously.

The most commonly used method is the reflectron [7, 23, 26]. A reflectron is an ion mirror constructed at the end of the flight tube to reflect the analyte ions toward the detector thus effectively extends the length of the flight tube and increases the resolution of TOF analyzer. More importantly, ions with different kinetic energy penetrate the reflectron to different depths. Ions with higher kinetic energy will penetrate deeper and spend more time inside the reflectron, which compensates their shorter flight time outside of the reflectron. With judicious choice of the accelerating and reflectron voltages, ions with same *m/z* and different kinetic energies will strike the detector concurrently.

As a TOF analyzer works in the pulsed mode, it works well with a MALDI ionization source. Continuous ionization sources can also be coupled to TOF analyzers, although special gating methods are usually needed [23]. A TOF requires high vacuum

system to avoid frequent collisions between the analyte ions and the background gas molecules, which will significantly deteriorate its performance.

TOF analyzers have many advantages. They are very fast and can be easily adapted to the high performance liquid chromatography (HPLC) system for high throughput analysis. Since almost all the ions flying through the tube can be detected, TOFs have high sensitivities and require relatively small amount of samples. Theoretically, there is no limitation for its mass range, although the upper mass limit is often determined by post-source decay. With the implementation of various focusing schemes, modern TOF instruments can easily reach a resolving power of 20,000 and mass accuracy of <10 ppm [7].

Fourier transform ion cyclotron resonance (FT-ICR) mass analyzer

The FT-ICR MS was introduced in 1974 by Comisarow and Marshall [27, 28]. The FT-ICR MS determines the mass-to-charge ratio of the analyte ions by measuring their cyclotron frequency in a magnetic field [7, 26, 29-33]. Although there are several types of magnets available, the superconducting magnet is by far the best choice for FT-ICR MS. The major events of FT-ICR MS occur in an ICR cell, which is located in the homogeneous region of the magnetic field and functions to store, excite and detect the analyte ions. The principle of FT-ICR analysis is briefly described as follows [29, 30]: the trapped analyte ions are first excited by a resonant RF field applied to the excitation plates to a large cyclotron orbit. The coherent cyclotron motion of a given ion packet induces image currents on the detection plates, which are further amplified and digitized to generate the time domain transient. The transient can be Fourier transformed to

produce a frequency spectrum, which is then converted to the mass spectrum via proper mass calibration.

Ion cyclotron motion [7, 26, 30]. In a magnetic field B, a charged particle with mass m, charge q, and velocity v will experience the Lorentz force F and move along a circular trajectory with the radius r. According to Newton's second law of mechanics, the force can also be expressed as the product of mass and acceleration a. The following equation can be derived:

$$F = ma = \frac{mv^2}{r} = q(v \times B) \qquad (1.10)$$

Recall that the angular velocity ω of the charged particle is:

$$\omega = \frac{v}{r} \qquad (1.11)$$

Combine the above two equations and we have:

$$\omega = \frac{qB}{m} \qquad (1.12)$$

The cyclotron frequency f equals to $\omega/2\pi$, and can be calculated as:

$$f = \frac{qB}{2\pi m} \qquad (1.13)$$

Therefore, the cyclotron frequency of a charged particle in a constant magnetic field is inversely proportional to its mass-to-charge ratio, which is the basic principle used in FT-ICR MS.

In FT-ICR MS, the combination of the electric and magnetic fields will also induce magnetron motion of a charged particle [29]. Although the magnetron motion is not directly related to the mass-to-charge ratio of the analyte ions, its presence will affect the

mass analysis, and a proper calibration equation, other than equation 1.12 is required [34].

Ion cyclotron resonance cell [29, 30, 35]. There are many types of ICR cells. The cubic cell is the original type and is still used in FT-ICR MS today. It is a cubic chamber with six plates arranged in a cubic shape, as shown in Figure 1.2 [29]. For illustration purpose, we have placed it with its z axis along the magnetic field, and its y and x axes perpendicular to the magnetic field. The two plates perpendicular to the magnetic field are called end-caps, which function to trap the ions along the z axis. There are holes on the end-caps for the introduction of ions into the cell. The two pairs of opposing plates parallel to the magnetic field axis are excitation and detection plates, respectively.

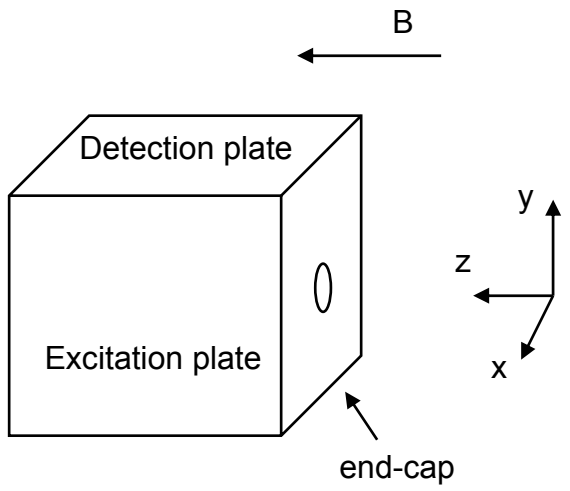

Figure 1. 2 Scheme represents the cubic cell.

The open-ended cylindrical cell is another commonly used ICR cell in FT-ICR MS [29]. The open-ended cylindrical cell consists of three cylinders, as shown in Figure 1.3. The center cylinder contains four plates: two function as excitation plates and the

remaining two are detection plates. The two cylinders at the end of the cell are trapping electrodes, to confine the ions along the magnetic field axis. The open ends allow easy access of the ions into the cell as well as passages of electrons and/or laser beams in tandem MS analysis. An important property of the open-ended cylindrical ICR cell is its ability to generate a uniform excitation electric field [35].

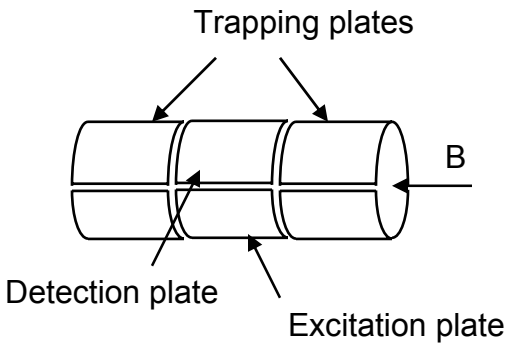

Figure 1. 3 Scheme represents the cylindrical cell.

The principles, geometry and electric configurations of many types of ICR ion traps were discussed in a review paper [35].

Ion excitation and detection in ICR cell. The ionization process can happen both inside and outside the ICR cell, as in internal and external ionizations, respectively [30]. Some ionization methods, such as EI and CI, can be used to generate ions in the ICR cell. More recently, the external ionization method has become the predominantly used one, especially electrospray ionization, because many biological samples are nonvolatile and the sample introduction needs to be accessed and operated in the high pressure region of the instrument. With external ionization, the ions need to be transferred into the

ICR cell through several stages of the instrument, with the pressure gradually decreasing in each stage, achieved by differential pumping.

Once inside the ICR cell, the ions are trapped axially by the end trapping plates and radially by the magnetic field, and they will have initial cyclotron motion under the influence of the magnetic field. However, the radius of the initial thermal cyclotron motion is too small to induce a detectable image current on the detection plates. Furthermore, the thermal cyclotron motion of the ions is incoherent and will generate zero net image current on the detection plates. This is because the ions with same cyclotron frequency but different phase may induce image current simultaneously on each of the detection plate to counteract each other and get no net current [30, 35].

A spatially uniform electric field E oscillating at the cyclotron frequency of a given *m/z* value can be applied to achieve the resonant excitation [30]. After excitation, all ions with the same *m/z* value will move coherently as a tight packet at a large cyclotron radius, which can induce an alternating image current on the two opposing detection plates. The post-excitation ion cyclotron radius r is described as [30, 32]:

$$r = \frac{ET_{excite}}{2B} \qquad (1.14)$$

where T_{excite} is the resonant excitation time and B is the magnetic field strength. In practice, a broadband excitation is usually used to achieve the simultaneous detection of all the ions in the ICR cell [29]. The broadband excitation is performed by applying a rapid frequency sweep or chirp over a wide range of frequency. Consequently the ions with its cyclotron frequency in this range will be excited and detected. It is important to note that the final cyclotron radius is independent of *m/z*. This is particularly desirable, as all ions will be excited to the same radius, regardless of *m/z*, provided that the excitation

field and time are constant throughout the *m/z* range. Ion packets with different *m/z* values will induce their own corresponding image currents, which can be detected and stored as a superimposed time-domain transient.

The ICR mass analyzer is characterized by the simultaneous detection with a wide *m/z* range. In addition, this detection is non-destructive by using the image current [29].

High vacuum and high magnetic field. The FT-ICR mass analyzer requires a high vacuum system, usually ~10^{-10} Torr [7]. This is essential for the ultra high mass resolution of the FT-ICR MS. If the pressure in the ICR cell is too high, collisions between ions and neutral gas molecules will destroy the coherent cyclotron motion of the ion packet and the time-domain transient will decay very fast. The resolution R of the FT-ICR MS can be calculated as [29]:

$$R \cong \frac{fT}{2} \qquad (1.15)$$

where f is the cyclotron frequency and T is the length of the transient. It is immediately evident from equation 1.15, that a reduced time-domain transient T will lead to lower resolution R. Therefore, the ultra high vacuum in the FT-ICR MS is usually maintained via differential pumping in several stages [26].

. It is also evident from equation 1.15 that the mass resolving power in FT-ICR MS increases linearly with the strength of the magnetic field, since cyclotron frequency f is proportional to magnetic field strength B [36]. In addition, many other performing characteristics of FT-ICR MS, including data acquisition speed, upper mass limit, mass accuracy, and dynamic range, will improve as the magnetic field strength increases. The

detailed discussion about the advantages of high magnetic field in FT-ICR MS has been reported [32, 36]. However, the high superconducting magnets are usually very expensive, which limits the broad application of the FT-ICR MS.

The FT-ICR MS can routinely achieve ultra high mass resolution of about 500,000 with typical mass accuracy <2 ppm [7]. Many tandem MS methods can be performed on FT-ICR MS, such as collision activated dissociation (CAD) [37], electron capture dissociation (ECD) [38], infrared multiphoton dissociation (IRMPD) [39]. Combining with online HPLC system further expands the capability of the FT-ICR MS to high throughput analysis. The FT-ICR MS is widely used in proteomics for performing both top-down and bottom-up analyses [33]. The high resolving power and mass accuracy of the FT-ICR MS make it particularly suited for the top-down analysis, where the intact proteins are measured in FT-ICR MS directly followed by tandem MS analysis.

1.2.3 Tandem mass spectrometry methods

Tandem mass spectrometry (MS/MS or MS^n) [7, 26, 40] can provide detailed structure and sequence information for biological samples by decomposing the molecular ions. In MS/MS, the precursor or parent ions are usually isolated in the first stage of the mass analyzer, followed by a dissociation process and the detection of the fragment or daughter ions in the second stage of the mass analyzer. The two stages of mass analyses can be arranged tandem in space, such as in a triple-quadrupole (QqQ), or in time, such as in an FT-ICR mass spectrometer. Several types of scan are used in MS/MS, including the product ion scan, the precursor ion scan, and the neutral loss scan, etc [7]. Most of the experiments involved in this thesis were performed in the product ion scan mode in FT-ICR mass spectrometers.

Many different dissociation methods can be used in MS/MS to generate different types of fragment ions. Based on the masses of the fragment ions, the detailed sequence information of the precursor ions can be deduced. Figure 1.4 shows the general types of fragment ions observed in MS/MS spectra of peptides and proteins, using the nomenclature proposed in 1984 by Roepstorff, et al. [41, 42] The nomenclature of the fragment ions of carbohydrate generated in the MS/MS analysis was proposed later in 1988 by Domon and Costello [43]. Peptide sequencing by tandem mass spectrometry is based on the knowledge of amino acid sequence deduced from the mass spectrum, with the mass of each amino acid corresponding to the mass difference between two adjacent fragment ions of the same type. For example, the mass difference between the y_n and y_{n+1} ions corresponds to the mass of an amino acid located in the n+1 position in the peptide.

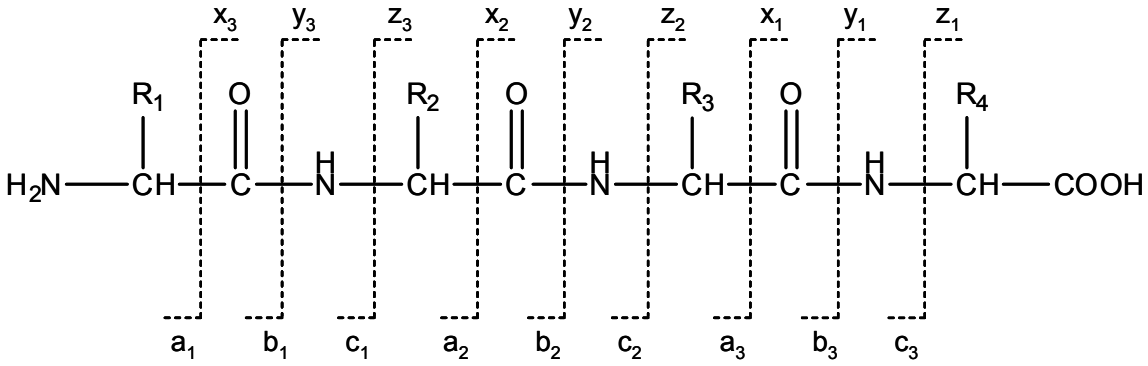

Figure 1. 4 Nomenclature of peptide N- and C-terminal sequence ions used in mass spectrometry.

Collisionally activated dissociation

CAD, also known as collision induced dissociation (CID) [7, 26, 37, 44] is the most routinely employed tandem mass spectrometry method. In CAD, the molecular ions collide with the neutral gas molecules, resulting in the energy conversion into the internal energy of the molecular ions. The commonly used neutral gases are helium, nitrogen, and argon. The excited molecular ions can then undergo framentation. Because the intermolecular vibrational energy redistribution (IVR) in the molecular ions occurs prior to the decomposition [45], the molecular ions usually dissociate by the breakage of the weakest bonds. In unmodified peptides, this typically occurs at the backbone amide bond, leading to the formation of b and y ions. The y ions represent the truncated peptides. The b ions can have acylium or oxazolone structures. Preferential cleavages at the N-terminal side of proline residue and at the C-terminal side of aspartic acid residue have been reported [45-47].

There are two categories of CAD: the high energy CAD and the low energy CAD [37, 44]. In high energy CAD, the molecular ions with the initial kinetic energy of several kiloelectron volts (keV) collide a few times (usually less than 5) with the gas molecules to induce fragmentation. It can be performed in the electromagnetic sectors or TOF-TOF instruments, with good reproducibility. In addition to b and y ions, the high energy CAD can also induce side chain cleavages to form d and w ions, which can be used to differentiate the isomeric amino acids. On the other hand, the presence of many d and w ions may also introduce complexity to the interpretation of the CAD spectra. The low energy CAD is usually performed in triple quadrupoles (QqQ), with q representing a RF only quadrupole as the collision cell, in quadrupole ion traps and in FT-ICR mass spectrometers (as in sustained off resonance irradiation, or SORI-CAD) [48]. In low energy CAD, the molecular ions with low kinetic energy, less than one hundred electron

volts (eV), are allowed to collide multiple times with the neutral gas molecules to obtain sufficient internal energy to induce fragmentations. The low energy CAD can also occur at the interface region of the ESI source, known as the in-source or nozzle/skimmer CAD [49], although without the isolation of precursor ions.

CAD is a powerful technique in proteomics, by providing extensive sequence or structure information of peptides and proteins. The oligosaccharide and lipid samples can also be analyzed by CAD. However, CAD also has some limitations, particularly in the PTM analysis. This is because the labile groups in PTMs can fall off easily in CAD, making the determination difficult. The PTMs, however, can be measured by other non-ergodic methods, which will be discussed later.

Electron capture dissociation

ECD is a relatively new tandem mass spectrometry method which was discovered by Roman Zubarev, in 1998 [38]. ECD is generally believed to be a non-ergodic process. In ECD, the multiply charged peptide ions interact with low energy electrons (~0.2 eV), inducing the nonselective homolytic cleavages of the backbone N-C_α bond and generating c and z• fragment ions, as shown in Figure 1.5. As an exception, the N-terminal side of proline residue is resistant to ECD cleavage. In addition to N-C_α bond cleavages, the disulfide bond cleavages are also favored in ECD [38, 50]. A minor fragmentation channel in ECD is the formation of a• and y ions [51].

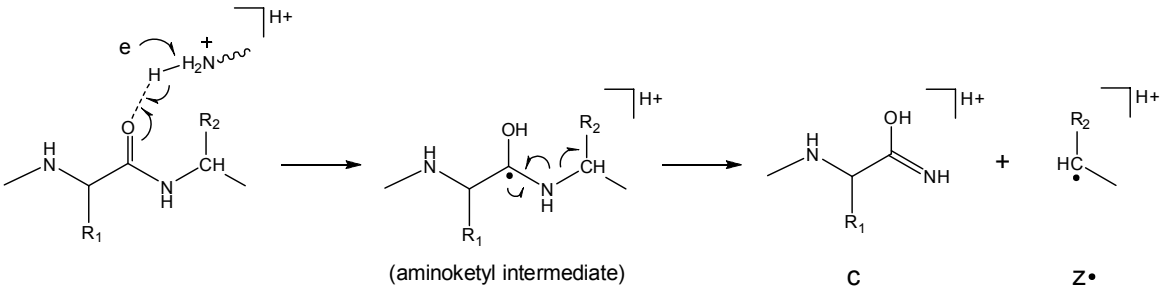

Figure 1. 5 Scheme of ECD process.

Several mechanisms have been proposed for ECD. In the dissociation-recombination mechanism [45], the electron capture happens at the charged groups of the peptide, followed by charge neutralization and repulsion of a hydrogen atom. This hydrogen atom can subsequently be captured at the carbonyl oxygen of an adjacent amide bond to form an intermediate aminoketyl radical, which dissociates by cleaving the N-C_α bond. However, it is also known that the capture cross sections of the hydrogen atom in the gas-phase peptide ions are low, making the dissociation-recombination rather unattractive. Later, an amide-superbase mechanism was proposed [52]. In this mechanism, the electron capture occurs at the amide bond oxygen, creating an anion radical, which can abstract a proton from a nearby group and form an aminoketyl radical to undergo N-C_α bond cleavage.

Secondary fragmentation and amino acid side chain loss in ECD. After the generation of the c and z• fragments, the α-carbon radical located at the N-terminus of the z• fragment can migrate and induce secondary fragmentations, involving the partial or entire side chain loss of amino acids in conventional ECD [53, 54]. The presence of

the partial or entire amino acid side chain losses can be used to infer the existence of certain amino acid residues, which will help the protein identification. In addition, some w ions can be used to distinguish isomeric amino acids, such as Ile and Leu [55]. On the other hand, the secondary fragmentation will also complicate the interpretation of ECD spectra, especially when using the database search.

Free radical cascade mechanism in ECD. In addition to linear peptides, ECD has also been performed on doubly charged cyclic peptides [56]. In that study, many peaks corresponding to losses of one or several amino acid residues were observed, which required the cleavage of multiple backbone bonds. Since the capture of two electrons by a doubly charged precursor ion would lead to complete neutralization of the precursor and render all products undetectable, the presence of these fragment ions indicated that a single electron capture can result in multiple backbone cleavages. A free radical cascade (FRC) mechanism was proposed, which suggested that the initial α-carbon radical formed can propagate to induce secondary fragmentations along the peptide backbone or on various side chain groups.

Biological applications of ECD. There are two major applications of ECD in proteomics: characterization of the post-translational modifications and top-down analysis [57, 58]. ECD is very suitable for the PTM studies, because of its preference to cleave backbone bonds while leaving the labile PTM groups intact [59]. Many kinds of PTMs have been identified in proteins by ECD, including glycosylation, phosphorylation, sulfation, methionine oxidation, and acylation, etc. Deamidation as one kind of PTMs has also been studied by ECD, which will be discussed in detail in the following chapters.

Characterization of PTMs by ECD is very different from slow-heating methods [57], such as CAD, which usually follow the lowest energy pathways. Consequently, in CAD, the labile PTMs could easily fall off, with the loss of PTM information.

ECD can non-selectively cleave the backbone bonds of peptides and proteins, providing extensive sequence information, which is particularly beneficial in top-down analysis. However, in top-down analysis of large proteins by ECD, the non-covalent interactions between large fragments may hold them together and hinder the separation and detection of each fragment. Several methods have been employed to mitigate this problem. Plasma ECD was used to increase the performance of conventional ECD by introducing pulsed gas during electron injection, as the analyte ions were introduced into the ICR cell [60]. Ion activation can also be used to disrupt the noncovalent interactions to promote fragment ion separation, as employed in activated ion ECD (AI-ECD) [61]. The commonly used activation methods include the collisional activation, and infrared irradiation.

ECD can also be used in bottom-up analysis, de novo sequencing, and protein folding studies. Finally, ECD has also found wide applications in the analysis of other biomolecules, such as oligonucleotides and carbohydrates.

EXD methods related to ECD

Hot ECD (HECD) [62, 63]. In conventional ECD, the most efficient fragmentations were usually induced by low energy electrons (~0.2 eV). As the electron energy increases, the fragmentation efficiency decreases initially, and then increases again to a second maximum at ~10 eV electron energy. This hot (3-13 eV) ECD can also generate c and z• fragment ions, similar to conventional ECD. Although the electron

capture efficiency in HECD is two orders of magnitude smaller than that in the conventional ECD, the larger electron current produced by the indirectly-heated cathode partially compensates leading to a similar overall fragmentation efficiency [45]. An important feature of HECD is its tendency to induce secondary fragmentation of z• and a• ions, because of the excess of energy. The resulting w and d ions can be used to differentiate the isomeric leucine (Leu) and isoleucine (Ile) residues.

Electron transfer dissociation (ETD). ETD was first introduced in 2004 by Syka, et al. [64] Contrast to the limitation of ECD to FT instrument, this technique can be performed in relatively inexpensive and rf-field trapping instruments, such as quadrupole linear ion trap (QLT). In ETD, singly charged anions interact with multiply protonated peptides/proteins, generating c and z• ions. In the original design, the ESI source and CI source were located at the two ends of the QLT instrument. A mixture of anthracene $C_{14}H_{10}$ and CI reagent gas, methane, were used to generate anthracene radicals, which can interact with multiply charged proteins to induce homolytic backbone cleavage. Other commonly used anion reagents include fluoranthene and azulene. In a similar way, the interaction between radical cations and multiply deprotonated peptide anions can also induce peptide backbone cleavage, as employed in negative ETD (nETD) [65]. Like ECD, ETD also has the ability to detect the labile PTMs of peptides and proteins [66]. The cleavage efficiency of ETD decreases as the charge state of the precursor ions decreases. A supplemental collisional activation method (ETcaD) that activated the charge reduced precursor ions after the electron transfer and before the backbone dissociation, can be applied to increase the cleavage efficiency in ETD, especially for doubly charged precursor ions [67].

Electron-induced dissociation (EID), or electron-impact excitation of ion from organics (EIEIO) [68]. In EID, the multiply or singly charged precursor ions interact with 6-20 eV electrons, which are energetic enough to induce electronic excitation of the precursor ions to generate fragments [69, 70]. Without the requirement of multiply charged precursor ions as in ECD studies, EID has a major application area in the analysis of singly charged precursor ions, which are readily generated in MALDI sources [71].

Electron detachment dissociation (EDD). EDD was first discovered by Zubarev and co-workers in 2001 [72]. In EDD, instead of the multiply charged precursor cations, the multiply deprotonated precursor anions interact with high energy electrons (>10 eV), resulting in the electron ejection/detachment from the precursor ions and the formation of the nitrogen centered radical anions, which can undergo the C_{α}-C bond cleavages and side chain losses [73]. The efficiency of EDD can be improved by increasing the charge state of the precursor ions, and by adjusting the voltages on the cathode and the extraction lens [74]. EDD is useful for the analysis of peptides/proteins containing large amount of acidic residues, e.g. Asp, Glu.

Electron excitation dissociation (EED). EED contains two steps: ionization and electron capture [75]. In the first step, the protonated polypeptides interact with electrons with energy >10 eV, which induces the ionization of precursor ions and the ejection of slow electrons. In the second step, the slow electrons are reflected back and captured by the ionized precursor radical ions, resulting in fragmentation. Because the ionization

process in EED can increase the charge state of precursor ions, it is amenable in the analysis of singly charged ions generated from MALDI ion sources [76].

1.2.4 ESI qQq-FT ICR mass spectrometer

Most of the experiments in this thesis were performed on a custom-built, hybrid 7 Tesla ESI qQq-FT ICR mass spectrometer [77, 78]. The configuration of this instrument is shown in Figure 1.6. This instrument consists of two regions: a front end qQq region modified from an AB/MDS Sciex API 365 instrument and an FT ICR mass analyzer modified from an IonSpec FT-ICR MS with interface built by our lab. The front end is controlled by the Sciex LC2Tune 1.5 software and the FT ICR MS part is controlled by the IonSpec99 software. The 7 Tesla actively shielded magnet was manufactured by Cryomagnetics Inc., Oak Ridge, TN. This FT instrument is equipped with an external electrospray ionization source in the atmosphere. After the ionization process, the ions are transmitted through the ion path into the ICR cell by both a potential gradient and multipole ion guides along the instrument.

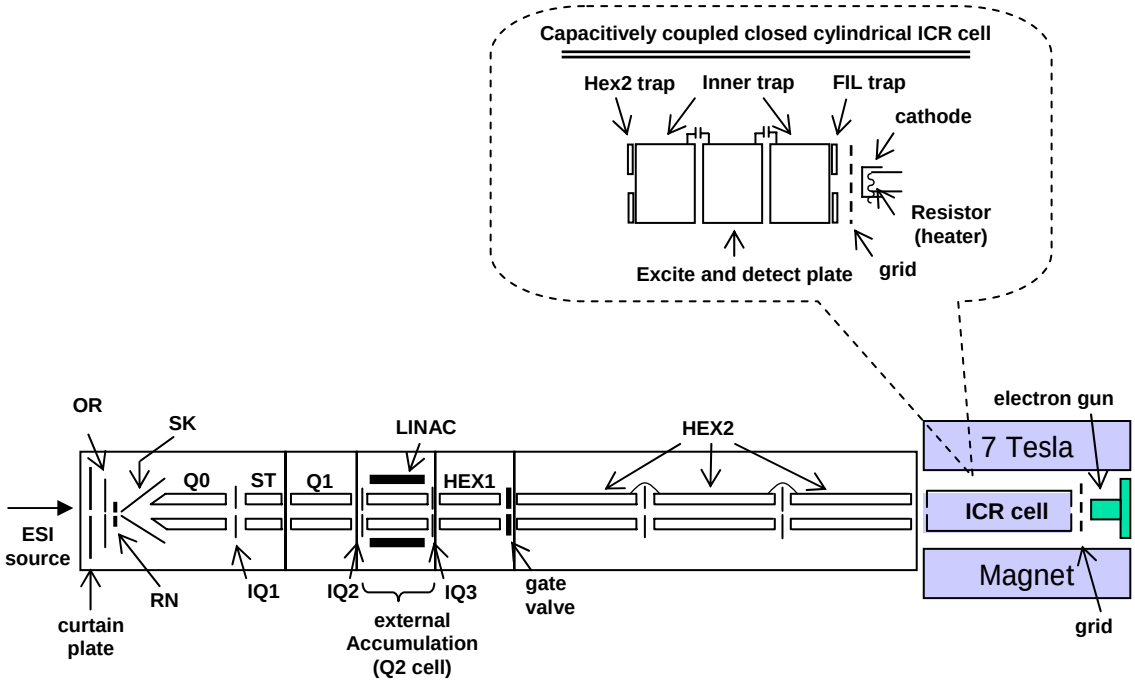

Figure 1. 6 Scheme of 7 Tesla ESI qQq-FT ICR mass spectrometer. FIL trap is filament trapping.

A typical ECD experiment is as follows [77]: The normal electrospary is performed at 1100-1200 V with a steady spray current of 10^{-7}-10^{-6} A. The ions are desolvated in the high pressure region between the curtain plate and the orifice (OR) and then focused at the ring electrode (RNG). After they pass through the skimmer (SK), they are focused again in the first quadrupole Q0. The IQ1, IQ2, and IQ3 are ion lenses for both focusing and gating. The stubby quadrupole (ST) is used to improve ion transmission. Ions of interest can be isolated by quadrupole Q1 and trapped in quadrupole Q2 for external ion accumulation. The normal accumulation time is about 300-1000ms. Q2 can also function as a collision cell, where collisionally activated dissociation can be performed. After sufficient ions are accumulated in Q2 or the

products are generated by CAD in Q2, these ions can be guided and transmitted through transfer hexapoles 1 and 2 (HEX1 and HEX2) into the ICR cell. The LINAC is used to help reduce the TOF spread during ion extraction. A gated valve located between HEX1 and HEX2 physically separates the instrument into low and high vacuum regions allowing for easy maintenance.

The potential on the Hex2 trapping plate (Hex2 trap) located between HEX2 and the ICR cell is first dropped to a negative value to allow ions fly into the cell. Once inside the ICR cell, the Hex2 trapping voltage is increased to help trap these ions. This is known as gated trapping. The capacitively coupled closed cylindrical ICR cell has been discussed previously. Briefly, it contains two inner traps and one middle section, which contains two excitation plates and two detection plates. The indirectly heated cathode dispenser, or the electron gun located on the other side of the ICR cell can generate thermal electrons for ECD experiments. The electron gun has a BaO coated surface which can generate electrons, when the resistor inside the cathode is heated. This resistor typically operates with a heating current of 1.6-1.8 A. The surface voltage of the electron gun is normally kept at +9.9 V to confine the electrons. During the ECD event, this voltage drops to a negative value (-0.2 V to -1.5 V) to repel the electrons from the surface. The length of the electron irradiation time is typically around 30-100 ms. The grid located between the ICR cell and the electron gun is kept at a constant positive voltage of +10 V to help extract the electrons into the ICR cell. Trapped ions interact with electrons in the center of the ICR cell to produce ECD fragments. A typical spectrum is obtained by averaging multiple scans, usually between 20 to 200 scans, to improve the signal-to-noise ratio.

This custom-built FT instrument needs fine tuning of many parameters to achieve optimal performance. An example of an ECD experimental setup is shown in Figure 1.7. The cathode surface voltage is provided by Blade off. Although the tuning process is complex, this hybrid FT instrument has the ability to perform many kinds of tandem MS experiments, including Q2 CAD, SORI CAD, ECD, EDD, and IRMPD. It has been extensively used in the characterization of peptides, proteins, and carbohydrates, providing high broadband mass resolving power (>100,000) and high mass accuracy (~2-5 ppm).

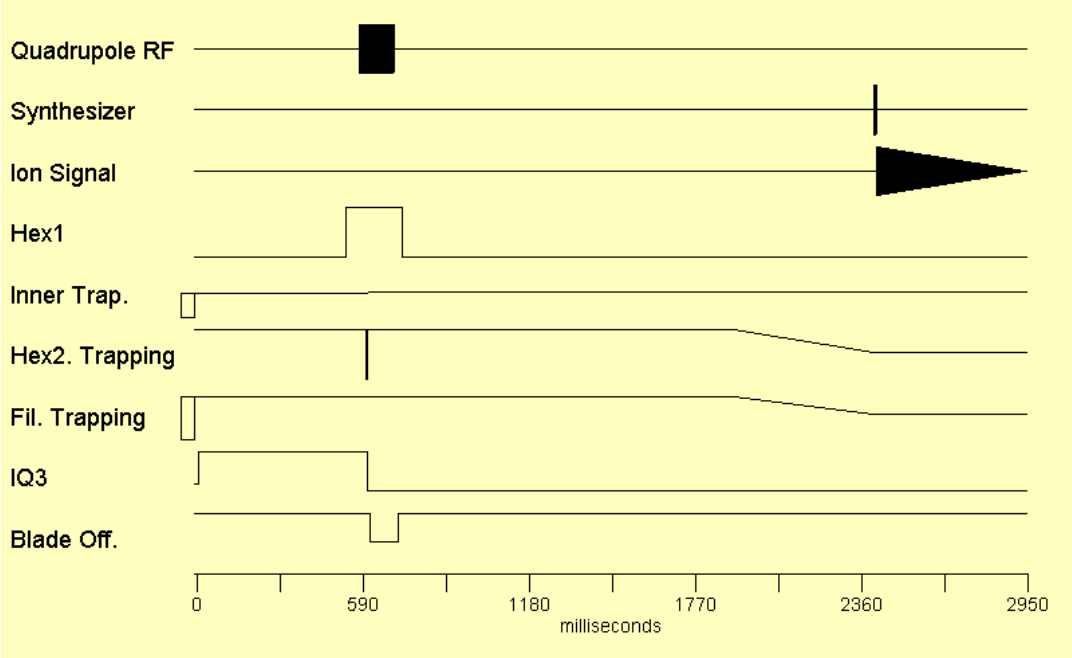

Figure 1. 7 Pulse sequences used in a typical ECD experiment.

1.2.5 12 Tesla solariX FT ICR mass spectrometer

Another instrument used in this thesis is a commercial 12 Tesla solariX hybrid Qq-FT MS instrument from Bruker Daltonics, Billerica, MA. The schematic of this 12 Tesla solariX FT instrument is shown in Figure 1.8 (Courtesy of Bruker Daltonics). This

instrument can provide extremely high mass resolving power (>1,000,000) and mass accuracy (~0.5 ppm). Most of the experiments in this thesis were performed by using the external ESI source in positive mode. After the ions are desolvated by the heated glass capillary, they are delivered through ion funnel and skimmer region. Ions are focused and pre-accumulated in the source octopoles, isolated by the quadrupole if needed, before entering the hexapole collision cell, where CAD can be performed. ETD may also be performed in the collision cell, with radical anions generated by an nCI source mounted off-axis above the split octapole. Ions can be externally accumulated in the collision hexapole and fly through the transfer hexpoles to enter the ICR cell, where ECD and IRMPD can be performed. The hollow electron gun is located on the other side of the ICR cell, with an extraction lens located between the ICR cell and the electron gun. The hollow electron gun design allows the on-axis introduction of an IR laser beam and performance of IRMPD and AI-ECD experiments.

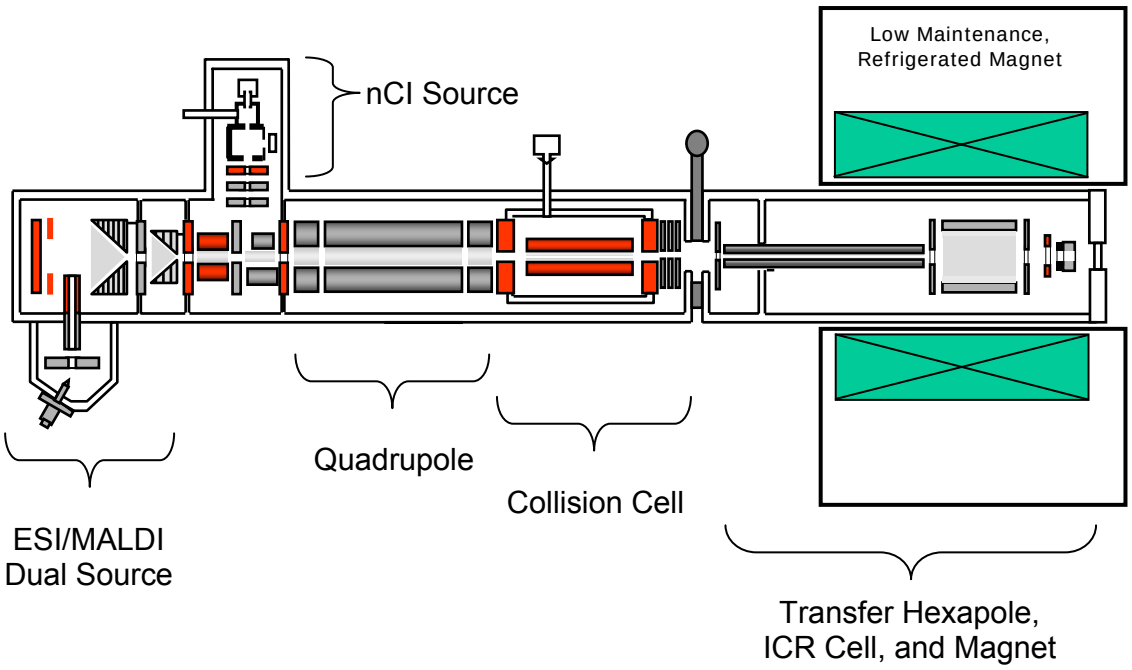

Figure 1. 8 Schematic of 12 Tesla solariX FT mass spectrometer (Bruker Daltonics).

1.3 Introduction to protein deamidation and related diseases

1.3.1 Protein deamidation

Deamidation is an important PTM in peptides and proteins [79]. Of the total 20 amino acids, only Asn and Gln are relatively unstable and undergo spontaneous deamidation under physiological conditions. The product of deamidation is the replacement of the side chain amino group of Asn/Gln by a hydroxyl group, resulting in an increase of mass by +0.984 Da and an introduction of a negative charge to the peptide or protein. As a result, the protein confirmation will change significantly, which will further influence their stabilities and biological activities.

Deamidation can happen both in vitro and in vivo. Deamidation is usually a non-enzymatic process, whose products accrue with the increase of age. The enzymatic deamidation is only reported for Gln resiudes [79]. The enzymes include transglutaminase, and glutaminases, etc. Transglutaminase can catalyze both the Gln-Lys linkage formation and the Gln deamidation, while glutaminase only promote the Gln deamidation.

Figure 1.9 illustrates the Asn (top) and Gln (bottom) deamidation processes in neutral or basic solutions, respectively [79, 80]. At pH>7, Asn and Gln deamidation processes involve the formation of succinimide and glutarimide intermediate, respectively, followed by hydrolysis process. The water molecule can attack either carbonyl group in the cyclic intermediates, generating a mixture of Asp/isoAsp or Glu/isoGlu. In acidic solutions, deamidation occurs via direct hydrolysis and only Asp or

Glu are produced. In general, the deamidation rate of Asn is much faster than that of Gln. The only exception is that when Gln is located at the N-terminus of the peptide, which deamidates faster than Asn.

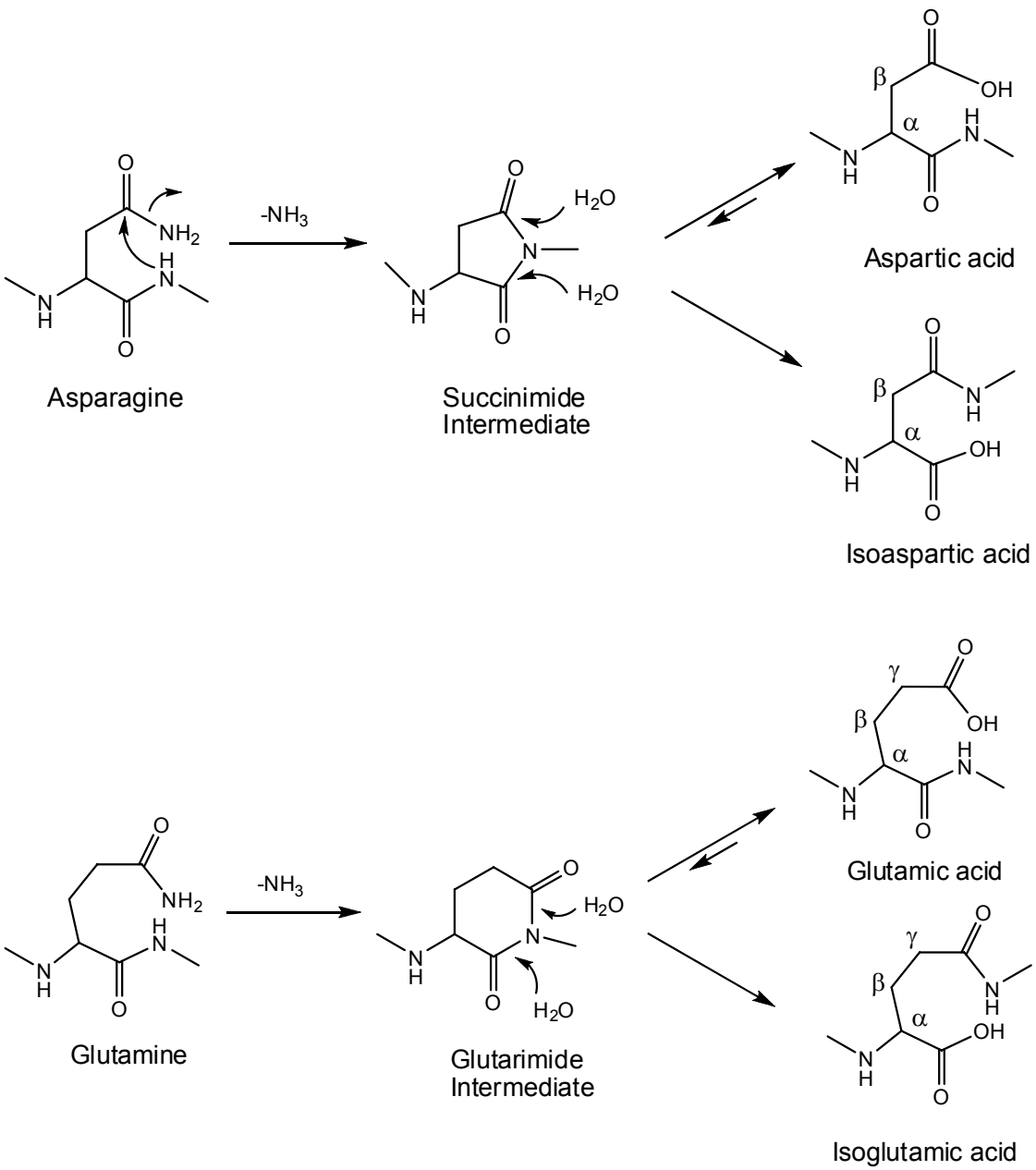

Figure 1. 9 Asn and Gln deamidation process.

There are many factors influencing Asn and Gln deamidation rates, among which the primary sequence is the most important one. It was found that in proteins, Asn deamidation depends 60% on primary structure and 40% on three dimensional structure [81]. For example the -NG- sequence has the fastest deamidation rate [79, 82]. The amino acid residue located C-terminal to Asn influences the deamidation rate a lot more than that located N-terminal to Asn. Due to the limited number of Gln deamidation studies, the influence of the neighboring amino acids on Gln deamidation rate is not clear. The protein secondary structures, α-helix and β-sheet, were found to stabilize protein structures and hinder the Asn deamidation [83]. Tertiary structure is believed to be a principal determinant of protein deamidation, which usually leads to a slower deamidation rate [82]. It was also reported that in vivo, the Gln deamidation rate in peptides was five fold faster than in proteins, while Asn was four fold quicker [84].

Deamidation can be both acid and base catalyzed, and its rate reaches a minimum in the pH range between 4 to 6 [79, 85]. Deamidation rate also increases with increasing temperature [79, 86, 87]. In many in vitro experiments, high pH and high temperature conditions are used to accelerate the deamidation process. Buffers and ionic strength can also influence the deamidation rate, especially the phosphate buffer [79, 88]. The common buffer system used in this thesis is the ammonium bicarbonate buffer.

1.3.2 Isomerization and racemization of asparatic acid

Both isomerization and racemization processes of Asp are non-enzymatic modifications [89]. Asp isomerization rate is much slower than Asn deamidation, and has

a similar mechanism to that of Asn deamidation (Figure 1.9), which proceeds through the succinimide intermediate to generate isoAsp residues [79, 90]. It was reported that isomerization of Asp in some tetrapeptides was reversible [91]. The Asp isomerization rate can also be influenced by pH, temperature, and other solvent conditions. A detailed comparison between the influence of these factors on Asn deamidation and Asp isomerization can be found in a review paper [90].

Amino acid racemization is the process that converts the normal L-amino acids to D-amino acids. Racemization can occur to most amino acids, among which Asp shows the fastest racemization rate. Asp racemization usually happens together with Asn deamidation, resulting a mixture of L-Asp, D-Asp, L-isoAsp, and D-isoAsp products [79, 92].

1.3.3 Protein L-isoaspartyl O-methyltransferase

Protein L-isoaspartyl O-methyltransferase (PIMT, EC 2.1.1.77) functions as an important repair enzyme to reduce the accumulation of damaged proteins in biological systems, both in vitro and in vivo [93]. PIMTs are ubiquious and highly conserved enzymes, which are found in bacteria, plants, animals, and humans. Most of PIMTs are cytosolic enzymes [94]. The first reported crystal structure of a PIMT from *Thermotoga maritima* contained three subdomains: N-terminal helical subdomain, central subdomain, and unique C-terminal subdomain [95]. The crystal structure of human PIMT enzyme also had a central $\alpha/\beta/\alpha$ sandwich structure [96]. PIMTs catalyze the transfer of a methyl group from S-adenosylmethionine (AdoMet) to the a-carboxyl group of L-isoAsp, with S-adenosyl-L-homocysteine (AdoHcy) as a by-product. The resulting methyl ester can spontaneously hydrolyze and form a cyclic succinimide intermediate, which then

hydrolyze to generate an Asp and isoAsp mixture, in a similar manner to the deamidation process [97, 98]. Since PIMTs only target isoAsp residues, after many cycles, the isoAsp content will be significantly reduced. In the PIMT knock-out mice, the accumulation of L-isoAsp was detected in many tissues, especially in the brain, and the mice showed enlargement of brains, growth retardation, a fatal seizure disorder, and fatal progressive epilepsy phenotypes [99, 100]. On the contrary, the overexpression of PIMT extended the lifespan of *Drosophila* [101]. These and many other studies indicated the biological importance of PIMT enzymes in biological systems.

A simple scheme showing the relationship among deamidation, isomerization, and PIMT enzymes is shown in Figure 1.10.

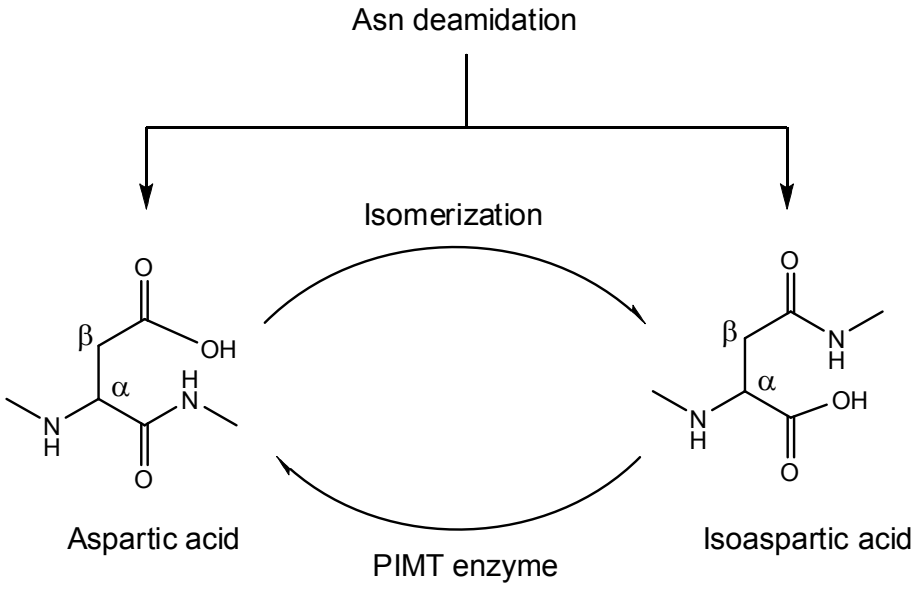

Figure 1. 10 Scheme presents the relation among deamidation, isomerization, and the repairment by PIMT enzyme.

1.3.4 Deamidation related diseases

Deamidation and Aging [79]. Aging is a complex process, with the accumulation of altered cellular proteins as one of its most important features. There are many kinds of modifications involved in aging process, such as oxidation, glycation, glycoxidation, deamidation, ubiquitination, and lipid peroxidation, etc. [102, 103] Although the exact mechanism of aging in unclear, there are many aging hypotheses, such as the oxidative stress hypothesis, and the free radical hypothesis [104-106]. Because deamidation happened in a variety of proteins in biological organisms and the deamidation extent is associated with age, a deamidation based molecular clock hypothesis in regulation of aging was proposed by Robinson and co-workers in 1970 [107].

Deamidation and Cancer. It was demonstrated that Bcl-x_L deamidation was a critical switch in the selective tumor cell death induced by DNA damaging agents [108, 109]. The Bcl-x_L deamidation is normally suppressed by retinoblastoma protein (RB) via an unclear mechanism. It is known that RB is an important tumor suppressor. RB represses transcription by forming complexes with the E2F transcription factors, which then recruit histone deacetylases (HDACS) and other factors to block the promoters and inhibit gene expression [110-112]. Rb itself is regulated by cyclin-dependent kinase (CDK), with a phosphorylated inactive form and a dephosphorylated active form. Rb is lacking in most tumor cells, which releases the inhibition of Bcl-x_L deamidation. Bcl-x_L is an anti-apoptotic protein, which when activated, can inhibit the BAX and BAK mediated mitochondrial apoptosis. The deamidation at Asn_{52}, Asn_{66} sites in a flex region of Bcl-x_L was reported to induce the inactivation of Bcl-x_L. Thus, tumor cells died, while normal cells survived [108, 113-115].

Deamidation and Alzheimer's Disease. Alzheimer's disease is one kind of neurodegenerative diseases. Although the exact molecular mechanism of Alzheimer's disease is still unknown, many studies suggested that amyloid β peptide (Aβ) played an important role in Alzheimer's disease, by forming the amyloid fibril deposition. The Aβ peptides, ~4 KDa, are derived from the amyloid precursor proteins (APP). There are three major Aβ peptides with different length: $A\beta_{1-38}$, $A\beta_{1-40}$, and $A\beta_{1-42}$ [116, 117]. During aging, many post-translational modifications occur in Aβ peptides, such as glycation, sulfation, and phosphorylation. High levels of isomerization and racemization products of Asp residue at positions 1, 7, and 23 were detected from the brains of patients with Alzheimer's disease. It was suggested that the isomerization might change the solubility, the conformation, and even the function of Aβ peptides [118, 119].

Deamidation and crystallin proteins. Many deamidations have been found in aged or diseased lens crystallin proteins, especially Gln deamidation. It was suggested that deamidation could reduce crystallin solubility, change lens transparency and induce cataract formation [120]. Three major classes of crystallins are: alpha (α), beta (β), and gamma (γ). Alpha crystallins consist of up to three types of monomers: αA, αB, and αA insert, and are typically present as oligomers and function as chaperons [121]. The first deamidation study of αA crystallin protein was reported in 1975 [122]. Deamidation sites of αA crystallin have been found at N101, Q6, Q50, Q90, Q140, and Q147 [121, 123-125]. Beta and gamma crystallins have similar structures, containing two domains, each of which is made up of two Greek key motifs connected by a short peptide. Beta crystallin proteins consist of three basic (B1-B3) and four acidic (A1-A4) β crystallin

proteins, which can assemble into homo- or hetero-dimers. The water soluble βB2 is the main β crystallin [121]. Deamidation sites of βB2 crystallin were found at N15, Q5, Q7, Q12, Q70, Q162, Q182, and Q184 [120, 126-128]. Gamma crystallins generally do not associate. The seven γ crystallin proteins are γ(A-F) and γS. Gamma (A-F) crystallins are water insoluble and lens only. Gamma S crystallin is water soluble and present in numerous tissues outside the lens as well [121]. Deamidation sites of γS crystallin were found at N14, N37, N53, N76, N143, Q16, Q63, Q70, Q92, Q106, Q120, Q148, and Q170 [121, 125, 129, 130].

Deamidation and Celiac disease. Celiac disease is a life-long autoimmune disease of small intestine. The dietary gluten after ingestion was digested into small peptides, including a 33-mer Pro and Gln rich peptide. When this 33-mer peptide was deamidated by tissue transglutaminase at the Gln site(s), it became an antigenic epitope recognized by CD4+ T cells, resulting in immunological reaction [131-133]. Currently gluten-free diet is the only solution to this disease. Gln deamidation is also involved in many bacterial toxins, such as cytotoxic necrotizing factors (CNFs) [134].

Deamidation and the Stability of Protein Drugs. Due to the fast deamidation rate in peptides and proteins containing the -NG- sequence, many protein drugs are facing the deamidation, oxidation, and aggregation problems in purification and storage processes [135, 136].

1.4 Overview of this thesis

This thesis focuses on the mechanism of electron capture dissociation and its application to protein deamidation studies, involving both Asn deamidation and Gln deamidation. The ECD mechanism research includes: Chapter 2, the effect of fixed charge modifications on ECD; Chapter 3, charge remote fragmentation in ECD and ETD; and Chapter 4, cyclic rotational heterogeneity of b ions probed by ECD. The protein deamidation studies include: Chapter 5, use of ^{18}O labels to monitor deamidation during protein and peptide sample processing; and Chapter 6, glutamine deamidation: differentiation of glutamic acid and γ-glutamic acid in peptides by ECD. Chapter 7 is the conclusion and future work. This thesis demonstrates the utility of ECD as a powerful method for protein deamidation studies.

Chapter 2

The Effect of Fixed Charge Modifications on ECD

2.1 Introduction

2.1.1 ECD and primary mechanisms

Different from many slow heating fragmentation methods such as infrared multiphoton dissociation (IRMPD) [39] and CAD [48], where IVR precedes fragmentation, ECD [38] of multiply charged peptide/protein ions is often considered as a "directed" tandem MS/MS method since it non-specifically cleaves many backbone bonds while frequently leaving the more labile side chain groups [57, 137-140] and non-covalent interactions [61, 141-144] intact. Because of these unique properties, it has significant applications in both top-down and bottom-up sequencings for protein identification [38, 57, 145-147], as well as in PTM characterizations [45, 137, 148]. The ECD process is the dissociative recombination of multiply charged molecular ions with low energy electrons (<0.2 eV) [38, 45, 52]. The major ECD products are often the charge reduced species, $[M+nH]^{(n-1)+\bullet}$, and the H• loss product, $[M+(n-1)H]^{(n-1)+}$ [149]. There are generally two backbone fragmentation pathways: the major one produces c and z• (or c• and z) ions via N-C_α bond cleavage and the minor pathway generates a• and y ions [38, 45, 52]. In addition, ECD may also produce some amino acid side-chain cleavages [53, 55, 150] and secondary fragment ions [54, 56, 62].

---

[1]This chapter has been partially/entirely reproduced from
Xiaojuan Li, Jason J. Cournoyer, Cheng Lin, and Peter B. O'Connor. The effect of fixed charge modifications on electron capture dissociation. *Journal of the American Society for Mass Spectrometry.* 2008, 19, 1514-1526. Copyright 2010 Elsevier.

Two primary mechanisms have been proposed to explain the abundant c and z• type ions observed in ECD spectra of peptides. In the dissociation-recapture mechanism, the initially captured electron in a high-lying Rydberg state may land in one of the protonated sites and the resultant H• from the dissociation of the neutralized ammonium group (or other charged groups) can be recaptured by a nearby carbonyl oxygen atom, yielding an aminoketyl intermediate that dissociates via the N-C_α bond cleavage [45]. Since the cross section for gas phase peptide ions to capture a free hydrogen atom is low [52, 151], it is unlikely that the abundant backbone cleavages were induced by the mobile hot hydrogen from the neutralization of a charged amino or guanidine group. Such cleavages were probably initiated by a concerted dissociation-recapture process upon electron capture due to the extensive solvations of the charged sites by multiple backbone carbonyls, which may also be followed by secondary fragmentations [56]. The low selectivity in backbone cleavages and retention of labile groups during ECD were attributed to the non-ergodic nature of this process, i.e. the N-C_α bond cleavage occurs before the ~6 eV recombination energy was randomized among the 3N-6 normal vibrational modes in the peptide molecule via intramolecular vibrational energy redistribution (IVR), which would result in milli-eV's of energy per mode, clearly far below the normal adiabatic bond dissociation thresholds [38, 45]. The non-ergodic premise has been scrutinized heavily as of late [52, 152], and the necessity of the presence of a hydrogen atom to initiate N-C_α bond cleavages was also under debate [140, 153]. In the recently proposed amide-superbase mechanism, it was argued that the electron is first captured in the remote-charge (Coulomb) stabilized π^* orbital of a backbone carbonyl, generating an aminoketyl anion radical (a super base) which abstracts a nearby proton,

and the resultant aminoketyl radical undergoes facile cleavage of the adjacent N-C_α bond with a very low (or nonexistent) energy barrier, thus eliminating the need to evoke non-ergodic hypothesis, as well as the necessity of the presence of a hydrogen atom [52, 154]. Furthermore, many H• abstraction reactions in peptides, in addition to having low activation barriers, also are net exothermic reaction, as the radical moves to a more stable site. It was further suggested that both mechanisms might be at work depending on the electronic states of the peptide ions [52, 155].

2.1.2 ECD and secondary mechanism: free radical cascade (FRC)

However, either of these above two mechanisms addresses only the formation of the c and z• type ions, but does not explain the many other types of fragment ions also present in the ECD spectra. In particular, in the ECD spectra of doubly charged cyclic peptide ions, many backbone fragment ions were observed, which requires multiple backbone cleavages induced by a single electron capture. It was proposed that these ions resulted from the FRC, i.e., the radical site on the initially produced z• ion could propagate along the peptide backbone or side chain to initiate secondary fragmentations via hydrogen abstraction and/or loss of neutrals such as diketopiperazines [56]. For linear peptides, hydrogen atom migrations within the post-ECD complex are also frequently observed. In an ECD study of peptides with all glycine alpha hydrogens replaced by deuterons, many fragment ions showed extensive H/D scramblings [156]. Moreover, c• and z ion formations are common in peptide ion ECD spectra [157], which has been demonstrated to be the result of the intra-complex hydrogen transfer between the originally formed c/z• ion pair [144, 157, 158]. A double resonance (DR)-ECD experiment showed that a long-lived free radical intermediate existed in the ECD

process [142], and that its lifetime was often much longer than the time it took for the intra-complex hydrogen transfer [144]. However, evidence for multiple backbone cleavages resulting in the formation of internal ions in the ECD of linear peptide ions was lacking to date, most likely due to the location of charges near the termini for the tryptic peptides studied. Experimental evidence linking the formation of smaller z• ions to the FRC of larger ones was also lacking, as the resonant ejection of the latter during ECD did not lead to appreciable decrease in smaller z• ion abundances [142]; thus, if the FRC is to account for some of the smaller z• ion formation, it must have taken place on a timescale shorter than the ejection time (typically milliseconds). Nevertheless, the FRC may still play an important role in the ECD of linear peptides, as evidenced by the abundant secondary side-chain cleavages and radical rearrangement, particularly when there is extra energy deposited in the precursor ions [54, 62, 144, 159, 160].

The importance of the radical in ECD was investigated further by several research groups by adding radical trap moieties in peptides [161, 162]. In one study, coumarin labels were attached to the N-terminal and/or lysine side-chain amine groups to serve as radical traps, which appeared to inhibit the c/z• ion formation while enhancing the side-chain cleavages in ECD [161]. In another study, a 2-(4´-carboxypyrid-2´-yl)-4-carboxamide group (pepy) moiety was used as the stable trap for both the electron and the hydrogen, which resulted in abundant electron capture without backbone dissociation. When the precursor ions were preheated by an IR laser near the dissociation threshold, subsequent electron capture did trigger backbone dissociation, but only produced b type ions [162]. These studies demonstrated the instrumental role of the mobility of the radical in peptide ion ECD.

In this study, a different radical trap, 2,4,6-trimethylpyridinium (TMP), was used. In addition to its potential of being a stable radical trap, TMP also functions as a fixed charge that inhibits the H atom formation upon electron capture and does not form hydrogen bonds with backbone carbonyls in the precursor ions. This may shed light on our understanding of both the primary and secondary ECD mechanisms. Charge derivatization methods using both positively and negatively charged derivatives have been used in mass spectrometry research to control the type of fragment ions generated from peptides and to facilitate the interpretation of the mass spectral data [163-168]. In several recent ECD and the related ETD [64] studies, fixed charge derivatization was used to increase the sequence coverage, investigate the role of excited electronic states, study the effects of cation charge-site identity, and examine the mechanism of disulfide bond cleavages [155, 169-171].

2.2 Experimental section

2.2.1 Materials

Amyloid β peptides (20-29, FAEDVGSNKG, hereafter abbreviated as Aβ 20) and (25-35, GSNKGAIIGLM, hereafter abbreviated as Aβ 25) were purchased from Bachem AG (Philadelphia, PA) and used without further purification. 2,4,6-trimethylpyrylium tetrafluoroborate was purchased from Alfa Aesar (Ward Hill, MA). Poros 50 R1 material was purchased from Applied Biosystems (Foster City, CA). All other chemicals were purchased from Sigma (St. Louis, MO).

2.2.2 Peptide derivatization

Potassium carbonate buffer solution (0.1 M K_2CO_3 and 0.1 M $NaHCO_3$) containing ~0.05 M 2,4,6-trimethylpyrylium tetrafluoroborate was prepared, whose pH was adjusted to ~9 using ~10 µl of HCl. 20 nmol of each peptide was dissolved in 50 µl of this buffer solution respectively, vortexed, and purged with nitrogen gas. The reaction was allowed to proceed for 18-24 hrs at room temperature. The final reaction solutions were dried and the peptide derivatives were purified by Poros 50 R1 material in custom solid phase microextraction (SPME) tips. Each fraction of the eluate was analyzed, and the unlabeled, singly-labeled, and doubly-labeled fractions were identified by ESI FT-ICR mass spectrometry.

2.2.3 ECD experiments

Unlabeled, singly-labeled, and doubly-labeled model peptides were analyzed by ECD at ~10^{-5} M concentration in 49.5:49.5:1 methanol:water:formic acid spray solution. The ECD analysis was performed on a custom qQq-FT-ICR-MS equipped with an external nano-spray source and a 7 Telsa actively shielded superconducting magnet as described previously [77, 78]. Multiply charged precursor ions were isolated by the front-end quadrupole (Q1) followed by external accumulation in the collision cell (Q2) for about 100-600 ms, before they were transferred via two rf-only hexapoles and trapped in the ICR cell using the gated trapping. These trapped ions were then irradiated with low-energy electrons (~0.2 eV) for 50-120 ms, generated by the indirectly heated dispenser cathode (Heatwave, Watsonville, CA). A chirp excitation/detection sequence was used and the signal was averaged for 20 scans. All spectra were zero filled once without apodization and Fourier transformed to give the magnitude mode spectra. Internal

calibration using the molecular ion and the charge reduced species gave a typical mass accuracy of less than 2 ppm for most of the peaks identified.

2.3 Results and discussion

The derivatization reaction of peptides with 2,4,6-trimethylpyrylium was previously used to convert the ε-amino group of the lysine side chain to the charged TMP group (Figure 2.1) [172-174]. Even though each of the Amyloid β peptides studied here only has one lysine residue, some doubly tagged peptides were also generated, where the second tag must have been attached to the N-terminal amino group. The singly tagged peptides may exist in one of the two forms, with either the lysine side-chain or the N-terminal amino group modified. Since the TMP tagging causes a mass shift of ~104 Da (from the *charged* amino group as it introduces a fixed charge) per modification, it was possible to localize the TMP group in the lysine residue rather than at the N-terminus (*vide infra*). The TMP group also fixed the charge at the nitrogen atom on the pyridinium ring, eliminating the existence of (relatively) free protons in the doubly tagged peptides, which allows the study of the role of hydrogen atom in the ECD process. Furthermore, the aromatic structure of the pyridinium ring could trap the radical generated near the TMP group, making it unlikely to propagate and induce further reactions.

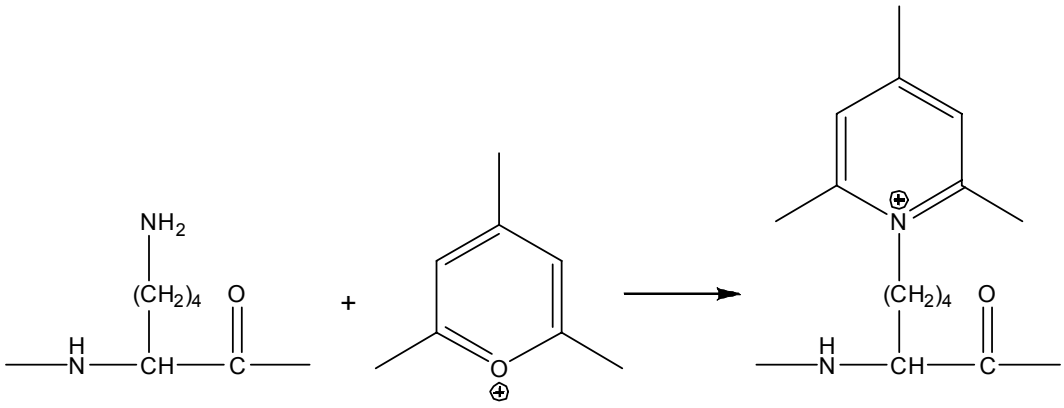

Figure 2. 1 The ε-amino group of the lysine side-chain was selectively converted to a 2,4,6-trimethylpyridinium salt.

Before analyzing the results obtained in the ECD studies of these modified peptides and attempting to draw conclusions on the ECD mechanism, it is important to point out that the modification also significantly changes the peptide conformational and electronic structures, which may influence the outcome of the electron capture, such as the preferential neutralization site and the ECD product branching ratios for different fragmentation channels.

2.3.1 Backbone cleavages

The ECD spectra of the unlabeled, singly- and doubly-labeled Amyloid β peptides are shown in Figure 2.2 (Aβ 20) and Figure 2.3 (Aβ 25), with the insets showing the cleavage patterns for the corresponding peptides. ECD of the unmodified Aβ 20 gave rise to many c and z type ions (Figure 2.2 a), reflecting the charge locations near both the N- and C-termini, as well as the similar recombination energy of the charged N-terminal amino group and the lysine side chain. On the other hand, ECD of the

unmodified Aβ 25, with both charges located near its N-terminus, produced mostly N-terminal (b- and c-type) ions, with the only z ion (z_8) being the one that contains the lysine residue (Figure 2.3 a). Some a and y ions were also present, likely the products of the minor channel in ECD that produces a- and y-type ions [51]. In addition, abundant b ions were observed in both spectra, a phenomenon that was previously investigated by Copper et al., who found that the b ion formations were common in ECD of peptides, particularly those containing lysines but not arginines [54, 175]. Such would be the case if the electron capture deposited sufficient energy into the precursor ion that resulted in the formation of the excited $[M+(n-1)H]^{(n-1)+}$ ion (the hydrogen atom loss product), which was an even electron species that could follow the mobile proton dissociation pathway to produce b-type ions.

ECD spectra of the singly labeled Aβ 20 and Aβ 25 are shown in Figures 2.2 b and 2.3 b, respectively. For Aβ 20 peptide, all z ions and the c_9 ion displayed a ~104 Da mass shift from those produced in the ECD of its unmodified counterpart, but smaller c ions that do not contain the lysine residue showed no such mass shift; thus, the TMP tag was added to the lysine residue rather than at the N-terminus. Likewise, for Aβ 25 peptide, all fragment ions containing the lysine residue displayed the characteristic ~104 Da mass shift, while those without the lysine residue showed none, unambiguously locating the TMP tag at the side chain of the lysine residue.

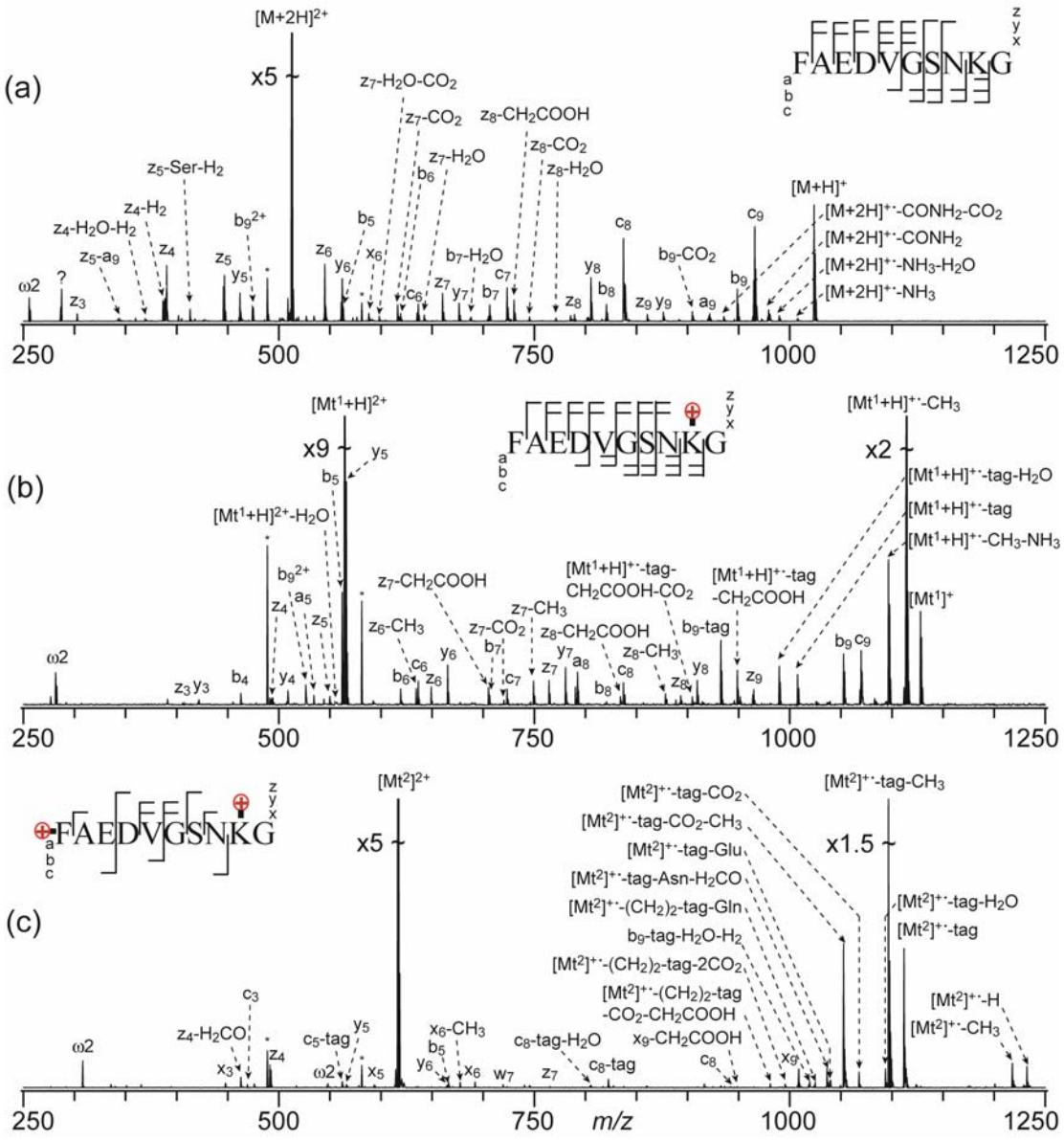

Figure 2. 2 ECD spectra of the (a) unlabeled, (b) singly-labeled and (c) doubly-labeled Amyloid β peptide (20-29). ∗ marks the electronic noise peak, ω2 marks the first harmonic peak of the precursor ion, peaks marked with "-amino acid residue" resulted from cleavage at the C_α-C_β bond, and partial side-chain losses were represented by molecular formula of the departing group(s). Tagged precursor ions were labeled as

$[Mt^1+H]^{2+}$ and $[Mt^2]^{2+}$ for singly- and doubly-labeled peptides, respectively. Cleavage patterns are shown as the insets.

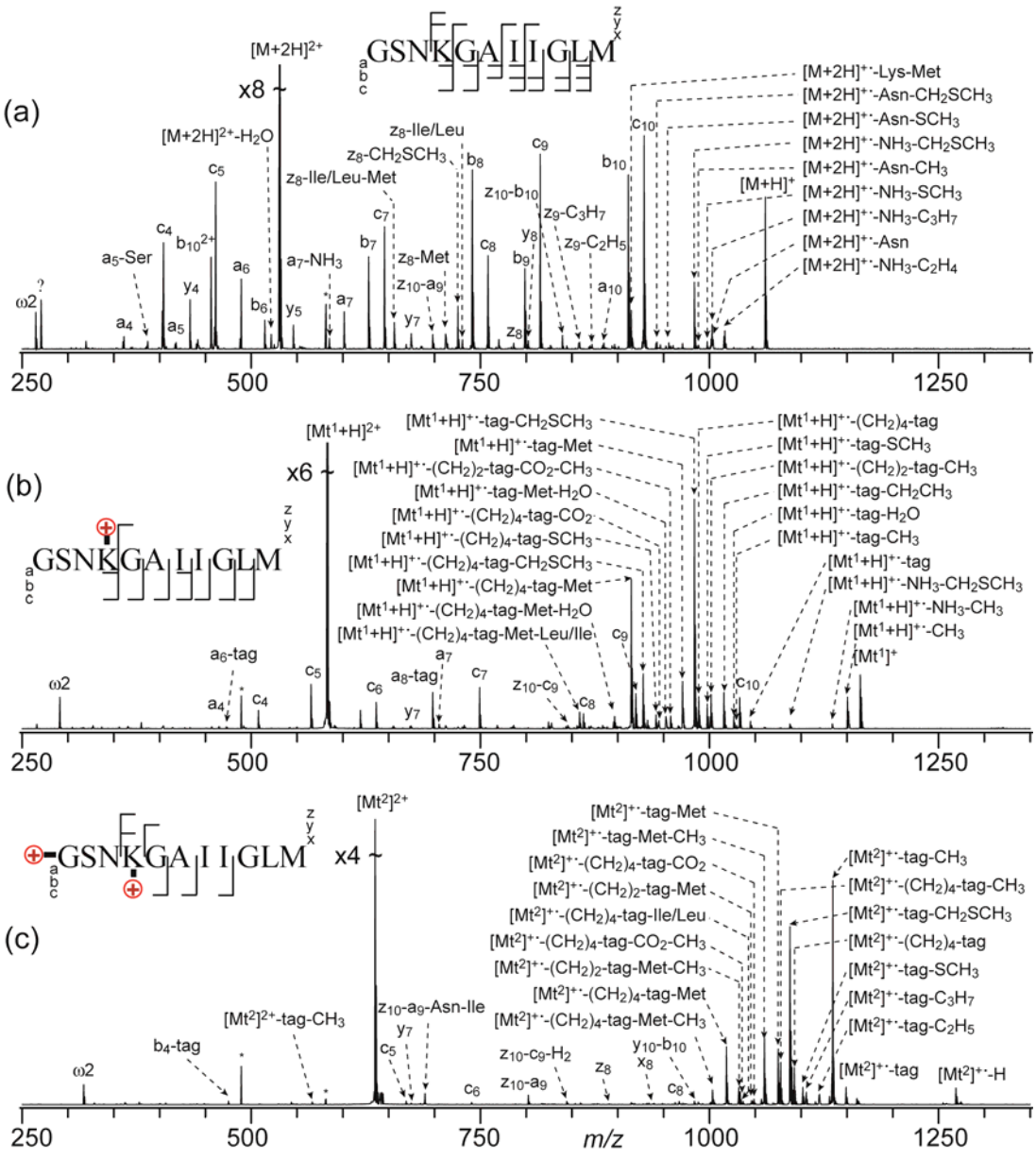

Figure 2. 3 ECD spectra of the (a) unlabeled, (b) singly-labeled and (c) doubly-labeled Amyloid β peptide (25-35). Peak labeling follows the same convention as in Figure 2.2. Cleavage patterns are shown as the insets.

The addition of a single TMP tag appeared to greatly reduce the abundance of the backbone fragments, but not the number of cleavages. The intrinsic recombination energy of the pyridinium ion (4.71 eV) [176] is much greater than that of the N-terminus protonated peptide (3.71 eV) [177]. After the initial electron capture in a high-lying Rydberg state, the pyridinium is far more likely to be the eventual neutralization site than the protonated N-terminal amino group. This resulted in the formation of a stable radical that was unlikely to undergo the typical c/z• dissociations. However, it appeared that there was still a small but significant probability that the electron ended up at the N-terminus, leading to the observed N-C_α cleavages (*vide infra*).

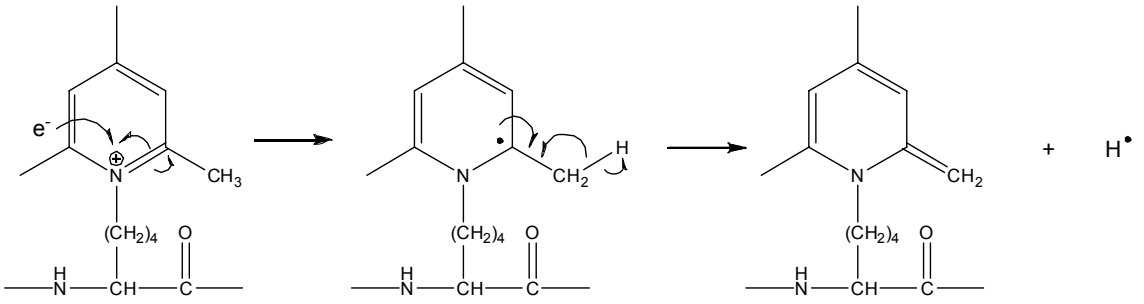

Figure 2. 4 H loss from the TMP tag upon electron capture.

Both the abundance and frequency of the backbone N-C_α cleavages were greatly reduced with the addition of a second TMP tag at the N-terminus (Figures 2.2 c and 2.3 c), as one would expect from the dissociation-recapture mechanism, since both charges were “fixed”, and no H atom formation was expected upon electron capture. However, N-C_α cleavages were not completely eliminated from the ECD of these doubly tagged peptides, and there were also some H loss products present, albeit in much lower

abundance. These H atoms were probably lost from the methyl groups on the pyridinium ring after it was neutralized, as shown in Figure 2.4, leading to the formation of stable even electron species, which could not undergo further radical driven processes. Since the recapture cross section of a free H atom by a gas phase peptide ion was very low, and the solvation of the TMP group by backbone carbonyls leading to the concerted H atom transfer from the methyl group to the carbonyl oxygen appeared unlikely, there must existed a second pathway to account for the observed c/z• ions in the ECD spectra of these doubly labeled peptides.

One possibility is that the electron was first neutralized near the TMP moiety, and the resulting radical at the alpha carbon on the pyridine ring could abstract a hydrogen atom from a nearby (through space) amino acid residue side-chain beta carbon, generating a beta radical that could lead to c/z and a/x ion formations (Figure 2.5). Free radical driven backbone cleavages have been reported by Beauchamp and coworkers in their free radical initiated peptide sequencing (FRIPS) studies [178], and were recently applied in the radical-directed dissociation of whole proteins in the gas phase [179]. In this study, however, the initially produced alpha radical on the pyridine ring was supposed to be fairly stable and unlikely to propagate; more importantly, the FRIPS mechanism (Figure 2.5) calls for the formation of c• ions and z•-H ions, while in the ECD spectra, only the even electron c ions and odd electron z• ions were observed. Thus, the FRIPS-like mechanism cannot account for all the backbone fragment ions observed here. A second possibility is that an amide superbase mechanism could be at work, where coulomb-assisted dissociative electron attachment at the backbone carbonyls generated an aminoketyl anion radical that abstracted a nearby proton to produce an aminoketyl radical that could undergo facile N-C_α bond cleavages. The proton most likely came from

the methyl group on the pyridinium ring, as its acidity was increased by the positive charge on the nitrogen atom. Further experiments employing a deuterium labeled TMP tag would be helpful in determining the origin of the protons.

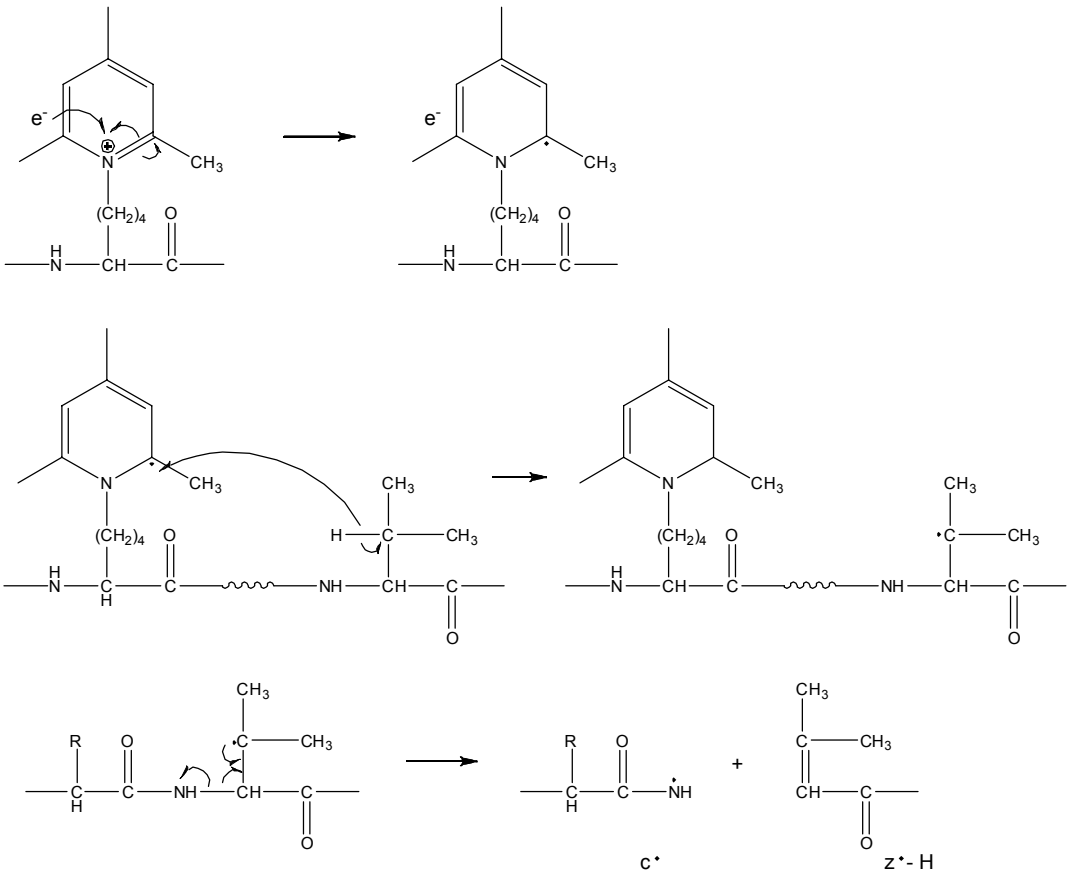

Figure 2. 5 One possible mechanism for c/z ion formations in doubly tagged peptides.

While the number of the fixed charge tags appeared to have a profound effect on the abundance and frequency of the backbone cleavages, the position of these tags seemed to have a less dramatic influence. For the doubly tagged Aβ 20, either of the two TMP tags could be the neutralization site, or the site that provided the proton during ECD, as substantiated by the observation of the c_3, c_8 ions which must have retained the charge at the N-terminal TMP tag, and the z_4, z_7 ions which must have had the lysine

side-chain TMP tag as the charge carrier (Figure 2.2 c). For the doubly tagged Aβ 25, the N-terminal TMP tag was a possible neutralization site as indicated by the presence of z_8, and x_8 ions (Figure 2.3 c), but it was unclear if the tag on the lysine side chain could also contribute to provide the proton necessary for backbone cleavages since all observed fragments contained the lysine residue. Moreover, the cleavages did not appear to be limited to regions that were adjacent to the charged sites in the sequence. This would certainly be true for remote charge assisted electron capture at backbone carbonyls, and it would also be expected if these cleavages were the results of the through-space radical propagation. Previously, cleavages occurring spatially but not necessarily sequentially close to the initially formed radical site have been observed [180].

The singly tagged peptides did show some differences in backbone cleavage abundances. When the tag was far away from the protonated site as in the case of the Aβ 20 peptide, only moderate drops in z ion abundances were observed (Figures 2.2 a, b). The c ions showed slightly more abundance decrease because their formations required the TMP tag site to be neutralized, which did not easily lead to N-C_α bond cleavages. For the Aβ 25 peptide (Figures 2.3 a, b), almost all fragment ions showed significant decrease in abundance in the ECD spectrum of the singly labeled peptide. This might be due to the close proximity of the protonated site and the TMP tagged site in the Aβ 25 peptide, which would greatly reduce the probability that the electron capture occurred on the protonated N-terminal site. In addition, tag locations also seemed to influence the abundances of various side-chain loss and tag loss products (*vide infra*).

Aside from backbone cleavages, fragment ions that resulted from small molecule losses, single or multiple side-chain cleavages as well as a combination of backbone,

side-chain cleavages and small molecule losses were also observed in the ECD spectra of all Amyloid β peptides studied here. These fragment ions were labeled in Figures 2.2 and 2.3, as well. All observed cleavages were also summarized in Figures 2.6 and 2.7.

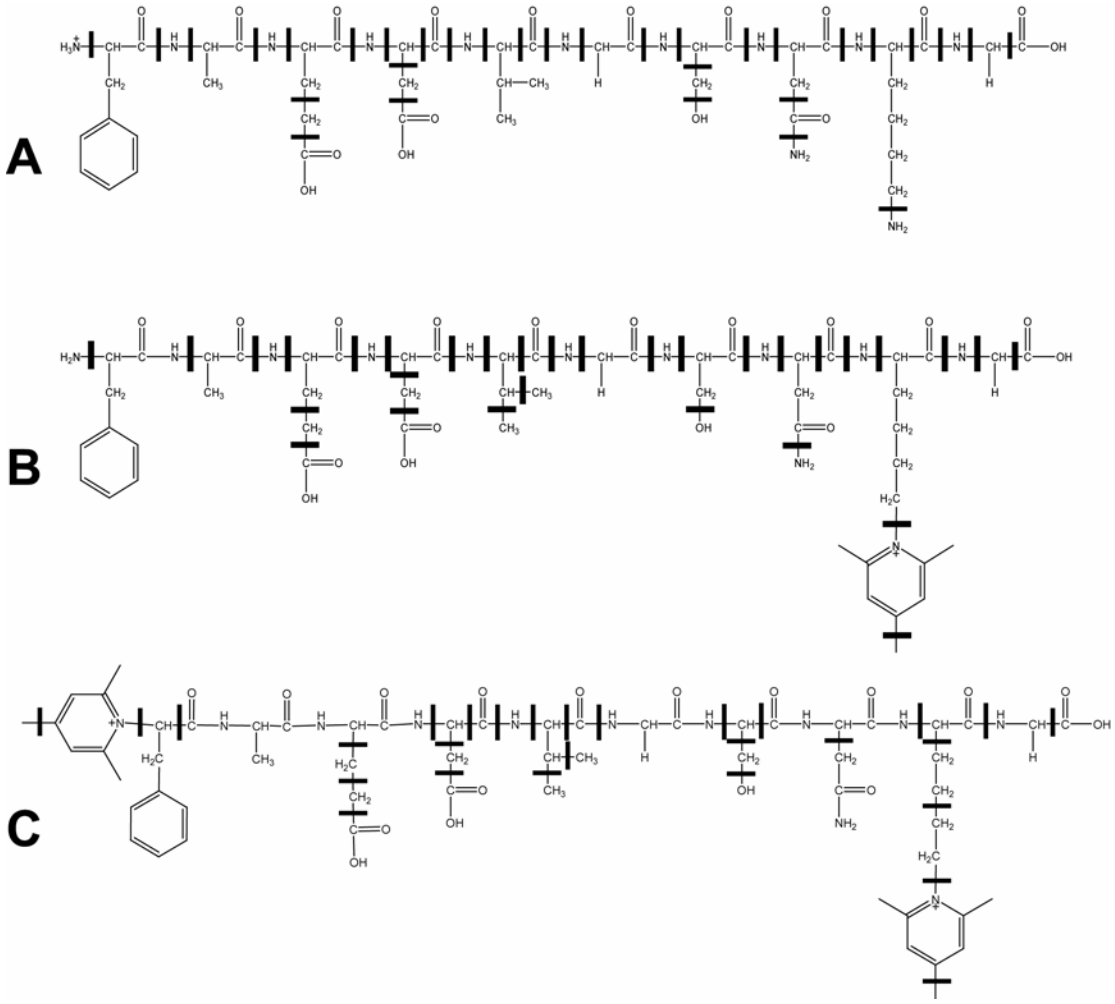

Figure 2. 6 All observed ECD cleavages of the (a) unlabeled, (b) singly-labeled and (c) doubly-labeled Aβ peptide (20-29).

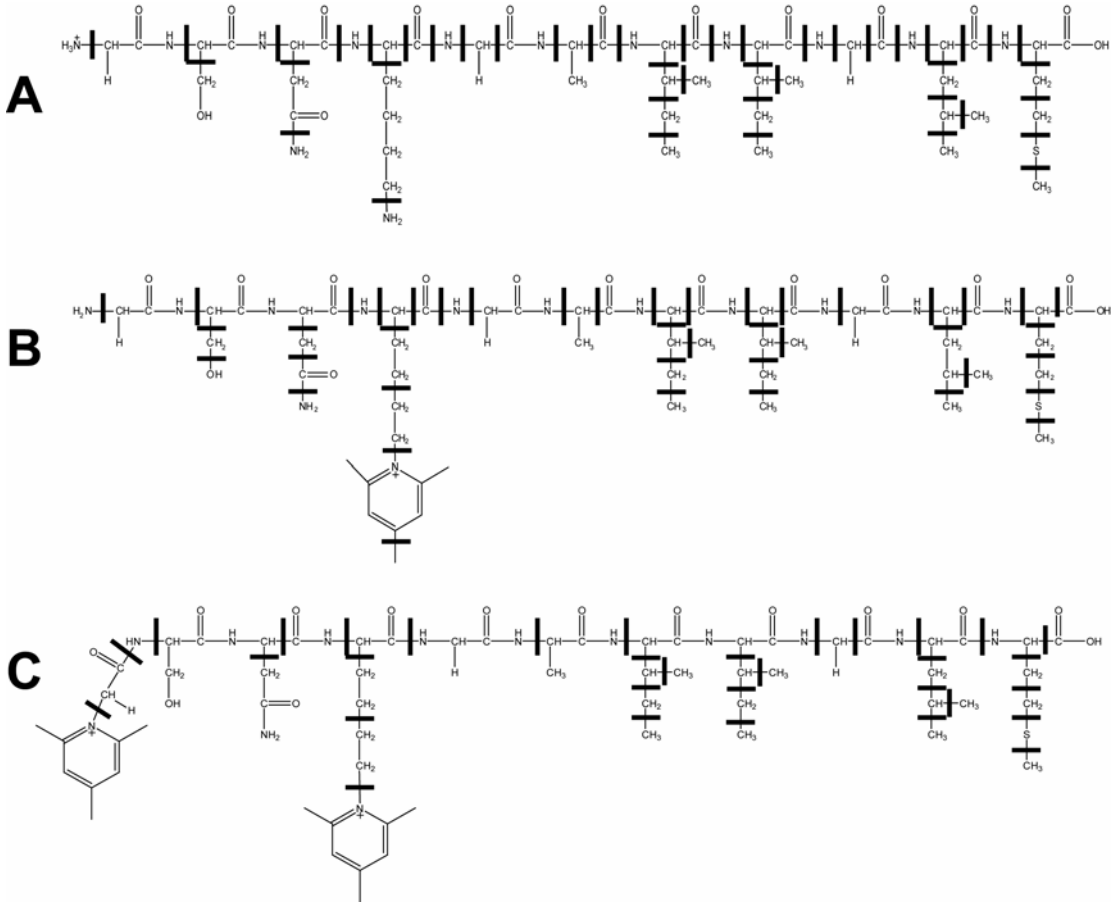

Figure 2. 7 All observed ECD cleavages of the (a) unlabeled, (b) singly-labeled and (c) doubly-labeled Aβ peptide (25-35).

2.3.2 Tag and alkyl group losses

It has been shown previously in a neutralization-reionization study of gas-phase pyridinium ion that the pyridinium radical preferentially lost the N-bound H or D atom to reform the aromatic ring [176], which competed favorably over the hydrogen rearrangement within the pyridinium ring. For the doubly TMP tagged peptides studied here, this implied that loss of the whole tag should be a favored process upon electron capture (Figure 2.8). However, as can be seen from Figures 2.2 c and 2.3 c, the tag loss

peaks were much weaker (by as much as an order of magnitude in the latter case) than the corresponding peaks with loss of the tag and an additional methyl group. Figure 2.9 represents two possible pathways for the generation of the tag loss product with an additional methyl loss, which led to the formation of a charged even electron species that was detected, and a stable radical species with the radical residing on the alpha carbon. The latter may also exist in several other possible resonance structures. Figure 2.9 a represent the McLafferty rearrangement pathway, which may be readily present because of the low activation barrier.

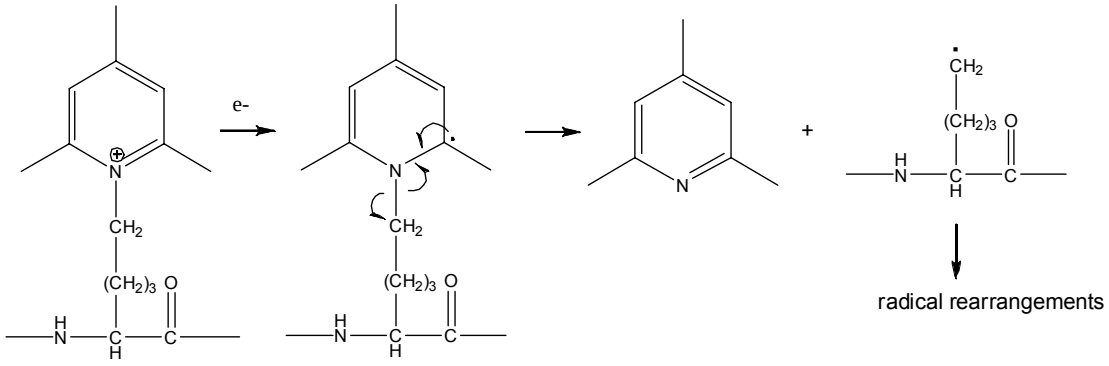

Figure 2. 8 Tag loss after the electron capture.

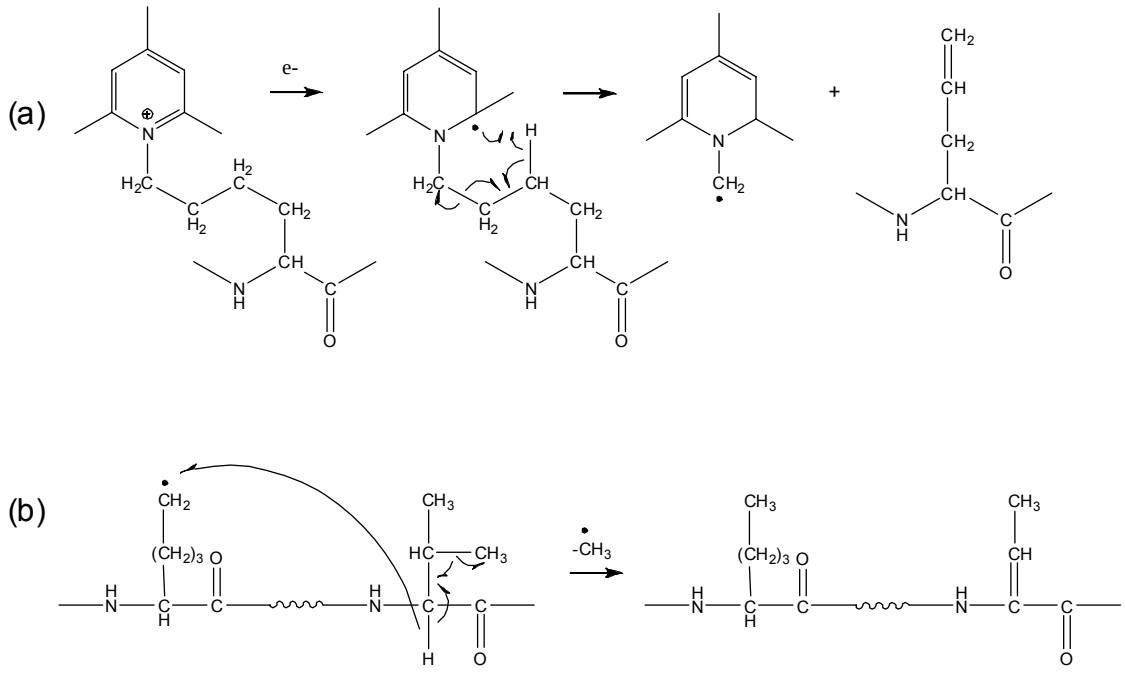

Figure 2. 9 Methyl group loss from the tag loss product.

Alternatively, the methyl group lost could come from elsewhere on the peptide such as the valine side chain (Figure 2.9 b). The loss of the TMP tag left the radical site on the ε-carbon of the lysine side-chain, which was an unconjugated primary radical, a fairly reactive species prone to further radical rearrangements. This radical may abstract a hydrogen atom from the alpha carbon of the valine residue, leading to the additional loss of methyl group (Figure 2.9 b). This mechanism was actually supported by the following observations. First of all, the relative abundance of the tag loss product with additional methyl group loss to that without was much higher for the doubly labeled Aβ 25 than the doubly labeled Aβ 20. Since the Aβ 25 has several leucine and isoleucine residues which could also lead to methyl loss from the tag loss product upon H atom abstraction from the alpha or beta carbon, this observation lends same support to the model in Figure 2.9 b; whereas in the case of the Aβ 20, for this model to be correct, the

H atom abstraction would have to take place at the alpha carbon of the single valine residue. Secondly and more importantly, fragment ions corresponding to additional loss of other alkyl groups such as the ethyl and propyl were only observed in ECD of the Aβ 25, corresponding to the presence of multiple leucine/isoleucine residues. Had Figure 2.9 a been the major pathway for the combined loss of tag and methyl groups, tag plus ethyl loss would only have been observed if the originally abstracted H atom was from the beta rather than the gamma carbon of the lysine side-chain.

For singly labeled peptides, the methyl loss peaks were much stronger than the tag loss peaks, particularly for the singly labeled Aβ 20, where it was the most abundant fragment ion (Figure 2.2 b). The methyl group did not appear to come from the TMP tag, since the addition of a second tag greatly reduced the abundance of the methyl loss product for both peptides. Once again, the most likely source of the methyl group was the side chain of the valine residue, where the initially formed radical could abstract a hydrogen atom from the alpha carbon of the valine residue, and the resultant alpha radical could lose one of the two methyl groups to form a stable even electron species (Figure 2.10). Selectively deuterating the TMP tag or the valine residue would help to identify the source of the lost methyl group. For Aβ 25, the alpha radical on the one of the isoleucine residues or the beta radical on either the isoleucine or leucine residue could also lead to the loss of a methyl group (Figure 2.10), although the methyl loss peak there was much weaker than in the ECD spectrum of the Aβ 20. This might be due to the different conformations of the two peptides, with the Aβ 20 having the valine residue closer to the TMP tag on lysine, and the Aβ 25 having the tag farther away from the isoleucine/leucine residues. Likewise, the dramatic abundance drop of the methyl

loss product ions when a second TMP tag was added to the N-terminus may also be due to the conformational changes.

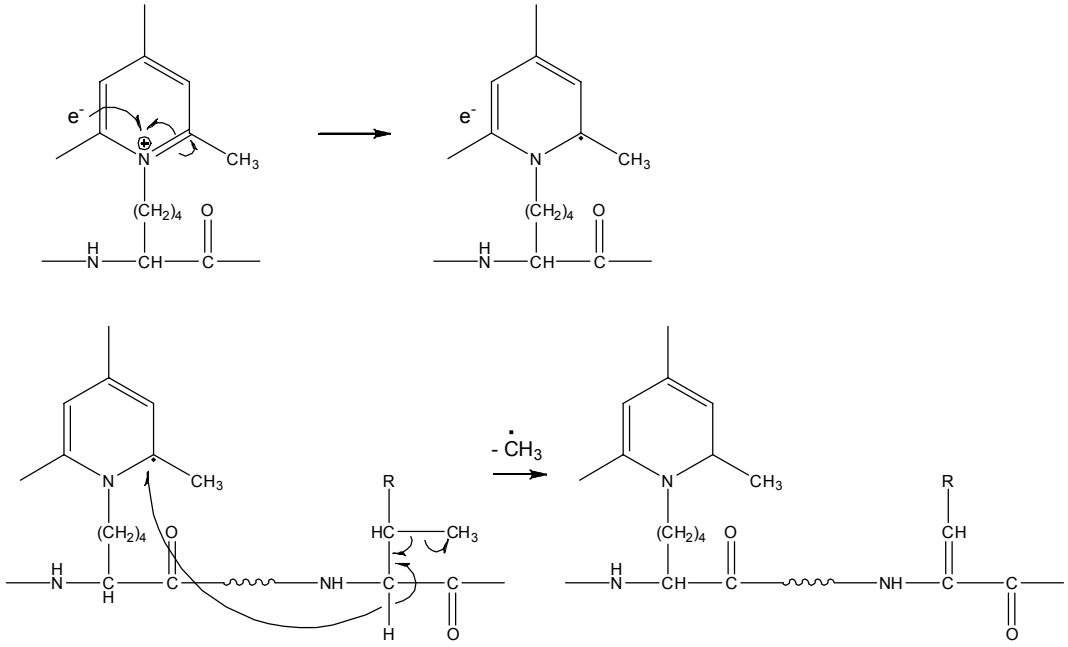

Figure 2. 10 Methyl loss from the valine (R = CH_3) and isoleucine (R = CH_2CH_3) side-chains.

2.3.3 Other small molecule and side-chain losses

Small molecule and side-chain losses are common in ECD of multiply protonated peptides [53]. The hydrogen atom generated from the neutralized protonated site plays an instrumental role in the proposed mechanism. Such was also the case for the ECD of the unlabeled peptides studied here, where ammonia and water losses as well as side-chain losses from serine, asparagine, lysine, isoleucine, leucine, and methionine residues were observed.

In a previous study, ECD of substance P modified with coumarin tags produced far more side-chain cleavages than the unmodified peptide, and the abundances of these side-chain cleavage products appeared to increase with the number of the tags [161]. It was believed that the presence of radical traps inhibited the backbone cleavage pathways, thus redirecting the radical to the side chains, possibly by changing the gas phase conformation of the peptide. A closer examination revealed that the great majority of the side-chain loss products from the ECD of the tagged substance P were also accompanied by tag loss. The (singly) lysine tagged substance P did produce some "pure" side-chain loss products, albeit in lower abundances. Similar trends were observed here, where most enhanced side-chain cleavages were primarily observed when they were also accompanied by tag loss. One notable difference is the abundant solo methyl loss peak observed in singly tagged Amyloid peptides and the doubly tagged Aβ 20.

These trends can be explained by the number of available protonation sites, and the tag's ability to stabilize a racial. For the singly tagged substance P, the likely charged sites were the arginine side-chain guanidine group and the remaining untagged amino group, which upon electron capture could produce the hydrogen atom initiating side-chain cleavages. For the doubly tagged substance P, one of the charge carriers was the protonated guanidine group, and the other most likely was the protonated amide nitrogen on the tagged site. The latter would be the favored neutralization site upon electron capture, which led to the loss of the neutral tag and left the radical site on the peptide lysine side-chain, capable of inducing secondary side-chain cleavages. As a result, for doubly tagged substance P, all observed side-chain cleavages were from the tag loss products [161].

Unlike the singly tagged substance P, all tagged Aβ peptides studied here contained at least one non-protonated charge carrier (the fixed charge tag), which also happened to be the preferred neutralization site due to its larger recombination energy. As discussed earlier, the electron capture at the TMP tag resulted in the loss of the neutral tag as a primary product (although not necessarily the most abundant product), which could undergo secondary side-chain losses as the radical site remaining on the peptide was a primary radical with relatively low stability (Figure 2.8). Consequently, in the ECD spectra of the TMP tagged peptides, whether with one or two tags, most observed side-chain loss products were secondary fragment ions from the tag loss product, just like what have been observed in the ECD of the doubly tagged substance P. However, in the ECD spectra of singly labeled Aβ peptides, some side-chain losses without accompanying tag loss were also observed. These were often accompanied by NH_3 loss instead, such as the -CH_3-NH_3 peaks in Figures 2.2 b and 2.3 b, and the -NH_3-CH_2SCH_3 peak in Figure 2.3 b. Thus, the protonated N-terminal amino group may also be a possible neutralization site, even though it may not be the favored one, in accordance with the observation of multiple z ions in Figure 2.2 b.

2.3.4 Secondary and internal fragment ions

Both d and w ion formations resulting from secondary side-chain cleavages after the primary N-C_α bond cleavage were common in ECD of multiply protonated peptide ions. Their abundances were often dramatically increased with increased precursor ion internal energy, such as in hot ECD or AI-ECD, which was very useful in differentiating the isomeric leucine and isoleucine residues [62, 160]. Other types of secondary fragments requiring radical migration from the alpha carbon at the cleavage site prior to

secondary side-chain cleavages have also been observed previously [54, 144]. For the unlabeled peptides studied here, many z ions experienced secondary side-chain cleavages (Figures 2.2 a and 2.3 a), but none of the c ions displayed any secondary side-chain losses, as the latter did not contain a radical site. Some secondary fragment ions resulted from loss of different groups from the same side-chain. Thus, the hydrogen atom abstracted did not appear to be limited to those on the backbone alpha carbons; some of the ions observed would require the hydrogen atom on the side-chain to be abstracted prior to secondary cleavages. For example, the z_8 ion from the ECD of the Aβ 25 peptide could lose either the even electron CH_3-S-CH=CH_2 molecule or the odd electron CH_3-S-CH_2• radical (Figure 2.11). Complete side-chain loss from the leucine or isoleucine residue was also apparent, which left the radical on the peptide backbone that could initiate further cleavages. This was evident in Figure 2.3 a, where z_8 ion with multiple side-chain losses was observed.

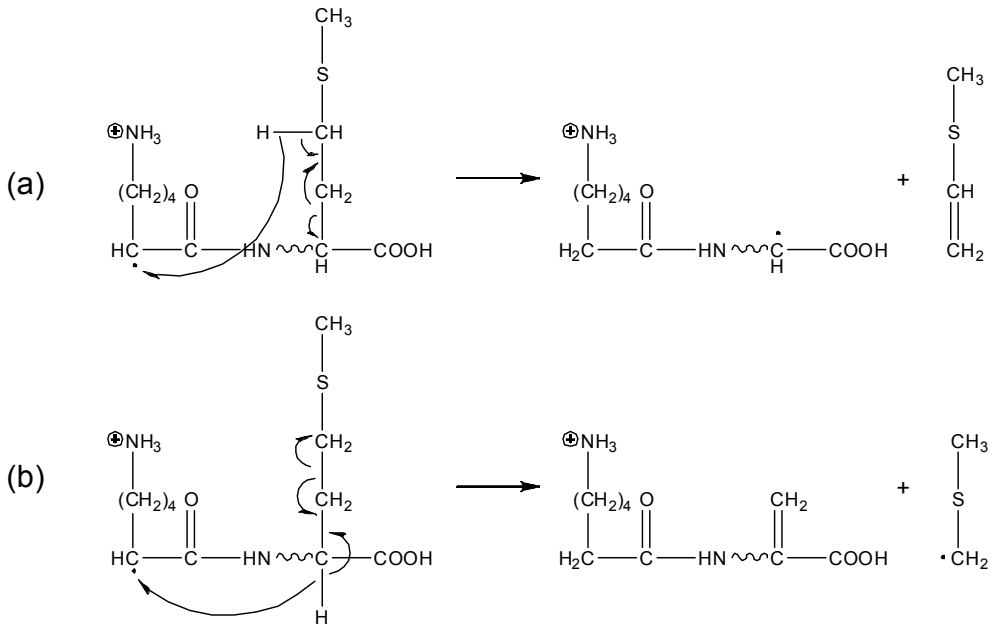

Figure 2. 11 Methionine side-chain losses from z8 ion.

The ECD spectrum of the singly tagged Aβ 20 peptide contained many similar secondary fragment ions as seen in that of the unlabeled peptide. These [z – R] ions (where R denotes a side-chain) were almost certain to result from the electron capture by the protonated N-terminal amino group, as the lysine TMP tag must retain its charge so that they could be detected. Furthermore, several methyl loss peaks from various z ions were present in the ECD spectrum of the singly labeled Aβ 20 peptide, but were absent in that of the unlabeled peptide. No z ions smaller than z_6 experienced the methyl loss, thus the methyl group most likely were lost from the valine side-chain, instead of from the TMP tag. It was unclear, however, why the presence of a TMP tag enhanced the methyl loss from both the charge reduced molecular ion and the primary z ions, as it did not appear to be directly involved (i.e. the methyl was unlikely to come from the TMP tag). For the singly tagged Aβ 25 peptide, neither z ions nor secondary fragment ions from z ions were observed. This was probably due to the close proximity of the N-terminus and the TMP tag, which made the electron capture at the N-terminus less likely than when they were farther apart as in the case of the singly tagged Aβ 20 peptide. However, extensive secondary fragmentation was observed on the molecular ion that had lost the neutral tag only or the neutral tag along with partial or full loss of the lysine side-chain (Figure 2.3 b), provided that the radical still resided within the peptide after the tag or lysine side-chain loss. ECD of both doubly tagged peptides produced plenty of secondary side-chain loss products after the initial tag or lysine side-chain loss, just like the singly tagged Aβ 25 peptide. In absence of a protonated site, the electron capture was certain to take place at the TMP tagged site, generating a radical upon neutral tag loss, which can initiate further cleavages.

Finally, some internal fragments were observed with high mass accuracy in both the unlabeled and labeled peptides (Figures 2.2 a and 2.3 a-c). These have not been previously reported, most likely because of the charge locations near the termini for substance P and the tryptic peptides commonly studied. The two peptides studied here have one of the charge carriers, the lysine residue, in the middle of the sequence, thus making possible the detection of internal fragment ions generated, particularly when the charge was fixed on the lysine residue. Their abundances were fairly low compared with those of the terminal fragment ions, probably because of the many other channels, such as the secondary side-chain loss channels, present that were more favorable due to low activation energies or less stringent conformational requirements. Nonetheless, the presence of these internal fragments demonstrated further that the free radical cascade mechanism could play an important role in the backbone cleavages during ECD of linear peptides as well.

2.4 Conclusion

The addition of fixed charge groups (TMP) significantly changed the ECD behavior of two amyloid β peptides. In general, a higher number of TMP tags correlated with fewer backbone cleavages and more abundant side-chain cleavages. The TMP tag was chosen because of its ability to stabilize (trap) the originally formed radical upon electron capture, as well as its non-protonated nature which was postulated to inhibit the hydrogen atom formation that was essential for the N-C_α bond cleavage in the dissociation-recapture mechanism. Although low abundance H loss products were observed in the ECD spectra of doubly tagged peptides, the H atoms generated there were not expected to play an important role in backbone cleavages due to the small

cross section for its recapture by the peptide and the unlikelihood of the fixed charge site to form a hydrogen bond with backbone carbonyls to initiate concerted hydrogen atom transfer for N-C_α bond cleavages during ECD. Still, some c and z type ions were observed in the ECD of doubly tagged peptides, demonstrating that there existed other, non-H atom mediated, pathways for c/z• ion formations in ECD, which may be radical driven, or resulted from the coulomb-assisted dissociative electron transfer. However, because the modified peptides often have very different electronic and conformational properties from the unmodified ones, these results did not necessarily undermine the importance of the hydrogen atom in the ECD of peptides. In fact, the opposite might be true as the doubly tagged peptides without a protonated site produced far fewer and less abundant backbone cleavages.

The apparent blocking of the backbone fragmentation channels seemed to open up new channels for side-chain cleavages, possibly as a result of the redirection of the radical site towards side chains. Most side-chain cleavages from the TMP tagged Aβ peptides were accompanied by the tag loss. This reaffirmed that the charge neutralization predominantly occurred at the TMP tag, which could easily lose the tag and generate a primary radical that can initiate further side-chain cleavages. Secondary fragment ions were abundant in the ECD spectra of both Aβ peptides, with or without the TMP tag(s). Frequently, these ions were the results of secondary cleavages following through-space hydrogen atom abstraction. Future experiments employing selectively deuterated TMP tag or amino acid side-chains can help to explain different processes in the ECD of these modified peptides. Finally, several internal fragments were observed in the spectra, which provide strong support to the free radical cascade mechanism.

Chapter 3

Charge Remote Fragmentation in ECD and ETD

3.1 Introduction

3.1.1 Free radicals generated by various MS methods

Free radical induced gas-phase fragmentation processes in peptides/proteins have been extensively studied. A variety of methods have been employed to generate free radicals in gas phase peptides/protein ions, including homolytic cleavages of covalent bonds that couple the chemical/chromophore groups or radical initiators to peptides, dissociation of noncovalent complexes of peptides, and peptide ion-electron/ion-ion interaction methods. For example, the weak covalent bonds in the lysine peroxycarbamates (LPC) and the free radical initiator Vazo 68-peptide conjugates may be collisionally activated to generate free radicals in peptide ions [178, 181, 182]. CID may also be used to generate radical cations from the S- and N-nitrosopeptides or sodiated nitrate esters of serine and homoserine derivatives [183, 184]. Site specific radical directed dissociations can be induced by photodissociation (PD) of a carbon-sulfur (C-S) bond introduced at phosphorylated serine and threonine residues through elimination of the phosphate in basic solution followed by addition of a thiol with an attached naphthyl based chromophore group [185], or PD/CID of a carbon-iodine (C-I) bond at iodinated tyrosine, and to a lesser extent, iodinated histidine [179]. CID of the

[1]This chapter has been partially/entirely reproduced from
Xiaojuan Li, Cheng Lin, Liang Han, Catherine E. Costello, and Peter B. O'Connor. Charge remote fragmentation in electron capture and electron transfer dissociation. *Journal of the American Society for Mass Spectrometry.* 2010, 21, 646-656. Copyright 2010 Elsevier.

ternary complex [Metal(L)(M)]$^{n+\bullet}$ that contains a metal ion such as Cu(II) or Co(III), an auxiliary ligand L (typically an amine) and oligopeptide M has been shown to generate molecular radical cations ($M^{+\bullet}$) [186-189]. The PD-CID of the crown ether based photolabile iodonaphthyl radical precursor/peptide complexes can also generate radicals on the side chain, which mediates the backbone fragmentation [190]. Most of these methods require re-isolation of the radical peptide ions and further collisional activation. On the other hand, ion-electron/ion-ion interaction methods can simplify the analysis process by avoiding the prior covalent modification, formation of complexes, and/or additional isolation/reactivation steps. Multiply protonated peptides can interact directly with high energy (>10 eV) and low energy (< 0.2 eV) electrons to generate radical peptide ions, as observed in EID [70, 71, 191] and ECD [38, 45, 52], respectively. Radical anions may also be used to transfer an electron to the multiply protonated peptides to induce backbone fragmentation pathways similar to those observed in ECD, as demonstrated in ETD [64-66].

3.1.2 Free radicals in ECD and ETD

As described in the previous chapters, in ECD, after electron capture by the multiply protonated peptide ion, the subsequent non-selective N-C_α bond cleavage generates an even-electron c ion and a radical z• ion [38, 45, 52]. The radical located on the N-terminal α-carbon of the z• ions may initiate further rearrangement reactions to induce many kinds of secondary fragmentations along the peptide backbone or on the side chain. A common fragmentation channel is the alpha cleavage of the C_β-C_γ bond of the N-terminal residue of the z• ion, resulting in the formation of w-ions. However, the radical may also migrate to other positions via hydrogen abstraction to induce bond

cleavages remote from the initial radical site, similar to the dissociation pathways observed in the vacuum ultraviolet (VUV) photodissociation of peptide ions, and the surface induced dissociation (SID) and CID of peptide radical cations [192, 193]. In ECD, the likelihood of radical rearrangement generally decreases as the distance between the primary cleavage site and the hydrogen abstraction site along the peptide backbone increases, although through-space hydrogen abstraction does occur [142, 156]. Neutral losses from the reduced precursor ions and secondary side chain losses from z• ions in ECD have been studied extensively in linear peptides [53-55, 150, 159, 194-196]. Loss of the entire or partial side chain from z• ions was considered to be associated with the γ- or α-radical formation on the corresponding amino acid, respectively [55, 194]. Because these secondary fragmentations do not involve the charge directly, and the bond cleavage sites are spatially remote from the charge carrier site, they can be considered as “charge-remote fragmentations” (CRFs) [189, 197-202]. CRFs are not as common in ETD, presumably because of the less energy deposited upon electron transfer, as well as the collisional cooling effect present in the ion trap commonly used to carry out ETD experiments. However, when z• ions from ETD were collisionally activated, extensive radical induced fragmentations were also readily observed [203]. CRF may also lead to secondary backbone cleavages, as evident in the ECD of doubly charged cyclic peptides, where multiple backbone cleavages and side chain losses were observed with the capture of a single electron [56]. A free radical cascade (FRC) mechanism was proposed, in which the initial α-radical can propagate along the peptide backbone to generate another α-radical with a stable even-electron neutral as the leaving group. FRC also predicts the formation of internal fragments in ECD of linear peptides. However, since most peptide ions studied in ECD experiments are ESI-

generated tryptic peptides with charges located near the termini, the internal fragments, even if formed, would be neutral and undetectable. Nevertheless, for non-tryptic peptides, or for tryptic peptides with basic residues(s) located in the middle of the sequence either due to missed cleavage(s) or the presence of histidine residue(s), internal fragments may be detected. To test this hypothesis, three synthetic peptides were investigated by ECD and ETD. Internal fragment ions were observed and the postulated mechanisms were discussed. Side chain losses were also investigated to help further understand the radical's fate in z• ions.

3.2 Experimental section

3.2.1 Materials and ECD experiments

Human αA crystallin peptide (1-11, MDVTIQHPWFK), the deamidated form of human βB2 crystallin peptide (4-14, HETEAGKPESL) (both from Anaspec, Fremont, CA, USA), and amyloid β peptide (25-35, GSNKGAIIGLM) (Bachem AG, Philadelphia, PA, USA) were used without further purification. All other chemicals were purchased from Sigma (St. Louis, MO, USA). The peptides were analyzed by ECD at ~10^{-5} M concentration in the spray solution containing 49.5:49.5:1 (v/v/v) methanol: water: formic acid. ECD analysis was performed on the custom built ESI qQq- FT-ICR mass spectrometer equipped with an external nanospray source and a 7 Tesla actively shielded magnet as described previously [77, 78]. In the ECD experiments, the multiply charged precursor ions were isolated in the front end quadrupole (Q1), and externally accumulated in the collision cell (Q2). These ions were then transmitted to and trapped in the cylindrical ICR cell by gated trapping. The trapped ions were irradiated with low

energy electrons (~0.2 eV), generated by an indirectly heated dispenser cathode (Heatwave, Watsonville, CA, USA). A grid, located in front of the cathode, was kept at +10 V to help guide the electrons into the ICR cell. The transients were zero-filled twice and Fourier transformed without apodization. All spectra were internally calibrated using the precursor and charge reduced ions.

3.2.2 ETD experiments

The ETD experiments of these three peptides were performed on an AmaZon (Bruker Daltonics, Bremen, Germany) Ion Trap instrument equipped with an Apollo II ion source, at the concentration of ~1 μM in the same spray solution as used in ECD experiments. The low mass cutoff value was *m/z* 100-120 and the reaction time was between 100-120 ms. Smart Decomposition was employed to improve fragmentation [67].

3.3 Results and discussion

ECD measurements of three synthetic peptides were performed, with one mimicking a tryptic peptide and two being non-tryptic peptides. Figure 3.1 shows the ECD spectrum of the tryptic peptide (αA crystallin peptide, 1-11) with a histidine residue in the middle of the sequence. Figure 3.2 and Figure 3.3 show the ECD spectra of two non-tryptic peptides (amyloid β peptide, 25-35 and the deamidated form of βB2 crystallin peptide, 4-14) each containing a lysine residue in the middle of the peptide sequence. In the ECD and ETD spectra of this study, peaks corresponding to both the charge-reduced molecular ions and its hydrogen loss products ($[M+nH]^{(n-1)+\bullet}$ and $[M+(n-1)H]^{(n-1)+}$) were observed. These spectra were dominated by c and z• ion series, as expected.

There were also several b ions present in the spectra, particularly in Figure 3.2, in agreement with previous studies [175, 204]. In addition, peaks corresponding to entire and partial side chain losses from z• ions, as well as internal fragments were observed.

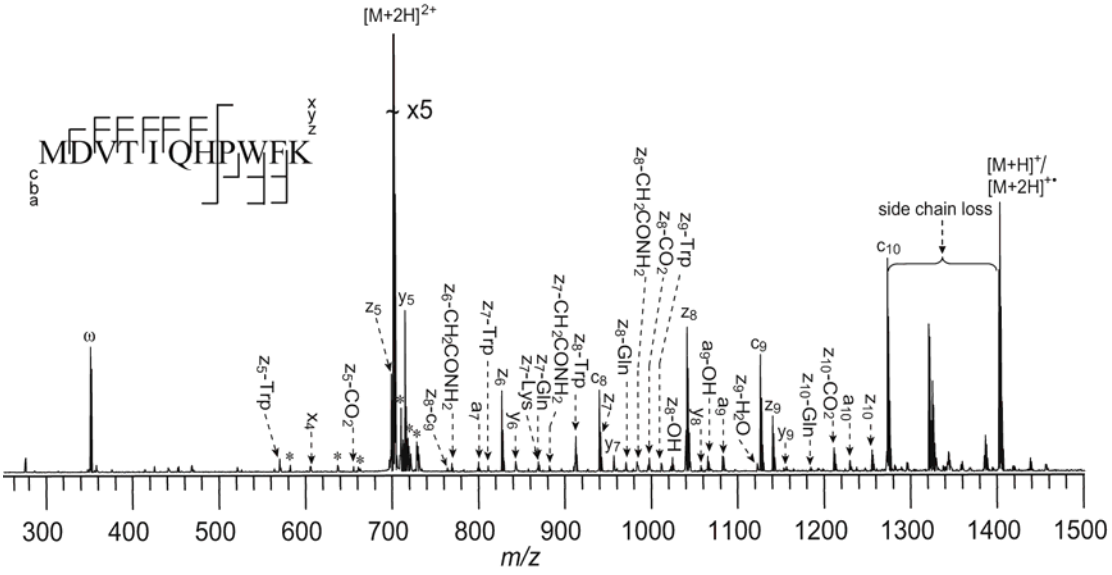

Figure 3. 1 ECD spectrum of αA crystallin peptide (1-11). ∗ represents the electronic noise peak or salt adducts, ω represents the harmonic peaks. Peaks marked with "-amino acid residue" represent the entire side chain losses, and the partial side chain losses are represented by the molecular formulas of the departing group(s). Side chain loss means loss from the charge-reduced molecular ions. The cleavage pattern is shown as the inset.

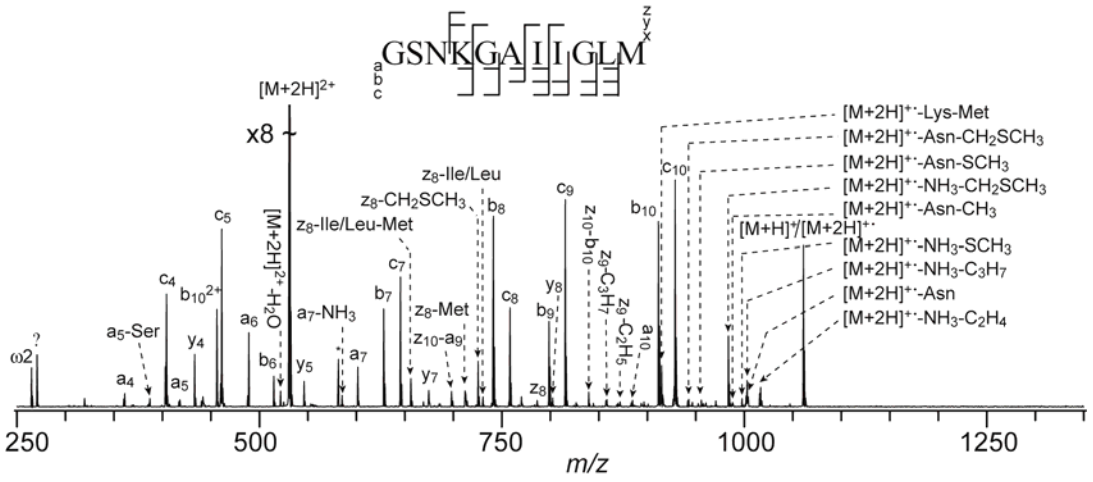

Figure 3. 2 ECD spectrum of amyloid β peptide (25-35). Peak labeling follows the same convention as in Figure 3.1. The cleavage pattern is shown as the inset.

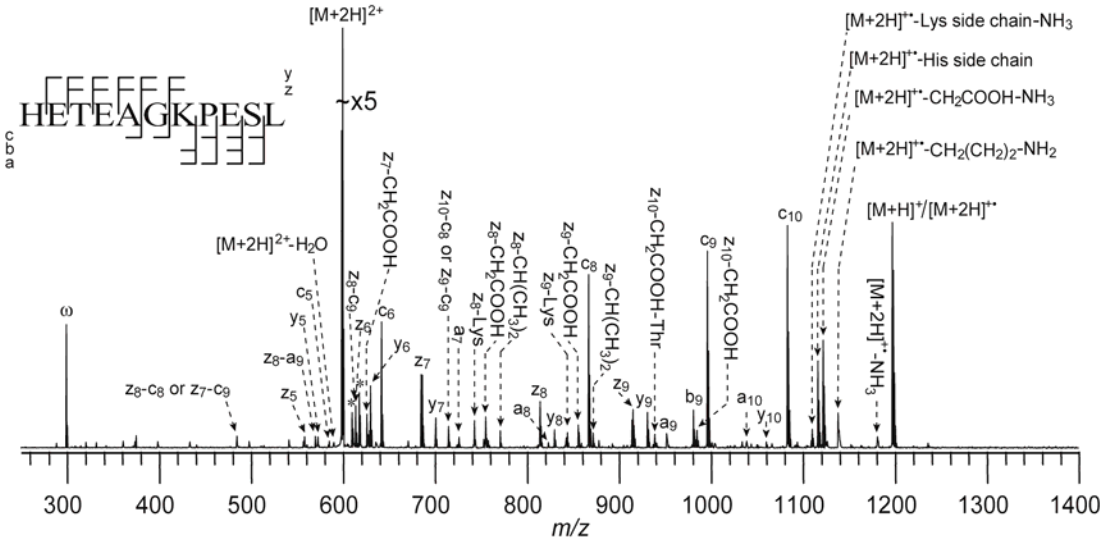

Figure 3. 3 ECD spectrum of the deamidated form of βB2 crystallin peptide (4-14). Peak labeling follows the same convention as in Figure 3.1. The cleavage pattern is shown as the inset.

3.3.1 Entire side chain loss from z• Ions associated with γ-radical formation on the side chain

For amino acids containing γ-hydrogen(s) on their side chains, entire side chain losses from z• ions may be observed, usually at sites remote from the primary backbone cleavage sites [189, 190, 193, 194]. These amino acids include: Ile/Leu, Lys, Arg, Glu, Gln, Cys, Met, and Val. Figure 3.4 illustrates a possible mechanism for the loss of the entire side chain, using glutamine as an example. After the initial z• fragment formation, the α-radical on the N-terminal carbon of the z• fragment may abstract one hydrogen from the γ-carbon of the glutamine side chain, and the newly formed γ-radical can undergo an α-cleavage reaction and release the side chain as an even-electron, neutral species from the peptide, leaving the radical on the peptide backbone. For example, in the ECD spectrum of the αA crystallin peptide (1-11), the entire glutamine side chain was lost from the z_7• and z_8• ions, and the lysine side chain was lost from the z_7• ions (Figure 3.1); in none of these cases is the backbone cleavage site adjacent to the site of side chain loss. In other ECD spectra, glutamic acid side chain losses from z• fragments were also detected with low abundance (data not shown here). In the ECD spectrum of amyloid β peptide (25-35), peaks corresponding to entire side chain losses from z• fragments of leucine/isoleucine, or methionine were also observed (Figure 3.2) [205].

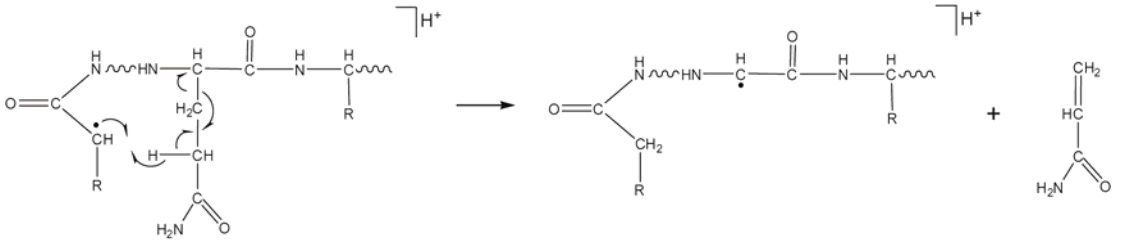

Figure 3. 4 Entire side chain loss from z• ions via gamma hydrogen abstraction.

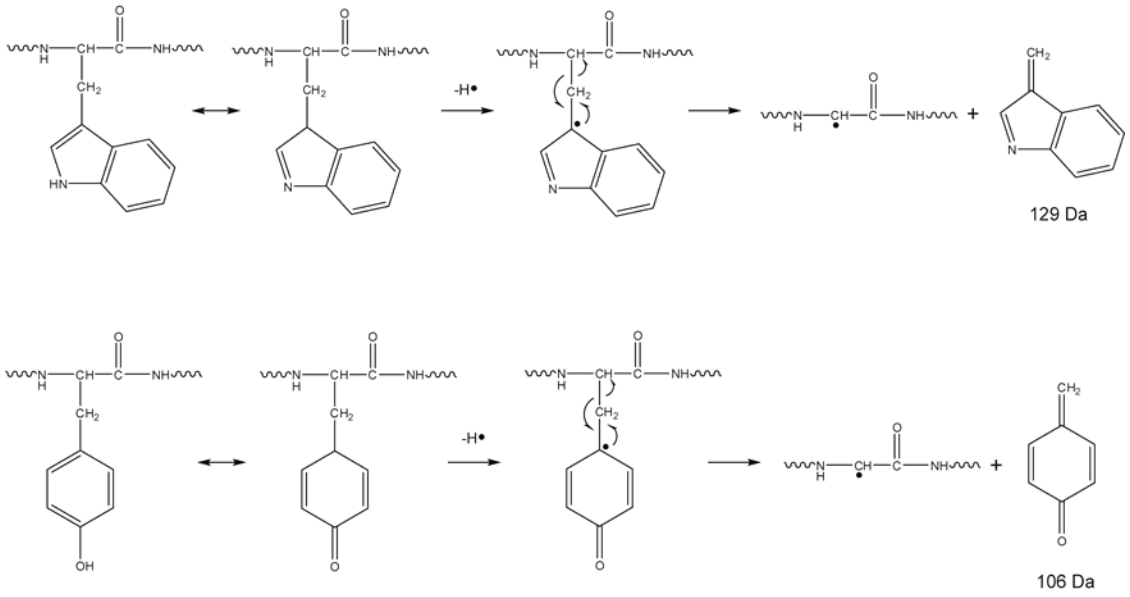

Figure 3. 5 Entire side chain loss from z• ions via gamma hydrogen abstraction involving aromatic amino acids.

In the ECD spectrum of the αA crystallin peptide (1-11) (Figure 3.1), a series of peaks corresponding to loss of the entire side chain of a tryptophan residue (129 Da) from the z• fragments were observed, some of which have relatively high abundance, such as the z_8•-Trp at *m/z* 911. For all of these z•-Trp ions, the backbone cleavage sites were remote from the tryptophan residue. This remote loss of tryptophan side chain from

z• ions has been reported previously in ECD and ETD studies, the latter of which required additional collisional activation [194, 203]. Siu and coworkers have observed the 129 Da loss of the tryptophan side chain in the CID mass spectra of the $M^{+\bullet}$ ion of WGG formed by the collisional induced dissociation of the $[Cu^{II}(dien)M]^{2+\bullet}$ complex [187], where they proposed that the tryptophan side chain was lost as a carbene species, following the 1,4-proton transfer that puts the charge on the backbone carbonyl and the radical on the β-carbon. Although there is no γ-hydrogen in the common canonical representation of the tryptophan structure as previously suggested [193, 194], a tautomeric form of tryptophan does contain a γ-hydrogen, which can be used to explain the abundant tryptophan side chain losses present here, as illustrated in Figure 3.5. This postulated mechanism may also account for the side chain loss from tyrosine residue (106 Da), as seen in both ECD of protonated peptide ions [194] and CID of peptide radical ions [186]. Phenylalanine does not have a hydroxyl group to generate the tautomeric structure like tyrosine, and loss of the entire phenylalanine side chain from z• ions has seldom been observed, except once as reported in the literature, but under unusual conditions [161]. The histidine residue can assume a γ-hydrogen containing tautomeric form as well, which may lead to a complete side chain loss of ~80 Da, although it has not been observed in ECD to date. Nonetheless, histidine side chain loss has been reported in the dissociation of the hydrogen deficient peptide radicals [190], as well as in the CID and SID spectra of $M^{+\bullet}$ ions [189]. This potential ~80 Da loss is different from the ~82 Da loss from the charge reduced species reported in previous studies [53, 196]. The ~82 Da loss proceeds via a different mechanism, where the charge neutralization at the protonated imine nitrogen site generates a stable carbon radical to induce loss of the entire side chain. It is important to note that these neutral

side chain losses are different from the cationic side chain losses in the EID spectra of protonated aromatic amino acid or peptides containing aromatic moieties, where the electron ejected by EI is typically from the aromatic ring itself, leaving both the charge and the radical on the aromatic ring. This radical cation may rearrange to lose a cationic species which is one Da higher than that of the neutral loss (tryptophan: 130 Da, phenylalanine: 91 Da, tyrosine: 107 Da, and histidine: 81 Da) [71].

Multiple side chain losses from z• ions were also observed in ECD spectra. For example, in the ECD spectrum of the amyloid β peptide (25-35), peaks corresponding to the losses of Ile/Leu and Met side chains from the z_8• fragment were observed (z_8 - Ile/Leu-Met) (Figure 3.2). This is expected, as loss of the entire side chain leaves the radical on the backbone, which may induce further fragmentations. As long as the radical still remains on the backbone, the side chain loss cascade may continue.

3.3.2 Partial side chain loss from z• ions associated with α-radical formation on the side chain

Furthermore, in Figure 3.1, there were a series of peaks corresponding to the partial side chain losses of glutamine residue (C_2H_4NO) from z• ions, with the glutamine residue located either directly at the backbone cleavage site or several amino acids away from it. In this peptide, the z_6• -C_2H_4NO fragment was assigned as the w_6 ion resulting from the direct cleavage of the C_β-C_γ bond adjacent to the initial radical site, because the side chain loss occurred at the site N-terminal to the only glutamine residue in the sequence. The other partial side chain losses of glutamine from z• ions had to be formed via through space radical rearrangement. The detailed mechanisms for the partial glutamine side chain losses from z• ions are shown in Figure 3.6, similar to those

proposed by other groups [56, 190, 193, 194]. The α-carbon radical, either in the original position or as a result of the α-hydrogen abstraction will initiate an α-cleavage reaction to break the bond between the β- and γ-carbons of the side chain. This will induce the partial loss of the side chain while the radical remains on the lost neutral species, and an even-electron species is formed for the remaining z fragment. Thus, the α-radical, N-terminal to the z• fragment may induce the partial side chain losses in ECD via through-bond (w ion formation, Figure 3.6 a) or through-space (Figure 3.6 b) mechanisms. The remaining z fragments contain no radicals to initiate further reaction.

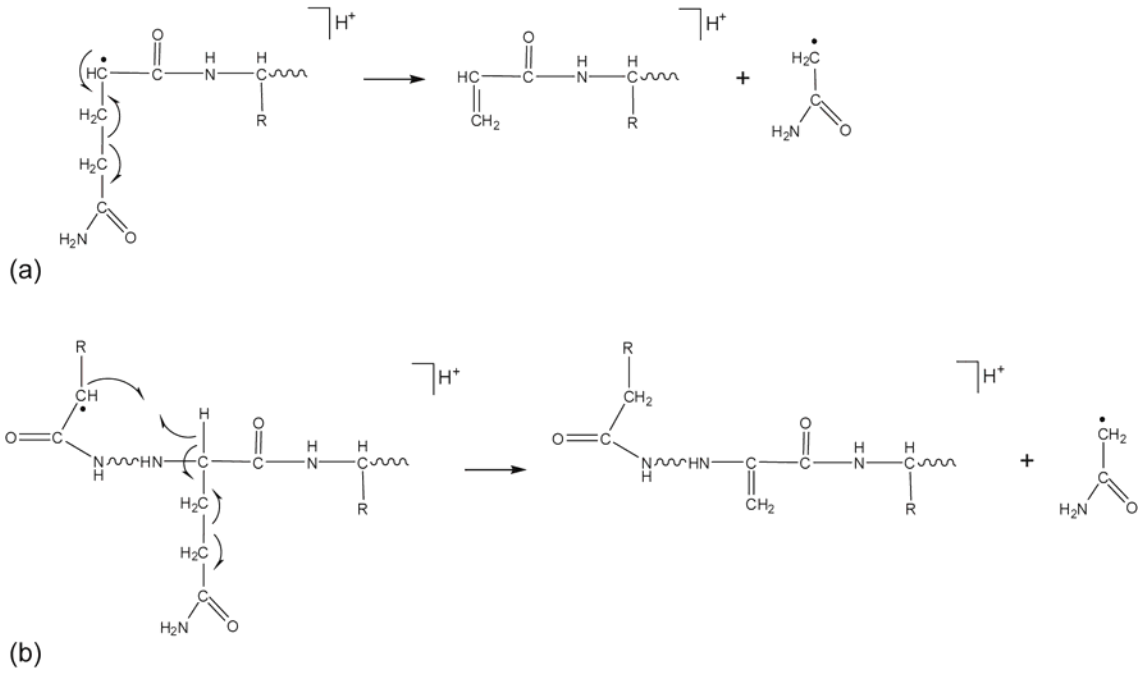

Figure 3. 6 Partial side chain loss from z• ions via alpha hydrogen abstraction [through-bond, (a) and through-space, (b)]

A series of partial glutamic acid side chain losses ($C_2H_3O_2$) from the corresponding z• ions were observed in the ECD spectrum of the deamidated form of the

βB2 crystallin peptide (4-14) as well (Figure 3.3). For this peptide, some of the side chain loss fragment ions contain multiple glutamic acid residues located either directly at, or remote from, the backbone cleavage sites. The z_8• -$C_2H_3O_2$ and z_{10}• -$C_2H_3O_2$ ions may be generated either as the w ions or formed following radical migration, while the other z• -$C_2H_3O_2$ ions had to be formed subsequent to through-space hydrogen abstraction. The high frequency of the partial side chain losses of z• ions indicates that, after the formation of z• ions in ECD, the radical on the z• ions will have ample time to migrate and induce further cleavages, without the need of additional activation. These secondary fragmentations usually do not depend on the charge location in the peptides. Thus, the CRF may be a common pathway for partial side chain losses from z• ions, especially in tryptic peptides which usually have a charge carrier at the C-terminus, that permits the detection of secondary C-terminal fragments.

This phenomenon has important implications in de novo sequencing. A specific side chain loss from z• ions does not warrant the assignment of that amino acid at the cleavage site because the loss may occur at remote sites. For example, in the differentiation of Leu/Ile, it is not sufficient to identify Leu/Ile solely based on the mass difference between the w- and the corresponding z• ions, because the partial side chain loss of Leu/Ile may not come from the N-terminus of the z• ions at all [54, 62]. In the ECD spectrum of the amyloid β peptide (25-35) (Figure 3.2), partial side chain losses of leucine and isoleucine (C_3H_7 and C_2H_5) from z_9• fragment were observed to occur several residues away from the backbone cleavage site. In addition, for the partial side chain losses of the leucine residue from z• ions in the ECD spectrum of the deamidated form of βB2 crystallin peptide (4-14) (Figure 3.3), the backbone cleavage sites were seven or eight residues away from the C-terminal leucine. Thus, it is important to assign

the residue as a Xle (meaning either Leu or Ile) based on the mass difference between adjacent backbone fragment ions before looking at the side chain loss peak for differentiation of Leu and Ile residues, and if several different Leu/Ile residues exist on the same peptide, the assignments may be ambiguous. In addition to Ile/Leu isomer differentiation, ECD can also be used to distinguish aspartic acid (Asp) and isoaspartic acid (isoAsp) based primarily on the presence of diagnostic c+57 and z•-57 ions for isoAsp containing peptides [206-210]. The Asp/isoAsp result is likely to be less affected by secondary side chain cleavages as it results from the primary backbone cleavage of the C_α-C_β bond, but for cases where several Asp/isoAsp residues are available in the same peptide, similar ambiguity to the Leu/Ile question discussed above could arise.

It has been suggested that α-hydrogen abstraction proceeds via a stepwise mechanism [55]. However, in the current study, partial side chain loss of methionine residue (C_2H_5S) from z_8• ions was observed abundantly (Figure 3.2) with the methionine residue located at the C-terminus of the amyloid β peptide (25-35), which was seven residues away from the backbone cleavage site. This suggests that α-hydrogen abstraction may also proceed through space in a single step and that the abundance of the CRF fragments is influenced by both the spatial proximity and the sequence proximity of the amino acid side chain to the backbone cleavage site. Similar through space hydrogen transfer may also occur in γ-hydrogen abstraction leading to the entire side chain losses from residues distant from the original radical site. This hypothesis is supported by the presence of a strong peak corresponding to the z_8•-Trp ion, which is not only much more abundant than the smaller z_n•-Trp (n=5-7) ions despite the comparable intensity of the related z• ions, but also has an intensity higher than that of any other side-chain losses from z_8• ions, even though the threonine and the glutamine

residues are both closer to the backbone cleavage site than the tryptophan residue. Of course, one has to take into account the reactivity of the originally formed α radical and the stability of the radical in its new position, which can also affect the abundance of the side chain losses. Nevertheless, the abundant distant side chain losses observed in the present study underscore the importance of gas phase peptide ion conformations in secondary fragment ion formations in ECD.

In addition, it was found that the w-ions are not always more abundant than the same side chain losses in longer fragment ions. For example, in Figure 3.1, the most abundant partial Gln side chain loss was from the z_8• ion, rather than the z_6• ion, the latter of which produced w_6. This is in contrast with the observation in a previous study [194], where the intensity of w_5 ions was found to be consistently at least twice as high as those resulting from the same side chain loss from larger z_n• ions, where n≥6. In that previous study, ECD was applied to synthetic peptides with mostly glycine residues which can only induce limited side-chain interactions. In more complicated peptides as those studied here, gas phase conformations will influence the secondary fragment ion abundances, even to the extent that could invalidate the criterion for differentiating w ions from u ions as proposed in earlier studies [63, 194].

3.3.3 Internal fragments associated with β-radical formation on the side chain from z• ions

Four peaks corresponding to internal fragments were found in the ECD spectrum of the deamidated βB2 crystallin peptide (4-14) (Figure 3.3). Three of them, z_8-c_8/z_7-c_9, z_8-c_9, z_{10}-c_8/z_9-c_9 are even-electron species, and one (z_8-a_9•) contains a radical. The internal fragments discussed in this study were labeled by the ion types at both ends,

with each named after the backbone fragment ion that would have been generated, had the other end been the uncleaved C- or N-terminus of the peptide. The N-terminal ends of all these internal fragments result from N-C_α bond cleavage, while the C-terminal ends mimic either a c- or an a-type fragment ion. This suggests that the internal fragment was generated from a z• ion with its radical initiating the secondary cleavage on the peptide backbone. Figure 3.7 illustrates the postulated mechanisms for the internal fragment formation. The z• radical can abstract a hydrogen atom from the β-carbon of the amino acid side chain to generate a β-radical, which can then induce α-cleavage to generate the secondary cleavage on the peptide backbone. If the α-cleavage occurs toward the C-terminal side of the β-radical, it will generate a z-a type internal fragment ion (Figure 3.7 a). However, the resulting internal fragment would be an even-electron species, which is inconsistent with the experimental observation. The α-cleavage may also proceed toward the N-terminal side of the β-radical, which will generate a z-c• type internal ion (Figure 3.7 b). After the secondary backbone cleavage, the radical on the NH- group is not stable, and it can abstract a hydrogen via the intra- or inter-molecular hydrogen transfer to become an even-electron species (pathway I in Figure 3.7 b). According to the literature, histidine and glutamine residues in c ions are good H• donors for H• transfer to z• ions [157]. In this deamidated βB2 crystallin peptide (4-14), the histidine residue is located at the N-terminus, which could be an active H• donor. The unstable N-radical may also lose an O=C=NH molecule to generate a radical z-a• type internal fragment, such as the z_8-a_9• ion observed here (pathway II in Figure 3.7 b).

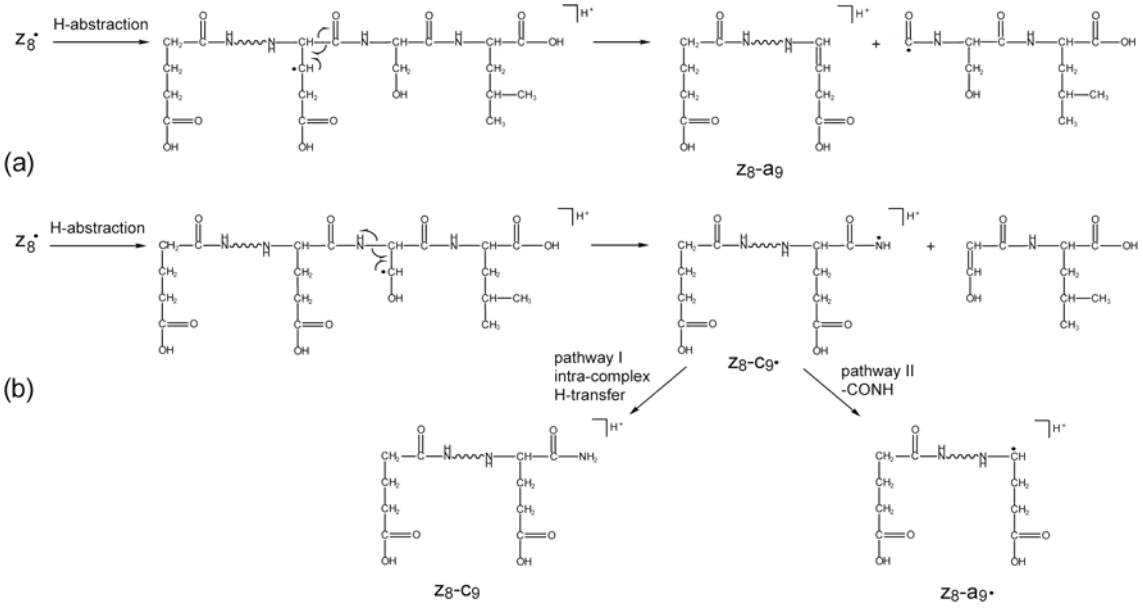

Figure 3. 7 Postulated mechanisms for the formation of internal fragments z_8-a_9 (a); z_8-a_9• and z_8-c_9 (b) via beta hydrogen abstraction in ECD of the βB2 crystallin peptide (4-14).

In the ECD spectrum of the αA crystallin peptide (1-11) (Figure 3.1), one internal fragment z_8-c_9 was also observed with double H• losses, which is known to be promoted when a threonine residue is located C-terminal to the backbone cleavage site [157]. In addition, there were two internal fragments z_{10}-a_9, z_{10}-b_{10} in the ECD spectrum of amyloid β peptide (25-35) (Figure 3.2). The internal fragment z_{10}-a_9 also had double H• loss, because of a serine residue located C-terminal to the backbone cleavage site. Radical induced b/y cleavage has been discussed in the literature, where a mechanism involving the McLafferty rearrangement was proposed to explain the unusual radical y ions observed in the CID spectra of ETD generated z• ions [203]. Similar mechanism cannot be invoked here, however, as the z_{10}-b_{10} ion is a normal even electron species. Most likely, it was formed from the internal fragment z_{10}-c_{10} with the loss of NH_3. Internal

fragments in the ECD spectra of other peptides were also observed (data not shown here), such as the βB2 crystallin peptide (4-14) in its native form. All these peptides contain basic residue(s) located in the middle of the sequences, rendering the internal fragments detectable.

The abundances of internal fragments are generally lower than the normal c/z fragments and side chain losses from z• ions, possibly due to the higher C_β-H bond dissociation energy (BDE) [190]. As reported, almost all of the amino acids have lower C_α-H BDE than C_β-H BDE [190]. Thus, it is easier to generate an α-radical to induce double bond formation between the α- and β-carbon of the side chain and the accompanying radical partial side chain loss, as shown in Figure 3.6. In addition, there also exist other radical stabilization pathways, such as intra-complex hydrogen transfer [144, 157], which can further reduce the possibilities of β hydrogen abstraction, and hence the abundances of internal ions. The internal fragments observed here provide strong supports for the free radical cascade mechanism, although their low abundances also indicate a minor role FRC may play in the formation of c and z• ions. Finally, like in the case of side chain losses, both the radical stability and the peptide conformation could play important roles in the internal fragment formation.

3.3.4 Side chain loss from z• ions and internal fragments studied in ETD

Because ECD and ETD appear to have similar fragmentation mechanisms, the CRF was also studied in ETD. In comparison, fewer CRF fragments were observed in the ETD spectra of the deamidated form of βB2 crystallin peptide, 4-14 (Figure 3.8) than in its ECD spectrum (Figure 3.3). ETD spectra of the doubly charged αA crystallin peptide and amyloid β peptide are shown in Figures 3.9 and 3.10, respectively.

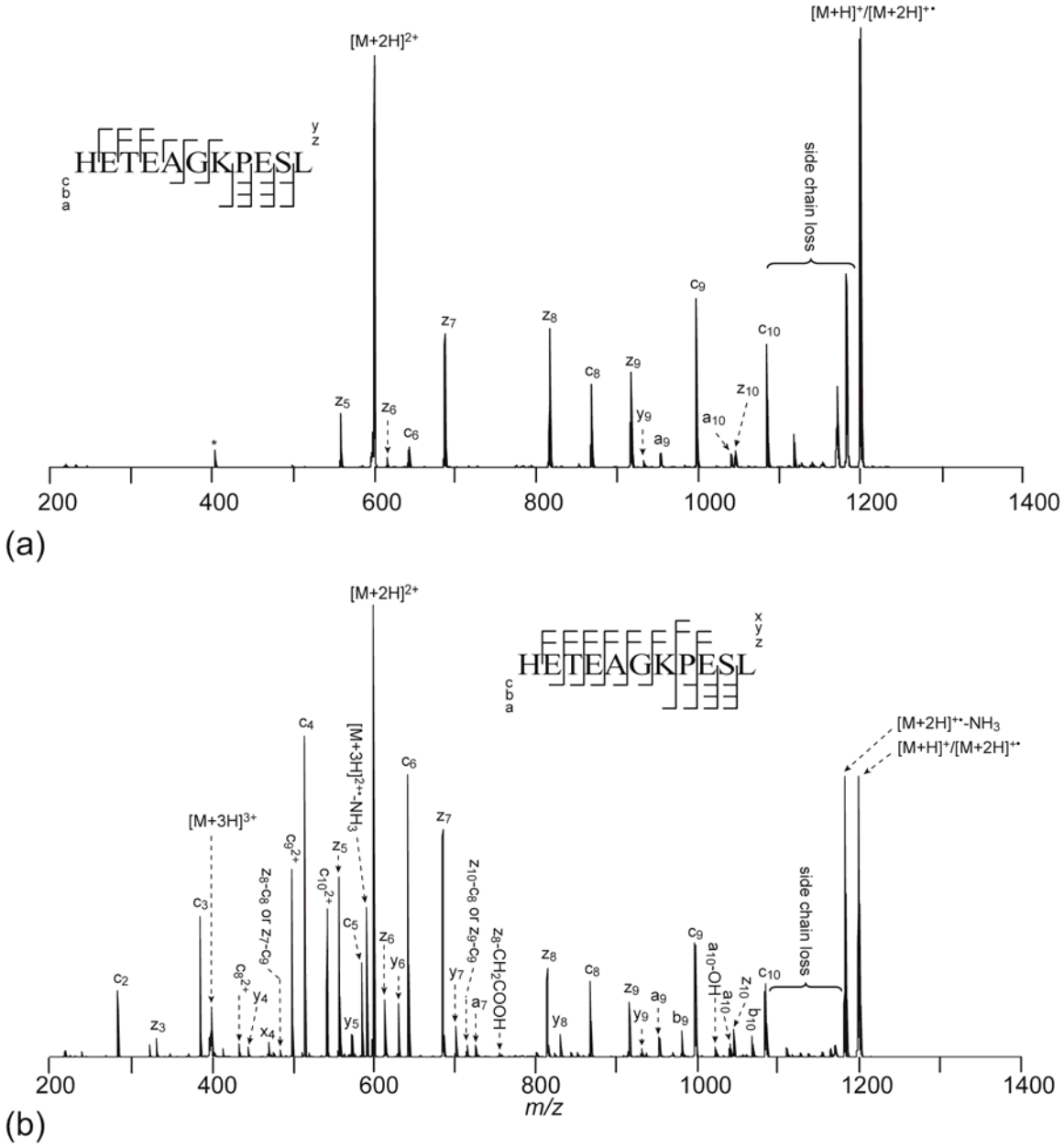

Figure 3. 8 ETD spectra of the deamidated form of βB2 crystallin peptide (4-14) generated from 2+ charge state (a) and 3+ charge state (b). ∗ represents two fluoranthene molecules. Side chain loss means loss from the charge-reduced molecular ions. Cleavage patterns are shown as the insets.

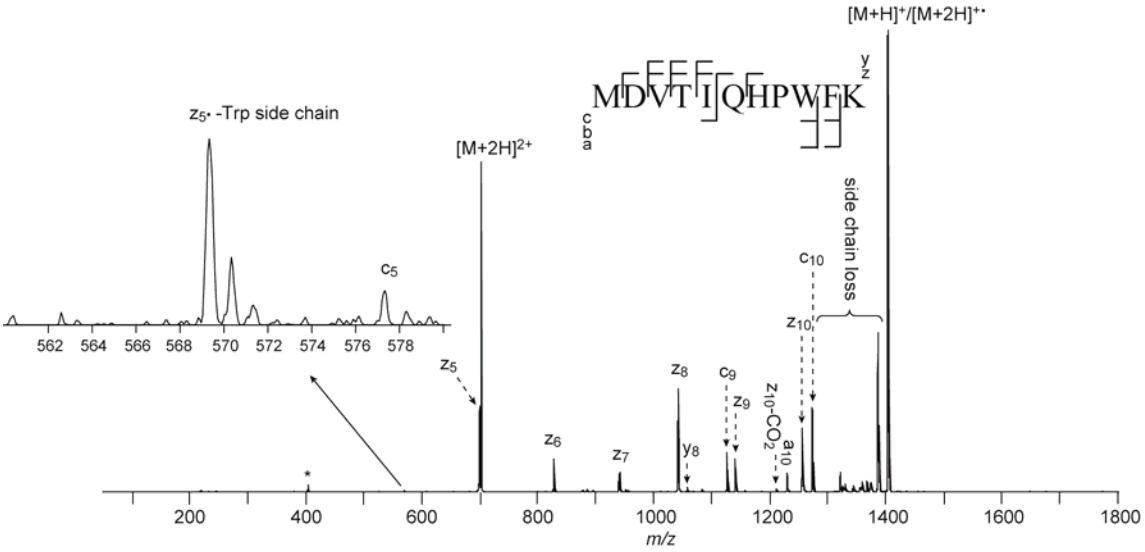

Figure 3. 9 ETD spectrum of the doubly charged αA crystallin peptide (1-11).

∗ represents two fluoranthene molecules. The cleavage pattern is shown in the inset.

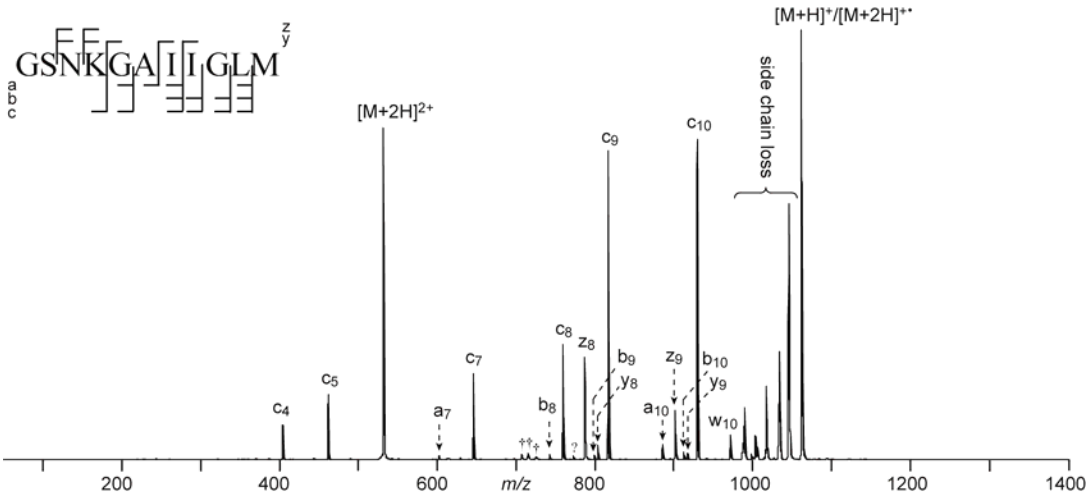

Figure 3. 10 ETD spectrum of the doubly charged amyloid β peptide (25-35). † indicates peaks that can not be assigned due to low resolution. The cleavage pattern is shown in the inset.

Figure 3.8 a shows the ETD spectrum of the doubly charged deamidated βB2 crystallin peptide (4-14). No partial/entire side chain losses from z• ions were present in this spectrum, and the only internal fragment (z_{10}-c_8/z_9-c_9) observed is of very low abundance and not labeled in the spectrum. The dramatically reduced CRF fragmentations in ETD is likely due to the smaller energy deposits in ETD than that in ECD, with the difference being the ionization potential of the anion radical. Collisional cooling in the low vacuum ion-trap instrument may also contribute to the stabilization of the radicals in z• ions and the decrease in the abundance of fragment ions formed via CRF. The ETD spectrum of the triply charged deamidated βB2 crystallin peptide (Figure 3.8 b) showed slightly more CRFs than the doubly charged one. However, the few peaks corresponding to partial side chain losses from z• ions were still of much lower intensity compared to those in the ECD spectrum of this peptide (Figure 3.3). In addition, two low abundance internal fragments, z_8-c_8/z_7-c_9 and z_{10}-c_8/z_9-c_9, were observed and are labeled, and another internal fragment z_8-a_9 had very low abundance and thus is not labeled. Although the internal fragment z_8-c_9 and the z_6• ion produced by ECD can be easily distinguished based on their accurate masses measured by the FT-ICR mass analyzer, such differentiation is impossible in ETD performed in a low resolution ion trap (Figure 3.8 b). It is also unclear whether the internal fragments in ETD of the triply charged βB2 crystallin peptide (4-14) were produced via CRF mechanism, or they were generated from double electron captures, as the doubly reduced precursor ion is readily observed in this ETD spectrum. ETD of the doubly charged αA crystallin peptide (1-11) and amyloid β peptide (25-35) were also performed, and they both showed significantly reduced secondary fragmentations (Figures 3.9 and 3.10, respectively). This reduced

CRF fragmentation in ETD could be beneficial, as it will make database searching and/or de novo sequencing a less complex task. On the other hand, ECD's ability to generate w ions and other secondary fragments makes it a valuable tool for isomer differentiation, which may otherwise be difficult when using ETD alone.

3.4 Conclusion

Two non-tryptic peptides and one tryptic peptide with histidine in the middle were used as model peptides to study the secondary fragmentation in ECD/ETD. Radical rearrangement of z• ions may proceed through three possible pathways: α-radical formation along the backbone can induce partial side chain losses from z• ions; β-radical formation in the side chain may produce internal fragments; γ-radical formation in the side chain will generate entire side chain losses from z• ions, and this may induce further radical rearrangement, leading to multiple side chain losses. All three secondary fragmentations took place at sites remote from the charge sites. Fewer CRF fragments were observed in ETD than in ECD. Entire and/or partial side chain losses from z• ions in ECD can provide additional information for isomer differentiation, help with de novo sequencing, and increase the confidence of database searching. Although in general they can not be used to identify the location of certain amino acids, they do indicate the existence of specific amino acids. The current study also indicates that the low occurrence of internal fragments in peptide ECD/ETD spectra is likely due to several reasons: lack of charge carriers in the middle of the sequence of the commonly studied tryptic peptides; the relatively higher C_β-H BDE than the C_α-H BDE, as a β-radical is needed to initiate the secondary backbone cleavage; and the low stability of the radical intermediates involved. Understanding the secondary fragmentation of z• ions is

important for the interpretation of ECD spectra with high confidence and accuracy, because in some peptide ECD spectra, many major peaks are generated from entire/partial side chain losses of z• ions. The existence of these CRFs may aid the peptide identification, but could also complicate database searching.

Chapter 4

Cyclic Rotational Heterogeneity of b Ions

4.1 Introduction

4.1.1 MS^3 methods of CAD/CAD and CAD/ECD

Tandem mass spectrometry is a powerful technique in peptide sequencing and protein identification (proteomics), with CAD [37, 44] being the most routinely used method. In CAD, energy transfer through collisions with inert gas molecules can lead to internal excitation and eventual dissociation of the precursor ions, usually via backbone amide bond cleavages, producing b- and y-type ions. The mass difference between fragment ions of the same type resulting from cleavages of adjacent amide bonds can be used to deduce the identity of the amino acid residue in between. When such a series of fragment ion masses are present in the tandem MS spectrum, the peptide sequence may be reconstructed. CAD has been extended to large biological ions [211, 212], and in-source CAD of intact protein ions up to 200 kDa in mass has been reported [213]. However, because of CAD's tendency to preferentially break the weakest bond in peptides [38, 45, 52], high sequence coverage is often difficult to achieve, particularly in the presence of labile amide bonds, such as the Asp/Glu-Pro sequence [46, 47]. Multiple stages of CAD may be performed to improve the sequence coverage. However, in such MS^n experiments, sequence rearrangements of b ions may occur as evidenced by the observation of non-direct sequence fragment ions with loss of internal amino acid residues, which can lead to erroneous peptide sequence assignments [214, 215].

On the other hand, the recently developed ECD method tends to cleave, nonselectively, many more inter-residue N-C_α bonds along the peptide backbone, and has proved to be an extremely valuable tool in post translational modification characterization because of its ability to preserve labile modifications while breaking backbone bonds. In general, though, as the size of the protein increases, ECD efficiency decreases, often due to the existence of extensive non-covalent interactions which both restrict the conformational space and prevent fragment ion separation and detection. The ECD efficiency and sequence coverage can be improved by precursor ion activation, via either infrared irradiation or collisions with inert gases, as employed in activated ion ECD [61]. It is often best to perform CAD and ECD in duet, where the complementary information provided by each method individually can be combined to allow higher confidence in sequence assignment and protein identification, either *de novo* or through database searching [216]. Conceivably, sequence coverage may also be increased by performing CAD and ECD in tandem, where a large protein ion is first dissociated by CAD, and a fragment ion which is both smaller in size and somewhat activated is then subjected to ECD [217]. Because sequence rearrangement has been observed in b-ion CAD experiments, it is important to investigate whether it also occurs when ECD is used in the second tandem MS stage. Since the fragmentation behavior of an ion is influenced by its structure, a better understanding of the fragment ion structure is beneficial for spectral interpretation and protein sequencing using the MS^3 approach.

4.1.2 The b ion structures

Of the major product ions produced by CAD, the y ions generally have the same structure as the protonated truncated peptides [218], but the b ions may exist as several

structural variants. The structure of peptide b ions has been the subject of a long-standing debate. Originally the structure of b ion was proposed as an acylium [219], although the oxazolone structure is now generally accepted as the most stable form based on its fragmentation behavior, a conclusion that is also supported by both the theoretical modeling [220] and the infrared (IR) spectroscopic study [221]. There has been growing evidence recently, showing that b ion may also assume a macro-cyclic form Figure 4.1, which can lead to sequence rotation upon CAD [214, 215, 222-229]. Most of the macro-cyclic structures were formed via the nucleophilic attack on the C-terminus by the N-terminal amino group, while in some lysyl and ornithyl peptides, the ε-amino group on the basic amino acid side chain may also be involved [230, 231]. Upon further collisional activation, these cyclic b ions can reopen at various positions to form a mixture of linear oxazolones giving rise to non-direct sequence ions. A recent review presented an extensive discussion on the structures of small b_{1-4} ions and medium-sized b_n ions generated in CAD [232].

Factors influencing the b ion cyclization have been investigated, although no obvious correlation was established. Medium-sized b ions were generally considered to have a greater potential to form macro-cyclic structure than large b ions or small b_2 to b_4 ions, which follows stepwise degradation via “the oxazolone rule” [225, 229, 233, 234]. The effect of amino acid composition was also investigated. The aliphatic amino acids, such as Ile, Leu, Val, and Ala were found prone to undergo internal elimination [214]. Selective ring opening of protonated cyclic peptides [227] may be influenced by the Pro [235] and the Asn/Gln effects [236], as well as certain acidic, basic, and amide side chains [237]. The doubly charged b ions have a higher tendency to form cyclic structures than their singly charged counterparts [214]. Further, activation methods and collisional

cooling rates may also play important roles in CAD chemistry [233], and the experimental conditions, such as the collisional activation energy and activation time, can affect the formation of macro-cyclic structure as well [228].

Very few ECD studies on b ions have been performed. In one ECD study, abundant CO loss was observed and used as evidence to support the acylium structure [238], although it was shown and later demonstrated that CO may also be lost from the oxazolone form [239]. In the current study, ECD was performed on various doubly charged medium-sized b_n ions (n=5-10) from several tachykinin peptides with multiple basic residues near their N-termini to investigate whether sequence scrambling presents a problem in the tandem CAD/ECD experiments, and to probe the b-ion structures based on their fragmentation behaviors. Theoretical calculations were also performed to identify the low energy conformers of selected b ions.

(a)

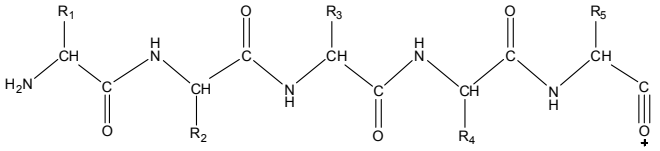

(b)

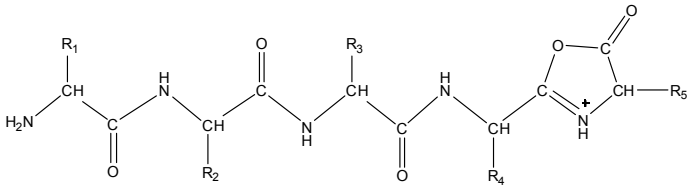

(c)

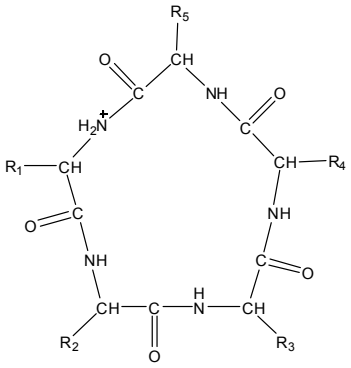

Figure 4. 1 The structures of b ions (a) acylium structure, (b) oxazolone structure, and (c) macro-cyclic structure.

4.2 Experimental section

4.2.1 Materials

Substance P (RPKPQQFFGLM-NH_2) and neurokinin A (HKTDSFVGLM-NH_2) were purchased from Sigma-Aldrich (St. Louis, MO). Two variants of substance P (RPKPEEFFGLM-OH and RPKPγEγEFFGLM-OH) and Eledoisin ($_p$EPSKDAFIGLM-NH_2) (pyrogluatmic acid, Pry, $_p$E) was custom synthesized by AnaSpec (Fremont, CA). These

peptides were used without further purification. All the other chemicals were purchased from Sigma (St. Louis, MO). Peptides were dissolved in standard electrospray solution containing 49.5:49.5:1 methanol: water: formic acid (v/v/v) to a concentration of ~2 μM for MS analysis.

4.2.2 ECD experiments

All experiments were performed on a solariX 12 T hybrid Qh-FT-ICR mass spectrometer (Bruker Daltonics, Billerica, MA), as discussed in the introduction part of this thesis. Micro-electrospray was used to introduce the sample into the mass spectrometer with a flow rate of ~100 μl/hr. In-source dissociation in the funnel-skimmer region was used to fragment the precursor ions, and the collisional energy was adjusted to maximize the abundance of the specific fragment ion for further ECD analysis. All fragment ions were focused by and pre-stored in the source octopole, and the doubly charged b ions of interest were isolated by the mass filtering quadrupole with an isolation window of ~2 *m/z* unit, accumulated in the collision cell hexapole for up to 8 ms before being transferred to the ICR cell. Low energy electrons (~1 eV) were generated by a hollow cathode dispenser mounted on the rear side of the ICR cell, with an extraction lens located between the cathode and the cell to help guide the electrons into the ICR cell. The spectra were internally calibrated by fragment ions, analyzed using the DataAnalysis software (Bruker Daltonics, Billerica, MA) and manually interpreted, with a typical mass accuracy around 0.5 ppm.

4.2.3 Theoretical calculation

The conformations of the b_6^{2+} and b_8^{2+} ions of peptide substance P were investigated theoretically. First, molecular dynamics (MD) simulations were performed to generate low energy conformer candidates. The CHARMm force field was applied in MD simulations, using the NVT canonical ensemble technique. In order to explore the conformation space as comprehensive as possible, the system temperature was chosen at 1000K. Each MD step was integrated at 1 fs interval, and each trajectory lasted 200 ps. For each trajectory, geometries were recorded every 5 ps, and then subjected to temperature-independent energy minimization using molecular mechanics methodology. The MD simulations were performed using the Discovery Studio 5.0 software (Accelrys, CA).

The energetics of conformer candidates generated by MD simulations were calculated using quantum chemistry methodologies. Due to the relatively large size of these peptide ions, restricted self-consistent field based *ab initio*- (RHF) approach with small 3-21G basis set was utilized for geometry optimization. In order to minimize the energy inaccuracy resulted from the omission of correlation energy, density functional theory (DFT)-based single point energy calculations were carried out on optimized HF/3-21G geometries using the hybrid of Becke's exchange and Lee-Yang-Parr's correlation functionals (B3LYP) with 6-31G(d) basis set. The B3LYP/6-31G(d) electronic energies were used as zero Kelvin enthalpy without zero-point vibrational energy correction. All HF and DFT calculations were carried out using the Gaussian 03 program suite [240] installed on the IBM katana cluster at Boston University.

4.3 Results and discussion

Three tachykinin neuropeptides [241-243] (neurokinin A, eledoisin, and substance P), and two potential deamidated forms of substance P were used as model peptides. The tachykinin peptides are neurotransmitters and can rapidly induce the contraction of gut tissue [244]. They have a common C-terminal sequence of: Phe-Xxx-Gly-Leu-Met-NH_2, which is considered as the message domain, with Phe important for receptor binding and the Xxx important for receptor selectivity [245].

4.3.1 ECD of b ions from neurokinin A and eledoisin

Neurokinin A (HKTDSFVGLM-NH_2), also known as substance K, is a homologue of substance P (RPKPQQFFGLM-NH_2) [242]. In Figure 4.2 a and b, ECD of the b_9^{2+} and b_8^{2+} ions from neurokinin A generated a near complete series of c ions, which can be produced from the linear oxazolone structure. However, these c ions comprise only a small portion of the product ions. In the ECD spectrum of the b_9^{2+} (HKTDSFVGL^{2+}) ion of neurokinin A, the most intense peaks correspond to a series of sequence rotated ions of the z-b type with HK as their C-terminal sequence: LHK, GLHK, VGLHK, FVGLHK, SFVGLHK, and DSFVGLHK. A z-b ion is a fragment ion which resembles a normal z• ion at its N-terminus and a normal b ion at its C-terminus. Other types of sequence rearranged fragments were also present, labeled as the z-a and z-c ions in the spectrum. These other ions do not necessarily terminate with the HK at their C-termini, and were in general of lower abundances. The ECD spectrum of the b_8^{2+} (HKTDSFVG^{2+}) ion of neurokinin A showed a similar cleavage pattern to the b_9^{2+} ion, with the major peaks corresponding to the normal c ions and sequence rotated GHK, VGHK, FVGHK, SFVGHK, and DSFVGHK (z-b ion) fragments. The z-a and z-c ions were also observed at lower abundances, again not necessarily with an HK C-terminal sequence. ECD of the

smaller b_7^{2+} ($HKTDSFV^{2+}$) ions from neurokinin A produced predominantly sequence rotated fragment ions, VHK, FVHK, and SFVHK (z-b ion), with no c ions, Figure 4.2 c.

The abundant z-b ions observed may be explained by the formation of a macro-ring structure of the original b ion, connecting its C-terminal carbonyl group to its N-terminal amino group, followed by ring reopenings to form new sequence rotated linear oxazolones, predominantly with lysine as its C-terminus, Figure 4.3. The preference is likely driven by the favorable formation of an oxazolone with histidine as the amino acid residue next to the C-terminus, characteristic of an ergodic process [246]. ECD of the sequence rotated linear b ions can produce a series of z-b fragment ions as observed in Figure 4.2 a and b. As the charge carrying histidine and lysine residues were located near the C-terminus of the newly formed linear oxazolone, no sequence rearranged c ions were observed. Meanwhile, ring reopening by cleaving the N-C_α or C_α-C(=O) bond is energetically unfavorable, thus the z-a and z-c ions observed were likely formed via a different mechanism. Note that, b ions, if assuming a macro-cyclic form have essentially the same structures as the cyclic peptide ions. It has been reported that ECD of doubly charged cyclic peptides can generate numerous internal fragment ions, which were proposed to be formed via the free radical cascade mechanism [56]. Likewise, the z• radical produced by the N-C_α bond cleavage within the macro-ring of the b ions studied here can also initiate free radical cascade, leading to the formation of the z-a and z-c ions, via apparent loss of one or multiple internal amino acid residues (Figure 4.3). The major difference between the formation of the z-b ions, and that of the z-a and z-c ions is that the former proceeds via ring-opening prior to ECD and the latter via ECD before ring-opening followed by FRC. Thus, z-b ions were selectively formed with HK as their C-terminal sequence, as expected from an ergodic ring-opening process; while z-a and

z-c ions tend to contain more random sequences, as expected from the non-statistical behavior of ECD. These results indicated that b ions can exist as a mixture of linear and cyclic structures, and their interconversion in the gas phase occurred prior to ECD. Since the sequence rearrangement occurred before ECD, peptide sequencing using the MS^3 data could be erroneous, even when ECD was used in the second tandem MS stage.

Although eledoisin ($_pEPSKDAFIGLM\text{-}NH_2$) has a similar C-terminal sequence as that of the neurokinin A, sequence scrambling was not observed in the ECD spectra of its b_{10}^{2+} and b_9^{2+} ions, as shown in Figure 4.4 a and b, respectively. This is perhaps not surprising in light of the presence of the N-terminal pyroglutamic acid residue, as its N-terminal amino group is blocked by the succinimide structure, thus preventing its conversion to the cyclic form via the N- and C-termini connection. This phenomenon is similar to the previous observation that the N- and C-termini cyclization of b ions can be effectively blocked by acetylation of the N-terminal amino group [214, 222-224].

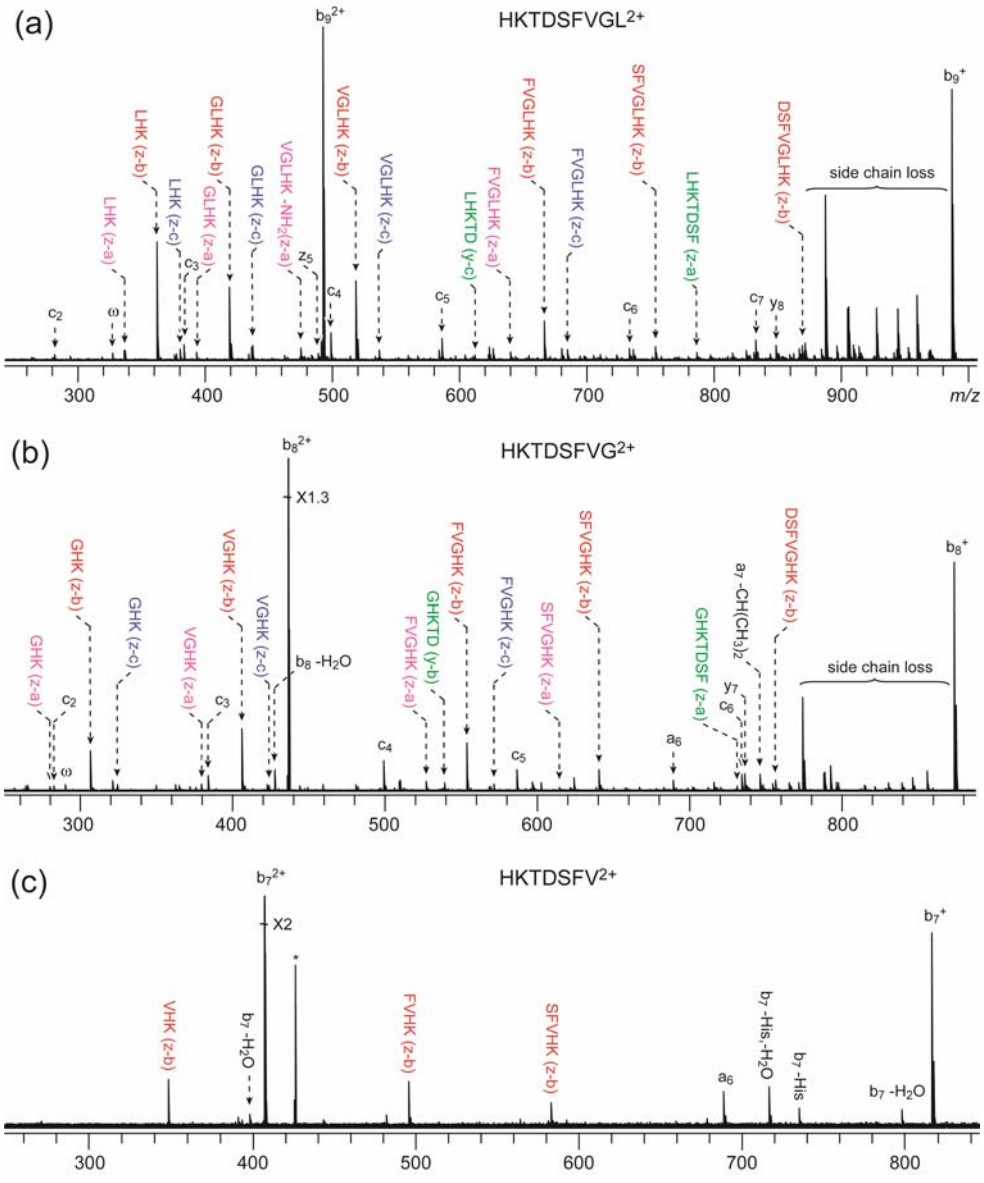

Figure 4. 2 ECD spectra of doubly charged b_9 (a), b_8 (b), and b_7 (c) ions from neurokinin A (HKTDSFVGLM-NH_2). The z-b, z-a, and z-c resembles the N- and C-terminal structures. Partial side chain loss and small molecule loss are labeled as molecular composition. Peaks marked with "-amino acid residue" represent the entire side chain loss. ∗ stands for noise peak. ω stands for harmonic peak.

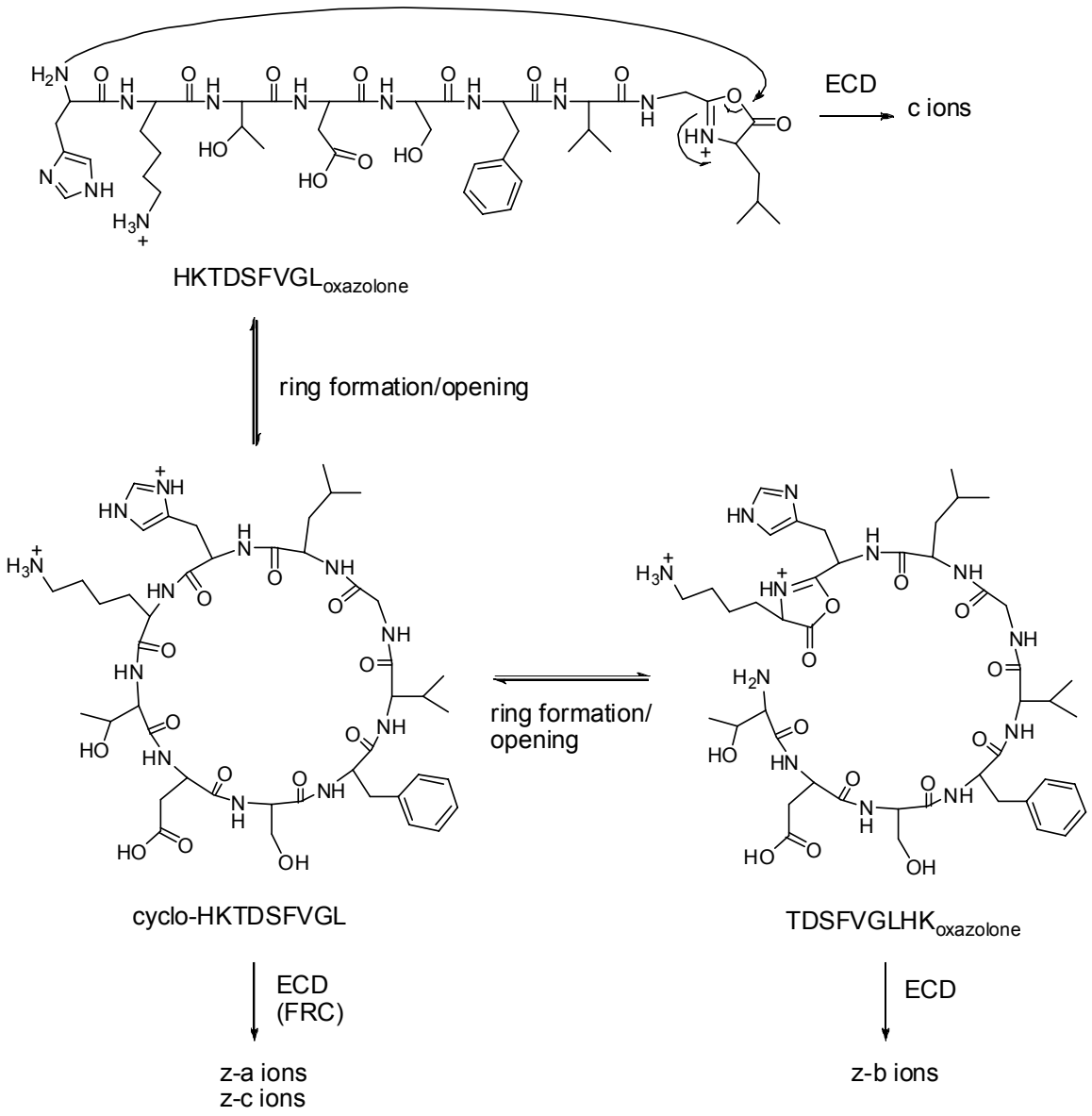

Figure 4. 3 Proposed ECD fragmentation pathway of neurokinin A b_9^{2+} ion. FRC means free radical cascade.

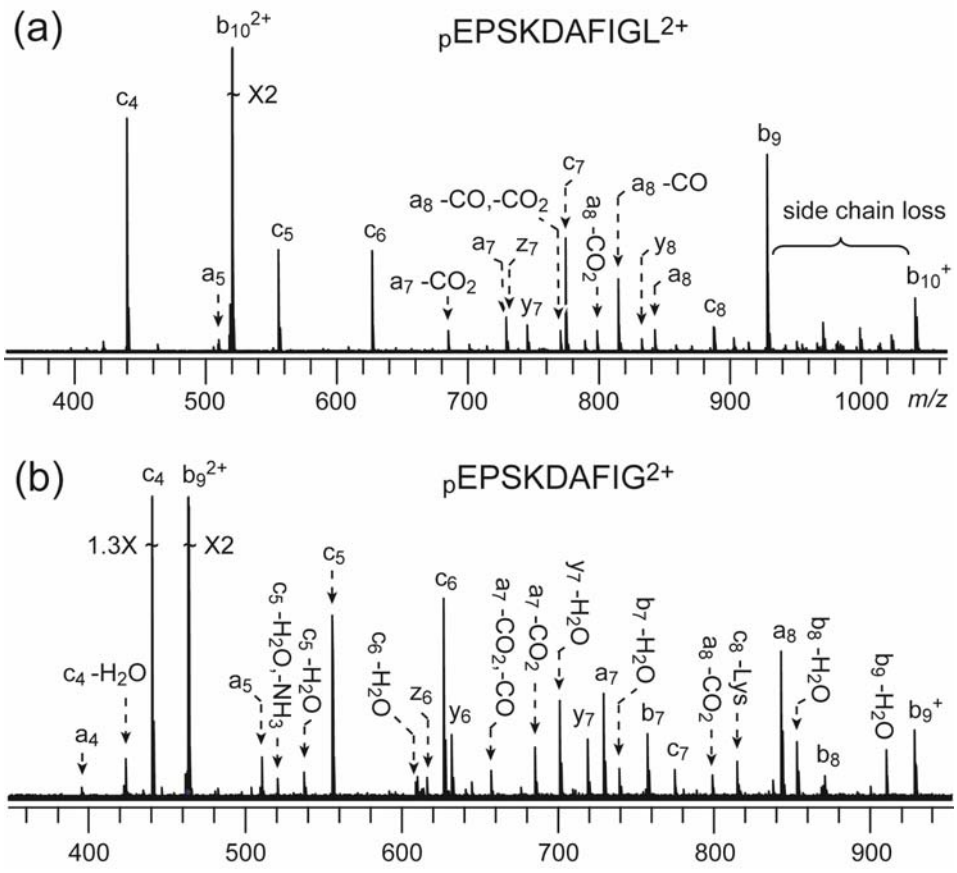

Figure 4. 4 ECD spectra of doubly charged b_{10} (a) and b_9 (b) ions from eledoisin ($_pEPSKDAFIGLM\text{-}NH_2$). Peak labeling follows the same convention as in Figure 4.2.

4.3.2 ECD of b ions from substance P

In addition to the normal c ions, ECD of doubly charged b_n^{2+} ions (n = 10 to 5) from substance P (RPKPQQFFGLM-NH_2) produced a series of fragment ions that correspond to c ions with additional lysine side-chain loss, labeled as c_m-Lys, m = 4 to (n-1), Figure 4.5 and 4.6. This is at first surprising, because c ions do not usually contain a radical that is capable of initiating further side-chain losses as in the case of z• ions

[190, 193, 194, 247]. The formation of these unusual fragments may be explained by the presence of another type of cyclic b ion structure, where the C-terminal carbonyl group forms an amide bond with the lysine side-chain amino group. In ECD of this C-terminus-Lys linked cyclic b ion, the initial N-C_α bond cleavage will not result in the formation of individual c and z• fragments, as they are still held together by a covalent bond. The radical on the α-carbon of the z• moiety can migrate through space to induce the lysine side-chain loss and produce the c-Lys fragment (Figure 4.7). Because the initial N-C_α bond cleavage within the ring can occur at various positions, a series of c_m-Lys fragments can be generated. Similar cyclization involving the ε-NH_2 group of the Lys side chain to form a caprolactam structure has been reported previously [248].

The relative abundance of the c_m-Lys fragments to that of the c_m ions depends on the size of the precursor b_n ions: going up from n = 10 to 8 (Figure 4.5) and then down from n = 7 to 5 (Figure 4.6). The c_4-Lys fragment ions in the ECD spectrum of the b_5^{2+} ions was assigned with a relatively big error (~2 ppm) compared to the ~0.5 ppm mass accuracy in all other data generated in this study. This may be due to the very low signal-to-noise ratio (S/N) of the monoisotopic peak of the c_4-Lys fragment in the b_5^{2+} ion ECD spectrum, as it was difficult to isolate and accumulate the very low abundance b_5^{2+} precursor ions generated by funnel-skimmer dissociation. The ECD spectrum of the b_8^{2+} ions was dominated by the c_m-Lys ions, with almost no c ions. Thus, the majority of b_8^{2+} ions were likely present in the C-terminus-Lys cyclized form, which is consistent with the previous study of oligoglycine b_8 ions by another group [233]. For most other b_n^{2+} ions, both the c_m and c_m-Lys ions were abundantly present in the ECD spectra, indicating that these b ions likely existed as a mixture of the two forms, both in appreciable quantities. No sequence rearranged fragment ions were observed in any substance P b ion ECD

spectrum. Thus, the N- and C-termini connected macro-ring structure was either not formed, or formed but preferentially reopened at its original position.

In addition, the ETD study [64] of the doubly charged b_{10} ion of substance P was performed on an ion-trap instrument as described previously [247]. Although a series of peaks corresponding to the c_m-Lys fragment ions were also observed, they were in general present in much lower abundances (data not shown here). The lower abundance of the c_m-Lys fragment ions in ETD might be due to the lower amount of energy available comparing to ECD, reducing the likelihood of secondary fragmentations.

Cyclic structure formation involving the Lys side chain has been proposed previously. In a CAD study of the doubly charged b_{10}, b_9 and b_7 ions of substance P, wholesale transfer of one (L) or two (GL) residues from the C-terminus of b ions to lysine side chain were observed, suggesting the formation of a cyclic structure connecting the lysine side chain to the C-terminus [230, 231]. For other peptides, fragmentation after ring opening at one of the several ring positions was also observed. The presence of proline residue close to the lysine or ornithine residue on the C-terminal side was considered to promote the ring structure formation.

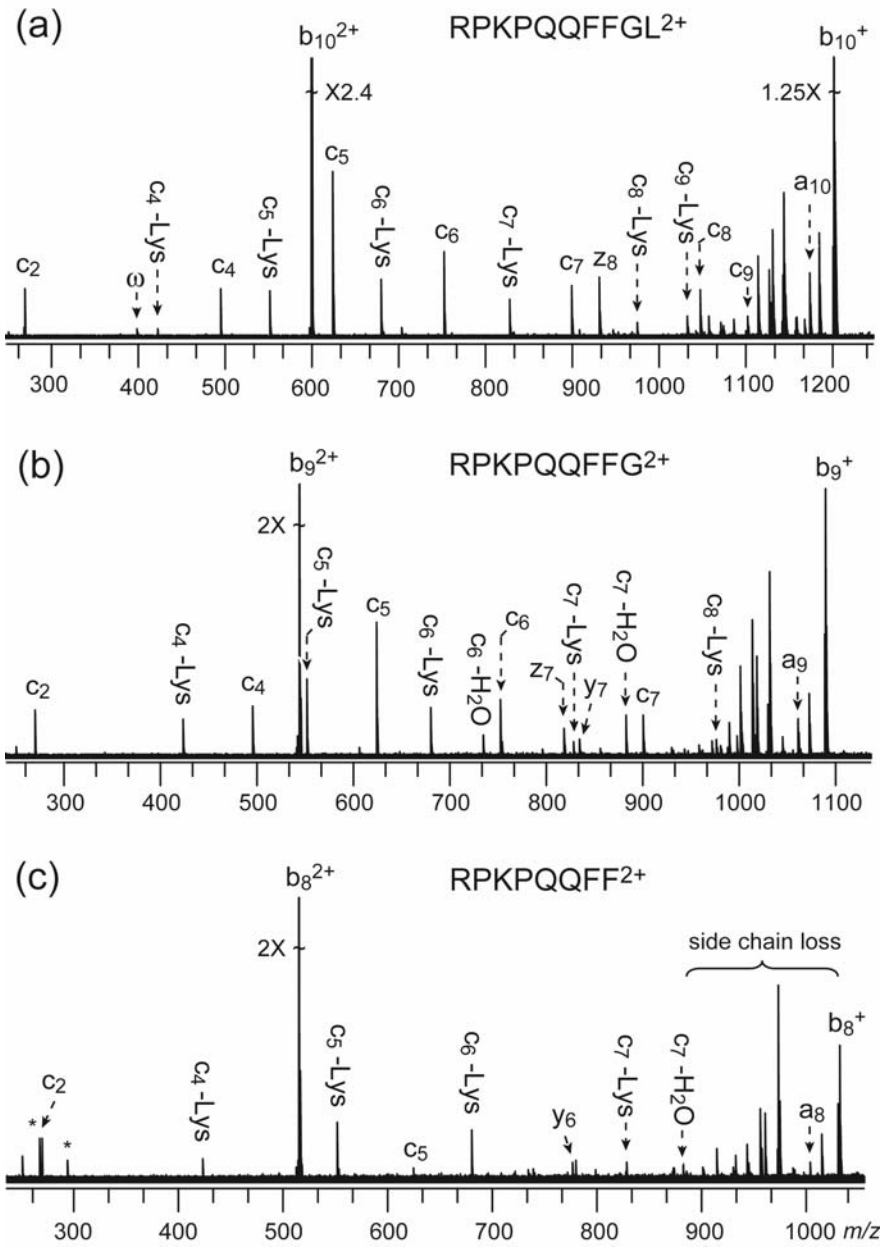

Figure 4. 5 ECD spectra of doubly charged b_{10} (a), b_9 (b), and b_8 (c) ions from substance P (RPKPQQFFGLM-NH_2). Peak labeling follows the same convention as in Figure 4.2.

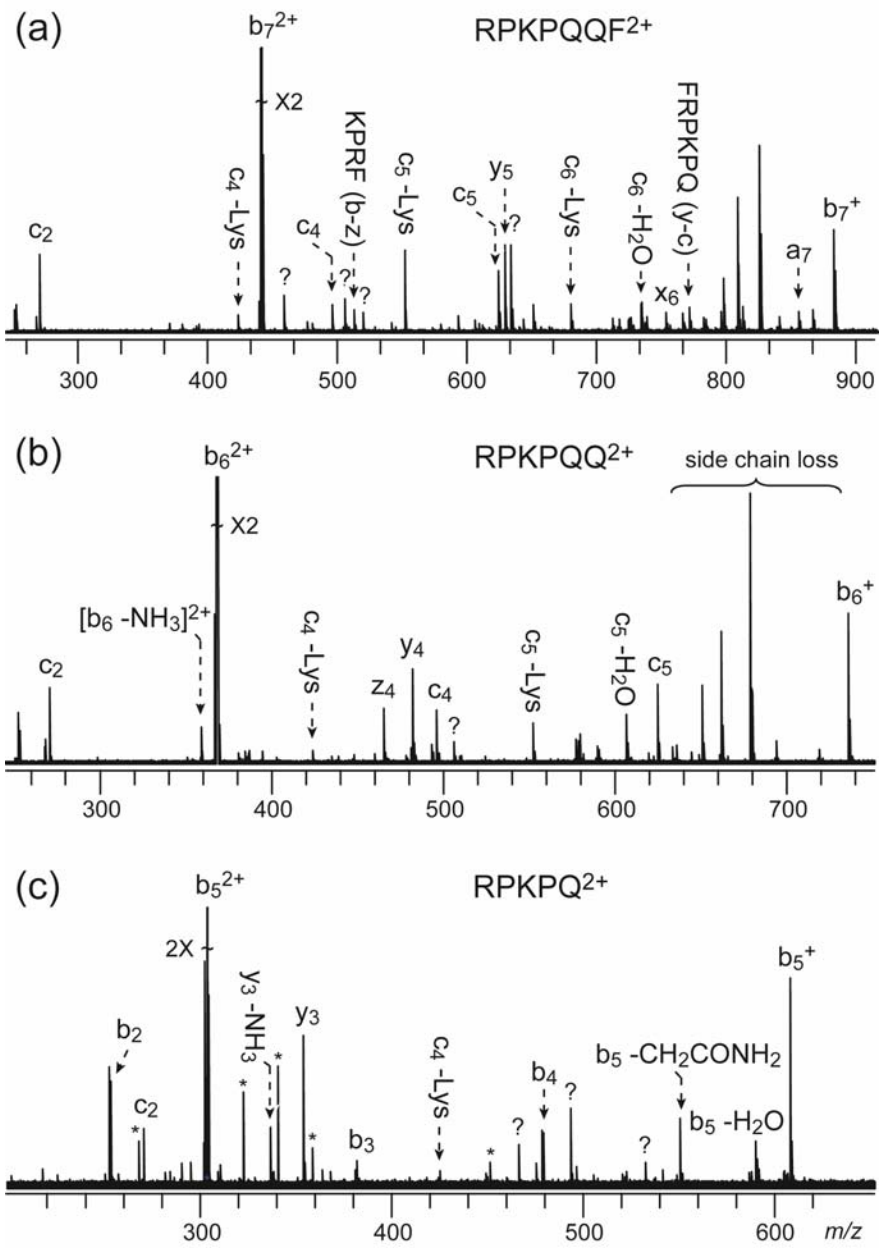

Figure 4. 6 ECD spectra of doubly charged b_7 (a), b_6 (b), and b_5 (c) ions from substance P (RPKPQQFFGLM-NH_2). Peak labeling follows the same convention as in Figure 4.2.

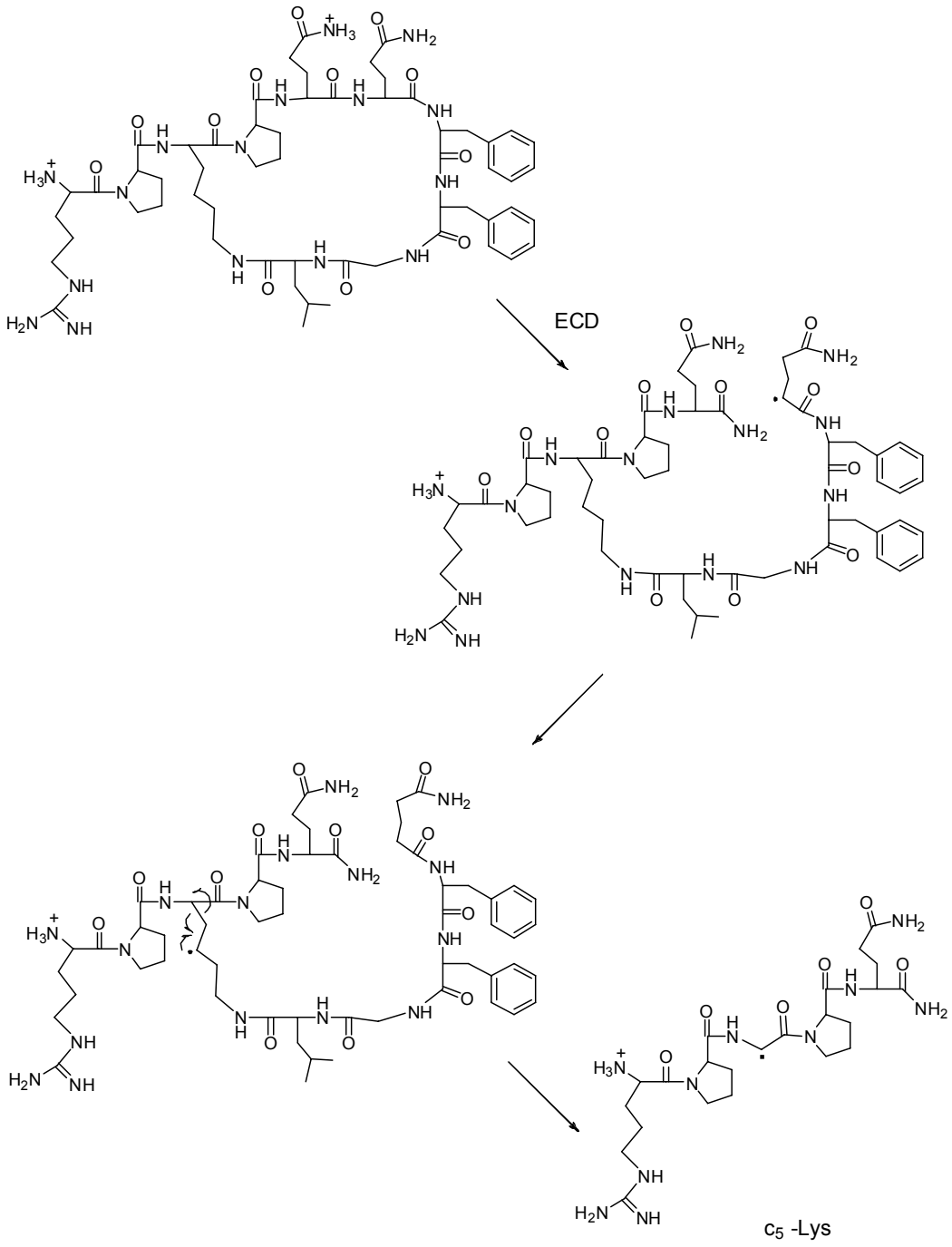

Figure 4. 7 Proposed mechanism for the formation of c_m-Lys side chain ions in ECD of substance P b_{10}^{2+} ion.

To better understand the structure and ECD behavior of these doubly charged b ions, the geometries and energetics of lower energy conformers of substance P b_6^{2+} and b_8^{2+} ions generated by MD simulations were studied at B3LYP/6-31G(d)//HF/3-21G level of theory. The optimized structures and relative stabilities of the lowest energy linear (oxazolone), C-terminus-Lys linked, and C- and N-termini linked cyclic structures of b_8^{2+} and b_6^{2+} ions generated from substance P were shown in Figure 4.8 and Figure 4.9, respectively.

For the b_8^{2+} ($RPKPQQFF^{2+}$) ion, the lowest energy oxazolone structure (which has protonated guanidine and oxazolone groups solvated by N-terminal amino nitrogen and backbone carbonyl oxygen, respectively) is 6.6 kcal/mol higher in energy compared to its FK-linked cyclic counterpart (Figure 4.8) that has both positive charge sites solvated by backbone carbonyl oxygen atoms. Consequently, c_m-Lys ions are expected to be the dominant fragments in the ECD spectrum of b_8^{2+}, as observed experimentally.

For the b_6^{2+} ($RPKPQQ^{2+}$) ion, the QK-linked cyclic structure (Figure 4.9 a) is 12.7 kcal/mol energetically preferred over oxazolone structure (Figure 4.9 b). If energetics is the only factor taken into consideration, one should expect the predominance of QK-linked cyclic structure over the linear oxazolone one, which would lead to predominant formation of c_m-Lys fragment ions as well. The coexistence of both c_m and c_m-Lys ions with comparable abundance in b_6^{2+} ion's ECD spectrum indicates that other factors may also play important roles in the ECD process. One possibility is that, although the QK-linked cyclic structure has lower energy than the oxazolone one, it might not be easily accessed due to the entropy effect. Therefore, both types of structures are abundantly populated.

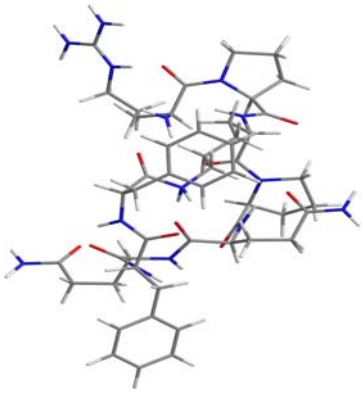

(a) 0.0

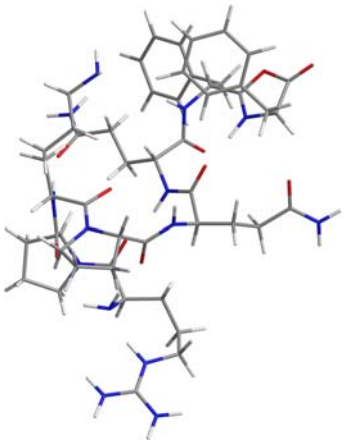

(b) 6.6

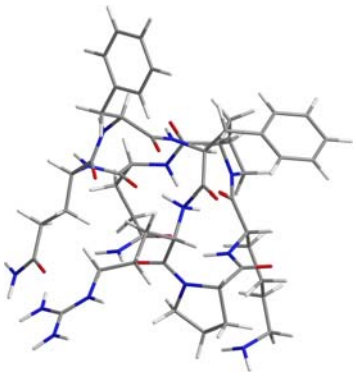

(c) 16.3

Figure 4. 8 Calculated lowest energy structures of substance P b_8^{2+} ion and their relative energetic stability obtained at B3LYP/6-31G(d)//HF/3-21G level of theory: (a) FK-linked cyclic structure, (b) linear oxazolone structure, and (c) FR-linked cyclic structure. Numbers are in the unit of kcal/mol.

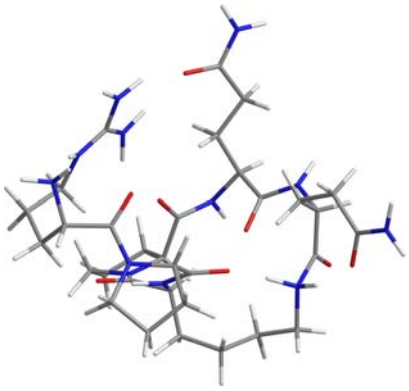

(a) 0.0

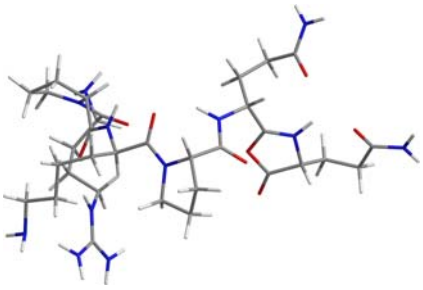

(b) 12.7

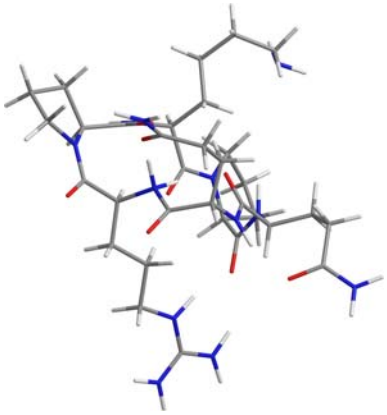

(c) 16.0

Figure 4. 9 Calculated lowest energy structures of substance P b_6^{2+} ion and their relative energetic stability obtained at B3LYP/6-31G(d)//HF/3-21G level of theory: (a) QK-linked cyclic structure, (b) linear oxazolone structure, and (c) QR-linked cyclic structure. Numbers are in the unit of kcal/mol.

Finally, as shown in Figure 4.9 and Figure 4.8, the N-C termini linked cyclic structures, QR-linked for the b_6^{2+} and FR-linked for the b_8^{2+}, are about 16 kcal/mol higher in energy compared to the lysine linked cyclic structures. Therefore, they are not expected to comprise an appreciable fraction of the total ion population. This is consistent with the experimental observation that no sequence rotated fragment ions were observed in the ECD spectra of either b_8^{2+} or b_6^{2+} ions.

4.3.3 ECD of b ions from two variants of substance P

The ECD spectra of the doubly charged b_{10} and b_9 ions from two potential deamidated forms of substance P peptides (RPKPEEFFGLM-OH and RPKPγEγEFFGLM-OH) are shown in Figure 4.10 and Figure 4.11, respectively. Series of C_m-Lys fragment ions were observed, similar to the ECD spectra of b ions from substance P. This suggested that the substitution of these middle amino acids did not influence the Lys and C-terminus linked cyclic structure formation of b ions in gas phase. In the insets of Figure 4.11, there were peaks corresponding to c+57 ions, which were the characteristic ions for γGlu containing peptides and will be discussed in chapter 6.

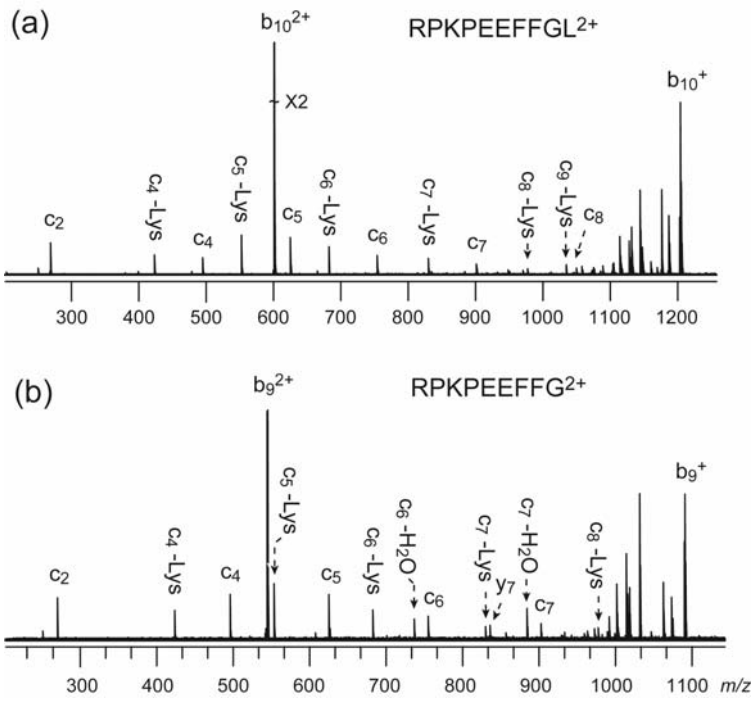

Figure 4. 10 ECD spectra of doubly charged b_{10} (a) and b_9 (b) ions from substance P variant peptide (RPKPEEFFGLM-OH). Peak labeling follows the same convention as in Figure 4.2.

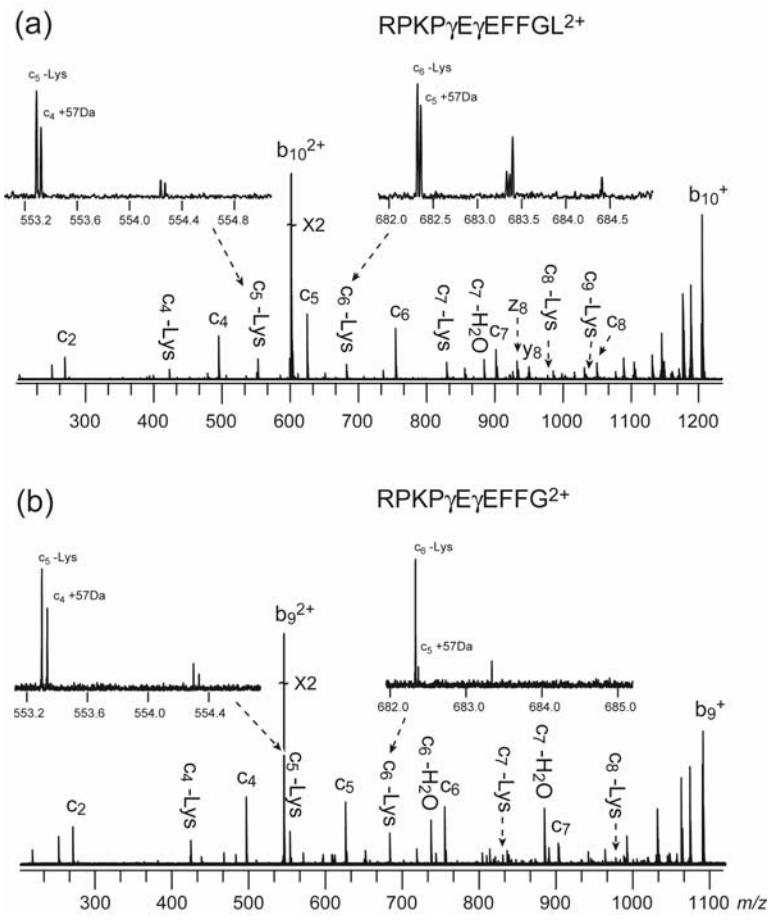

Figure 4. 11 ECD spectra of doubly charged b_{10} (a) and b_9 (b) ions from substance P variant peptide (RPKPγEγEFFGLM-OH). Peak labeling follows the same convention as in Figure 4.2.

With the sole exception of the b ions from eledosin, which does not contain a free N-terminal amino group, macro-ring formation was observed in all b ions studied here, either via the N- and C-termini linkage or via the Lys side chain and C-terminus connection. The identity of the C-terminal amino acid residues, on the other hand, did not seem to play an important role in the cyclic structure formation of the limited samples studied here. The macro-cyclic structure appeared to be abundantly formed in medium-

sized b ions studied here, with sizes ranging from b_6^{2+} to b_{10}^{2+}. The abundance of the cyclic structure in smaller b ions (e.g. the b_5^{2+} ion from substance P) is significantly lower, possibly due to the severe ring strain. Meanwhile, the trend observed in ECD of substance P b_n ions (n = 8 to 10) indicated that the cyclic structure formation may also be disfavored as the size of the b ions increases. This could be due to the entropic factor, i.e. it is more difficult for larger b ions to find the low-energy conformation that brings the N-terminal or side-chain amino group close to the C-terminal oxazolone in the increased conformational space. ECD of even larger b_n ions (n>10) is currently under investigation.

Finally, it is important to note that while sequence scrambling seems to be a common feature among ECD of smaller b_n ions (n≤10), ECD of small b ions are rarely needed in peptide sequencing and protein identifications, as the N-terminal sequence of a protein is usually adequately covered in MS^2 experiments. In a recent study done here [217], it has been reported that the CAD/ECD approach can be a valuable tool to provide sequence information in regions where CAD or ECD alone or CAD based MS^n can not access. In that study, no sequence scrambled fragment ions have been observed in ECD of large b_n ions (n>30) from medium-sized proteins, hemoglobin and transthyretin (TTR). In addition to the entropic factor mentioned above, lack of cyclization in these very large b ions may also be due to the extensive charge solvations that stabilize the oxazolone structure.

4.4 Conclusion

Both the ECD experimental and theoretical works clearly demonstrated that a peptide b ion may exist as a mixture of several different forms in the gas phase, with their propensities influenced by its size, N-terminus, and possibly the side chains of

basic amino acid residues. Blockage of the N-terminal amino group eliminated the formation of the N- and C- termini linked cyclic structure. When a lysine residue is present in the sequence, cyclization via the C-terminus-Lys linkage may also occur. The possibility of cyclization is the highest in medium-sized b ions, and becomes lower in very small b ions due to the ring strain, as well as in large b ions due to the decreased likelihood of finding the geometry necessary for ring formation. Sequence rotated fragment ions can be formed from the cyclized structure after ring reopening at different positions from the original linkage site, with ring-opening following the common preference observed in CAD experiments. When the C-terminus-Lys linkage was formed, unusual fragments corresponding to the lysine side-chain loss from the c ions were observed. The presence of these sequence rotated and unusual secondary fragment ions can complicate the spectral interpretation and may also lead to errors in peptide sequencing. The current results underscored a potential problem in protein identification and peptide sequencing based on the data generated from multiple stages of tandem mass spectrometry. However, such problem may not be as serious when using the CAD/ECD approach to sequence large proteins, where MS^3 is needed the most.

Chapter 5

Use of ^{18}O Labels to Monitor Deamidation during Protein Trypsin Digestion Processes

5.1 Introduction

5.1.1 Deamidation and its mechanism

As a spontaneous nonenzymatic PTM of proteins, deamidation plays an important role in protein degradation and is postulated to function as a timer in aging [79, 249-251]. As it has been discussed in previous chapters, deamidation occurs on Asn and Gln residues, and has been observed and characterized in a wide variety of proteins *in vivo* and *in vitro*. The Asn deamidation takes place much more rapidly than that of Gln, because the latter requires the formation of a six-membered cyclic imide intermediate which is entropically less favorable [94, 252]. Upon deamidation, the asparaginyl residue is converted to a mixture of isoAsp and Asp residues.

Factors that influence deamidation rates include: protein sequence [89, 252, 253], secondary structure [83], local three-dimensional structure [81], pH, temperature, ionic strength, buffer ions, turnover of the protein and other solution properties [80, 88], etc. In many cases, the deamidation rate is strongly influenced by the primary structure and the neighboring amino acids. It is well known that Gly and Ser located on the C-terminal side of Asn greatly accelerates Asn deamidation. Ser, and to a lesser extent, Thr and Lys

---

[1]This chapter has been partially/entirely reproduced from Xiaojuan Li, Jason J. Cournoyer, Cheng Lin, and Peter B. O'Connor. Use of ^{18}O labels to monitor deamidation during protein and peptide sample processing. *Journal of the American Society for Mass Spectrometry.* 2008, 19, 855-864. Copyright 2010 Elsevier.

preceding Asn (at its N-terminal side) can also facilitate the Asn deamidation [80, 88]. The small side chains of Gly and Ser allow extensive conformational changes, while amino acids with branched, bulky, hydrophobic side chains or Asn/Gln located close to intramolecular disulfide bonds reduce the conformational flexibility necessary for the intermediate formation [252]. Furthermore, the secondary and tertiary structures can also determine whether or not deamidation actually occurs [94]. Stabilization of Asn residues by higher order structures has been observed, which may result from conformational restrictions and the reduced nucleophilic reactivity of the backbone NH centers due to hydrogen bonding [82, 83]. Also, the structural change induced by one deamidation site may further influence the deamidation rates at other sites [252].

Deamidation may occur via two different pathways depending on the pH of the solution which can also affect the product abundances. In acidic conditions (pH < 5), deamidation proceeds via the acid-catalyzed pathway, where direct hydrolysis of the Asn residue side-chain amide group results in the formation of Asp as the only product. When pH value is higher than 5, deamidation primarily occurs via a base-catalyzed pathway, in which the Asn residue is converted to a succinimide intermediate that can then hydrolyze rapidly to produce L-Asp and L-isoAsp, typically in a 1:3 ratio for random-coil peptides, see Figure 1.9 in chapter 1 [89]. This reaction is reversible in aqueous solution. The deamidation rate reaches a minimum at approximately pH = 5. In basic conditions, the rate-limiting step is the intramolecular nucleophilic attack on the side chain carbonyl by the nitrogen. In acidic conditions, the rate limiting step is the direct elimination of NH_2- from the anionic tetrahedral intermediate [79, 80, 85, 254].

5.1.2 Asn deamidation detection methods

Charge sensitive techniques can be used for the detection of deamidation, because deamidation introduces negative charges to a protein which shifts its isoelectric point (pI). MS methods can also be used in deamidation studies, based on the a +0.984 Da mass shift introduced by each deamidation, which can be detected and the extent measured using the mass defect and the envelope deconvolution method [255-258]. The advantages of these techniques are that protein samples can be introduced into a Fourier transform mass spectrometer without sample pretreatment (e.g. digestion, separation, absorption, and ionization), and that protein deamidation can be measured quantitatively without tandem MS/MS analysis. While determining the conversion of Asn to Asp/isoAsp is relatively straightforward, distinguishing the isomeric products Asp and isoAsp is more challenging. Several methods for the Asp/isoAsp differentiation exist, including nuclear magnetic resonance (NMR) [259], HPLC [260], Edman-based sequencing [261], and antibody detection [262], although they all have certain limitations: the former three typically require relatively large quantity of protein samples, and the latter requires highly specific and expensive antibodies.

MS/MS methods can facilitate the detection and quantification of deamidation while only requiring very small amount of samples, e.g. fmol to pmol. In addition, they can also provide very specific information on the deamidation sites and help differentiate and quantify the ratio of the Asp and isoAsp products. In CAD, the two isomers have different, identifiable side-chain fragmentation patterns for the C-terminal ions [261, 263, 264]. In ECD [38, 45, 52, 56] and ETD [64, 265], their fragmentations can produce different diagnostic ions, i.e., the $[(M+nH)^{(n-1)+\cdot} - 60]$ fragment ion for the detection of the

Asp residue, and the c• + 58 and z• – 57 ions for the detection and location of the isoAsp residue, Figure 5.1 [206-208, 210].

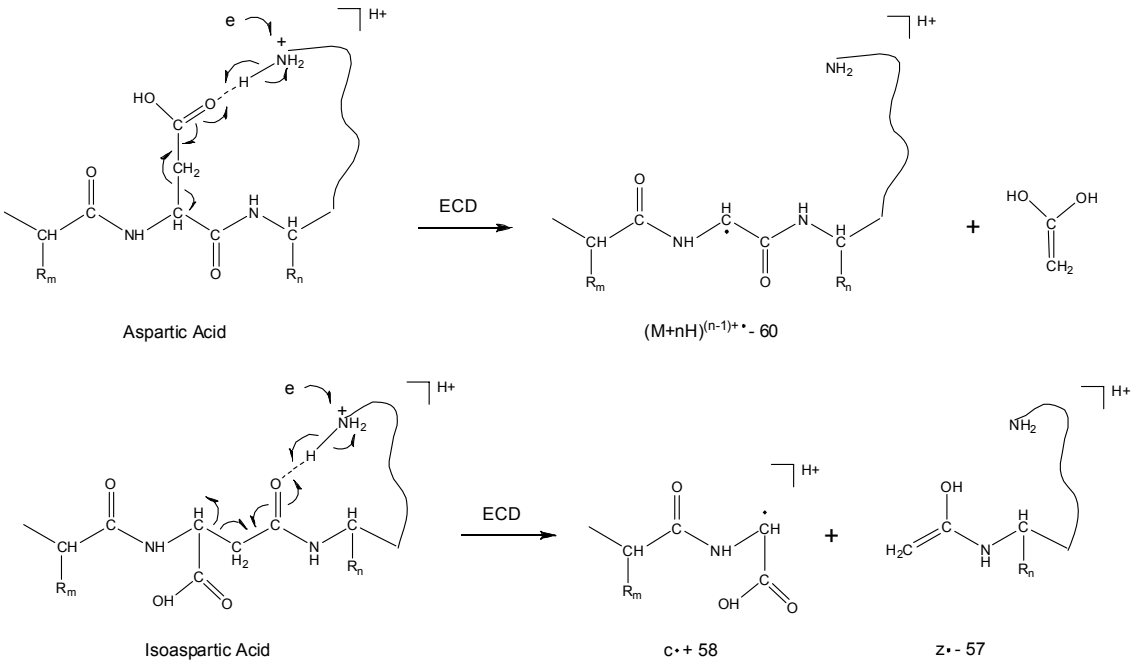

Figure 5. 1 Proposed mechanism for the formation of the $[(M+nH)^{(n-1)+\bullet} - 60]$ ions from Asp; and c• + 58 and z• – 57 ions from isoAsp in ECD.

However, ECD of intact proteins is often inefficient, because the number of available fragmentation channels is large and the resulting fragments frequently remain bound by noncovalent interactions, and hence undetectable. In most cases, the proteins need to be digested to into small peptides, most commonly by trypsin, before they are tested [61]. Trypsin digestion, which usually occurs at pH ~8 and results in many small random coil peptides, is well known to accelerate base mediated deamidation process. Thus, it is important to distinguish the artificial deamidations introduced during the

sample processing steps from those that have occurred naturally to decrease the uncertainty about the biological relevance of any observed modifications.

5.1.3 The $H_2{}^{18}O$ labeling method

One commonly used method to monitor artificial, spontaneous reactions in mass spectrometry field is to incorporate stable isotopic mass labels. For example, proteolytic ^{18}O labeling and hydrogen/deuterium (H/D) exchange have been used extensively in studies of protein modification, such as comparative proteomics [266-269], quantitative proteomics [270], protein conformational studies [271], protein dynamics analysis [272], protein-ligand interactions [273], and protein aggregates research [274, 275]. Proteolytic ^{18}O labeling, in particular, has been used in the identification and quantification of succinimide [276] and citrullination [277] in proteins.

The mechanism of protease catalyzed incorporation of ^{18}O into peptide fragments has been studied extensively [278, 279]. For trypsin, it usually results in up to two ^{18}O atoms incorporation into the peptide C-terminus, causing a mass shift of +2 Da per ^{18}O atom substitution. Since deamidation involves hydrolysis, sample preparation procedures performed in $H_2{}^{18}O$ will also offer the possibility of direct incorporation of a mass label during the reaction. Therefore, if a peptide deamidates in $H_2{}^{18}O$, it not only gets the +0.984 Da mass shift from the deamidation reaction, but also incorporates an ^{18}O atom in the newly formed Asp/isoAsp residue to get a total mass shift of +2.988 Da, as shown in Figure 5.2.

This chapter demonstrates the use of this simple $H_2{}^{18}O$ mass labeling procedure for distinguishing the artificial deamidation occurred during the tryptic digestion process which leads to a +3 Da mass shift, from the preexisting deamidation in the sample which

causes a +1 Da mass shift. Furthermore, fragment ions containing the artificial deamidation site will also be 2 Da heavier than those containing the natural deamidation site, providing additional insight into the origin and location of the deamidation. A time course study monitoring the extent of deamidations in three rapidly deamidating peptides released from tryptic digestions of three proteins were also performed.

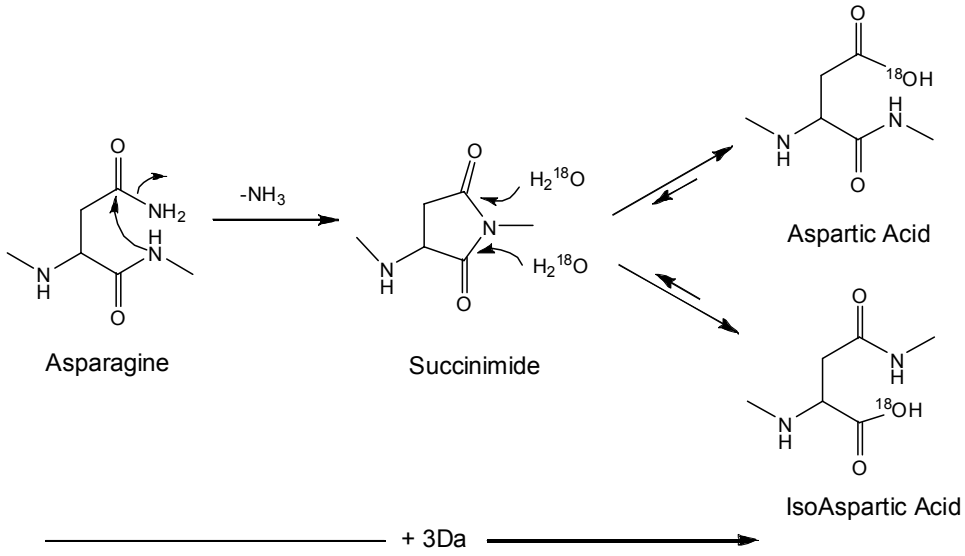

Figure 5. 2 Scheme of ^{18}O incorporation in asparagine deamidation.

5.2 Experimental section

5.2.1 Materials

Sequencing grade trypsin was purchased from Roche Applied Science (Indianapolis, IN). HPLC grade $H_2{}^{16}O$ was purchased from Honeywell/Burdick & Jackson (Muskegaon, MI). All other chemicals, proteins, and $H_2{}^{18}O$ (95% ^{18}O) were purchased from Sigma (St. Louis, MO).

5.2.2 Reduction and alkylation of ribonuclease A and lysozyme proteins

Ribonuclease A (RNase A) and lysozyme each have four disulfide bonds, which were reduced and alkylated prior to analysis as described previously [207]. Briefly, proteins were reduced in 6 M urea and 50 mM ammonium bicarbonate at pH 6, with 10-fold molar excess of dithiothreitol over disulfide bonds and the resultant mixtures were incubated for 1 hr at 37 °C. After the reaction solutions were cooled to room temperature, iodoacetamide was then added in 5-fold molar excess over cysteine residues and the resultant mixtures were incubated for 1 hr in the dark at room temperature. The samples were dried and purified by home-made Poros 50 R1 packed solid phase microextraction tip (Applied Biosystems, Foster City, CA). At each stage of sample processing, the elute fractions were monitored by ESI FT-ICR mass spectrometer. The reduced and alkylated RNase A and lysozyme were then dried for use in the time course digestion.

5.2.3 ^{18}O labeled time course digestion

Calmodulin (20 µg), RNase A and lysozyme (both 20 µg, denatured and purified) were each dissolved into 50 µl of 0.1 M ammonium bicarbonate buffer (pH 8.3) prepared using $H_2{}^{18}O$. Trypsin (1 µg) was added to each solution yielding a w/w ratio of 1:20. Each vial was then purged with N_2 gas, sealed and incubated at 37 °C. Aliquots were taken at 2, 4, 6, 8, and 24 hr, with an additional aliquot taken at 48 hrs for RNase A and lysozyme, due to their relatively slower deamidation rates. Each aliquot was immediately frozen at -80°C to stop the reaction and washed twice later by equal volume of $H_2{}^{18}O$ to desalt prior to mass spectrometry analysis.

5.2.4 ^{16}O labeled control experiments

Control experiments were performed by using the same proteins and methods described above in the ^{18}O labeled time course digestion section, except that $H_2{}^{16}O$ was used in place of $H_2{}^{18}O$.

5.2.5 Calmodulin ^{18}O labeled triplicate experiments

The digestion of 30 µg of calmodulin powder with 1.5 µg dried trypsin in 75 µl of 0.1 M ammonium bicarbonate buffer (pH 8.3) was performed in triplicate. The ammonium bicarbonate buffer was prepared by $H_2{}^{18}O$. The digestion solutions were incubated at 37°C. Sample aliquots were taken according to the time course, frozen, washed, and analyzed as above.

5.2.6 Mass spectrometry analysis

ESI FT-ICR mass spectrometry analysis was performed on the custom qQq-FT-ICR MS instrument equipped with an external nanospray ion source, as described earlier [77, 78]. Electrons in ECD experiments were generated by an indirectly heated dispenser cathode placed ~3 cm from the cell [280-282]. The control samples were electrosprayed at ~10^{-5} M concentration in 49.5:49.5:1 of methanol:water:formic acid spray solution, while the ^{18}O labeled samples were electrosprayed at the same concentration, but in 24.5:74.5:1 of methanol:water:formic acid spray solution. The different spray solution used was necessary to avoid ESI tip clogging, so that stable spray could be achieved for the ^{18}O labeled samples. Multiply charged precursor ions were isolated using the front-end resolving quadrupole (Q1), followed by external accumulation in the CAD cell (Q2) before being transferred to and trapped in the ICR cell by gated trapping. In the ICR cell, these ions were then irradiated with low-energy

electrons (~0.2 eV) for time periods ranging from 50-120 ms to generate ECD fragments. A conventional FTMS excitation/detection sequence was used and the signal was averaged over 20 to 50 scans. All ECD spectra were internally calibrated with the precursor ion and the charge reduced species.

5.3 Results and discussion

5.3.1 Calmodulin tryptic peptide ESI FTMS spectra (^{16}O vs. ^{18}O)

Calmodulin is a small (148 amino acids) and highly conserved protein, expressed in all eukaryotic cells. It has four EF-hand motifs in its structure, with the first two EF-hand motifs forming the N-terminal domain and the other two motifs forming the C-terminal domain. A short helix region connects the N- and C-terminal domains [283-285]. Calmodulin is the primary cellular calcium receptor, which mediates calcium concentration and regulates calcium-dependent enzymes [286, 287]. Calmodulin contains a total of six Asn residues, with two NG sequences in its primary structure, Asn60 and Asn97. Deamidation at these two sites was reported by Johnson, et al [288]. Another *in vitro* study also found that the Asn97-Gly98 was the greatest contributor to the isoAsp formation in calmodulin [289].

In this study, bovine calmodulin was used. Figure 5.3 shows the ESI mass spectra of the triply charged calmodulin tryptic peptide (^{91}VFDKDGNGYISAAELR$_{106}$) ion in a tryptic digestion time course study over 24 hrs in $H_2{}^{16}O$ and $H_2{}^{18}O$. The inset shows the theoretical isotopic distribution of this peptide, which was calculated and generated using the Yergey algorithm as implemented in Isopro 3.0 (IonSource.com).

In the control experiment performed in $H_2{}^{16}O$, there was a ~1 Da mass shift in the monoisotopic peak from the 2 hr spectrum to the 24 hr spectrum, indicating the onset

of one deamidation in this peptide during the 24 hr incubation period at 37 °C. The monoisotopic peak in the 2 hr ^{18}O labeled spectrum showed a ~2 Da mass difference from that in the control spectrum, resulting from one ^{18}O incorporation. The third isotopic peak had the highest intensity in the mass spectrum of this 2 hr ^{18}O labeled peptide, and its mass was shifted by an additional ~2 Da, corresponding to a second ^{18}O incorporation. The sixth isotopic peak became significant in the isotopic cluster in the 6 hr spectrum, continued to increase in intensity in the 8 hr spectrum, and became the most abundant peak in the 24 hr spectrum, right column. This peak showed a mass shift of ~7 Da from the monoisotopic peak in the corresponding control spectrum, with the addition of ~4 Da coming from the double ^{18}O substitution, and the remaining ~3 Da being the result of one deamidation occurring during the course of the tryptic digestion (Figure 5.2). During the deamidation process, the amide group of the Asn residue was substituted by a hydroxyl group (-^{18}OH) via the hydrolysis of the succinimide intermediate in $H_2{}^{18}O$, leading to an increase in the mass of a peptide by 0.984 + 2.0043 = 2.988 Da.

These results show that although deamidation readily occurred during a 24 hr tryptic digestion of this easily deamidating calmodulin peptide (91-106), a short trypsin digestion (~4 hr) would not introduce detectable deamidation(s). The first two ^{18}O atoms were incorporated into this peptide's C-terminus, which will be further confirmed by the tandem MS experiment (*vide infra*).

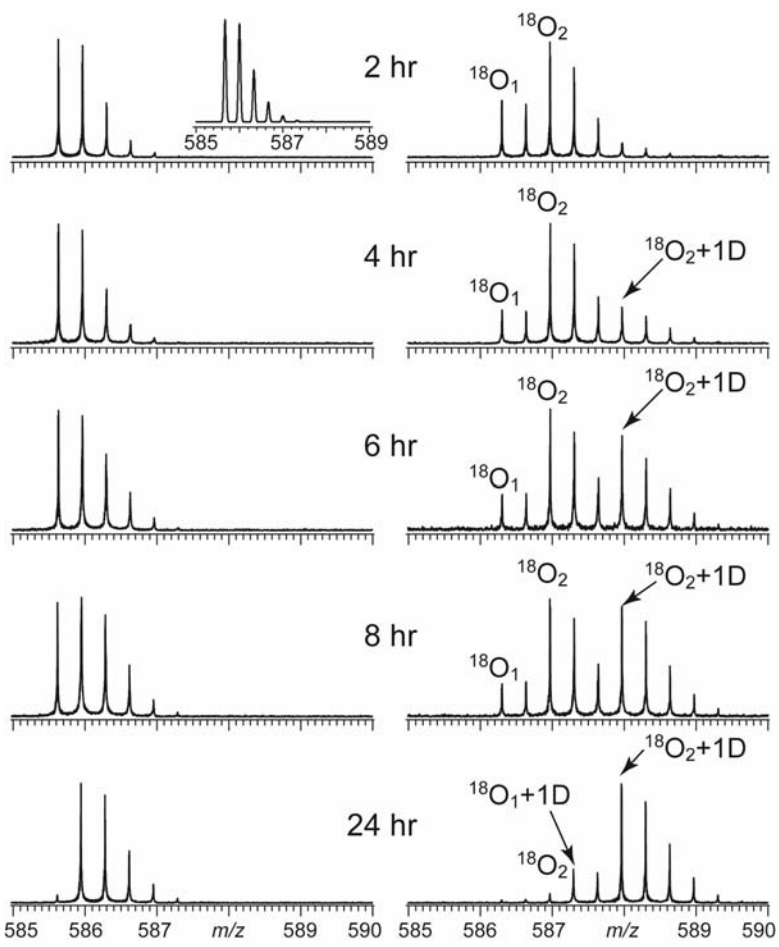

Figure 5. 3 Mass spectra of the triply charged calmodulin peptide (^{91}VFDKDGNGYISAAELR$_{106}$) extracted at different time from the tryptic digestion solution in $H_2{}^{16}O$ (left column) and in $H_2{}^{18}O$ (right column). The inset shows the theoretical isotopic distribution of this peptide. The isotopic clusters were assigned in the ^{18}O spectra as $^{18}O_m$ + nD, where m and n indicate the number of ^{18}O incorporations and deamidations, respectively.

5.3.2 RNase A and lysozyme tryptic peptides ESI FTMS spectra (^{16}O vs. ^{18}O)

RNase A is a widely studied enzyme in biology. It is a small protein containing 124 amino acids and four disulfide bonds, Cys26-Cys84, Cys40-Cys95, Cys58-Cys110, and Cys65-Cys72. Its structure has a kidney shape, including four long β-sheets and three short α-helixes [290, 291]. Although RNase A contains several Asn residues in its sequence, it only has one NG sequence, at Asn67, which is located in the β-turn of residues 66 to 68, and also near the Cys65-Cys72 disulfide bond. Thus in its native state, the three dimensional structure of RNase A will inhibit the Asn67 deamidation. However, it was reported that in the reduced and alkylated RNase A, Asn67 deamidation was observed [292]. Furthermore, a stepwise deamidation study of RNase A was demonstrated by using top down mass spectrometry method, where five deamidation sites were reported: Asn67, Asn71, Asn94, Asn34, and Gln74 [293]. In this chapter, bovine RNase A was used and one of its tryptic peptides containing Asn67 and Asn71 residues was studied.

Lysozyme is also a small protein, containing 129 amino acids, with only one NG sequence and four disulfide bonds: Cys6-Cys127, Cys30-Cys115, Cys64-Cys80, and Cys76-Cys94. The hen egg-white lysozyme was the first enzyme with its crystallin structure determined in 1965 [294]. Later, the crystallin structure of monoclinic turkey egg lysozyme was reported with similar backbone structure [295]. Lysozyme catalyzes the hydrolysis of specific kinds of polysaccharides from the cell wall of bacteria [296]. Deamidation of lysozyme was reported during the storage of egg white [297], and the sequence dependent deamidation was also studied by using model peptides derived from hen egg white lysozyme [298]. In this chapter, the chicken egg white lysozyme was

used and one of its tryptic peptides containing two Asn residues, Asn46 and Asn50, was studied.

The ESI FTMS spectra of the trypsin digestion time course for tryptic peptides from RNase A and lysozyme in $H_2{}^{16}O$ and $H_2{}^{18}O$ are shown in Figure 5.4 and Figure 5.5, respectively. Once again, the insets show the theoretical isotopic distributions of the corresponding peptides. The results from these time course studies are similar to the calmodulin tryptic peptide results in Figure 5.3, except that both of these RNase A and lysozyme peptides, which are also the most rapidly deamidating peptides from their respective proteins, contain two potential deamidation sites. Again, rapid digestion resulted in no detectable deamidation (< 6 hr for RNase A, < 24 hr for lysozyme) in these tryptic peptides. The RNase A tryptic peptide showed little incorporation of a second ^{18}O at its C-terminus, but demonstrated an abundant amount of double deamidation. The lysozyme tryptic peptide showed abundant double ^{18}O substitutions at its C-terminus, but only one deamidation over the 48 hr time course.

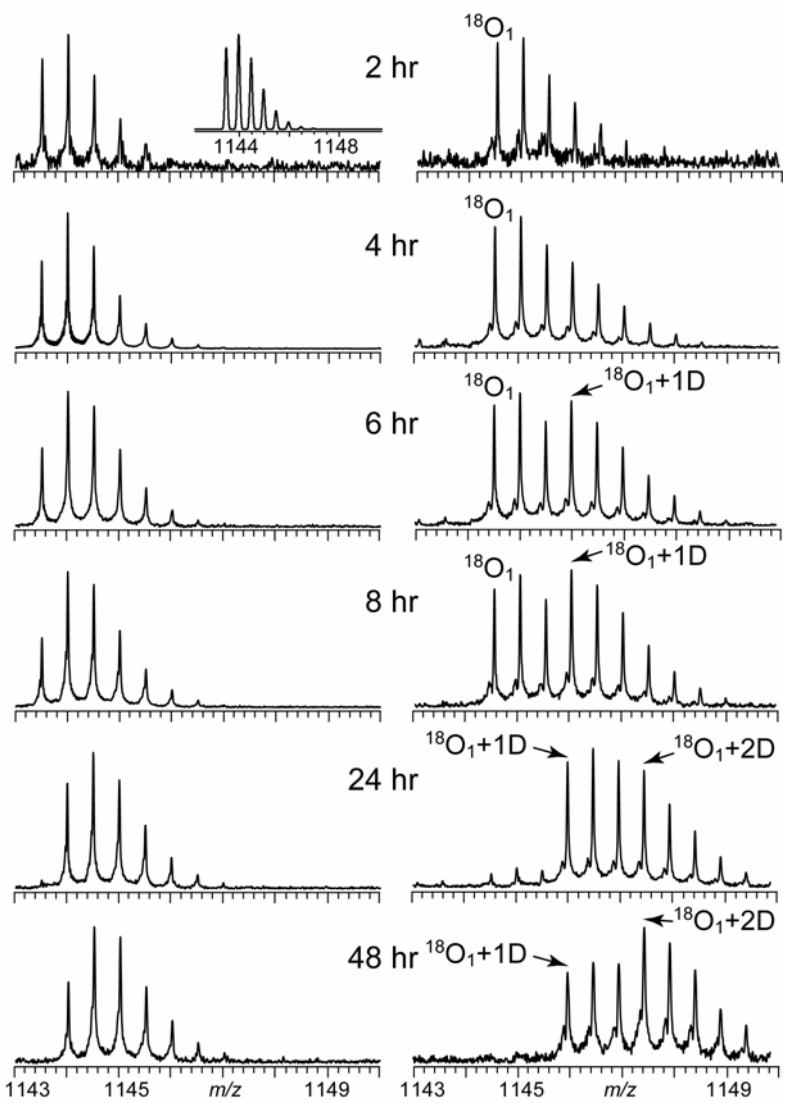

Figure 5. 4 Mass spectra of the doubly charged RNase A peptide (^{67}NGQTNCYQSYSTMSITDCR$_{85}$) extracted at different time from the tryptic digestion solution in $H_2{}^{16}O$ (left column) and in $H_2{}^{18}O$ (right column). The inset shows the theoretical isotopic distribution of this peptide. The isotopic clusters were assigned in the ^{18}O spectra in the same way as in Figure 5.3.

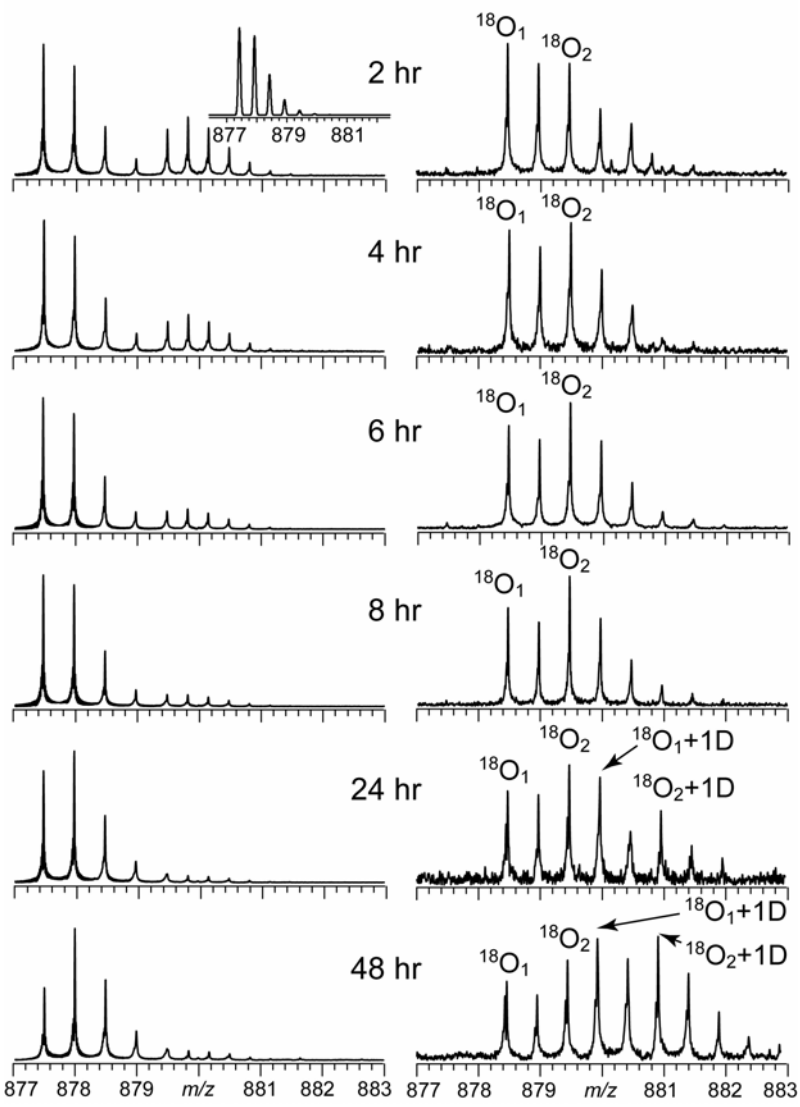

Figure 5. 5 Mass spectra of the doubly charged lysozyme peptide (^{46}NTDGSTDYGILQINSR$_{61}$) extracted at different time from the tryptic digestion solution in $H_2{}^{16}O$ (left column) and in $H_2{}^{18}O$ (right column). The inset shows the theoretical isotopic distribution of this peptide. The isotopic clusters were assigned in the ^{18}O spectra in the same way as in Figure 5.3.

The RNase A tryptic peptide (^{67}NGQTNC*YQSYSTMSITDC*R$_{85}$) contains the fast deamidating NG sequence at its N-terminus, near the exposed and flexible part of the peptide, where C* denotes the carbamidomethylated cysteine residue. There is little steric hindrance for the deamidation reaction, which may facilitate the succinimide intermediate formation and the hydrolysis in $H_2{}^{18}O$, thus making the deamidation process even faster than the second ^{18}O atom incorporation into the peptide C-terminus. The Thr located at the N-terminal side of the Asn71 residue is also known to accelerate deamidation [80], which may help to explain the second deamidation in this peptide. Moreover, deamidation in one site often causes protein conformational change and accelerates deamidation at a second site [252]. Since the TN is located near the N-terminal NG, a conformational change at the NG site will influence the TN local conformation, which may further contribute to the second site deamidation.

The lysozyme tryptic peptide (^{46}NTDGSTDYGILQINSR$_{61}$) has the NT located at its N-terminus and the NS located near its C-terminus. The deamidation rate of this peptide was substantially slower than the calmodulin tryptic peptide and the RNase A tryptic peptide, which was evident from the control spectra. The one deamidation site of this lysozyme tryptic peptide is likely the Asn residue in the NS sequence for two reasons. First, a Ser residue following an Asn residue is known to promote Asn deamidation due to conformational flexibility and its polar side chain which increases the deamidation rate compared to neutral groups [80]. Second, the NS is located near the C-terminus which has little steric hindrance for nucleophilic attack. The assigned NS site deamidation also corroborates with the previous study, which found the deamidation site at Asn59 of the lysozyme peptide Asp48 to Trp62 was recognized by T cells, with a measured deamidation half-life of about 10 days in PBS buffer (pH 7.5) at 37 °C [79].

Unlike the NG and TN sites in the RNase A peptide, the NT and NS sites in this lysozyme tryptic peptide are distant from each other so the conformational change induced by deamidation at one site may not have large influence on the local conformation of the other.

Finally, in all spectra of this lysozyme peptide, the major isotopic cluster was followed by another triply charged isotopic cluster which was an unrelated tryptic peptide fragment, containing residues (74-97). However, as evident from the control spectra, this second peptide was much less abundant than the peptide of interest in the 24 hr and 48 hr samples, where appreciable deamidations were observed. Furthermore, in the ^{18}O labeled spectra of samples taken after at least 6 hours of digestion, there was no evidence for a triply charged peptide in the mass range of interest, which would have shown up in between adjacent isotopic peaks of the doubly charged peptide of interest due to its different charge state. Thus, its interference to the quantification of deamidation extent was expected to be minimal, and no correction was attempted in the following analysis.

5.3.3 Quantification of the extent of the ^{18}O incorporation and deamidation during the digestion time course

The isotopic distribution in each ^{18}O labeled peptide spectrum was deconvolved using the least square fitting method. The initial values were obtained step by step, from the lightest isotopic cluster to the heaviest one. Using the 8 hr ^{18}O labeled calmodulin tryptic peptide spectrum as an example, the abundance of the $^{18}O_1$ cluster was taken directly from the peak height of the first isotopic peak (A) and then its contribution (A+2) to the third isotopic peak was calculated based on its theoretical isotopic distribution

which, finally, was subtracted from the peak height of the third isotopic peak to give the abundance of the $^{18}O_2$ cluster. This procedure was repeated until the abundances of all isotopic clusters were obtained. These initial abundance values were normalized to give the percentages, which were adjusted iteratively until the resulted sum of all isotopic distributions from the fitting gave the least sum of square deviations from the experimental distribution. The final percentages of all isotopic clusters as a function of digestion time were plotted in Figures 5.6 a, b and c for the calmodulin, RNase A and lysozyme peptides, respectively.

In order to test the variance of these abundances, triplicate experiments of the ^{18}O labeled calmodulin tryptic peptide were done using the same method as described above and the results were plotted in Figure 5.6 d, which correlate well with the results from the single time experiment shown in Figure 5.6 a.

After the deconvolution, it was easier to follow the deamidation process taking place during the tryptic digestion in $H_2{}^{18}O$. In general, the results agreed with those from the control experiment, showing that a short (4 hr for the calmodulin peptide and 8 hr for the RNase A and lysozyme peptides) tryptic digestion would not introduce detectable artificial deamidations.

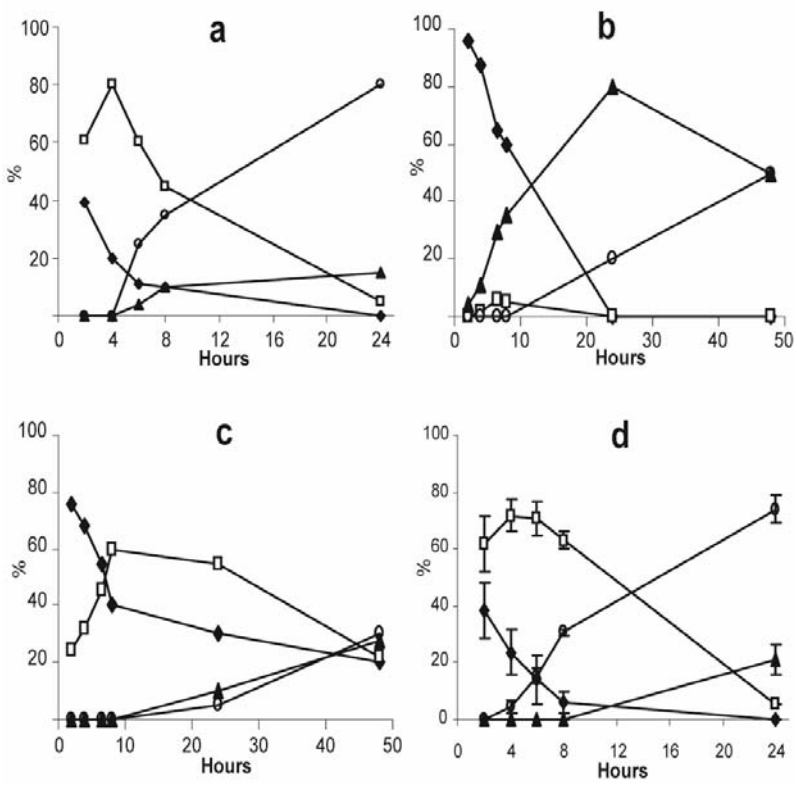

Figure 5. 6 The percentage of each isotopic cluster at different digestion time as calculated using the least squares method for the ^{18}O labeled: (a) calmodulin tryptic peptide (91-106), (b) RNase A tryptic peptide (67-85), (c) lysozyme tryptic peptide (46-61) and (d) calmodulin tryptic peptide (91-106) triplicate experiments. (a-d) -♦-: $^{18}O_1$, -□-: $^{18}O_2$, -▲-: $^{18}O_1$ + 1D, -○-: $^{18}O_2$ + 1D, except in (b) $^{18}O_1$ + 2D.

5.3.4 ECD of ^{18}O labeled calmodulin tryptic peptide at time points 2 hr and 24 hr

Figure 5.7 shows the ECD spectra of the 2 hr and 24 hr time point of ^{18}O labeled samples from Figure 5.3. As it has been discussed in the introduction chapter, ECD is based on the dissociative recombination of multiply charged polypeptide molecules with

low-energy electrons [299], which cleaves the N-C_α bond non-specifically and generates mostly c and z• ions [45, 52, 56].

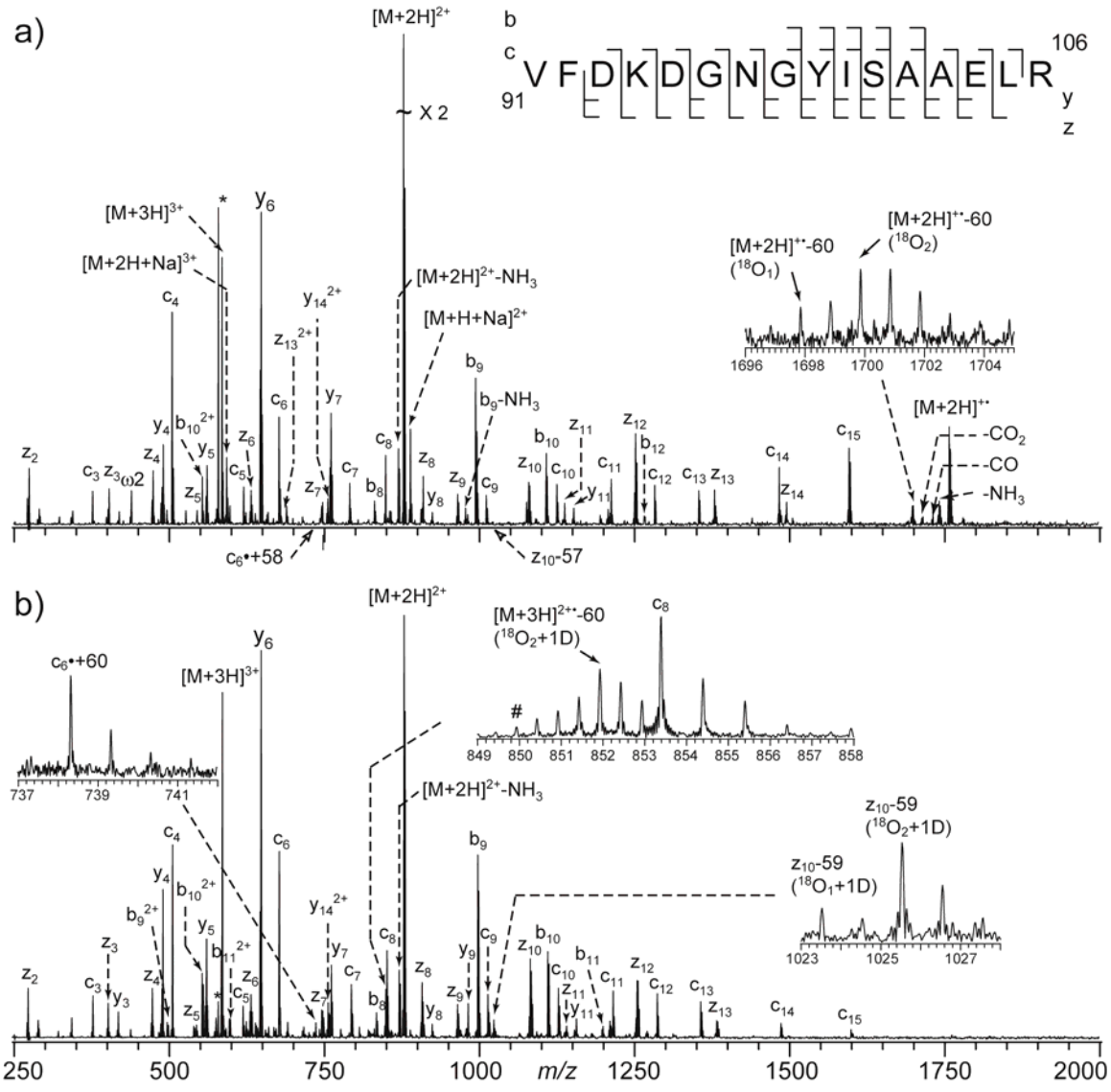

Figure 5. 7 ECD spectra of the triply charged calmodulin tryptic peptide (91-106) labeled in $H_2{}^{18}O$ at different time points: (a) 2 hr, (b) 24 hr. The insets of (a) show the [M – 60] ion (left) and the cleavage pattern (right). The insets of (b) show the isotopic distributions

of the c_6• + 60 (left), [M – 60] (middle), and z_{10}• – 59 (right) ions. ∗: electronic noise, ω2: harmonics.

The 2 hr ECD spectrum showed c_3 to c_{15} ions and z_2• to z_{14}• ions (Figure 5.7 a). Neither c_6• + 58 nor z_{10}• – 57 ion was observed in this spectrum to indicate the deamidation of Asn97 to isoAsp. Although the [M - 60] fragment ion was observed (Figure 5.7 a, inset), it most likely arose from the side chain loss of the two pre-existing Asp residues (Asp93 and Asp95), since all c ions that contain the Asn97 residue (c_7 to c_{15} ions) showed no +3 Da mass shift as one would expect if the Asn97 had deamidated in $H_2{}^{18}O$. Furthermore, none of the c ions (particularly the c_{15} ion) showed any mass shift compared to its normal counterpart produced in the control experiment, while all z• ions appeared to contain two adjacent isotopic clusters that were ~2 Da and ~4 Da heavier than their ^{16}O counterparts. These results indicated that the first and second ^{18}O atoms were incorporated into the peptide's C-terminal carboxyl group, and no detectable deamidation occurred during the first two hours of the tryptic digestion.

The 24 hr ECD spectrum showed c_3 to c_{15} ions and z_2• to z_{13}• ions as well (Figure 5.7 b). Like in the 2 hr ECD spectrum, all z• ions contained two adjacent clusters of isotopic peaks, indicating one and two ^{18}O atom incorporations at the C-terminus. For z_{10}• to z_{13}• ions, both isotopic clusters were shifted in mass by an additional ~3 Da, as they all included the Asn97 deamidation site. While the c_3 to c_6 ions showed no mass shifts, the mass of c_7 to c_{15} ions increased by ~3 Da when compared to their ^{16}O counterparts, once again indicative of the deamidation occurred at the Asn97 residue. Moreover, both complementary diagnostic ions for the Asn97 deamidation to isoAsp, the c_6• + 60 and z_{10}• - 59 ions, were observed with ~1 ppm mass accuracy, with the 2 Da

mass difference comparing with the normal diagnostic ions being the result of one ^{18}OH instead of one ^{16}OH substitution at the deamidation site (Figure 5.7 b, insets). Like all other z• ions, the z_{10}• - 59 ion also had two isotopic clusters corresponding to one and two ^{18}O atom incorporations at the C-terminus.

In the 24 hr ECD spectrum, the [M ($^{18}O_2$ + 1D) – 60] ion corresponding to the Asp side chain loss was observed, as expected because of the two pre-existing Asp residues in this peptide. The side chain loss peak of the Asp97 (as the result of Asn97 deamidation) should instead give rise to an [M ($^{18}O_2$ + 1D) – 62] ion, because of the ^{18}OH substitution at the deamidation site. Although this ion was indeed observed, it might also come from the normal Asp side chain loss of the singly ^{18}O labeled molecular ion which consisted of a significant portion of the total molecular ion population (Figure 5.6 a, d), i.e., it was actually an [M ($^{18}O_1$ + 1D) – 60] ion. The best evidence for the Asp formation from the Asn97 deamidation was perhaps the observation of an isotopic peak at another ~2 Da lighter than the [M ($^{18}O_1$ + 1D) – 60] peak (Figure 5.7 b, inset, marked by the number sign, #), which could only be the [M ($^{18}O_1$ + 1D) – 62] ion, since there was little [M ($^{18}O_0$ + 1D)] in the 24 hr sample (bottom right spectrum, Figure 5.3).

There are several factors which can significantly affect the accuracy of the ^{18}O labeling experiment. First, formic acid should not be used to halt the digestion reaction [278]. Apparently the acidic environment influenced the ^{18}O incorporation and the ^{18}O labeling ratio (data not shown). Second, the back exchange reaction should be considered and only $H_2{}^{18}O$ should be used in the desalting step. If $H_2{}^{16}O$ was used instead in this step, the ^{18}O atom which had already been incorporated into the tryptic peptides might be exchanged by the ^{16}O atom in the solvent, which would lead to erroneous ^{18}O incorporation measurement (data not shown). Centrifugation under

vacuum appeared to further accelerate the back exchange with $H_2{}^{16}O$. Finally, excessive desalting should also be avoided. If $H_2{}^{18}O$ was used more than three times to wash out the salts, it could also distort the ^{18}O incorporation ratio (data not shown).

5.4 Conclusion

During trypsin digestion, deamidation rate of the released peptides increases which may introduce unwanted artificial deamidation that is of no biological relevance. This chapter demonstrated the use of $H_2{}^{18}O$ as a mass labeling reagent during the trypsin digestion process to distinguish between the deamidation that occurred during sample handling processes (+3 Da mass increases) and the deamidation that was native to the sample (+1 Da). Tandem MS methods, such as ECD, can further help locate the sites of deamidation and ^{18}O incorporation. The use of $H_2{}^{18}O$, however, generated complex isotopic patterns that must be deconvolved first. In addition, care must be taken so that the isotopic distributions would not be distorted artificially during the digestion, centrifugation, and desalting steps.

This study showed that fast trypsin digestion (~4 hr) generally would not introduce additional detectable deamidations, even for the most rapidly deamidating peptides studied here. This result should increase the confidence in the quantification of Asn, Asp and isoAsp residues, when samples need to be digested first to small peptides to facilitate the mass spectrometry analysis. Finally, this ^{18}O labeling methodology can be easily extended to study the artificial deamidation taking place in other protein sample preparation procedure.

Chapter 6

Glutamine Deamidation: Differentiation of Glutamic Acid and γ-Glutamic Acid in Peptides by ECD

6.1 Introduction

6.1.1 Asn deamidation and the fate of the deamidated proteins in cells

Deamidation contributes to aging process, plays an important role in many diseases (such as celiac disease, urinary tract infection, cataract formation, cancer, and neurodegenerative diseases, e.g. Alzheimer's, Huntington's, and Parkinson's diseases), and affects the purity and shelf life of pharmaceutical products [79]. It is well known that under physiological conditions, nonenzymatic deamidation of Asn residues may occur both *in vivo* and *in vitro*, which generates acidic isomers, Asp and isoAsp residues, with + 0.984 Da mass shift per deamidation site [79, 80]. In cells, the deamidated proteins which generate an isoAsp residue can be partially repaired by PIMT enzymes to convert the isoAsp to Asp, but often the modified proteins are degraded by proteasomes [93, 300]. Proteasome is a very important enzyme located in both cytosol and nucleus, which controls the turnover of the abnormal proteins generated in cells. Inefficient degradation, caused by either increased deamidation products and decreased proteasome activity with age [102] or proteasomal dysfunction [301], may lead to accumulation of the damaged or modified proteins and related diseases.

---

[1]This chapter has been partially/entirely reproduced from
Xiaojuan Li, Cheng Lin, and Peter B. O'Connor. Glutamine deamidation: Differentiation of glutamic acid and γ-glutamic acid in peptides by electron capture dissociation. *Analytical Chemistry* 2010, 82, 3606-3615.
Copyright 2010 American Chemical Society.

6.1.2 Gln deamidation

Like Asn, Gln deamidates by direct hydrolysis under acidic conditions, and proceeds via a cyclic intermediate at neutral or alkaline conditions [80, 302], as discussed previously. The deamidation rate of Gln is much slower than that of Asn [79], except when Gln is located at the N-terminus of the peptide, under which condition it deamidates more rapidly than Asn to form a cyclic pyroglutamic acid [80]. For example, even the fastest deamidating QG sequence has a median deamidation half-life of about 660 days as measured in the pentapeptide GXQGG [84], as opposed to less than one day for Asn deamidation in the NG sequence [303]. In general, the half-lives of the sequence-dependent Asn peptide deamidation at neutral pH and physiological temperature range from about 0.5 to 500 days, while those of Gln range from about 600 to 20,000 days [79]. Consequently, most known Gln deamidation are present in long lived proteins, such as eye lens crystallins. Crystallins are highly soluble structural proteins and comprise 90% of lens proteins, which include three classes: alpha (α), beta (β), and gamma (γ) proteins. They undergo little turnover during their life spans, allowing accumulation of many kinds of modifications [129, 304, 305]. Among these, deamidation is one of the most prevalent, which decreases crystallin solubility, alters lens transparency, and is associated with cataract formation, a leading cause of blindness [120]. Extensive Gln deamidation has been reported in aged or diseased lens crystallin proteins [120, 121, 123-129, 130], which has been discussed in detail in the introduction part of this thesis.

6.1.3 Gln deamidation detection methods

As discussed previously, the Asn deamidation in peptides/proteins is extensively studied, both to determine the deamidation site(s) and to differentiate the isomeric deamidation products [206-209]. A variety of methods have been developed to differentiate the isomeric Asp and isoAsp residues, including the NMR, Edman sequencing, HPLC, and antibody based detection methods [210], etc. All these methods have their limitations, and they either require a relatively large quantity of peptide samples or are time consuming. Mass spectrometry has become a powerful tool for deamidation studies, because of its small sample amount requirement, fast and accurate detection, as well as the more detailed information provided by the tandem MS experiments. Recently, a fast and accurate ECD [38, 45, 52] based method has been developed to distinguish the Asp and isoAsp residues. The additional methylene group inserted into the backbone of the isoAsp containing peptide creates a second fragmentation channel, which proceeds via direct cleavage of the C_α-C_β bond, generating the diagnostic ions (c+57 and z•-57) for isoAsp containing peptides [206, 207, 209]. In addition, this ECD based method can provide the quantitative measurement of the relative abundance of the isoAsp residues in deamidated proteins [208]. The same diagnostic fragments have also been detected using the ETD method [210], which has a similar backbone fragmentation mechanism to ECD [64-66].

However, there have only been a limited number of Gln deamidation studies, even at the peptide level [84]. The first Gln deamidation study was reported in 1991 on a dipeptide, which showed the formation of glutarimide intermediate and deamidation products, α- and γ-glutamate (Glu) [302]. Recently, a few studies have been performed to determine the number of Gln deamidation site(s) in peptides/proteins based on the ~+1 Da mass shift per site, and to identify the exact Gln deamidation site(s) by using one

of the tandem MS methods, CAD, or by using amino acid sequencing methods [306-308]. Several methods, including hydrolysis, Edman degradation, and NMR, have been developed to distinguish the isomeric α- and γ-glutamyl peptides, but each has its own disadvantages [309, 310].

There have also been a number of MS studies on the differentiation of the α- and γ-glutamyl residues. Okada and Kawase used the electron impact (EI) mass spectrometry to differentiate the Z- or Dec-derivatives of α- and γ-glutamyl oligopeptides, containing two to four amino acid residues with most having the glutamyl residue at the N-terminus [311]. The ions due to ring formation of the glutamyl chain were associated with γ-isomers. Nevertheless, this method was limited by the size of the peptides (unsuccessful in even pentapeptides), the nature of the connected amino acid, and the type of the mass spectrometer employed. In addition to the extra chemical derivatization step, this method also required the use of the intensity ratios of the characteristic peaks than the relative peak intensity alone.

Nagasawa, et al. employed the chemical ionization (CI) mass spectrometry method to differentiate the α- and γ-glutamyl dipeptides with the glutamyl residue at the N-terminus [309]. While the α-glutamyl dipeptides lost one or two H_2O molecules from the protonated molecular ion, the characteristic fragment ions for γ-isomer were the protonated pyroglutamic acid ion and the protonated C-terminal amino acid. Although no chemical derivatization is required, this method can only be used in dipeptides with glutamyl at its N-terminus.

Lloyd, et al. used fast atom bombardment (FAB)/collisional activation tandem mass spectrometry to distinguish α- and γ-glutamyl underivatized dipeptides, with glutamyl at the N-terminus, based on the ratio of the ions with different relative stabilities

[310]. Capillary electrophoresis (CE) was also used for the separation of two α-glutamyl tripeptides and their potential degradation and isomerization products at pH 3 and pH 7, based on the different acidity and basicity between the α- and γ-isomers [312]. Recently, CAD was used to characterize the α- and γ-glutamyl dipeptides in negative ion mode [313]. All of these methods were limited to small peptides with less than five amino acids, and most of these methods can only be applied to peptides with glutamyl residue located at the N-terminus to form the cyclic structure for identification.

Because of the importance of Gln deamidation in many pathological processes and the limitations of the existing methods discussed above, there is a clear need for a fast, sensitive and accurate method to differentiate the α- and γ-Glu residues in relatively large peptides. In this chapter, three human crystallin peptides in their potentially Gln deamidated forms, with sizes ranging from eleven to twenty amino acid residues, were studied by ECD to develop an ECD based method for direct differentiation of the α- and γ-Glu residues in longer peptides, based on the knowledge of the Asp/isoAsp differentiation.

6.2 Experimental section

6.2.1 Materials

Human crystallin peptides αA (1-11: MDVTIQHPWFK), βB2 (4-14: HQTQAGKPQSL), and γS (52-71: PNFAGYMYILPQGEYPEYQR) in their native and two potentially deamidated forms were purchased from AnaSpec (Fremont, CA) and used without further purification. Other chemicals used in this work were purchased from Sigma (St. Louis, MO).

6.2.2 ECD experiments

The above peptides were analyzed by ECD at ~10^{-5} M concentration in the spray solution containing 50:50 (v/v) methanol: water with 1% formic acid. ECD analysis was performed on the custom built qQq-FT-ICR mass spectrometer equipped with a nano-spray source and a 7T actively shielded magnet [77, 78]. The ECD experiments were performed as described previously. Briefly, multiply charged precursor ions were isolated in the front end quadrupole (Q1) and externally accumulated in the collision cell (Q2). After that, ions were transmitted to and trapped in the cylindrical ICR cell to interact with low energy electrons (~0.5 eV), generated by the indirectly heated dispenser cathode (Heatwave, Watsonville, CA). A grid located in front of the cathode was set at +10 V to help guide the low energy electrons into the ICR cell. The time domain signals were Fourier transformed and the spectra were internally calibrated with the precursor and charge-reduced ions. The peak assignments were done manually.

6.3 Results and discussion

6.3.1 Identification of Gln deamidation site(s)

The ECD spectra of three human crystallin peptides αA(1-11), βB2 (4-14), and γS (52-71), and their corresponding potentially deamidated forms are shown in Figure 6.1, Figure 6.2, and Figure 6.3, respectively.

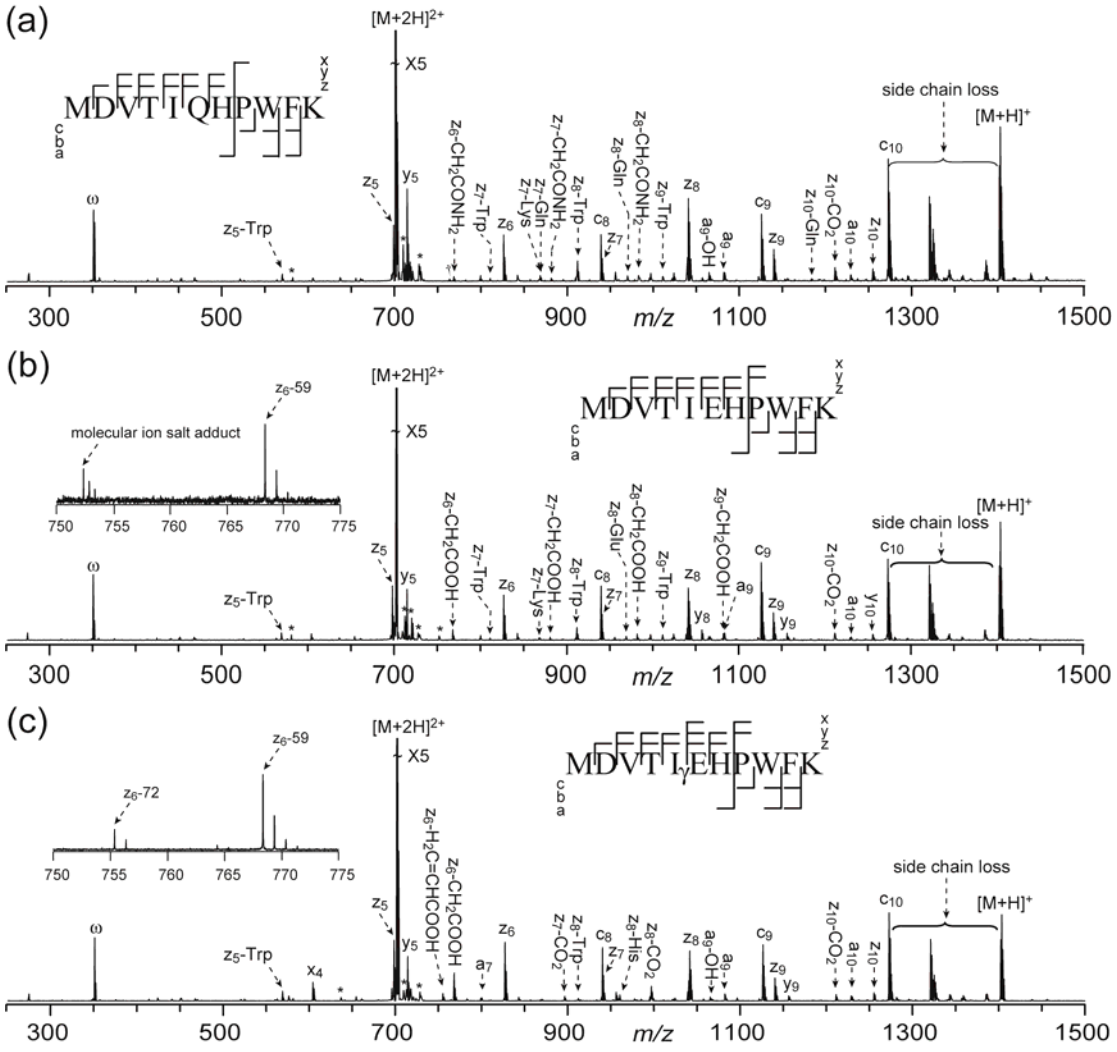

Figure 6. 1 ECD spectra of αA crystallin peptide (1-11) in its Gln (a), Glu (b), and γGlu (c) forms. The insets show the enlarged regions of interest. Peaks marked with "-amino acid residue" represent the entire side chain losses, and the partial side chain losses are represented by the molecular formulas of the departing group(s). ω: harmonic peaks. ∗: electronic noise peaks or salt adducts. †: internal fragments. Cleavage patterns are shown as the insets.

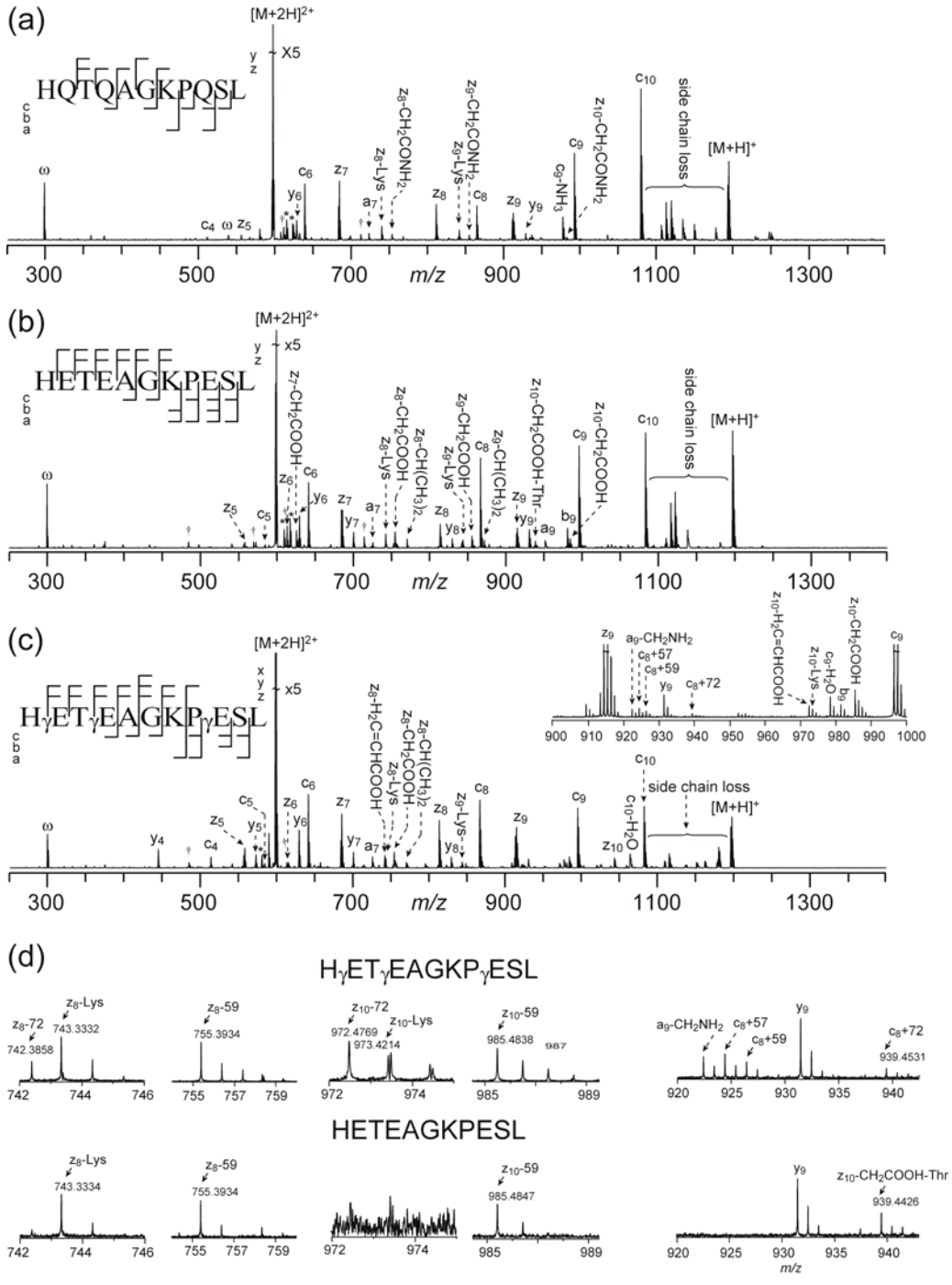

Figure 6. 2 ECD spectra of βB2 crystallin peptide (4-14) in its Gln (a), Glu (b), and γGlu (c) forms. The comparison of the enlarged regions of interest is shown in (d). Peak

labeling follows the same convention as in Figure 6.1. Cleavage patterns are shown as the insets.

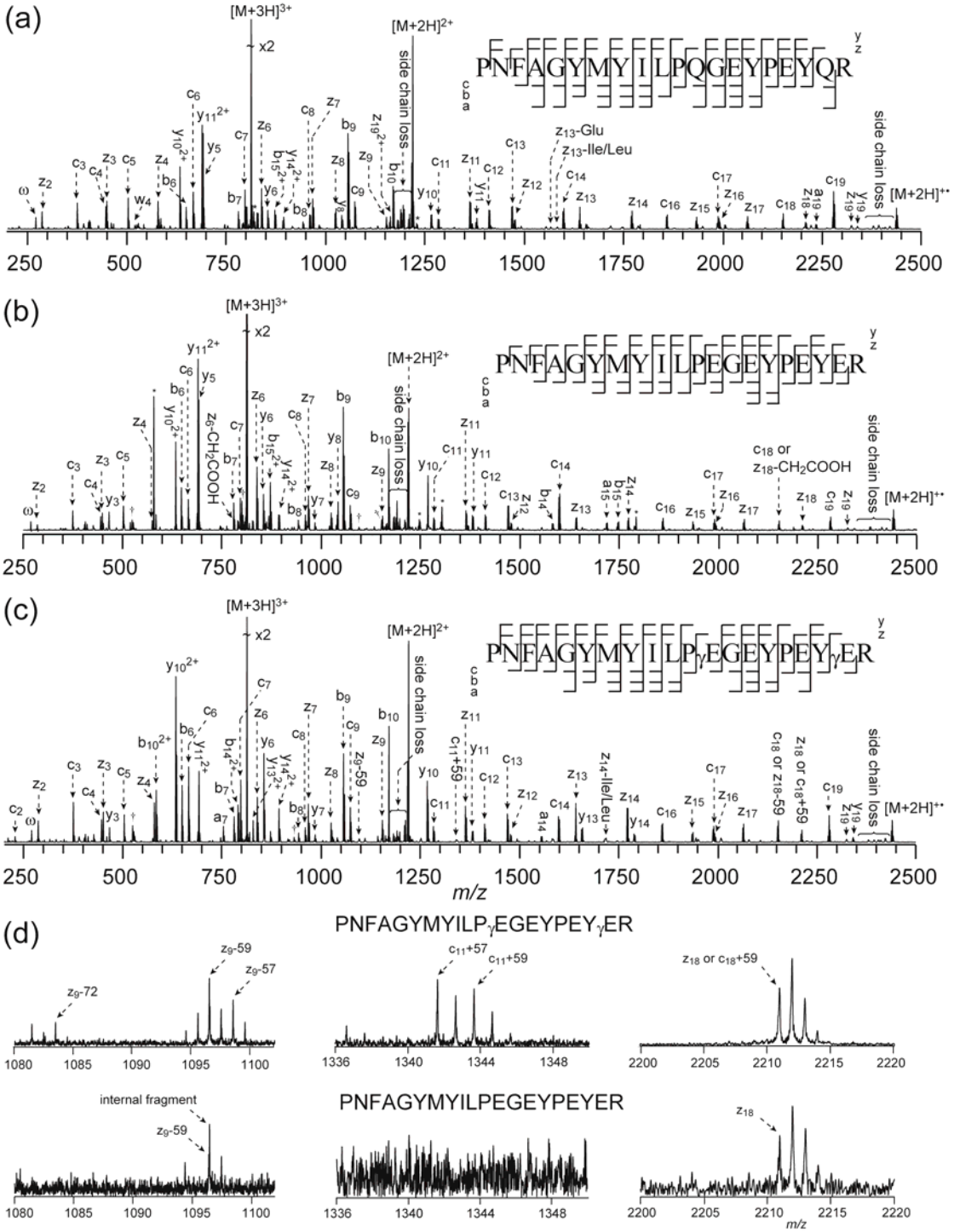

Figure 6. 3 ECD spectra of γS crystallin peptide (52-71) in its Gln (a), Glu (b), and γGlu (c) forms. The comparison of the enlarged regions of interest is shown in (d). Peak labeling follows the same convention as in Figure 6.1. Cleavage patterns are shown as the insets.

The Gln deamidation site(s) in peptides or proteins can be easily and accurately identified by ECD, based on the ~+1 Da mass shift per site caused by deamidation in the fragment ions containing the deamidated Gln residue. For example, Figure 6.4 shows the comparison of several c ions generated from the ECD experiments of the βB2 crystallin peptide (4-14) in its Gln and γ-Glu forms. In the ECD spectrum of this γ-Glu containing peptide, c_4 ion at *m/z* 514 shows a mass shift of ~+2 Da, consistent with the substitution of the first two Gln residues with γ-Glu. Further, c_8 ion at *m/z* 867 shows a ~+2 Da mass shift, while c_9 ion at *m/z* 996 shows a ~+3 Da mass shift, unambiguously identifying the Gln residue at position 9 as the third Gln residue being replaced by γ-Glu.

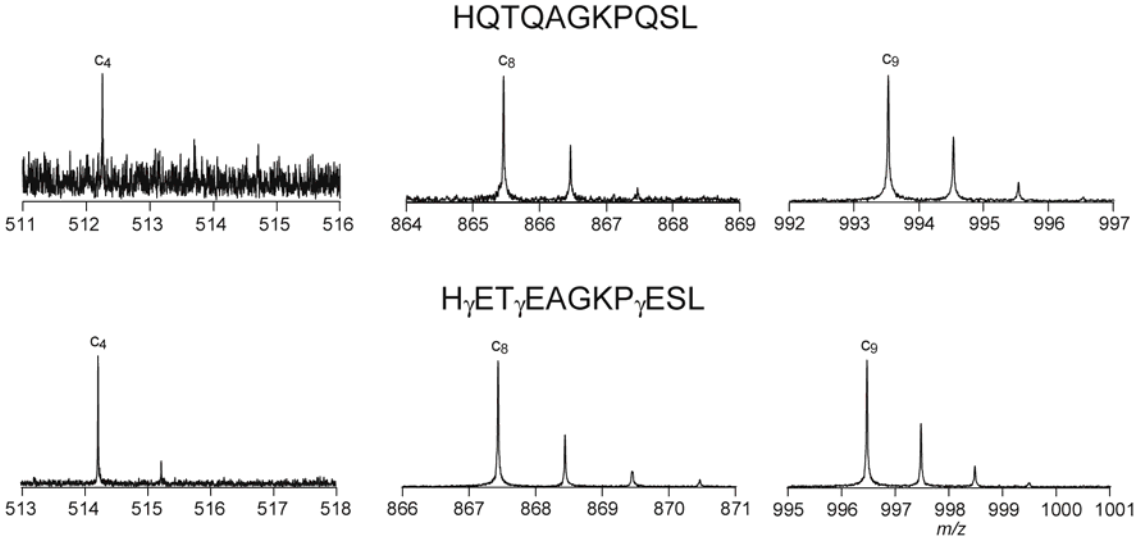

Figure 6. 4 Comparison of several c ions from ECD of βB2 crystallin peptide (4-14) in its Gln and γGlu forms, upper and lower panel, respectively.

6.3.2 Characteristic ions for the differentiation of the α- and γ-Glu containing peptides

Alpha A crystallin peptide (1-11)

As shown in Figure 6.1, the αA crystallin peptide (1-11) represents the simplest situation, where there is only one Gln residue in its peptide sequence that can undergo deamidation. The C-terminal lysine residue is the preferred site to retain the charge after the electron capture, and consequently the ECD spectra in Figure 6.1 are dominated by the C-terminal fragments, z• ions.

In addition to the z• ions, z• fragments with additional Gln/Glu side chain losses are also observed in Figure 6.1. The ECD spectra of both Glu and γ-Glu containing αA crystallin peptides have peaks corresponding to z_6•-59 ions (Figures 6.1 b and c, insets), although they are formed via different mechanisms. In ECD of the Glu containing αA crystallin peptide (Figure 6.1 b), the z_6•-59 ion is the w_6 ion, generated by the α-cleavage induced by the radical on the z_6• ion (Figure 6.5 a). In addition, a series of peaks corresponding to z_n•-59 ions (n>6) are also observed. These ions are generated from the partial loss of the Glu side chain from the corresponding z• ions, following through-space radical rearrangement (Figure 6.5 b) [144, 247]. Similar radical migration in larger z_n• ions (n>6) to the alpha position of the γ-Glu site may also occur in ECD of the γ-Glu containing αA crystallin peptide. However, because the C_β-C_γ bond is part of the

backbone in this γ-Glu peptide, its subsequent cleavage will not result in the formation of a series of z_n•-59 ions, but rather z_6•-59 ion only (Figure 6.5 c, Figure 6.1 c). Although the z•-59 ion is observed site specifically in γ-Glu peptides, it can not be used as the diagnostic ion, because of its presence in Glu peptides as well.

By contrast, the z_6•-72 ion is only present in the γ-Glu containing αA crystallin peptide, but not in the Glu peptide (Figures 6.1 b and c, insets). It may be formed via a similar mechanism to that of the isoAsp diagnostic ion formation in ECD [207]. In addition to the N-C_α bond cleavage, the electron capture at the protonated carbonyl group of the γ-Glu residue could also induce C_α-C_β cleavage at its N-terminal side, generating the c+71 and z•-71 ions. The primary carbon radical in the c+71 ion is unstable, which may abstract a hydrogen from the z•-71 ion species to form the stable c+72 and z•-72 ions (Figure 6.6 a). However, because of the unstable radical intermediates involved, this process is not expected to play a significant role. A more plausible mechanism is shown in Figure 6.6 b, where the radical on the N-terminal α-carbon of the z• ions can initiate α-cleavage along the peptide backbone to generate z•-72 ions.

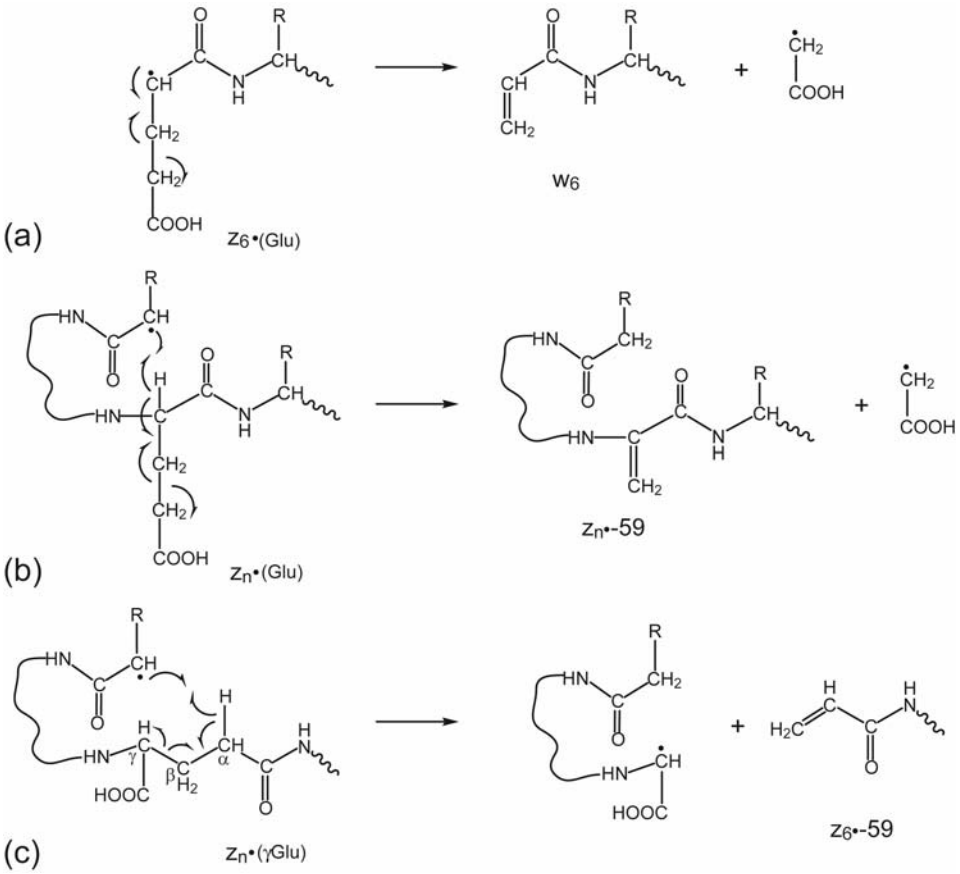

Figure 6. 5 Mechanisms for the formation of z•-59 ions in ECD of the Glu containing αA crystallin peptide (1-11) via (a) direct partial side-chain loss (w_6 ion formation) and (b) through-space radical rearrangement. (c) proposed mechanism for the formation of site specific z_6•-59 ions in ECD of the γGlu containing αA crystallin peptide (1-11).

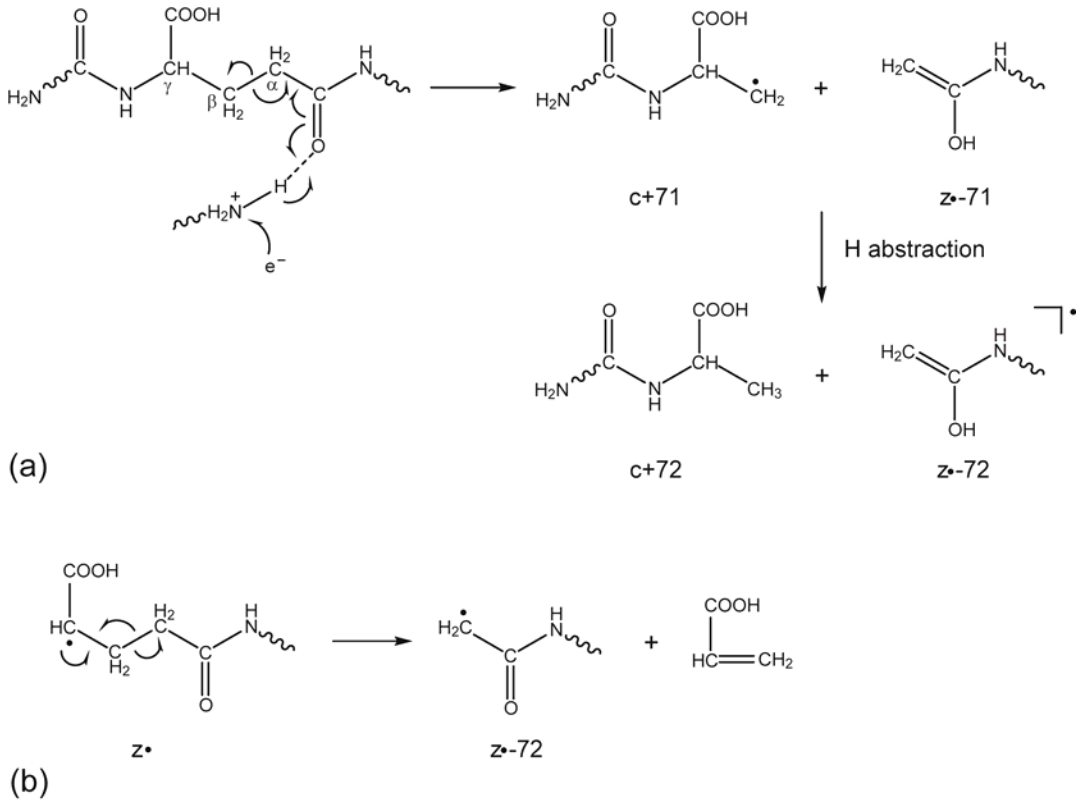

Figure 6. 6 Proposed mechanisms for the formation of z•-72 ions in the ECD of the γGlu containing peptide via (a) primary backbone cleavage and (b) secondary fragmentation.

In rare occasions, z•-72 ions corresponding to the entire Glu side chain loss from z• ions may also be present in the ECD spectra of Glu containing peptides. These ions are usually formed via α-cleavage following through-space radical migration to the γ-carbon of the Glu residue [247], and they almost never occur at sites directly N-terminal to the Glu residue. For example, in Figure 6.1 b, the z_8•-72 ion is observed, but the z_6•-72 ion is absent. Thus, the site specific z•-72 ions may serve as characteristic ions for the differentiation of the Glu and γ-Glu containing peptides. Due to the presence of the C-terminal lysine residue, in the ECD spectrum of the γ-Glu containing αA crystallin

peptide, no peaks corresponding to the N-terminal complementary (c+59 or c+72) ions are observed.

Beta B2 crystallin peptide (4-14)

The C-terminal fragments. The βB2 crystallin peptide (4-14) contains three Gln residues (Gln_2, Gln_4, and Gln_9) in its sequence and one lysine residue in the middle, presenting an opportunity to investigate both N- and C-terminal fragments in ECD. The ECD spectra of the βB2 crystallin peptide and two of its potentially deamidated forms are shown in Figure 6.2 a-c, respectively. Figure 6.2 d shows the comparison of several regions of interest between ECD spectra of the two potentially deamidated forms of βB2 crystallin peptide. ECD of the γ-Glu containing peptide generates site specific z_n•-59 ions N-terminal to the γ-Glu residues (n = 8 and 10, Figure 6.2 c), with the exception of the z_3•-59 ion, which is not observed due to its lack of a charge carrier. However, these z_n•-59 ions are also present in the ECD spectrum of the Glu containing peptide (Figure 6.2 b), as a result of the partial side chain losses from the Glu residues, preventing their use as diagnostic ions for γ-Glu residues.

On the other hand, the z_n•-72 peaks are present site specifically (n = 8 and 10) in the ECD spectrum of the γ-Glu containing βB2 peptide, but absent in that of the Glu containing βB2 peptide, Figure 6.2 d, similar to what was observed in the ECD study of the αA crystallin peptide. In the case of the βB2 crystallin peptide, however, there is an added complexity caused by the interference peaks of the lysine side chain loss from z• ions. For example, the first isotopic peak of the diagnostic z_8•-72 ion for the γ-Glu peptide at *m/z* 743.39 overlaps with the monoisotopic peak of the z_8•-Lys peak at *m/z* 743.33,

which is present in the ECD spectra of both the Glu and γ-Glu peptides. However, this interference peak does not present a problem for the identification of the γ-Glu here, as it can be easily distinguished from the diagnostic ion based on the accurate mass measurement afforded by the high performance FT-ICR instrument.

A further, and more serious, complication arises from the presence of multiple Glu residues in this peptide. In the ECD spectrum of the Glu peptide, there is a tiny peak at *m/z* ~742.38, which likely arises from the loss of Glu_9 side chain of the z_8• ion, via γ hydrogen abstraction at Glu_9. Since this z_8•-Glu ion has the same exact mass as that of the z_8•-72 diagnostic ion in the ECD spectrum of the γ-Glu peptide, they cannot be differentiated even by an FT-ICR mass analyzer. The result from this peptide illustrates a potential limitation of using z•-72 ion as the diagnostic ion for the identification of γ-Glu residue in peptides with multiple Glu residues. However, since side chain loss occurrence from a remote residue often decreases dramatically as its distance from the backbone cleavage site increases, such interference is likely to be minimal as evident from the very low abundance of the z_8•-72 ion and the absence of the z_{10}•-72 ion here.

Nonetheless, it would still be advantageous to identify additional characteristic ions for γ-Glu peptides to make the assignment with higher confidence. Of particular interest is the search for N-terminal diagnostic ions, since unlike z• ions, these ions usually do not contain a radical to initiate side chain losses which may produce interference peaks.

The N-terminal fragments and amino acid side chain loss from the charge reduced species. The right panel of Figure 6.2 d shows the difference associated with N-terminal fragments between ECD spectra of the two potentially deamidated forms of βB2

crystallin peptide. Of the three γ-Glu residues, only one site (γ-Glu_9) produced complementary diagnostic ions that correspond to the c_8+57, c_8+59, and c_8+72 ions. The potential characteristic N-terminal fragments for the other two γ-Glu sites do not contain the charge carrying lysine residue and are hence, unobservable. The peak at *m/z* 922.43 does not arise from the c_8+55 ion, but rather the a_9•-CH_4N ion. The peak at *m/z* 939.453 corresponding to the c_8+72 ions in the γ-Glu peptide ECD spectrum can be distinguished from the peak at *m/z* 939.442 in the Glu peptide ECD spectrum, which is the result of multiple side chain losses.

The c+72 ions may be formed via the C_α-C_β cleavage upon electron capture followed by intra-complex hydrogen transfer, although this process is disfavored because of the unstable primary carbon radical involved as discussed earlier (Figure 6.6a). An alternative mechanism is shown in Figure 6.7, which involves the ring opening process of proline residue. Dissociations of proline radicals formed by ECD/ETD have been studied in the past, where it was found that although H-atom loss is energetically favored over backbone dissociations, H-atom migrations may also occur [314], sometimes leading to secondary N-C or C-C bond cleavage at the proline side chain [54]. In this case, the C_α radical generated by the initial N-C_α bond cleavage at the proline residue can abstract one hydrogen from the α or γ position of the nearby γ-Glu residue to induce α-cleavage and form c+59 and c+72 ions, respectively. All intermediates in Figure 6.7 involved are resonantly stabilized by the conjugated carbonyl groups [315]. By contrast, in ECD of Glu containing peptides, because there are no additional methylene groups in the Glu peptide backbone, the hydrogen abstraction from the α or γ position of the Glu residue will only lead to partial or entire side chain loss from the molecular ions, as shown in Figure 6.8.

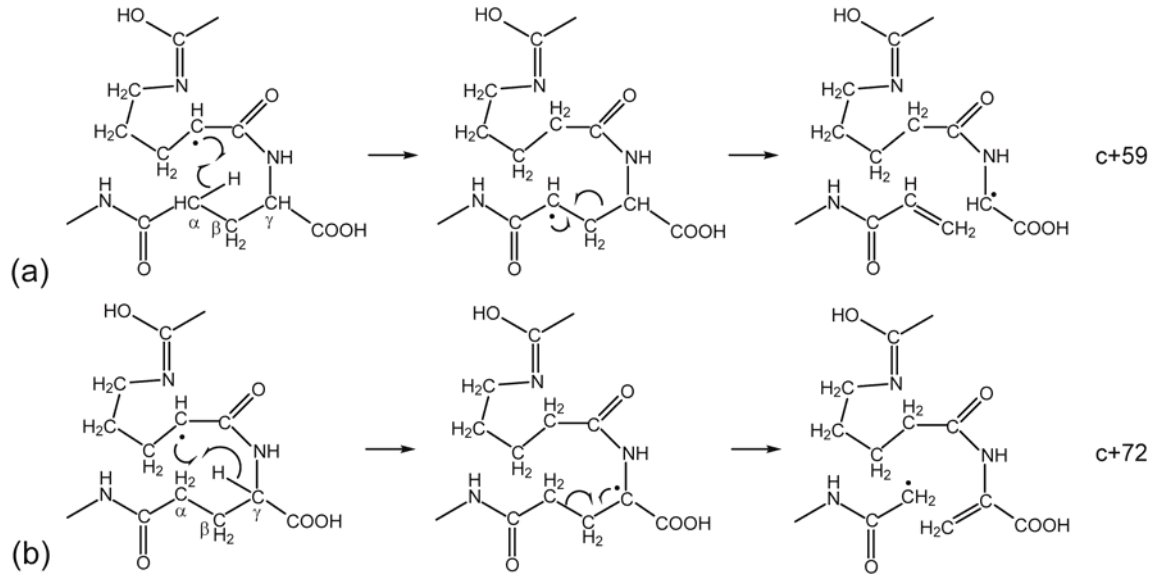

Figure 6. 7 Proposed mechanisms for the formation of (a) c+59 and (b) c+72 ions in the γGlu containing peptide via proline ring opening process.

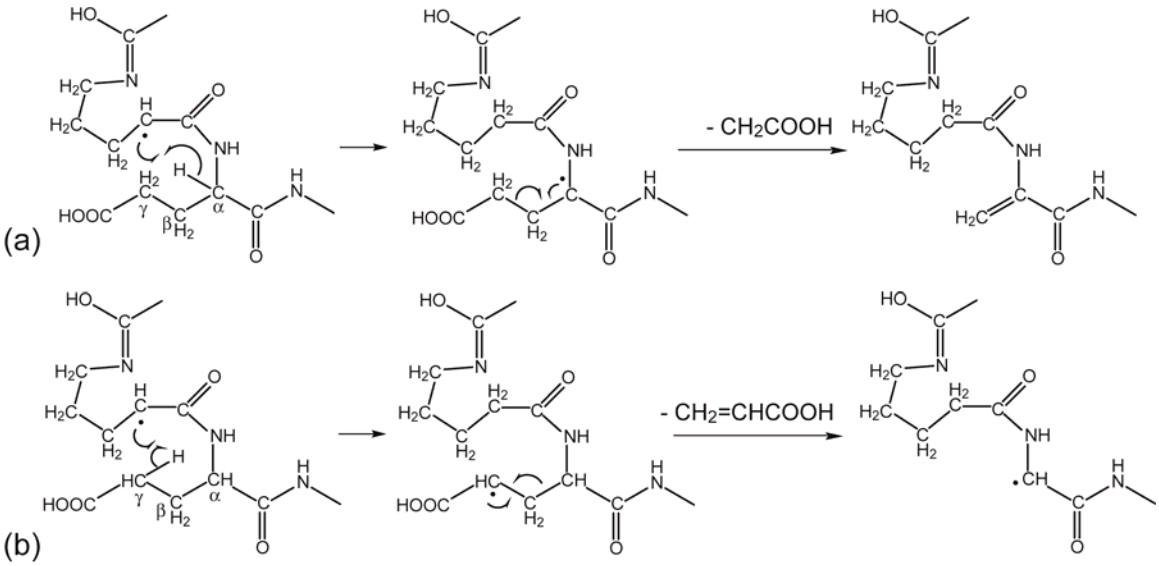

Figure 6. 8 Proposed mechanisms for the loss of (a) -CH_2COOH and (b) -CH_2=CHCOOH molecules in the Glu containing peptide via proline ring opening process.

The amino acid side chain losses from the charge reduced species are usually initiated by electron capture at either charged basic amino acid side chains (e.g. Arg, Lys,

and His), or amino acid residues capable of solvating the charge (e.g. Asp and Met). It has been shown that charge neutralization at the solvated Asp side chain can lead to the formation of the diagnostic $[M-60]^{+\bullet}$ ion by losing an even electron species, $CH_2=C(OH)_2$ [206]. The radical is left on the backbone α-carbon, which is stabilized captodatively by the neighboring amine and carbonyl groups. Although the carboxylic acid group of the Glu side chain is also capable of solvating the charge, a similar process is unlikely to occur at Glu residues, as the loss of the $CH_2=C(OH)_2$ group will result in the formation of an unstable primary radical on the β-carbon. Nonetheless, partial Glu side chain loss from the charge reduced species is present (peak at *m/z* 1139.57) in the ECD spectrum of the Glu containing βB2 peptide ECD spectrum here. This 59 Da loss corresponds to the loss of a radical $\bullet CH_2COOH$ species, most likely from the Glu side chain following the proline ring opening.

The proposed mechanisms for the c+57 ion formation are shown in Figure 6.9. The c_8+57 ion may be formed from the $a_9\bullet$ ion via loss of an ethylene molecule (Figure 6.9 a), although the $a_9\bullet$ ion itself contains an unstable primary carbon radical, which makes this mechanism an unattractive one. Alternatively, the c+57 ions could result from the intra-complex hydrogen transfer after the initial N-C_α bond cleavage. For any c ion that contains the γ-Glu residue, the radical on its complementary z• fragment may abstract a hydrogen atom from the α-carbon of the γ-Glu, and the resulting c• radical can undergo α-cleavage to produce the c+57 ion (Figure 6.9 b).

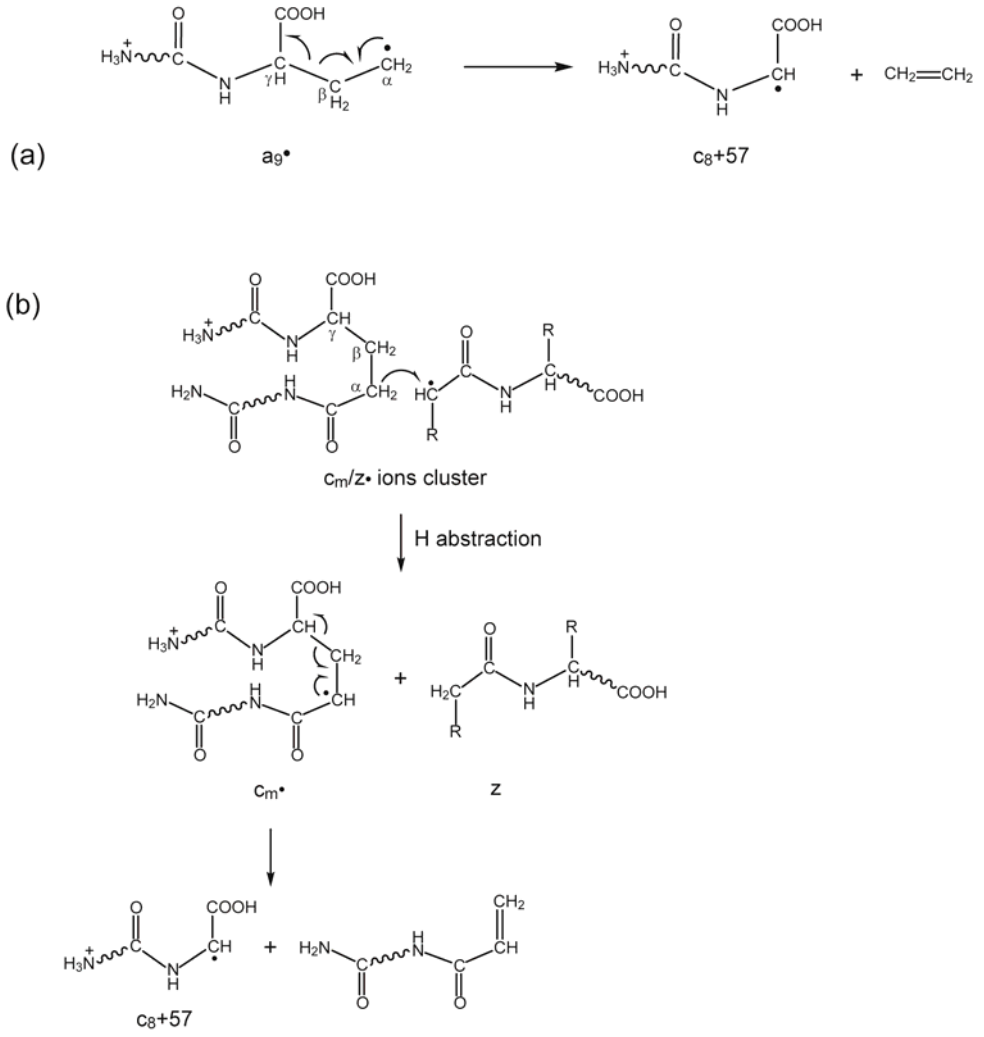

Figure 6. 9 Proposed mechanisms for the formation of c+57 ions in the γGlu containing βB2 peptide, from (a) a• ions and from (b) the intra-complex hydrogen transfer.

The site-specific occurrence of the c+57, c+59, and c+72 ions at the γ-Glu residue observed here suggests that they too can be used as diagnostic ions for the identification of γ-Glu residues.

Gamma S crystallin peptide (52-71)

Both αA crystallin peptide (1-11) and βB2 crystallin peptide (4-14) are short Gln containing peptides, without the interference of other existing Glu residues in their sequences. The γS crystallin peptide (52-71) contains two Gln residues and two Glu residues in its twenty amino acid-long peptide sequence, which makes the differentiation of Glu and γ-Glu residues more complex than in the αA and βB2 crystallin peptides. The two potentially deamidated forms studied here include one containing four Glu residues, and another containing two Glu and two γ-Glu residues.

The comparison of the relevant regions associated with fragmentations near the two γ-Glu sites (γ-Glu_{12} and γ-Glu_{19}) from Figure 6.3 c and the related Glu sites from Figure 6.3 b is shown in Figure 6.3 d. Peaks corresponding to z_9•-59, z_9•-57, and z_9•-72 ions as well as the complementary c_{11}+57 and c_{11}+59 ions, which are generated by cleavage within the γ-Glu_{12} residue, are present in the ECD spectrum of the γ-Glu containing γS crystallin peptide. However, the complementary c_{11}+72 ion is not observed here. Incidentally, in the γS crystallin peptide, the γ-Glu_{12} residue is also preceded by a proline residue, just like the γ-Glu_9 residue in the βB2 peptide. Thus, it is not clear whether the c+57 and c+59 ions are sequence specific or they may serve as general diagnostic ions. None of these N- and C-terminal characteristic ions are observed in the ECD spectrum of the Glu containing γS peptide. The tiny peak at *m/z* 1096 in the Glu peptide spectrum does not correspond to the z_9•-59 ion, but rather an internal fragment: MYILPEGEY, based on its accurate mass. Therefore, the presence of these complementary diagnostic ions provides high confidence for the identification and location of the γ-Glu_{12} residue, even in the presence of multiple Glu residues in the sequence.

For the γ-Glu_{19} residue in the γ-Glu containing γS crystallin peptide, the diagnostic z_2•-59 and c_{18}+59 ions have the same elemental composition as the c_2 and z_{18}• ions, respectively. This ambiguity has a similar origin as the homeometric peptides, which are different peptides with similar theoretical tandem mass spectra [216, 316]. This does not constitute a systematic limitation to the method developed here, since its occurrence is expected to be rare, although it does emphasize the importance of multiple diagnostic ions to increase the confidence in γ-Glu identification. Unfortunately, in this particular case, the z_2•-72 and c_{18}+72 ions are not observed in the γ-Glu peptide ECD spectrum either. Thus, the γ-Glu_{19} residue could not be identified by the N- or C-terminal characteristic ions established here.

There are, in general, no equivalent Glu diagnostic ions to the abundant $[M-60]^{+\bullet}$ ion present in the ECD spectra of Asp containing peptides [207]. The $[M-60]^{+\bullet}$ ion is produced via the charge neutralization at the solvated Asp side chain, a process that is inhibited at the Glu side chain, due to the instability of the resulting radical. Direct Glu side chain loss from the charge reduced species either partially or completely, is rarely observed in ECD. Of the three Glu containing peptides studied here, only one, the βB2 crystallin peptide, produced the partial Glu side chain loss peak at $[M-59]^{+\bullet}$, and it is likely an unusual case due to the presence of the proline residue. On the other hand, a series of z_n•-59 ions in the ECD spectra of the Glu containing peptides may be used to infer the existence of Glu residue(s), but they can not be generally used to locate the position or to determine the number of Glu residues. Finally, while it is possible to quantify the relative content of γ-Glu in a mixture of deamidation products, the presence of z_n•-59 and z_n•-72 ions due to remote Glu side chain losses makes the quantification of

α- and γ-Glu residues a much more difficult task, particularly when there are multiple Glu/γ-Glu residues present in the sequence.

6.4 Conclusion

Three synthetic human crystallin peptides and their potentially deamidated forms were analyzed by ECD in this study. The C- and N-terminal diagnostic ions associated with the γ-Glu residue were established and the fragmentation mechanisms were discussed. In the ECD spectra of these peptides, peaks corresponding to the z•-72 fragment ions were observed at multiple γ-Glu sites in the γ-Glu containing peptides, but were generally absent in the Glu containing peptides. Further, these z•-72 fragment ions happened only at sites N-terminal to the γ-Glu residues. Thus, the z•-72 fragment ions can be used as diagnostic ions for the differentiation of the α- and γ-Glu residues, and for the determination of the γ-Glu sites. This C-terminal diagnostic ion is especially useful in the bottom-up approach, which typically involves the analysis of tryptic peptides containing a C-terminal charge carrier that facilitates the detection of C-terminal fragments in ECD.

The z•-59 fragment ions, although detected site specifically in ECD of γ-Glu containing peptides, were also present in the ECD spectra of Glu containing peptides. This 59 Da loss from Glu containing z• ions arose from the partial loss of the Glu side chain, either directly at the cleavage site (w ion) or following through-space radical rearrangement within the corresponding z• ions, which led to the formation of a series of z_n•-59 ions. The presence of a series of z_n•-59 ions is suggestive of the existence of Glu residue(s), but cannot be used to determine their exact locations.

In the ECD spectra of the three crystallin peptides studied, the N-terminal diagnostic ions (c+57, c+59 and/or c+72 ions) were only observed at two γ-Glu sites, both of which contain proline residue located directly before γ-Glu residue. Because of the relative location of the γ-Glu residues and the charge carriers, the only γ-Glu residue in a non-Pro-γGlu sequence capable of generating detectable N-terminal diagnostic ions here is the γ-Glu_{19} in the γS crystallin peptide. However, it is impossible to either confirm or rule out the formation of the diagnostic c+59 ion related to this γ-Glu_{19} residue, due to the presence of an interference ion. Thus, it remains unclear whether the N-terminal diagnostic ions are Pro-γ-Glu sequence specific or they may serve as general diagnostic ions. Even if the proline effect is generally applicable, the c+59 and c+72 ions will still be useful in the study of Gln deamidations in the Pro-Gln rich regions of crystallin, gluten and other biological proteins [317, 318].

In conclusion, multiple diagnostic ions including both N- and C-terminal fragments for the identification of γ-Glu residue were established using ECD, which provided confident differentiation of the Glu and γ-Glu residues at the peptide level. This knowledge will facilitate the bottom-up analysis of Gln deamidations in aged or diseased proteins. The high mass accuracy afforded by the FT-ICR instrument is crucial for confident identification, particularly in larger peptides, where interference peaks abound.

Chapter 7

Conclusion and Future Work

7.1 Conclusion

Tandem mass spectrometry methods, such as CAD, ECD, ETD, have been widely used in protein characterization and peptide sequencing. Among these methods, ECD is the one with the greatest potential to induce extensive backbone cleavages and maintain labile PTMs. Although the exact mechanism of ECD is still under debate, great effort has been taken by many research groups. The dissociation-recombination mechanism and the amide-superbase mechanism were proposed to explain the primary backbone cleavages in ECD. The free radical cascade mechanism was proposed for the secondary fragmentation. In FRC, it is believed that the α-carbon radical generated from the primary backbone cleavage can further propagate along the peptide backbone by losing cyclic neutrals or hydrogen abstraction to induce secondary backbone cleavages, or induce small molecule and side-chain losses via hydrogen transfer or radical rearrangement. This dissertation focuses on the understanding of the secondary fragmentation mechanism of ECD and the application of ECD to the differentiation of isomeric protein deamidation products.

It was proposed that the inhibition of the generation of H• and migration of free radicals will significantly reduce the backbone cleavages in linear peptide ECD. In order to further test this hypothsis, the 2,4,6-trimethylpyridinium salt was used as the fixed charge tag, with the potential to both trap the originally formed radical upon electron capture and inhibit the H• generation. TMP was previously reported to specifically label

lysine residue in peptides. Two amyloid β peptides with each containing one lysine residue in its sequence were used as model peptides. Both singly labeled and doubly labeled Aβ peptides were formed, which suggested that the N-termini of these peptides were also labeled by TMP. ECD of the native peptides, singly labeled, and doubly labeled peptides were performed and the spectra were compared. It was found that both the number and location of the fixed charge groups influenced the backbone and side-chain cleavages of these modified peptides. In general, the frequency and extent of backbone cleavages decreased and those of side-chain cleavages increased with the addition of fixed charge tags. The few c and z• ions observed in ECD of the doubly labeled peptides indicated that although the hydrogen transfer was important for backbone fragmentation in ECD, other fragmentation channels involving radical migration may also exist. However, the modification of the peptides may alter the conformation and electronic structure of the peptides and influence the electron capture process and products.

To further explore the ECD mechanism, secondary fragmentation generated in ECD of several unmodified peptides was investigated as well. Abundant charge remote fragmentations of z• ions were observed, which were internal fragments or partial/entire side-chain losses from amino acids, sometimes several residues away from the backbone cleavage site. In addition, multiple side-chain losses were also observed. All of these fragments have the common feature that they all formed via cleavage spatially remote from the charge carrier site, referred to as CRFs. Abundant tryptophan side-chain losses from z• ions were observed, which was considered to be the result of the γ-hydrogen abstraction in the tautomeric structure of tryptophan. Similar γ-hydrogen abstraction from the aromatic and tautomeric structure may also induce the entire side-

chain loss from tyrosine residue. The low abundance internal fragments were observed in peptides with basic residues located in the middle of the sequences, which supported the FRC mechanism. In summary, these CRFs were formed via secondary cleavages initiated by hydrogen abstraction at the α-, β-, and γ-position of the amino acid side chain. Although the existence of abundant CRFs complicates the ECD spectra interpretation, it provides ECD with the ability to differentiate the isomeric residues in peptide sequence and helps de-novo sequencing. ETD has a similar fragmentation mechanism to ECD, generating c and z• fragment ions. In comparison, ETD of these unmodified peptides generates fewer CRF fragments than ECD, possibly due to the lower energy deposition in electron transfer and the collisional cooling effect present in the ion trap instrument. Fewer CRFs in ETD may simplify the database searching.

CAD is a commonly used tandem mass spectrometry method, producing b and y fragment ions for peptides and proteins. While the y ions represent the truncated and protonated peptides, the b ions are postulated to have multiple structures (acylium, oxazolone, and macro-cyclic structures, among others). Although the oxazolone and macro-cyclic b-ion structures have been studied by CAD, very few ECD studies of b ions have been performed. Since the combination of CAD and ECD in tandem will often provide comprehensive sequence information in peptide sequencing, the correct b-ion sequence determination will have fundamental role in peptide sequencing. Doubly charged b ions of several tachykinin peptides and two variants of substance P with varied sizes (b_5 to b_{10}) were investigated by ECD. Theoretical studies of selected doubly charged b ions of substance P were also performed to further check the experimental results, by the calculation of the energetics of conformer candidates generated from molecular dynamics simulations. The data showed that the formation of two different

types of macro-cyclic structures of medium-sized b ions probed by ECD, which may result in erroneous sequence assignment when the combined CAD and ECD methods are used in peptide sequencing. From the results, it also indicated that the N-terminus, rather than C-terminus, was important for the macro-cyclic structure formation, as these tachykinin peptides have a common C-terminal sequence, but different b-ion structures. The ECD results of the b ions from two variants of substance P suggested that the substitution of middle amino acid residues did not influence the macro-cyclic structure formation. Due to the somewhat non-selective cleavage feature of ECD, ECD of the macro-cyclic b ions can generate a series of fragment ions which can help assign the intermediate structure. On the other hand, ECD of large-sized b ions did not show undirected sequence fragments, which will be beneficial for the combination of CAD and ECD method in MS^3 and even higher level MS/MS study.

As an important non-enzymatic PTM, deamidation is involved in many biological processes, many of which are related to aging, such as Alzheimer's disease, and cataract formation, etc. A variety of methods have been developed to identify the deamidation sites in peptides and proteins, by measuring the +0.984 Da mass shift and/or the introduction of one negative charge per deamidation site, or the conformational change induced by the extension of the backbone in the deamidated products. Because of its high sensitivity, speed, accuracy, small sample requirement, and the production of detailed backbone cleavage information, tandem mass spectrometry has become the most widely used method in the identification of deamidation sites. More importantly, the isomeric deamidation products of Asn residues, Asp and isoAsp, can be distinguished by ECD based on the diagnostic ions formed from

each isomer, the c+57 and z•-57 ions for isoAsp residue and the M-60 corresponding to the side-chain loss from Asp residue. This method has been established to differentiate and quantify the relative abundance of the isomeric deamidation products of Asn in peptides by previous studies in our group.

Due to the fast deamidation rate of the NG sequence in flexible peptides ($t_{1/2}$ less than one day), it is important to determine whether the sample processing, particularly the commonly used trypsin digestion process, introduces artifical deamidation to the samples. In order to achieve an accurate measurement of the deamidation products, the $H_2{}^{18}O$ labeling method was used to monitor three rapidly deamidating peptides released from proteins: calmodulin, ribonuclease A, and lysozyme. These tryptic peptides contained fast deamidating NG or NS sequences. The ^{18}O atom would incorporate into the newly formed deamidation site and cause a mass increase by ~+3 Da per deamidation site, compared to the ~+1 Da mass shift in the pre-existing deamidation site. It was verified by the ESI spectra of these peptides during the trypsin digestion time course study and further confirmed by the backbone fragments and diagnostic ions generated in ECD experiments of the calmodulin tryptic peptide. The data indicated that a fast (~4 hr) trypsin digestion process generates minimal peptides deamidation(s). This result provides a general and reliable time period for the accurate deamidation measurement.

Compared to the extensively studied Asn deamidation, Gln deamidation study is very understudied due to its much slower deamidation rate than that of Asn. Gln deamidation has the similar mechanisms to that of Asn, either by direct hydrolysis or via the formation of cyclic intermediates depending on the reaction conditions. The difficulty for the formation of the six-membered ring structure of glutarimide intermediation may

contribute to its slow deamidation rate. One exception of Gln deamidation rate is when Gln is located at the N-terminus of the peptide sequence, in which case it deamidates more rapidly than Asn. Few studies of Gln deamidation have been reported, and even fewer were reported to differentiate its isomeric deamidation products, α- and γ-Glu residues. The existent methods for the differentiation of Gln deamidation products were only applicable to small peptides with less than five amino acids and most of them were limited to the situation where γ-Glu was located at the N-terminus. Despite its slower rate Gln deamidation still has important biological significance and is involved in many diseases, such as celiac diseases and aged or diseased lens crystallin proteins. Thus, establishing a fast and accurate detection method for the differentiation of the isomeric Gln deamidation products is necessary.

The ECD based method for the differentiation of isomeric deamidation products of Asn was extended to the Gln deamidation study. Three peptides from different types of human lens crystallins and their potentially Gln deamidated forms were used as model peptides to study the characteristic ions for isomeric Gln deamidation products in ECD. These three peptides present different situations: one Gln residue in the peptide sequence, multiple Gln residues in the peptide sequence, and multiple Gln residues with the co-existence of multiple Glu residues in the peptide sequence. The lengths of these peptides range from ten to twenty amino acids. It was found that the z•-72 ions can be used to identify the existence and locate the position of the γ-Glu resiudes. Although the z•-59 ions was also site specific to γ-Glu residue, the presence of a series of z•-59 ions in the Glu containing peptide made it unsuitable as diagnostic ions. When the peptide contains a charge carrier near its N-terminus, the c+57 and c+59 ions may also be produced at the γ-Glu site. It was unclear whether these N-terminal fragments were

sequence specific or may serve as general diagnostic ions, because their formation were associated with the Pro-γ-Glu sequence in the limited numbers of peptides studied here. Unlike the M-60 fragment ions generated from Asp containing peptide, the side-chain loss from Glu side chain generates an unstable radical, thus no characteristic ions were found for Glu.

7.2 Future work

PIMT is used as a repair enzyme in biological systems to recognize and catalyze the conversion of isoAsp to Asp, although during each cycle only 30% of isoAsp is converted to Asp. As the cycle goes on, it may eventually correct all isoAsp. Furthermore, Asn deamidation rate is largely influenced by the primary structure of the peptides, especially the neighboring amino acids. The commonly known Asn deamidation ratio has this sequence: NG < NS, NT< other NX (X means other amino acids). Thus a hypothesis is provided that there is also sequence specificity for PIMT enzyme. This may be studied by quantitatively measuring the PIMT reaction products from sequence specific isoAsp containing peptides. The quantitation method was previously established utilizing the linear relationship between the relative abundance of the isoAsp diagnostic ion z•-57 and the percentage of isoAsp content in the mixture.

Up until now, the ECD based method for the differentiation of the isomeric deamidation products was successfully applied to peptides mostly released from trypsin digestion, at the bottom-up level. During the sample processing, the artificial deamidation may be introduced into samples and influence the accuracy of the deamidation detection. The direct detection of deamidation products at the whole protein level by top-down ECD analysis may be used to avoid these problems and simplify the

sample handling process. However, the data analysis of the top-down ECD spectra will be much more complex than that of small peptides and the interference from other fragmentation channels in top-down analysis may also complicate the diagnostic ions identification.

Bibliography

1. Bode, A. M.; Dong, Z. G. Post-translational modification of p53 in tumorigenesis. *Nature Reviews Cancer* **2004,** *4*, 793-805.

2. Gong, C. X.; Liu, F.; Grundke-Iqbal, I.; Iqbal, K. Post-translational modifications of tau protein in Alzheimer's disease. *Journal of Neural Transmission* **2005,** *112*, 813-838.

3. Witze, E. S.; Old, W. M.; Resing, K. A.; Ahn, N. G. Mapping protein post-translational modifications with mass spectrometry. *Nature Methods* **2007,** *4*, 798-806.

4. Mann, M.; Jensen, O. N. Proteomic analysis of post-translational modifications. *Nature Biotechnology* **2003,** *21*, 255-261.

5. Fenn, J. B.; Mann, M.; Meng, C. K.; Wong, S. F.; Whitehouse, C. M. Electrospray ionization for mass-spectrometry of large biomolecules. *Science* **1989,** *246*, 64-71.

6. Fenn, J. B.; Mann, M.; Meng, C. K.; Wong, S. F.; Whitehouse, C. M. Electrospray ionization-principles and practice. *Mass Spectrometry Reviews* **1990,** *9*, 37-70.

7. Hoffmann, E. D.; Stroobant, V. Mass spectrometry: Principles and applications. John Wiley & Sons, Ltd. **2007**.

8. Munson, M. S. B.; Field, F. H. Chemical ionization mass spectrometry. I. Genral introduction. *Journal of the American Chemical Society* **1966,** *88*, 2621-2630.

9. Barber, M.; Bordoli, R. S.; Sedgwich, R. D.; Tyler, A. N. Fast atom bombardment of solids (F.A.B.): A new ion source for mass spectrometry. *Journal of the Chemical Society, Chemical Communications* **1981**, 325-327.

10. Beranova-Giorgianni, S.; Desiderio, D. M. Fast atom bombardment mass spectrometry of synthetic peptides. *Methods in Enzymology* **1997,** *289*, 478-499.

11. Karas, M.; Bachmann, D.; Bahr, U.; Hillenkamp, F. Matrix-assisted ultraviolet-laser desorption of nonvolatile compounds. *International Journal of Mass Spectrometry and Ion Processes* **1987,** *78*, 53-68.

12. Stults, J. T. Matrix-assisted laser-desorption ionization mass-spectrometry (MALDI-MS). *Current Opinion in Structural Biology* **1995,** *5*, 691-698.

13. Dreisewerd, K. The desorption process in MALDI. *Chemical Reviews* **2003,** *103*, 395-425.

14. Kebarle, P.; Verkerk, U. H. Electrospray: From ions in solution to ions in the gas phase, what we know now. *Mass Spectrometry Reviews* **2009,** *28*, 898-917.

15. Cech, N. B.; Enke, C. G. Practical implications of some recent studies in electrospray ionization fundamentals. *Mass Spectrometry Reviews* **2001,** *20*, 362-387.

16. Whitehouse, C. M.; Dreyer, R. N.; Yamashita, M.; Fenn, J. B. Electrospray interface for liquid chromatographs and mass spectrometers. *Analytical Chemistry* **1985,** *57*, 675-679.

17. Bruins, A. P.; Covey, T. R.; Henion, J. D. Ion spray interface for combined liquid chromatography/atmospheric pressure ionization mass-spectrometry. *Analytical Chemistry* **1987,** *59*, 2642-2646.

18. Wilm, M.; Mann, M. Electrospray and Taylor-cone theory, Dole's beam of macromolecules at last? *International Journal of Mass Spectrometry and Ion Processes* **1994,** *136*, 167-180.

19. Wilm, M.; Mann, M. Analytical properties of the nanoelectrospray ion source. *Analytical Chemistry* **1996,** *68*, 1-8.

20. Gaskell, S. J. Electrospray: Principles and practice. *Journal of Mass Spectrometry* **1997,** *32*, 677-688.

21. Kebarle, P. A brief overview of the present status of the mechanisms involved in electrospray mass spectrometry. *Journal of Mass Spectrometry* **2000,** *35*, 804-817.

22. Loo, J. A. Electrospray ionization mass spectrometry: a technology for studying noncovalent macromolecular complexes. *International Journal of Mass Spectrometry* **2000,** *200*, 175-186.

23. Guilhaus, M. Principles and instrumentation in time-of-flight mass-spectrometry - physical and instrumental concepts. *Journal of Mass Spectrometry* **1995,** *30*, 1519-1532.

24. Wollnik, H. Time-of-flight mass analyzers. *Mass Spectrometry Reviews* **1993,** *12*, 89-114.

25. Weickhardt, C.; Moritz, F.; Grotemeyer, J. Time-of-flight mass spectrometry: State-of-the-art in chemical analysis and molecular science. *Mass Spectrometry Reviews* **1996,** *15*, 139-162.

26. Downard, D. Mass spectrometry: A foundation course. Royal Society of Chemistry, Cambridge **2004**.

27. Comisaro.Mb; Marshall, A. G. Frequency-sweep fourier transform ion cyclotron resonance spectroscopy. *Chemical Physics Letters* **1974,** *26*, 489-490.

28. Comisaro.Mb; Marshall, A. G. Fourier transform ion cyclotron resonance spectroscopy. *Chemical Physics Letters* **1974,** *25*, 282-283.

29. Amster, I. J. Fourier transform mass spectrometry. *Journal of Mass Spectrometry* **1996,** *31*, 1325-1337.

30. Marshall, A. G.; Hendrickson, C. L.; Jackson, G. S. Fourier transform ion cyclotron resonance mass spectrometry: A primer. *Mass Spectrometry Reviews* **1998,** *17*, 1-35.

31. Marshall, A. G. Milestones in Fourier transform ion cyclotron resonance mass spectrometry technique development. *International Journal of Mass Spectrometry* **2000,** *200*, 331-356.

32. Marshall, A. G.; Hendrickson, C. L. Fourier transform ion cyclotron resonance detection: principles and experimental configurations. *International Journal of Mass Spectrometry* **2002,** *215*, 59-75.

33. Heeren, R. M. A.; Kleinnijenhuis, A. J.; McDonnell, L. A.; Mize, T. H. A mini-review of mass spectrometry using high-performance FTICR-MS methods. *Analytical and Bioanalytical Chemistry* **2004,** *378*, 1048-1058.

34. Zhang, L. K.; Rempel, D.; Pramanik, B. N.; Gross, M. L. Accurate mass measurements by Fourier transform mass spectrometry. *Mass Spectrometry Reviews* **2005,** *24*, 286-309.

35. Guan, S. H.; Marshall, A. G. Ion traps for Fourier-transform ion-cyclotron resonance mass-spectrometry: Principles and design of geometric and electric configurations. *International Journal of Mass Spectrometry* **1995,** *146*, 261-296.

36. Marshall, A. G.; Guan, S. H. Advantages of high magnetic field for Fourier transform ion cyclotron resonance mass spectrometry. *Rapid Communications in Mass Spectrometry* **1996,** *10*, 1819-1823.

37. Hayes, R. N.; Gross, M. L. Collision-induced dissociation. *Methods in Enzymology* **1990,** *193*, 237-263.

38. Zubarev, R. A.; Kelleher, N. L.; McLafferty, F. W. Electron capture dissociation of multiply charged protein cations. A nonergodic process. *Journal of the American Chemical Society* **1998,** *120*, 3265-3266.

39. Little, D. P.; Speir, J. P.; Senko, M. W.; Oconnor, P. B.; McLafferty, F. W. Infrared multiphoton dissociation of large multiply-charged ions for biomolecule sequencing. *Analytical Chemistry* **1994,** *66*, 2809-2815.

40. Dass, C. Principles and practice of biological mass spectrometry. Wiley, John & sons, Incorporated **2000**.

41. Roepstorff, P.; Fohlman, J. Proposal for a common nomenclature for sequence ions in mass spectra of peptides. *Biomedical Mass Spectrometry* **1984,** *11*, 601-601.

42. Jankowski, K.; Pare, J. R. J.; Belanger, J. Comments on a 'Proposal for a common nomenclature for sequence ions in mass spectra of peptides'. *Biomedical Mass Spectrometry* **1985,** *12*, 631-631.

43. Domon, B.; Costello, C. E. A systematic nomenclature for carbohydrate fragmentations in FAB-MS/MS spectra of glycoconjugates. *Glycoconjugate Journal* **1988,** *5*, 397-409.

44. Wells, J. M.; McLuckey, S. A. Collision-induced dissociation (CID) of peptides and proteins. *Metohds in Enzymology* **2005,** *402*, 148-185.

45. Zubarev, R. A.; Haselmann, K. F.; Budnik, B.; Kjeldsen, F.; Jensen, F. Towards an understanding of the mechanism of electron-capture dissociation: a historical perspective and modern ideas. *European Journal of Mass Spectrometry* **2002,** *8*, 337-349.

46. Loo, J. A.; Edmonds, C. G.; Smith, R. D. Tandem mass-spectrometry of very large molecules .2. Dissociation of multiply charged proline-containing proteins from electrospray ionization. *Analytical Chemistry* **1993,** *65*, 425-438.

47. Yu, W.; Vath, J. E.; Huberty, M. C.; Martin, S. A. Identification of the facile gas-phase cleavage of the Asp-Pro and Asp-Xxx peptide bonds in matrix-assisted laser-desorption time-of-flight mass spectrometry. *Analytical Chemistry* **1993,** *65*, 3015-3023.

48. Gauthier, J. W.; Trautman, T. R.; Jacobson, D. B. Sustained off-resonance irradiation for collision-activated dissociation involving Fourier-transform mass-spectrometry. Collision-activated dissociation technique that emulates infrared multiphoton dissociation. *Analytica Chimica Acta* **1991,** *246*, 211-225.

49. Loo, J. A.; Udseth, H. R.; Smith, R. D. Collisional effects on the charge distribution of ions from large molecules, formed by electrospry ionization mass spectrometry. *Rapid Communications in Mass Spectrometry* **1988,** *2*, 207-210.

50. Sawicka, A.; Skurski, P.; Hudgins, R. R.; Simons, J. Model calculations relevant to disulfide bond cleavage via electron capture influenced by positively charged groups. *Journal of Physical Chemistry B* **2003,** *107*, 13505-13511.

51. Zubarev, R. A.; Kruger, N. A.; Fridriksson, E. K.; Lewis, M. A.; Horn, D. M.; Carpenter, B. K.; McLafferty, F. W. Electron capture dissociation of gaseous multiply-charged proteins is favored at disulfide bonds and other sites of high hydrogen atom affinity. *Journal of the American Chemical Society* **1999,** *121*, 2857-2862.

52. Syrstad, E. A.; Turecek, F. Toward a general mechanism of electron capture dissociation. *Journal of the American Society for Mass Spectrometry* **2005,** *16*, 208-224.

53. Cooper, H. J.; Hudgins, R. R.; Hakansson, K.; Marshall, A. G. Characterization of amino acid side chain losses in electron capture dissociation. *Journal of the American Society for Mass Spectrometry* **2002,** *13*, 241-249.

54. Cooper, H. J.; Hudgins, R. R.; Hakansson, K.; Marshall, A. G. Secondary fragmentation of linear peptides in electron capture dissociation. *International Journal of Mass Spectrometry* **2003,** *228*, 723-728.

55. Savitski, M. M.; Nielsen, M. L.; Zubarev, R. A. Side-chain losses in electron capture dissociation to improve peptide identification. *Analytical Chemistry* **2007,** *79*, 2296-2302.

56. Leymarie, N.; Costello, C. E.; O'Connor, P. B. Electron capture dissociation initiates a free radical reaction cascade. *Journal of the American Chemical Society* **2003,** *125*, 8949-8958.

57. Cooper, H. J.; Hakansson, K.; Marshall, A. G. The role of electron capture dissociation in biomolecular analysis. *Mass Spectrometry Reviews* **2005,** *24*, 201-222.

58. Bakhtiar, R.; Guan, Z. Q. Electron capture dissociation mass spectrometry in characterization of post-translational modifications. *Biochemical and Biophysical Research Communications* **2005,** *334*, 1-8.

59. McLafferty, F. W.; Horn, D. M.; Breuker, K.; Ge, Y.; Lewis, M. A.; Cerda, B.; Zubarev, R. A.; Carpenter, B. K. Electron capture dissociation of gaseous multiply charged ions by Fourier-transform ion cyclotron resonance. *Journal of the American Society for Mass Spectrometry* **2001,** *12*, 245-249.

60. Sze, S. K.; Ge, Y.; Oh, H. B.; McLafferty, F. W. Plasma electron capture characterization of large dissociation for the proteins by top down mass spectrometry. *Analytical Chemistry* **2003,** *75*, 1599-1603.

61. Horn, D. M.; Ge, Y.; McLafferty, F. W. Activated ion electron capture dissociation for mass spectral sequencing of larger (42 kDa) proteins. *Analytical Chemistry* **2000,** *72*, 4778-4784.

62. Kjeldsen, F.; Haselmann, K. F.; Budnik, B. A.; Jensen, F.; Zubarev, R. A. Dissociative capture of hot (3-13 eV) electrons by polypeptide polycations : An efficient process accompanied by secondary fragmentation. *Chemical Physics Letters* **2002,** *356*, 201-206.

63. Kjeldsen, F.; Haselmann, K. F.; Sorensen, E. S.; Zubarev, R. A. Distinguishing of Ile/Leu amino acid residues in the PP3 protein by (hot) electron capture dissociation in Fourier transform ion cyclotron resonance mass spectrometry. *Analytical Chemistry* **2003,** *75*, 1267-1274.

64. Syka, J. E. P.; Coon, J. J.; Schroeder, M. J.; Shabanowitz, J.; Hunt, D. F. Peptide and protein sequence analysis by electron transfer dissociation mass spectrometry. *Proceedings of the National Academy of Sciences of the United States of America* **2004,** *101*, 9528-9533.

65. Coon, J. J.; Shabanowitz, J.; Hunt, D. F.; Syka, J. E. P. Electron transfer dissociation of peptide anions. *Journal of the American Society for Mass Spectrometry* **2005,** *16*, 880-882.

66. Mikesh, L. M.; Ueberheide, B.; Chi, A.; Coon, J. J.; Syka, J. E. P.; Shabanowitz, J.; Hunt, D. F. The utility of ETD mass spectrometry in proteomic analysis. *Biochimica Et Biophysica Acta-Proteins and Proteomics* **2006,** *1764*, 1811-1822.

67. Swaney, D. L.; McAlister, G. C.; Wirtala, M.; Schwartz, J. C.; Syka, J. E. P.; Coon, J. J. Supplemental activation method for high-efficiency electron-transfer dissociation of doubly protonated peptide precursors. *Analytical Chemistry* **2007,** *79*, 477-485.

68. Gord, J. R.; Horning, S. R.; Wood, J. M.; Cooks, R. G.; Freiser, B. S. Energy deposition during electron-induced dissociation. *Journal of the American Society for Mass Spectrometry* **1993,** *4*, 145-151.

69. Wolff, J. J.; Laremore, T. N.; Aslam, H.; Linhardt, R. J.; Amster, I. J. Electron-induced dissociation of glycosaminoglycan tetrasaccharides. *Journal of the American Society for Mass Spectrometry* **2008,** *19*, 1449-1458.

70. Budnik, B. A.; Haselmann, K. F.; Elkin, Y. N.; Gorbach, V. I.; Zubarev, R. A. Applications of electron-ion dissociation reactions for analysis of polycationic chitooligosaccharides in Fourier transform mass spectrometry. *Analytical Chemistry* **2003,** *75*, 5994-6001.

71. Lioe, H.; O'Hair, R. A. J. Comparison of collision-induced dissociation and electron-induced dissociation of singly protonated aromatic amino acids, cystine and related simple peptides using a hybrid linear ion trap-FT-ICR mass spectrometer. *Analytical and Bioanalytical Chemistry* **2007,** *389*, 1429-1437.

72. Budnik, B. A.; Haselmann, K. F.; Zubarev, R. A. Electron detachment dissociation of peptide di-anions: an electron-hole recombination phenomenon. *Chemical Physics Letters* **2001,** *342*, 299-302.

73. Anusiewicz, I.; Jasionowski, M.; Skurski, P.; Simons, J. Backbone and side-chain cleavages in electron detachment dissociation (EDD). *Journal of Physical Chemistry A* **2005,** *109*, 11332-11337.

74. Yang, J.; Hakansson, K. Characterization and optimization of electron detachment dissociation Fourier transform ion cyclotron resonance mass spectrometry. *International Journal of Mass Spectrometry* **2008,** *276*, 144-148.

75. Nielsen, M. L.; Budnik, B. A.; Haselmann, K. F.; Olsen, J. V.; Zubarev, R. A. Intramolecular hydrogen atom transfer in hydrogen-deficient polypeptide radical cations. *Chemical Physics Letters* **2000,** *330*, 558-562.

76. Nielsen, M. L.; Budnik, B. A.; Haselmann, K. F.; Zubarev, R. A. Tandem MALDI/EI ionization for tandem Fourier transform ion cyclotron resonance mass spectrometry of polypeptides. *International Journal of Mass Spectrometry* **2003,** *226*, 181-187.

77. Jebanathirajah, J. A.; Pittman, J. L.; Thomson, B. A.; Budnik, B. A.; Kaur, P.; Rape, M.; Kirschner, M.; Costello, C. E.; O'Connor, P. B. Characterization of a new qQq-FTICR mass spectrometer for post-translational modification analysis and top-down tandem mass spectrometry of whole proteins. *Journal of the American Society for Mass Spectrometry* **2005,** *16*, 1985-1999.

78. O'Connor, P. B.; Pittman, J. L.; Thomson, B. A.; Budnik, B. A.; Cournoyer, J. C.; Jebanathirajah, J.; Lin, C.; Moyer, S.; Zhao, C. A new hybrid electrospray Fourier transform mass spectrometer : Design and performance characteristics. *Rapid Communications in Mass Spectrometry* **2006,** *20*, 259-266.

79. Robinson, N. E.; Robinson, A. B. Molecular clocks: Deamidation of asparaginyl and glutaminyl residues in peptides and proteins. Althouse Press, Cave Junction, OR. 2004.

80. Wright, H. T. Nonenzymatic deamidation of asparaginyl and glutaminyl residues in proteins. *Critical Reviews in Biochemistry and Molecular Biology* **1991,** *26*, 1-52.

81. Robinson, N. E.; Robinson, A. B. Prediction of protein deamidation rates from primary and three-dimensional structure. *Proceedings of the National Academy of Sciences of the United States of America* **2001,** *98*, 4367-4372.

82. Kossiakoff, A. A. Tertiary structure is a principal determinant to protein deamidation. *Science* **1988,** *240*, 191-194.

83. Xie, M. L.; Schowen, R. L. Secondary structure and protein deamidation. *Journal of Pharmaceutical Sciences* **1999,** *88*, 8-13.

84. Robinson, N. E.; Robinson, Z. W.; Robinson, B. R.; Robinson, A. L.; Robinson, J. A.; Robinson, M. L.; Robinson, A. B. Structure-dependent nonenzymatic deamidation of glutaminyl and asparaginyl pentapeptides. *Journal of Peptide Research* **2004,** *63*, 426-436.

85. Peters, B.; Trout, B. L. Asparagine deamidation: pH-dependent mechanism from density functional theory. *Biochemistry* **2006,** *45*, 5384-5392.

86. Scotchler, J. W.; Robinson, A. B. Deamidation of glutaminyl residues: dependence on pH, temperature, and ionic strength. *Analytical Biochemistry* **1974,** *59*, 319-322.

87. Daniel, R. M.; Dines, M.; Petach, H. H. The denaturation and degradation of stable enzymes at high temperatures. *Biochemical Journal* **1996,** *317*, 1-11.

88. Tylercross, R.; Schirch, V. Effects of amino-acid-sequence, buffers, and ionic-strength on the rate and mechanism of deamidation of asparagine residues in small peptides. *Journal of Biological Chemistry* **1991,** *266*, 22549-22556.

89. Geiger, T.; Clarke, S. Deamidation, isomerization, and racemization at asparaginyl and aspartyl residues in peptides - succinimide-linked reactions that contribute to protein-degradation. *Journal of Biological Chemistry* **1987,** *262*, 785-794.

90. Wakankar, A. A.; Borchardt, R. T. Formulation considerations for proteins susceptible to asparagine deamidation and aspartate isomerization. *Journal of Pharmaceutical Sciences* **2006,** *95*, 2321-2336.

91. Capasso, S.; Kirby, A. J.; Salvadori, S.; Sica, F.; Zagari, A. Kinetics and mechanism of the reversible isomerization of aspartic-acid residues in tetrapeptides. *Journal of the Chemical Society-Perkin Transactions 2* **1995**, 437-442.

92. Ritz-Timme, S.; Collins, M. J. Racemization of aspartic acid in human proteins. *Ageing Research Reviews* **2002,** *1*, 43-59.

93. Reissner, K. J.; Aswad, D. W. Deamidation and isoaspartate formation in proteins: unwanted alterations or surreptitious signals? *Cellular and Molecular Life Sciences* **2003,** *60*, 1281-1295.

94. Lindner, H.; Helliger, W. Age-dependent deamidation of asparagine residues in proteins. *Experimental Gerontology* **2001,** *36*, 1551-1563.

95. Skinner, M. M.; Puvathingal, J. M.; Walter, R. L.; Friedman, A. M. Crystal structure of protein isoaspartyl methyltransferase: A catalyst for protein repair. *Structure* **2000,** *8*, 1189-1201.

96. Ryttersgaard, C.; Griffith, S. C.; Sawaya, M. R.; MacLaren, D. C.; Clarke, S.; Yeates, T. O. Crystal structure of human L-isoaspartyl methyltransferase. *Journal of Biological Chemistry* **2002,** *277*, 10642-10646.

97. Shimizu, T.; Matsuoka, Y.; Shirasawa, T. Biological significance of isoaspartate and its repair system. *Biological & Pharmaceutical Bulletin* **2005,** *28*, 1590-1596.

98. Zhu, J. X.; Doyle, H. A.; Mamula, M. J.; Aswad, D. W. Protein repair in the brain, proteomic analysis of endogenous substrates for protein L-isoaspartyl methyltransferase in mouse brain. *Journal of Biological Chemistry* **2006,** *281*, 33802-33813.

99. Kim, E.; Lowenson, J. D.; MacLaren, D. C.; Clarke, S.; Young, S. G. Deficiency of a protein-repair enzyme results in the accumulation of altered proteins, retardation of growth, and fatal seizures in mice. *Proceedings of the National Academy of Sciences of the United States of America* **1997,** *94*, 6132-6137.

100. Yamamoto, A.; Takagi, H.; Kitamura, D.; Tatsuoka, H.; Nakano, H.; Kawano, H.; Kuroyanagi, H.; Yahagi, Y.; Kobayashi, S.; Koizumi, K.; Sakai, T.; Saito, K.; Chiba, T.; Kawamura, K.; Suzuki, K.; Watanabe, T.; Mori, H.; Shirasawa, T. Deficiency in protein L-

isoaspartyl methyltransferase results in a fatal progressive epilepsy. *Journal of Neuroscience* **1998,** *18*, 2063-2074.

101. Chavous, D. A.; Jackson, F. R.; O'Connor, C. M. Extension of the *Drosophila* lifespan by overexpression of a protein repair methyltransferase. *Proceedings of the National Academy of Sciences of the United States of America* **2001,** *98*, 14814-14818.

102. Carrard, G.; Bulteau, A. L.; Petropoulos, I.; Friguet, B. Impairment of proteasome structure and function in aging. *International Journal of Biochemistry & Cell Biology* **2002,** *34*, 1461-1474.

103. Soskic, V.; Groebe, K.; Schrattenholz, A. Nonenzymatic posttranslational protein modifications in ageing. *Experimental Gerontology* **2008,** *43*, 247-257.

104. Robert, K. A.; Brunet-Rossinni, A.; Bronikowski, A. M. Testing the 'free radical theory of aging' hypothesis: physiological differences in long-lived and short-lived colubrid snakes. *Aging Cell* **2007,** *6*, 395-404.

105. Sohal, R. S.; Mockett, R. J.; Orr, W. C. Mechanisms of aging: An appraisal of the oxidative stress hypothesis. *Free Radical Biology and Medicine* **2002,** *33*, 575-586.

106. Sohal, R. S. Oxidative stress hypothesis of aging. *Free Radical Biology and Medicine* **2002,** *33*, 573-574.

107. Robinson, A. B.; McKerrow, J. H.; Cary, P. Controlled deamidation of peptides and proteins: an experimental hazard and a possible biological timer. *Proceedings of the National Academy of Sciences of the United States of America* **1970,** *66*, 753-&.

108. Deverman, B. E.; Cook, B. L.; Manson, S. R.; Niederhoff, R. A.; Langer, E. M.; Rosova, I.; Kulans, L. A.; Fu, X. Y.; Weinberg, J. S.; Heinecke, J. W.; Roth, K. A.; Weintraub, S. J. Bcl-X-L deamidation is a critical switch in the regulation of the response to DNA damage. *Cell* **2002,** *111*, 51-62.

109. Li, C.; Thompson, C. B. DNA damage, deamidation, and death. *Science* **2002,** *298*, 1346-1347.

110. Harbour, J. W.; Dean, D. C. The Rb/E2F pathway: expanding roles and emerging paradigms. *Genes & Development* **2000,** *14*, 2393-2409.

111. Nevins, J. R. The Rb/E2F pathway and cancer. *Human Molecular Genetics* **2001,** *10*, 699-703.

112. Sherr, C. J.; McCormick, F. The RB and p53 pathways in cancer. *Cancer Cell* **2002,** *2*, 103-112.

113. Gross, A.; McDonnell, J. M.; Korsmeyer, S. J. BCL-2 family members and the mitochondria in apoptosis. *Genes & Development* **1999,** *13*, 1899-1911.

114. Grubb, R. L.; Dho, S. H.; Manson, S.; Weintraub, S. J. Bcl-xL deamidation is regulated by NHE-1-mediated intracellular pH change. *Journal of the American College of Surgeons* **2008,** *207*, S23-S23.

115. Cimmino, A.; Capasso, R.; Muller, F.; Sambri, I.; Masella, L.; Raimo, M.; De Bonis, M. L.; D'Angelo, S.; Zappia, V.; Galletti, P.; Ingrosso, D. Protein isoaspartate methyltransferase prevents apoptosis induced by oxidative stress in endothelial cells: Role of Bcl-X-l deamidation and methylation. *PLoS One* **2008,** *3*.

116. Walsh, D. M.; Minogue, A. M.; Frigerio, C. S.; Fadeeva, J. V.; Wasco, W.; Selkoe, D. J. The APP family of proteins: similarities and differences. *Biochemical Society Transactions* **2007,** *35*, 416-420.

117. Sisodia, S. S.; Price, D. L. Role of the beta-amyloid protein in Alzheimers-disease. *FASEB Journal* **1995,** *9*, 366-370.

118. Shimizu, T.; Watanabe, A.; Ogawara, M.; Mori, H.; Shirasawa, T. Isoaspartate formation and neurodegeneration in Alzheimer's disease. *Archives of Biochemistry and Biophysics* **2000,** *381*, 225-234.

119. Orpiszewski, J.; Schormann, N.; Kluve-Beckerman, B.; Liepnieks, J. J.; Benson, M. D. Protein aging hypothesis of Alzheimer disease. *FASEB Journal* **2000,** *14*, 1255-1263.

120. Lampi, K. J.; Amyx, K. K.; Ahmann, P.; Steel, E. A. Deamidation in human lens beta B2-crystallin destabilizes the dimer. *Biochemistry* **2006,** *45*, 3146-3153.

121. Hoehenwarter, W.; Klose, J.; Jungblut, P. R. Eye lens proteomics. *Amino Acids* **2006,** *30*, 369-389.

122. Vankleef, F. S. M.; Dejong, W. W.; Hoenders, H. J. Stepwise degradations and deamidation of eye lens protein alpha-crystallin in aging. *Nature* **1975,** *258*, 264-266.

123. Miesbauer, L. R.; Zhou, X. J.; Yang, Z. C.; Yang, Z. Y.; Sun, Y. P.; Smith, D. L.; Smith, J. B. Posttranslational modifications of water-soluble human lens crystallins from young-adults. *Journal of Biological Chemistry* **1994,** *269*, 12494-12502.

124. Lund, A. L.; Smith, J. B.; Smith, D. L. Modifications of the water-insoluble human lens alpha-crystallins. *Experimental Eye Research* **1996,** *63*, 661-672.

125. Hanson, S. R. A.; Hasan, A.; Smith, D. L.; Smith, J. B. The major in vivo modifications of the human water-insoluble lens crystallins are disulfide bonds, deamidation, methionine oxidation and backbone cleavage. *Experimental Eye Research* **2000,** *71*, 195-207.

126. Zhang, Z. L.; Smith, D. L.; Smith, J. B. Human beta-crystallins modified by backbone cleavage, deamidation and oxidation are prone to associate. *Experimental Eye Research* **2003,** *77*, 259-272.

127. Zhang, Z. L.; David, L. L.; Smith, D. L.; Smith, J. B. Resistance of human beta B2-crystallin to in vivo modification. *Experimental Eye Research* **2001,** *73*, 203-211.

128. Feng, J. H.; Smith, D. L.; Smith, J. B. Human lens beta-crystallin solubility. *Journal of Biological Chemistry* **2000,** *275*, 11585-11590.

129. Wilmarth, P. A.; Tanner, S.; Dasari, S.; Nagalla, S. R.; Riviere, M. A.; Bafna, V.; Pevzner, P. A.; David, L. L. Age-related changes in human crystallins determined from comparative analysis of post-translational modifications in young and aged lens: Does deamidation contribute to crystallin insolubility? *Journal of Proteome Research* **2006,** *5*, 2554-2566.

130. Hanson, S. R. A.; Smith, D. L.; Smith, J. B. Deamidation and disulfide bonding in human lens gamma-crystallins. *Experimental Eye Research* **1998,** *67*, 301-312.

131. Mowat, A. M. Coeliac disease - a meeting point for genetics, immunology, and protein chemistry. *Lancet* **2003,** *361*, 1290-1292.

132. Shan, L.; Molberg, O.; Parrot, I.; Hausch, F.; Filiz, F.; Gray, G. M.; Sollid, L. M.; Khosla, C. Structural basis for gluten intolerance in Celiac sprue. *Science* **2002,** *297*, 2275-2279.

133. Kagnoff, M. F. Overview and pathogenesis of celiac disease. *Gastroenterology* **2005,** *128*, S10-S18.

134. Flatau, G.; Lemichez, E.; Gauthier, M.; Chardin, P.; Paris, S.; Fiorentini, C.; Boquet, P. Toxin-induced activation of the G protein p21 Rho by deamidation of glutamine. *Nature* **1997,** *387*, 729-733.

135. Cleland, J. L.; Powell, M. F.; Shire, S. J. The development of stable protein formulations: a close look at protein aggregation, deamidation, and oxidation. *Critical Reviews in Therapeutic Drug Carrier Systems* **1993,** *10*, 307-377.

136. Frokjaer, S.; Otzen, D. E. Protein drug stability: A formulation challenge. *Nature Reviews Drug Discovery* **2005,** *4*, 298-306.

137. Kelleher, R. L.; Zubarev, R. A.; Bush, K.; Furie, B.; Furie, B. C.; McLafferty, F. W.; Walsh, C. T. Localization of labile posttranslational modifications by electron capture dissociation: The case of gamma-carboxyglutamic acid. *Analytical Chemistry* **1999,** *71*, 4250-4253.

138. Stensballe, A.; Jensen, O. N.; Olsen, J. V.; Haselmann, K. F.; Zubarev, R. A. Electron capture dissociation of singly and multiply phosphorylated peptides. *Rapid Communications in Mass Spectrometry* **2000,** *14*, 1793-1800.

139. Shi, S. D. H.; Hemling, M. E.; Carr, S. A.; Horn, D. M.; Lindh, I.; McLafferty, F. W. Phosphopeptide/phosphoprotein mapping by electron capture dissociation mass spectrometry. *Analytical Chemistry* **2001,** *73*, 19-22.

140. Liu, H.; Hakansson, K. Electron capture dissociation of tyrosine O-sulfated peptides complexed with divalent metal cations. *Analytical Chemistry* **2006,** *78*, 7570-7576.

141. Breuker, K.; Oh, H. B.; Horn, D. M.; Cerda, B. A.; McLafferty, F. W. Detailed unfolding and folding of gaseous ubiquitin ions characterized by electron capture dissociation. *Journal of the American Chemical Society* **2002,** *124*, 6407-6420.

142. Lin, C.; O'Connor, P. B.; Cournoyer, J. J. Use of a double resonance electron capture dissociation experiment to probe fragment intermediate lifetimes. *Journal of the American Society for Mass Spectrometry* **2006,** *17*, 1605-1615.

143. Xie, Y. M.; Zhang, J.; Yin, S.; Loo, J. A. Top-down ESI-ECD-FT-ICR mass spectrometry localizes noncovalent protein-ligand binding sites. *Journal of the American Chemical Society* **2006,** *128*, 14432-14433.

144. Lin, C.; Cournoyer, J. J.; O'Connor, P. B. Probing the gas-phase folding kinetics of peptide ions by IR activated DR-ECD. *Journal of the American Society for Mass Spectrometry* **2008,** *19*, 780-789.

145. Zubarev, R. A.; Horn, D. M.; Fridriksson, E. K.; Kelleher, N. L.; Kruger, N. A.; Lewis, M. A.; Carpenter, B. K.; McLafferty, F. W. Electron capture dissociation for structural characterization of multiply charged protein cations. *Analytical Chemistry* **2000,** *72*, 563-573.

146. Zubarev, R. A. Reactions of polypeptide ions with electrons in the gas phase. *Mass Spectrometry Reviews* **2003,** *22*, 57-77.

147. Bakhtiar, R.; Guan, Z. Q. Electron capture dissociation mass spectrometry in characterization of peptides and proteins. *Biotechnology Letters* **2006,** *28*, 1047-1059.

148. Meng, F. Y.; Forbes, A. J.; Miller, L. M.; Kelleher, N. L. Detection and localization of protein modifications by high resolution tandem mass spectrometry. *Mass Spectrometry Reviews* **2005,** *24*, 126-134.

149. Breuker, K.; Oh, H. B.; Cerda, B. A.; Horn, D. M.; McLafferty, F. W. Hydrogen atom loss in electron-capture dissociation: a Fourier transform-ion cyclotron resonance study with single isotopomeric ubiquitin ions. *European Journal of Mass Spectrometry* **2002,** *8*, 177-180.

150. Cooper, H. J.; Hakansson, K.; Marshall, A. G.; Hudgins, R. R.; Haselmann, K. F.; Kjeldsen, F.; Budnik, B. A.; Polfer, N. C.; Zubarev, R. A. Letter: The diagnostic value of amino acid side-chain losses in electron capture dissociation of polypeptides. Comment on: "Can the (M-center dot-X) region in electron capture dissociation provide reliable information on amino acid composition of polypeptides?", *Eur. J. Mass Spectrom.* 8, 461-469 (2002). *European Journal of Mass Spectrometry* **2003,** *9*, 221-222.

151. Demirev, P. A. Generation of hydrogen radicals for reactivity studies in Fourier transform ion cyclotron resonance mass spectrometry. *Rapid Communications in Mass Spectrometry* **2000,** *14*, 777-781.

152. Turecek, F. N-C-alpha bond dissociation energies and kinetics in amide and peptide radicals. Is the dissociation a non-ergodic process? *Journal of the American Chemical Society* **2003,** *125*, 5954-5963.

153. Hudgins, R. R.; Hakansson, K.; Quinn, J. P.; Hendrickson, C. L.; Marshall, A. G. In *Electron capture dissociation of peptides and proteins does not require a hydrogen atom mechanism*, Proceedings of the 50th ASMS Conference on Mass Spectrometry and Allied Topics, Orlando, FL, 2000.

154. Sobczyk, M.; Anusiewicz, W.; Berdys-Kochanska, J.; Sawicka, A.; Skurski, P.; Simons, J. Coulomb-assisted dissociative electron attachment: Application to a model peptide. *Journal of Physical Chemistry A* **2005,** *109*, 250-258.

155. Chamot-Rooke, J.; Malosse, C.; Frison, G.; Turecek, F. Electron capture in charge-tagged peptides. Evidence for the role of excited electronic States. *Journal of the American Society for Mass Spectrometry* **2007,** *18*, 2146-2161.

156. O'Connor, P. B.; Lin, C.; Cournoyer, J. J.; Pittman, J. L.; Belyayev, M.; Budnik, B. A. Long-lived electron capture dissociation product ions experience radical migration via hydrogen abstraction. *Journal of the American Society for Mass Spectrometry* **2006,** *17*, 576-585.

157. Savitski, M. M.; Kjeldsen, F.; Nielsen, M. L.; Zubarev, R. A. Hydrogen rearrangement to and from radical z fragments in electron capture dissociation of peptides. *Journal of the American Society for Mass Spectrometry* **2007,** *18*, 113-120.

158. Tsybin, Y. O.; He, H.; Emmett, M. R.; Hendrickson, C. L.; Marshall, A. G. Ion activation in electron capture dissociation to distinguish between N-terminal and C-terminal productions. *Analytical Chemistry* **2007,** *79*, 7596-7602.

159. Kjeldsen, F.; Zubarev, R. Secondary losses via gamma-lactam formation in hot electron capture dissociation: A missing link to complete de novo sequencing of proteins? *Journal of the American Chemical Society* **2003,** *125*, 6628-6629.

160. Tsybin, Y. O.; Witt, M.; Baykut, G.; Kjeldsen, F.; Hakansson, P. Combined infrared multiphoton dissociation and electron capture dissociation with a hollow electron beam in Fourier transform ion cyclotron resonance mass spectrometry. *Rapid Communications in Mass Spectrometry* **2003,** *17*, 1759-1768.

161. Belyayev, M. A.; Cournoyer, J. J.; Lin, C.; O'Connor, P. B. The effect of radical trap moieties on electron capture dissociation spectra of Substance P. *Journal of the American Society for Mass Spectrometry* **2006,** *17*, 1428-1436.

162. Jones, J. W.; Sasaki, T.; Goodlett, D. R.; Turecek, F. Electron capture in spin-trap capped peptides. An experimental example of ergodic dissociation in peptide cation-radicals. *Journal of the American Society for Mass Spectrometry* **2007,** *18*, 432-444.

163. Roth, K. D. W.; Huang, Z. H.; Sadagopan, N.; Watson, J. T. Charge derivatization of peptides for analysis by mass spectrometry. *Mass Spectrometry Reviews* **1998,** *17*, 255-274.

164. Wagner, D. S.; Salari, A.; Gage, D. A.; Leykam, J.; Fetter, J.; Hollingsworth, R.; Watson, J. T. Derivatization of peptides to enhance ionization efficiency and control fragmentation during analysis by fast-atom-bombardment tandem mass-spectrometry. *Biological Mass Spectrometry* **1991,** *20*, 419-425.

165. Zaia, J.; Biemann, K. Comparison of charged derivatives for high-energy collision-induced dissociation tandem mass-spectrometry. *Journal of the American Society for Mass Spectrometry* **1995,** *6*, 428-436.

166. Vath, J. E.; Biemann, K. Microderivatization of peptides by placing a fixed positive charge at the N-terminus to modify high-energy collision fragmentation. *International Journal of Mass Spectrometry and Ion Processes* **1990,** *100*, 287-299.

167. Adamczyk, M.; Gebler, J. C.; Wu, J. Charge derivatization of peptides to simplify their sequencing with an ion trap mass spectrometer. *Rapid Communications in Mass Spectrometry* **1999,** *13*, 1413-1422.

168. Chagit, D.; Rabkin, E.; Tsoglin, A. A new charge derivatization procedure for peptide sequencing. *Organic & Biomolecular Chemistry* **2005,** *3*, 2503-2504.

169. Chamot-Rooke, J.; van der Rest, G.; Dalleu, A.; Bay, S.; Lemoine, J. The combination of electron capture dissociation and fixed charge derivatization increases sequence coverage for O-glycosylated and O-phosphorylated peptides. *Journal of the American Society for Mass Spectrometry* **2007,** *18*, 1405-1413.

170. Xia, Y.; Gunawardena, H. P.; Erickson, D. E.; McLuckey, S. A. Effects of cation charge-site identity and position on electron-transfer dissociation of polypeptide cations. *Journal of the American Chemical Society* **2007,** *129*, 12232-12243.

171. Gunawardena, H. P.; Gorenstein, L.; Erickson, D. E.; Xia, Y.; McLuckey, S. A. Electron transfer dissociation of multiply protonated and fixed charge disulfide linked polypeptides. *International Journal of Mass Spectrometry* **2007,** *265*, 130-138.

172. Johnson, R. S. Determination of peptide and protein structure by tandem mass spectrometry. *Ph.D Dissertation, M.I.T., Cambridge, MA* **1988**.

173. Johnson, R. S.; Martin, S. A.; Biemann, K. Collision-induced fragmentation of $(M+H)^+$ ions of peptides. Side-chain specific sequence ions. *International Journal of Mass Spectrometry and Ion Processes* **1988,** *86*, 137-154.

174. King, L. C.; Ozog, F. J. Reactions of pyrylium and pyridinium salts with amines. *Journal of Organic Chemistry* **1955,** *20*, 448-454.

175. Cooper, H. J. Investigation of the presence of b ions in electron capture dissociation mass spectra. *Journal of the American Society for Mass Spectrometry* **2005,** *16*, 1932-1940.

176. Nguyen, V. Q.; Turecek, F. Gas-phase protonation of pyridine. A variable-time neutralization-reionization and ab initio study of pyridinium radicals. *Journal of Mass Spectrometry* **1997,** *32*, 55-63.

177. Turecek, F.; Syrstad, E. A. Mechanism and energetics of intramolecular hydrogen transfer in amide and peptide radicals and cation-radicals. *Journal of the American Chemical Society* **2003,** *125*, 3353-3369.

178. Hodyss, R.; Cox, H. A.; Beauchamp, J. L. Bioconjugates for tunable peptide fragmentation: Free radical initiated peptide sequencing (FRIPS). *Journal of the American Chemical Society* **2005,** *127*, 12436-12437.

179. Ly, T.; Julian, R. R. Residue-specific radical-directed dissociation of whole proteins in the gas phase. *Journal of the American Chemical Society* **2008,** *130*, 351-358.

180. Ly, T.; Julian, R. R. In *Fast formation of sidechain aryl radicals by UV irradiation produces selective fragmentation of whole proteins*, 2008 Conference on Ion Chemistry and Mass Spectrometry, Lake Arrowhead, CA, 2008.

181. Masterson, D. S.; Yin, H. Y.; Chacon, A.; Hachey, D. L.; Norris, J. L.; Porter, N. A. Lysine peroxycarbamates: Free radical-promoted peptide cleavage. *Journal of the American Chemical Society* **2004,** *126*, 720-721.

182. Yin, H.; Chacon, A.; Porter, N. A.; Yin, H. Y.; Masterson, D. S. Free radical-induced site-specific peptide cleavage in the gas phase: Low-energy collision-induced dissociation in ESI- and MALDI mass spectrometry. *Journal of the American Society for Mass Spectrometry* **2007,** *18*, 807-816.

183. Hao, G.; Gross, S. S. Electrospray tandem mass spectrometry analysis of S- and N-nitrosopeptides: Facile loss of NO and radical-induced fragmentation. *Journal of the American Society for Mass Spectrometry* **2006,** *17*, 1725-1730.

184. Wee, S.; Mortimer, A.; Moran, D.; Wright, A.; Barlow, C. K.; O'Hair, R. A. J.; Radom, L.; Easton, C. J. Gas-phase regiocontrolled generation of charged amino acid and peptide radicals. *Chemical Communications* **2006**, 4233-4235.

185. Diedrich, J. K.; Julian, R. R. Site-specific radical directed dissociation of peptides at phosphorylated residues. *Journal of the American Chemical Society* **2008,** *130*, 12212-12213.

186. Chu, I. K.; Rodriquez, C. F.; Lau, T. C.; Hopkinson, A. C.; Siu, K. W. M. Molecular radical cations of oligopeptides. *Journal of Physical Chemistry B* **2000,** *104*, 3393-3397.

187. Bagheri-Majdi, E.; Ke, Y. Y.; Orlova, G.; Chu, I. K.; Hopkinson, A. C.; Siu, K. W. M. Copper-mediated peptide radical ions in the gas phase. *Journal of Physical Chemistry B* **2004,** *108*, 11170-11181.

188. Barlow, C. K.; McFadyen, W. D.; O'Hair, R. A. J. Formation of cationic peptide radicals by gas-phase redox reactions with trivalent chromium, manganese, iron, and cobalt complexes. *Journal of the American Chemical Society* **2005,** *127*, 6109-6115.

189. Laskin, J.; Yang, Z. B.; Lam, C.; Chu, I. K. Charge-remote fragmentation of odd-electron peptide ions. *Analytical Chemistry* **2007,** *79*, 6607-6614.

190. Sun, Q. Y.; Nelson, H.; Ly, T.; Stoltz, B. M.; Julian, R. R. Side chain chemistry mediates backbone fragmentation in hydrogen deficient peptide radicals. *Journal of Proteome Research* **2009,** *8*, 958-966.

191. Ly, T.; Yin, S.; Loo, J. A.; Julian, R. R. Electron-induced dissociation of protonated peptides yields backbone fragmentation consistent with a hydrogen-deficient radical. *Rapid Communications in Mass Spectrometry* **2009,** *23*, 2099-2101.

192. Laskin, J.; Futrell, J. H.; Chu, I. K. Is dissociation of peptide radical cations an ergodic process? *Journal of the American Chemical Society* **2007,** *129*, 9598-9599.

193. Zhang, L.; Reilly, J. P. Radical-driven dissociation of odd-electron peptide radical ions produced in 157 nm photodissociation. *Journal of the American Society for Mass Spectrometry* **2009,** *20*, 1378-1390.

194. Fung, Y. M. E.; Chan, T. W. D. Experimental and theoretical investigations of the loss of amino acid side chains in electron capture dissociation of model peptides. *Journal of the American Society for Mass Spectrometry* **2005,** *16*, 1523-1535.

195. Falth, M.; Savitski, M. M.; Nielsen, M. L.; Kjeldsen, F.; Andren, P. E.; Zubarev, R. A. Analytical utility of small neutral losses from reduced species in electron capture dissociation studied using SwedECD database. *Analytical Chemistry* **2008,** *80*, 8089-8094.

196. Haselmann, K. F.; Budnik, B. A.; Kjeldsen, F.; Polfer, N. C.; Zubarev, R. A. Can the (M center dot-X) region in electron capture dissociation provide reliable information on amino acid composition of polypeptides? *European Journal of Mass Spectrometry* **2002,** *8*, 461-469.

197. Cheng, C.; Gross, M. L. Applications and mechanisms of charge-remote fragmentation. *Mass Spectrometry Reviews* **2000,** *19*, 398-420.

198. Gross, M. L. Charge-remote fragmentation: an account of research on mechanisms and applications. *International Journal of Mass Spectrometry* **2000,** *200*, 611-624.

199. Jensen, N. J.; Tomer, K. B.; Gross, M. L. Gas-phase ion decompositions occurring remote to a charge site. *Journal of the American Chemical Society* **1985,** *107*, 1863-1868.

200. Adams, J.; Gross, M. L. Energy-requirements for remote charge site ion decompositions and structural information from collisional activation of alkali-metal cationized fatty alcohols. *Journal of the American Chemical Society* **1986,** *108*, 6915-6921.

201. Adams, J.; Gross, M. L. Charge-remote fragmentations of closed-shell ions - a thermolytic analogy. *Journal of the American Chemical Society* **1989,** *111*, 435-440.

202. Gross, M. L. Charge-remote fragmentations - method, mechanism and applications. *International Journal of Mass Spectrometry and Ion Processes* **1992,** *118*, 137-165.

203. Han, H. L.; Xia, Y.; McLuckey, S. A. Ion trap collisional activation of c and z(center dot) ions formed via gas-phase ion/ion electron-transfer dissociation. *Journal of Proteome Research* **2007,** *6*, 3062-3069.

204. Liu, H. C.; Hakansson, K. Abundant b-type ions produced in electron capture dissociation of peptides without basic amino acid residues. *Journal of the American Society for Mass Spectrometry* **2007,** *18*, 2007-2013.

205. Li, X.; Cournoyer, J. J.; Lin, C.; O'Connor, P. B. The effect of fixed charge modifications on electron capture dissociation. *Journal of the American Society for Mass Spectrometry* **2008,** *19*, 1514-1526.

206. Cournoyer, J. J.; Pittman, J. L.; Ivleva, V. B.; Fallows, E.; Waskell, L.; Costello, C. E.; O'Connor, P. B. Deamidation: Differentiation of aspartyl from isoaspartyl products in peptides by electron capture dissociation. *Protein Science* **2005,** *14*, 452-463.

207. Cournoyer, J. J.; Lin, C.; O'Connor, P. B. Detecting deamidation products in proteins by electron capture dissociation. *Analytical Chemistry* **2006,** *78*, 1264-1271.

208. Cournoyer, J. J.; Lin, C.; Bowman, M. J.; O'Connor, P. B. Quantitating the relative abundance of isoaspartyl residues in deamidated proteins by electron capture dissociation. *Journal of the American Society for Mass Spectrometry* **2007,** *18*, 48-56.

209. Li, X.; Cournoyer, J. J.; Lin, C.; O'Connor, P. B. Use of O-18 labels to monitor deamidation during protein and peptide sample processing. *Journal of the American Society for Mass Spectrometry* **2008,** *19*, 855-864.

210. O'Connor, P. B.; Cournoyer, J. J.; Pitteri, S. J.; Chrisman, P. A.; McLuckey, S. A. Differentiation of aspartic and isoaspartic acids using electron transfer dissociation. *Journal of the American Society for Mass Spectrometry* **2006,** *17*, 15-19.

211. Biemann, K.; Papayannopoulos, I. A. Amino-acid sequencing of proteins. *Accounts of Chemical Research* **1994,** *27*, 370-378.

212. Laskin, J.; Futrell, J. H. Activation of large ions in FT-ICR mass spectrometry. *Mass Spectrometry Reviews* **2005,** *24*, 135-167.

213. Han, X. M.; Jin, M.; Breuker, K.; McLafferty, F. W. Extending top-down mass spectrometry to proteins with masses greater than 200 kilodaltons. *Science* **2006,** *314*, 109-112.

214. Yague, J.; Paradela, A.; Ramos, M.; Ogueta, S.; Marina, A.; Barahona, F.; de Castro, J. A. L.; Vazquez, J. Peptide rearrangement during quadrupole ion trap fragmentation: Added complexity to MS/MS spectra. *Analytical Chemistry* **2003,** *75*, 1524-1535.

215. Bleiholder, C.; Osburn, S.; Williams, T. D.; Suhai, S.; Van Stipdonk, M.; Harrison, A. G.; Paizs, B. Sequence-Scrambling Fragmentation Pathways of Protonated Peptides. *Journal of the American Chemical Society* **2008,** *130*, 17774-17789.

216. Zubarev, R. A.; Zubarev, A. R.; Savitski, M. M. Electron capture/transfer versus collisionally activated/induced dissociations: Solo or duet? *Journal of the American Society for Mass Spectrometry* **2008,** *19*, 753-761.

217. Theberge, R.; Mccomb, M. E.; Lin, C.; Costello, C. E. In *Top-down sequencing of hemoglobin variants with multiple activation techniques*, *Proceedings from the 58th ASMS Conference on Mass Spectrometry and Allied Topics*, Salt Lake City, UT, 2010.

218. Papayannopoulos, I. A. The interpretation of collision-induced dissociation tandem mass-spectra of peptides. *Mass Spectrometry Reviews* **1995,** *14*, 49-73.

219. Biemann, K. Contributions of mass-spectrometry to peptide and protein-structure. *Biomedical and Environmental Mass Spectrometry* **1988,** *16*, 99-111.

220. Paizs, B.; Suhai, S. Towards understanding the tandem mass spectra of protonated oligopeptides. 1: Mechanism of amide bond cleavage. *Journal of the American Society for Mass Spectrometry* **2004,** *15*, 103-113.

221. Polfer, N. C.; Oomens, J.; Suhai, S.; Paizs, B. Spectroscopic and theoretical evidence for oxazolone ring formation in collision-induced dissociation of peptides. *Journal of the American Chemical Society* **2005,** *127*, 17154-17155.

222. Riba-Garcia, I.; Giles, K.; Bateman, R. H.; Gaskell, S. J. Evidence for structural variants of a- and b-type peptide fragment ions using combined ion mobility/mass spectrometry. *Journal of the American Society for Mass Spectrometry* **2008,** *19*, 609-613.

223. Harrison, A. G. Peptide sequence scrambling through cyclization of b_5 Ions. *Journal of the American Society for Mass Spectrometry* **2008,** *19*, 1776-1780.

224. Harrison, A. G. Cyclization of peptide b_9 ions. *Journal of the American Society for Mass Spectrometry* **2009,** *20*, 2248-2253.

225. Molesworth, S.; Osburn, S.; Van Stipdonk, M. Influence of size on apparent scrambling of sequence during CID of b-type ions. *Journal of the American Society for Mass Spectrometry* **2009,** *20*, 2174-2181.

226. Harrison, A. G.; Young, A. B.; Bleiholder, C.; Suhai, S.; Paizs, B. Scrambling of sequence information in collision-induced dissociation of peptides. *Journal of the American Chemical Society* **2006,** *128*, 10364-10365.

227. Jia, C. X.; Qi, W.; He, Z. M. Cyclization reaction of peptide fragment ions during multistage collisionally activated decomposition: An inducement to lose internal amino-acid residues. *Journal of the American Society for Mass Spectrometry* **2007,** *18*, 663-678.

228. Vachet, R. W.; Bishop, B. M.; Erickson, B. W.; Glish, G. L. Novel peptide dissociation: Gas-phase intramolecular rearrangement of internal amino acid residues. *Journal of the American Chemical Society* **1997,** *119*, 5481-5488.

229. Erlekam, U.; Bythell, B. J.; Scuderi, D.; Van Stipdonk, M.; Paizs, B.; Maitre, P. Infrared spectroscopy of fragments of protonated peptides: Direct evidence for macrocyclic structures of b_5 Ions. *Journal of the American Chemical Society* **2009,** *131*, 11503-11508.

230. Tang, X. J.; Thibault, P.; Boyd, R. K. Fragmentation reactions of multiply-protonated peptides and implications for sequencing by tandem mass-spectrometry with low-energy collision-induced dissociation. *Analytical Chemistry* **1993,** *65*, 2824-2834.

231. Tang, X. J.; Boyd, R. K. Rearrangements of doubly-charged acylium ions from lysyl and ornithyl peptides. *Rapid Communications in Mass Spectrometry* **1994,** *8*, 678-686.

232. Harrison, A. G. To b or not to b: The ongoing saga of peptide b ions. *Mass Spectrometry Reviews* **2009,** *28*, 640-654.

233. Chen, X.; Yu, L.; Steill, J. D.; Oomens, J.; Polfer, N. C. Effect of peptide fragment size on the propensity of cyclization in collision-induced dissociation: oligoglycine b_2-b_8. *Journal of the American Chemical Society* **2009,** *131*, 18272-18282.

234. Allen, J. M.; Racine, A. H.; Berman, A. M.; Johnson, J. S.; Bythell, B. J.; Paizs, B.; Glish, G. L. Why are a_3 ions rarely observed? *Journal of the American Society for Mass Spectrometry* **2008,** *19*, 1764-1770.

235. Grewal, R. N.; El Aribi, H.; Harrison, A. G.; Siu, K. W. M.; Hopkinson, A. C. Fragmentation of protonated tripeptides: The proline effect revisited. *Journal of Physical Chemistry B* **2004,** *108*, 4899-4908.

236. Jonsson, A. P.; Bergman, T.; Jornvall, H.; Griffiths, W. J.; Bratt, P.; Stromberg, N. Gln-Gly cleavage: Correlation between collision-induced dissociation and biological degradation. *Journal of the American Society for Mass Spectrometry* **2001,** *12*, 337-342.

237. Molesworth, S.; Osburn, S.; Stipdonk, M. V. Influence of amion acid side chains on apparent selective opening of cyclic b_5 ions. *Journal of the American Society for Mass Spectrometry* **2010,** *21*, 1028-1036.

238. Haselmann, K. F.; Budnik, B. A.; Zubarev, R. A. Electron capture dissociation of b^{2+} peptide fragments reveals the presence of the acylium ion structure. *Rapid Communications in Mass Spectrometry* **2000,** *14*, 2242-2246.

239. Chen, X. H.; Turecek, F. Simple b ions have cyclic oxazolone structures. A neutralization-reionization mass spectrometric and computational study of oxazolone radicals. *Journal of the American Society for Mass Spectrometry* **2005,** *16*, 1941-1956.

240. Frisch, M. J.; Trucks, G. W.; Schelegel, H. B.; Scuseria, G. E.; Robb, M. A.; Cheeseman, J. R.; Montgomery, Jr.; et al. Gaussian, Inc.: Pittsburgh, PA. **2001**.

241. Conlon, J. M.; Adrian, T. E.; Secor, S. M. Tachykinins (substance P, neurokinin A and neuropeptide gamma) and neurotensin from the intestine of the Burmese python, Python molurus. *Peptides* **1997,** *18*, 1505-1510.

242. Regoli, D.; Boudon, A.; Fauchere, J. L. Receptors and antagonists for substance P and related peptides. *Pharmacological Reviews* **1994,** *46*, 551-599.

243. Helke, C. J.; Krause, J. E.; Mantyh, P. W.; Couture, R.; Bannon, M. J. Diversity in mammalian tachykinin peptidergic neurons: multiple peptides, receptors, and regulatory mechanisms. *FASEB Journal* **1990,** *4*, 1606-1615.

244. Carter, M. S.; Krause, J. E. Structure, expression, and some regulatory mechanisms of the rat preprotachykinin gene encoding substance P, neurokinin A, neuropeptide K, and neuropeptide gamma. *Journal of Neuroscience* **1990,** *10*, 2203-2214.

245. Grace, R. C. R.; Chandrashekar, I. R.; Cowsik, S. M. Solution structure of the tachykinin peptide eledoisin. *Biophysical Journal* **2003,** *84*, 655-664.

246. Wysocki, V. H.; Tsaprailis, G.; Smith, L. L.; Breci, L. A. Special feature: Commentary - Mobile and localized protons: a framework for understanding peptide dissociation. *Journal of Mass Spectrometry* **2000,** *35*, 1399-1406.

247. Li, X.; Lin, C.; Han, L.; Costello, C. E.; O'Connor, P. B. Charge remote fragmentation in electron capture and electron transfer dissociation. *Journal of the American Society for Mass Spectrometry* **2010,** *21*, 646-656.

248. Yalcin, T.; Harrison, A. G. Ion chemistry of protonated lysine derivatives. *Journal of Mass Spectrometry* **1996,** *31*, 1237-1243.

249. Robinson, N. E. Protein deamidation. *Proceedings of the National Academy of Sciences of the United States of America* **2002,** *99*, 5283-5288.

250. Robinson, N. E.; Robinson, A. B. Molecular clocks. *Proceedings of the National Academy of Sciences of the United States of America* **2001,** *98*, 944-949.

251. Lindner, H.; Sarg, B.; Hoertnagl, B.; Helliger, W. The microheterogeneity of the mammalian H1(0) histone - Evidence for an age-dependent deamidation. *Journal of Biological Chemistry* **1998,** *273*, 13324-13330.

252. Bischoff, R.; Kolbe, H. V. Deamidation of asparagine and glutamine residues in proteins and peptides - structural determinants and analytical methodology. *Journal of Chromatography B-Biomedical Applications* **1994,** *662*, 261-278.

253. Capasso, S. Estimation of the deamidation rate of asparagine side chains. *Journal of Peptide Research* **2000,** *55*, 224-229.

254. Joshi, A. B.; Sawai, M.; Kearney, W. R.; Kirsch, L. E. Studies on the mechanism of aspartic acid cleavage and glutamine deamidation in the acidic degradation of glucagon. *Journal of Pharmaceutical Sciences* **2005,** *94*, 1912-1927.

255. Robinson, N. E.; Zabrouskov, V.; Zhang, J.; Lampi, K. J.; Robinson, A. B. Measurement of deamidation of intact proteins by isotopic envelope and mass defect with ion cyclotron resonance Fourier transform mass spectrometry. *Rapid Communications in Mass Spectrometry* **2006,** *20*, 3535-3541.

256. Robinson, N. E.; Lampi, K. J.; Speir, J. P.; Kruppa, G.; Easterling, M.; Robinson, A. B. Quantitative measurement of young human eye lens crystallins by direct injection Fourier transform ion cyclotron resonance mass spectrometry. *Molecular Vision* **2006,** *12*, 704-711.

257. Robinson, N. E.; Lampi, K. J.; McIver, R. T.; Williams, R. H.; Muster, W. C.; Kruppa, G.; Robinson, A. B. Quantitative measurement of deamidation in lens beta B2-crystallin and peptides by direct electrospray injection and fragmentation in a Fourier transform mass spectrometer. *Molecular Vision* **2005,** *11*, 1211-1219.

258. Schmid, D. G.; von der Mulbe, F.; Fleckenstein, B.; Weinschenk, T.; Jung, G. Broadband detection electrospray ionization fourier transform ion cyclotron resonance mass spectrometry to reveal enzymatically and chemically induced deamidation reactions within peptides. *Analytical Chemistry* **2001,** *73*, 6008-6013.

259. Chazin, W. J.; Kordel, J.; Thulin, E.; Hofmann, T.; Drakenberg, T.; Forsen, S. Identification of an isoaspartyl linkage formed upon deamidation of bovine calbindin-D_{9k} and structural characterization by 2D ^{1}H NMR. *Biochemistry* **1989,** *28*, 8646-8653.

260. Carlson, A. D.; Riggin, R. M. Development of improved high-performance liquid chromatography conditions for nonisotopic detection of isoaspartic acid to determine the extent of protein deamidation. *Analytical Biochemistry* **2000,** *278*, 150-155.

261. Carr, S. A.; Hemling, M. E.; Bean, M. F.; Roberts, G. D. Integration of mass-spectrometry in analytical biotechnology. *Analytical Chemistry* **1991,** *63*, 2802-2824.

262. Zhang, W.; Czupryn, M. J. Analysis of isoaspartate in a recombinant monoclonal antibody and its charge isoforms. *Journal of Pharmaceutical and Biomedical Analysis* **2003,** *30*, 1479-1490.

263. Gonzalez, L. J.; Shimizu, T.; Satomi, Y.; Betancourt, L.; Besada, V.; Padron, G.; Orlando, R.; Shirasawa, T.; Shimonishi, Y.; Takao, T. Differentiating alpha- and beta-aspartic acids by electrospray ionization and low-energy tandem mass spectrometry. *Rapid Communications in Mass Spectrometry* **2000,** *14*, 2092-2102.

264. Castet, S.; Enjalbal, C.; Fulcrand, P.; Guichou, J. F.; Martinez, J.; Aubagnac, J. L. Characterization of aspartic acid and beta-aspartic acid in peptides by fast-atom bombardment mass spectrometry and tandem mass spectrometry. *Rapid Communications in Mass Spectrometry* **1996,** *10*, 1934-1938.

265. Coon, J. J.; Syka, J. E. P.; Schwartz, J. C.; Shabanowitz, J.; Hunt, D. F. Anion dependence in the partitioning between proton and electron transfer in ion/ion reactions. *International Journal of Mass Spectrometry* **2004,** *236*, 33-42.

266. Yao, X. D.; Freas, A.; Ramirez, J.; Demirev, P. A.; Fenselau, C. Proteolytic O-18 labeling for comparative proteomics: Model studies with two serotypes of adenovirus (vol 73, pg 2836, 2001 correction). *Analytical Chemistry* **2004,** *76*, 2675-2675.

267. Stewart, II; Thomson, T.; Figeys, D. O-18 labeling: a tool for proteomics. *Rapid Communications in Mass Spectrometry* **2001,** *15*, 2456-2465.

268. Heller, M.; Mattou, H.; Menzel, C.; Yao, X. D. Trypsin catalyzed O-16-to-O-18 exchange for comparative proteomics: Tandem mass spectrometry comparison using MALDI-TOF, ESI-QTOF, and ESI-Ion trap mass spectrometers. *Journal of the American Society for Mass Spectrometry* **2003,** *14*, 704-718.

269. Yao, X. D.; Freas, A.; Ramirez, J.; Demirev, P. A.; Fenselau, C. Proteolytic O-18 labeling for comparative proteomics: Model studies with two serotypes of adenovirus. *Analytical Chemistry* **2001,** *73*, 2836-2842.

270. Miyagi, M.; Rao, K. C. S. Proteolytic O-18-labeling strategies for quantitative proteomics. *Mass Spectrometry Reviews* **2007,** *26*, 121-136.

271. Katta, V.; Chait, B. T. Hydrogen/deuterium exchange electrospray ionization mass spectrometry : A method for probing protein conformational changes in solution. *Journal of the American Chemical Society* **1993,** *115*, 6317-6321.

272. Wales, T. E.; Engen, J. R. Hydrogen exchange mass spectrometry for the analysis of protein dynamics. *Mass Spectrometry Reviews* **2006,** *25*, 158-170.

273. Garcia, R. A.; Pantazatos, D.; Villarreal, F. J. Hydrogen/deuterium exchange mass spectrometry for investigating protein-ligand interactions. *Assay and Drug Development Technologies* **2004,** *2*, 81-91.

274. Kheterpal, I.; Cook, K. D.; Wetzel, R. Hydrogen/deuterium exchange mass spectrometry analysis of protein aggregates. *Methods in Enzymology* **2006,** *413*, 140-166.

275. Kheterpal, I.; Wetzel, R. Hydrogen/deuterium exchange mass spectrometrys - A window into amyloid structure. *Accounts of Chemical Research* **2006,** *39*, 584-593.

276. Xiao, G.; Bondarenko, P. V.; Jacob, J.; Chu, G. C.; Chelius, D. O-18 labeling method for identification and quantification of succinimide in proteins. *Analytical Chemistry* **2007,** *79*, 2714-2721.

277. Kubota, K.; Yoneyama-Takazawa, T.; Ichikawa, K. Determination of sites citrullinated by peptidylarginine deiminase using O-18 stable isotope labeling and mass spectrometry. *Rapid Communications in Mass Spectrometry* **2005,** *19*, 683-688.

278. Schnolzer, M.; Jedrzejewski, P.; Lehmann, W. D. Protease-catalyzed incorporation of O-18 into peptide fragments and its application for protein sequencing by electrospray and matrix-assisted laser desorption/ionization mass spectrometry. *Electrophoresis* **1996,** *17*, 945-953.

279. Antonov, V. K.; Ginodman, L. M.; Rumsh, L. D.; Kapitannikov, Y. V.; Barshevskaya, T. N.; Yavashev, L. P.; Gurova, A. G.; Volkova, L. I. Studies on the mechanisms of action of proteolytic enzymes using heavy oxygen exchange. *European Journal of Biochemistry* **1981,** *117*, 195-200.

280. Tsybin, Y. O.; Witt, M.; Baykut, G.; Hakansson, P. Electron capture dissociation Fourier transform ion cyclotron resonance mass spectrometry in the electron energy range 0-50 eV. *Rapid Communications in Mass Spectrometry* **2004,** *18*, 1607-1613.

281. Tsybin, Y. O.; Hakansson, P.; Budnik, B. A.; Haselmann, K. F.; Kjeldsen, F.; Gorshkov, M.; Zubarev, R. A. Improved low-energy electron injection systems for high rate electron capture dissociation in Fourier transform ion cyclotron resonance mass spectrometry. *Rapid Communications in Mass Spectrometry* **2001,** *15*, 1849-1854.

282. Tsybin, Y. O.; Ramstrom, M.; Witt, M.; Baykut, G.; Hakansson, P. Peptide and protein characterization by high-rate electron capture dissociation Fourier transform ion cyclotron resonance mass spectrometry. *Journal of Mass Spectrometry* **2004,** *39*, 719-729.

283. Babu, Y. S.; Bugg, C. E.; Cook, W. J. Structure of calmodulin refined at 2.2 A resolution. *Journal of Molecular Biology* **1988,** *204*, 191-204.

284. Chattopadhyaya, R.; Meador, W. E.; Means, A. R.; Quiocho, F. A. Calmodulin structure refined at 1.7 angstrom resolution. *Journal of Molecular Biology* **1992,** *228*, 1177-1192.

285. Finn, B. E.; Forsen, S. The evolving model of calmodulin structure, function and activation. *Structure* **1995,** *3*, 7-11.

286. Cheung, W. Y. Calmodulin plays a pivotal role in cellular regulation. *Science* **1980,** *207*, 19-27.

287. Chin, D.; Means, A. R. Calmodulin: a prototypical calcium sensor. *Trends in Cell Biology* **2000,** *10*, 322-328.

288. Johnson, B. A.; Shirokawa, J. M.; Aswad, D. W. Deamidation of calmodulin at neutral and alkaline pH : Quantitative relationships between ammonia loss and the susceptibility of calmodulin to modification by protein carboxyl methyltransferase. *Archives of Biochemistry and Biophysics* **1989,** *268*, 276-286.

289. Potter, S. M.; Henzel, W. J.; Aswad, D. W. In-vitro aging of calmodulin generates isoaspartate at multiple Asn-Gly and Asp-Gly sites in calcium-binding domains II, III, and IV. *Protein Science* **1993,** *2*, 1648-1663.

290. Raines, R. T. Ribonuclease A. *Chemical Reviews* **1998,** *98*, 1045-1065.

291. Beintema, J. J.; Kleineidam, R. G. The ribonuclease A superfamily: general discussion. *Cellular and Molecular Life Sciences* **1998,** *54*, 825-832.

292. Wearne, S. J.; Creighton, T. E. Effect of protein conformation on rate of deamidation - ribonuclease-A. *Proteins: Structure, Function, and Genetics* **1989,** *5*, 8-12.

293. Zabrouskov, V.; Han, X. M.; Welker, E.; Zhai, H. L.; Lin, C.; van Wijk, K. J.; Scheraga, H. A.; McLafferty, F. W. Stepwise deamidation of ribonuclease A at five sites determined by top down mass spectrometry. *Biochemistry* **2006,** *45*, 987-992.

294. Blake, C. C. F.; Koenig, D. F.; Mair, G. A.; North, A. C. T.; Phillips, D. C.; Sarma, V. R. Structure of hen egg-white lysozyme - a 3-dimensional fourier synthesis at 2 A resolution. *Nature* **1965,** *206*, 757-&.

295. Harata, K. X-ray structure of monoclinic turkey egg lysozyme at 1.3-angstrom resolution. *Acta Crystallographica Section D-Biological Crystallography* **1993,** *49*, 497-504.

296. Kirby, A. J. The lysozyme mechanism sorted - after 50 years. *Nature Structural Biology* **2001,** *8*, 737-739.

297. Kato, A.; Shibata, M.; Yamaoka, H.; Kobayashi, K. Deamidation of lysozyme during the storage of egg white. *Agricultural and Biological Chemistry* **1988,** *52*, 1973-1978.

298. Robinson, A. B.; Tedro, S. Sequence dependent deamidation rates for model peptides of hen egg-white lysozyme. *International Journal of Peptide and Protein Research* **1973,** *5*, 275-278.

299. Zubarev, R. A. Electron-capture dissociation tandem mass spectrometry. *Current Opinion in Biotechnology* **2004,** *15*, 12-16.

300. Benaroudj, N.; Tarcsa, E.; Cascio, P.; Goldberg, A. L. The unfolding of substrates and ubiquitin-independent protein degradation by proteasomes. *Biochimie* **2001,** *83*, 311-318.

301. Halliwell, B. Proteasomal dysfunction: A common feature of neuro degenerative diseases? Implications for the environmental origins of neurodegeneration. *Antioxidants & Redox Signaling* **2006,** *8*, 2007-2019.

302. Capasso, S.; Mazzarella, L.; Sica, F.; Zagari, A. 1st evidence of spontaneous deamidation of glutamine residue via cyclic imide to alpha-glutamic and gamma-glutamic residue under physiological conditions. *Journal of the Chemical Society-Chemical Communications* **1991**, 1667-1668.

303. Hayes, C. S.; Setlow, P. Analysis of deamidation of small, acid-soluble spore proteins from Bacillus subtilis in vitro and in vivo. *Journal of Bacteriology* **1997,** *179*, 6020-6027.

304. Bloemendal, H.; de Jong, W.; Jaenicke, R.; Lubsen, N. H.; Slingsby, C.; Tardieu, A. Ageing and vision: structure, stability and function of lens crystallins. *Progress in Biophysics & Molecular Biology* **2004,** *86*, 407-485.

305. Wistow, G. J.; Piatigorsky, J. Lens crystallins - the evolution and expression of proteins for a highly specialized tissue. *Annual Review of Biochemistry* **1988,** *57*, 479-504.

306. Novak, P.; Man, P.; Tuckova, L.; Hogenova, H. T.; Bezouska, K.; Havlicek, V. Monitoring of in vitro deamidation of gliadin peptic fragment by mass spectrometry may reflect one of the molecular mechanisms taking place in celiac disease development. *Journal of Mass Spectrometry* **2002,** *37*, 507-511.

307. Joshi, A. B.; Kirsch, L. E. The relative rates of glutamine and asparagine deamidation in glucagon fragment 22-29 under acidic conditions. *Journal of Pharmaceutical Sciences* **2002,** *91*, 2332-2345.

308. Liu, H. C.; Gaza-Bulseco, G.; Chumsae, C. Glutamine deamidation of a recombinant monoclonal antibody. *Rapid Communications in Mass Spectrometry* **2008,** *22*, 4081-4088.

309. Nagasawa, H. T.; Magnan, S. D. J.; Foltz, R. L. Differentiation of alpha-glutamyl from gamma-glutamyl-transferase dipeptides by chemical ionization mass-spectrometry. *Biomedical Mass Spectrometry* **1982,** *9*, 252-256.

310. Lloyd, J. R.; Cotter, M. L.; Ohori, D.; Doyle, D. L. Distinction of Alpha-Aspartyl and Beta-Aspartyl and Alpha-Glutamyl and Gamma-Glutamyl-Transferase Peptides by Fast

Atom Bombardment Tandem Mass-Spectrometry. *Biomedical and Environmental Mass Spectrometry* **1988,** *15*, 399-402.

311. Okada, K.; Kawase, M. Mass-spectral differentiation of alpha-linkages and gamma-linkages in glutamyl oligopeptides and its application for structure elucidation of naturally occurring peptides. *Chemical & Pharmaceutical Bulletin* **1977,** *25*, 1497-1508.

312. Schucker, S. C.; Scriba, G. K. E. Analysis of isomeric glutamyl peptides by capillary electrophoresis - Application to stability studies. *Journal of Chromatography A* **2000,** *888*, 275-279.

313. Harrison, A. G. Characterization of alpha- and gamma-glutamyl dipeptides by negative ion collision-induced dissociation. *Journal of Mass Spectrometry* **2004,** *39*, 136-144.

314. Hayakawa, S.; Hashimoto, M.; Matsubara, H.; Turecek, F. Dissecting the proline effect: Dissociations of proline radicals formed by electron transfer to protonated pro-gly and gly-pro dipeptides in the gas phase. *Journal of the American Chemical Society* **2007,** *129*, 7936-7949.

315. Tsybin, Y. O.; Hamidane, H. B.; Vorobyev, A.; Wodrich, M.; Corminboeuf, C. In *Peptide conformation selectivity in electron capture and transfer dissociation.*, 57th ASMS conference on mass spectrometry, Philadelphia, Pennsylvania, 2009.

316. Frank, A. M.; Savitski, M. M.; Nielsen, M. L.; Zubarev, R. A.; Pevzner, P. A. De novo peptide sequencing and identification with precision mass spectrometry. *Journal of Proteome Research* **2007,** *6*, 114-123.

317. Qiao, S. W.; Bergseng, E.; Molberg, O.; Jung, G.; Fleckenstein, B.; Sollid, L. M. Refining the rules of gliadin T cell epitope binding to the disease-associated DQ2

molecule in celiac disease: Importance of proline spacing and glutamine deamidation. *Journal of Immunology* **2005,** *175*, 254-261.

318. Arentz-Hansen, H.; McAdam, S. N.; Molberg, O.; Fleckenstein, B.; Lundin, K. E. A.; Jorgensen, T. J. D.; Jung, G.; Roepstorff, P.; Sollid, L. M. Celiac lesion T cells recognize epitopes that cluster in regions of gliadins rich in proline residues. *Gastroenterology* **2002,** *123*, 803-809.

Curriculum Vitae

Xiaojuan Li

Education

- Ph.D., Biochemistry
  School of Medicine, Boston University, Boston, MA, anticipated September 2010
  Thesis title: Mechanism of electron capture dissociation and the application to protein deamidation.
  Advisor: Professor Peter B. O'Connor

- M. Sc., Microbiology and Biochemistry Pharmaceutics
  College of Life Science, Jilin University, Changchun, China 2003
  Thesis title: Research on the influence of aFGF antagonist on 3T3 cell protein profiles.

- B. Eng., Biopharmaceutics
  College of Life Science, Jilin University, Changchun, China 2000
  Thesis title: Study of alkaloids from seeds of Calonyction muricatum

Research Experience

2003-2005 Research associate, Center for Molecular Virology,
Institute of Microbiology, Chinese Academy of Sciences

Publications

- **Xiaojuan Li**, Cheng Lin, Peter B. O'Connor. "Top-down ECD and CID/ECD study of β_2-microglobulin protein deamidation." *(in preparation)*

- **Xiaojuan Li**, Peter B. O'Connor, Cheng Lin. "Multiple structures of b ions probed by electron capture dissociation." *(ready to be submitted)*

- **Xiaojuan Li**, Cheng Lin, Peter B. O'Connor. "Glutamine deamidation: Differentiation of glutamic acid and isoglutamic acid in peptides." *Analytical Chemistry* **2010,** 82, 3606-3615.

- **Xiaojuan Li**, Cheng Lin, Liang Han, Catherine E. Costello, and Peter B. O'Connor. "Charge remote fragmentation in electron capture and transfer dissociations." *J. Am. Soc. Mass Spectrom.* **2010,** 21(4), 646-656.

- **Xiaojuan Li**, Jason J. Cournoyer, Cheng Lin and Peter B. O'Connor. "The effect of fixed charge modifications on electron capture dissociation." *J. Am. Soc. Mass Spectrom.* **2008,** 19(10), 1514-1526.

- **Xiaojuan Li**, Jason J. Cournoyer, Cheng Lin, and Peter B. O'Connor. "Use of ^{18}O labels to monitor deamidation during protein and peptide sample processing." *J. Am. Soc. Mass Spectrom.* **2008,** 19(6), 855-864.

- Minghai Zhou, Dongping Xu, **Xiaojuan Li**, Hongtao Li, Ming Shan, Jiaren Tang, Min Wang, Fu-Sheng Wang, Xiaodong Zhu, Hua Tao, Wei He, Po Tien, and George F. Gao. "Screening and identification of severe acute respiratory syndrome-associated coronavirus-specific CTL epitopes." *The Journal of Immunology,* **2006**, 177, 2138–2145.

- Minghai Zhou, Yanhui Xu, Zhiyong Lou, David K. Cole, **Xiaojuan Li**, Yiwei Liu, Po Tien, Zihe Rao and George F. Gao. "Complex assembly, crystallization and preliminary X-ray crystallographic studies of MHC H-2K^{d} complexed with an HBV-core nonapeptide." *Acta Crystallographica Section D Biological Crystallography,* **2004**, 60, 1473-1475.

- **Xiaojuan Li**, Yuqin Fu, Gui Gao, Yinqiu Cui, Hui Zhou. "Research on the influence of aFGF antagonist on 3T3 cell protein profiles." *Chemical Journal of Chinese Universities,* **2004**, 25, 1268-1272. (in Chinese)

- **Xiaojuan Li,** Yuqin Fu, Hui Zhou. "Research progress of fibroblast growth factor (FGF) inhibitors." *Chinese Remedies and Clinics,* **2003**, 3, 326-328. (in Chinese)

- Yingming Wang, **Xiaojuan Li**, Yingwu Wang, Jingkai Gu, Hui Zhou. "Studies on alkaloids from seed of Calonyction muricatum." *Chinese Traditional and Herbal Drugs,* **2002**, 33, 111-113. (in Chinese)

Honors & awards

- The Myrna and Carl Franzblau Travel Award winner, Department of Biochemistry, Boston University (2009)
- ASMS student travel stipend (2009, 2007)
- Excellent Graduate Students Scholarship of Jilin University (2001~2002)
- Changchun Biology Scholarship (2001~2002)
- Dongrong Scholarship (1998~1999)
- Excellent Undergraduate Students Scholarship of Jilin University (1996~1999)